Single-Stream Spray Drying Process to Generate Uniform and Functional Powder Particles

Abdul Khaliq Elzhry Elyafi

Doctor of Philosophy

Aston University

September 2021

Aston University

Single-Stream Spray Drying Process to Generate Uniform and Functional Powder Particles

Abdul Khaliq Elzhry Elyafi
Doctor of Philosophy
September 2021

Thesis Abstract

Particle properties, especially size and shape, are considered critical attributes for many pharmaceutical materials as they affect the manufacturability of solid dosage forms and their critical quality attributes such as dose uniformity, dissolution rate and bioavailability. Regulatory guidelines e.g. ICH Q6A highlighted the need for controlling particle properties through setting acceptance criteria for particle size of drug substances. However, generating pharmaceutical ingredients with uniform and adjustable particle properties is faced with several challenges, most importantly a difficulty to control particle crystallisation. Thus, the interest in developing new technologies for engineering particles with controllable size and morphology has increased dramatically in the last two decades. Spray drying is at the forefront of industrial techniques used to produce complex microparticles at the desired scale. Nevertheless, this method generates polydisperse droplets with potential for their coalescence. Therefore, the particles may exhibit variation in size/morphology within the same batch, and semi-dried ones could agglomerate or deposit in the chamber.

This work aims to develop a novel spray drying-based technology for generating monodisperse pharmaceutical particles with controllable attributes (size and shape). This is expected to improve powders' processability during solid dosage manufacturing and reduce variation in quality attributes of final products. A custom-built lab-scale spray dryer for generating monodisperse particles, referred to as a single-stream spray dryer, is presented. It combines a monodisperse droplet generator (MDG) with a drying chamber and ancillary equipment to design particles with highly uniform size and shape. A stroboscopic imaging system was utilised as a process analytical technology tool to optimise the jet velocity and MDG vibration frequency necessary for generating monodisperse droplets. The performance of the new spray dryer was explored using model ingredients D-Mannitol, Metformin HCl and Felodipine. Monodisperse spray-dried (Mono-SD) powders were fabricated and compared with untreated and conventionally spray-dried (SD) ones. The impact of particle size/shape, powder mono-/polydispersity and excipient dilution on the homogeneity and content uniformity of binary blends containing a low-dose drug was also investigated. Several characterisation techniques were utilised, including Morphologi 4 and laser diffraction to study particle size and shape parameters, microscopy for morphology, shear cell for powder flow testing and differential scanning calorimetry along with x-ray powder diffraction for studying materials' crystallinity.

The generated Mono-SD particles exhibited spherical shapes with a very narrow size distribution. By contrast, conventional SD particles showed uncontrolled shape and size with agglomerates. As a result, Mono-SD powders showed significantly better bulk powder properties (e.g. flowability and packing density) even with particle sizes less than 50 μm. The repose angle for all Mono-SD powders was less than 16º, whereas it was above 42º for all other untreated/SD powders. This clearly indicates that Mono-SD powders exhibit superior flow compared to untreated/SD powders. Moreover, this high flowability of Mono-SD translated into significantly better blend homogeneity and content uniformity for binary mixtures containing Felodipine at low doses (< 10% w/w) compared to untreated and conventionally SD powders. On the other hand, no significant impact on material compressibility could be observed for Metformin HCl and D-mannitol Mono-SD powders. In fact, conventional SD powder for D-mannitol had significantly better compaction, potentially due to higher bonding generated between polydisperse particles during compression. The findings suggest that the novel single-stream spray dryer has a great promise for creating particles with the desired size and shape. In terms of functionality, the impact of Mono-SD properties on flowability and dose uniformity is overwhelmingly positive, while for compaction polydisperse particles were more useful due to their apparent higher bonding capacity.

Keywords: spray drying; monodisperse particles; flowability; content uniformity; solid dosage forms.

Acknowledgements

First of all, I would like to thank **Allah Almighty** for giving me the opportunity and guidance to achieving my goal and to complete my studies successfully.

Then, I would like to express my appreciation to my supervisor Dr. Ali Al-Khattawi who gave me this precious opportunity to undertake such an interesting project. The work that has resulted in this thesis would not have been possible without his guidance, inspiration, technical support, and constructive criticism throughout my years at Aston University. Working with Dr. Ali has provided me with many skills and has made me into a well-rounded scientific researcher.

My deep appreciation also goes to Prof. Afzal Mohammed (the associate supervisor) for his advice and academic support throughout my project.

Many thanks also go out to Aston Pharmacy School and its staff and technicians, for their kind advice and help on administrative and technical support and for creating a pleasant atmosphere for us to work as doctoral researchers.

I wish to thank Aston University for giving me a fully-funded doctoral scholarship.

I am indebted to many of my colleagues and friends in the pharmaceutical research group for their invaluable support and for making my postgraduate life more exciting and memorable. I enjoyed working with all of them, particularly Tu Tuan le, Annsar Warraich, Dilawar Khan, Carlo Curti, Basma Elbakary and Abdul Ershad. Our time together will never be forgotten!

I would also like to thank all those at Merlin Powder Characterisation Ltd. who have provided access to the hydraulic Compaction Simulator to undertake the Heckel profile analysis for the powder samples reported here. Elaine Harrop Stone and Charlotte Cartwright deserve special thanks for their efforts.

Last but certainly not least, I would also like to say a heartfelt thank you to my Dad, Mum, Siblings (Rida and Hadi) for always believing in me and encouraging me to follow my dreams. It is my pleasure to dedicate this thesis to them. Without their love and prayers, I most certainly would not be where I am today.

Table of Contents

List of Figures

List of Tables

Chapter 1

CHAPTER 1

Literature Review

1.1. Introduction:

Most pharmaceutical ingredients are polydisperse powders containing fine particles with different morphologies and agglomerates (1–4). The fundamental particle properties such as particle size and shape and their distributions are essential parameters to be considered during pharmaceutical formulation and process development. In many cases, any change to these parameters might easily cause problems in powder handling and flowability, which ultimately affect the drug's dose uniformity and bio-performance after administration (5–7). Therefore, maintaining powder batches uniformity and manufacturing consistency is crucial, especially during scale-up and technology transfer operations (1,8–12).

Unfortunately, the physical powder properties of pharmaceutical ingredients usually change throughout the active ingredient/product development course due to various routes of production and isolation parameters or conditions (13–15). In addition, given the diversity of ingredients' structure and sources, it is quite challenging to predict the particle properties and final powder's attributes of a given ingredient. Currently, many pharmaceutical scientists acknowledge this issue and attempt to control the physical powder properties using different systems or platforms. This is to ensure that the quality of the final drug product is consistently obtained and it matches the identified specifications according to regulatory agencies requirements (16–23). In this regard, one of the promising strategies to control the properties of ingredients is to develop them as "**monodisperse powders**". The term "**monodisperse powder**" as the antonym of "**polydisperse powder**" refers to a group of particles made with highly uniform size and shape (24). Ideally, suppose they are defined in terms of size distribution, the powdered materials could be considered monodisperse if at least 90% of the particle size distribution lies within 5% of the median size, according to the National Institute of Standards and Technology (25). Using such monodisperse particles with the ability to adjust their size on-demand could play an essential role in overcoming pharmaceutical production issues through reducing the variability within manufacturing processes and improving product quality.

In this literature review chapter, four main points will be addressed as follows:
Firstly, the chapter summarises the current state of solid dosage form design and manufacturing, highlighting some of the challenges resulting from variability in powder properties. Secondly, it presents the impact of using monodisperse particles in the pharmaceutical industry for better final product quality and performance and reviews the novel technologies that are utilised in generating multifunctional uniform particles with identical shapes. Thirdly, it highlights the spray drying process concept as a standard method

in the pharmaceutical industry for generating micro/nanoparticles with controlled properties. Finally, it provides an overview of the atomisation process with a focus on understanding the mechanism of droplet formation in order to generate droplets/particles with uniform diameters. This involves elucidating the principle of operation of monodisperse droplets generator (MDG) as a tool that creates a stream of uniform droplets with adjustable size.

1.2. The current state of solid dosage form design, development and manufacturing:

Generally, a key aim of pharmaceutical development is to design a robust formulation and manufacturing process that consistently produces drug products with desired properties and intended performance (26). Historically, solid dosage forms are the most popular commercial products used for drug administration in the global pharmaceutical market. According to the FDA (CDER reports), around 50% of new drug approvals are for oral delivery, especially in the form of tablets and capsules (27). This is mainly due to their advantages, such as accurate dosing, chemical stability, high patient compliance, flexibility in administration, established manufacturing processes, and low production cost, particularly when compared with other dosage forms (28,29).

Successful development of pharmaceutical dosage forms is heavily dependent on identifying the critical quality attributes (CQAs) and selecting the optimal quality target product profile (QTPP). These have a significant impact on designing a robust formulation with desired quality and clinical performance (26). According to the international conference on harmonisation guidelines, especially ICH Q8 (R2) (pharmaceutical development), the potential risks to QTPP and CQAs usually arise from critical material attributes (CMAs) and critical process parameters (CPPs) which need to be determined, controlled and monitored correctly during product design and proposed manufacturing (26).

Critical material attributes (CMAs) can be defined as any physical, chemical, biological, or microbiological property of a formulation ingredient which should be identified within appropriate limits in order to maintain consistent product CQAs such as assay, homogeneity, stability, content uniformity, *in vitro* drug release, etc. (26). In many cases, identifying CMAs is the essential criterion during formulation design and development to ensure meeting the predefined product quality specifications. Moreover, controlling CMAs helps to reduce the variation in product performance, improves manufacturing process efficiency and minimises the risk of failure, e.g. product recalls and shutdowns (30,31).

Specifically, one of common failure modes in the final product originate from the substantial variability in raw material specifications and the bulk powder properties (30). Conventionally, the chemical development of pharmaceutical ingredients (drug substances and excipients) and the pharmaceutical formulation development are commonly treated as independent activities (32). However, the interplay between these

two areas has been reported to have a critical role in the development of robust and cost-effective products (1,33).

Despite solid dosage form manufacturing looking simple at the outset, it is nevertheless a complicated process involving many pharmaceutical unit operations. According to pharmaceutical manufacturers, the link between raw material properties and final product development is still largely empirical, making some formulations challenging to design and develop (7,33,34). In addition, the diversity in raw material properties makes the development of solid dosage forms with desired pharmacokinetic profile and therapeutic efficacy a difficult task for many manufacturers, especially in achieving dosage uniformity and dissolution reproducibility of the produced batches (1,3,34,35). This is because the processability of the powders in the manufacturing unit operations depends heavily on the primary particle properties (e.g. particle size, morphology, porosity and density) and bulk properties (e.g. flowability and compressibility). Such that, even subtle changes in the fundamental particle properties of a drug could be amplified by the impact of factors such as processing conditions (temperature and humidity) and parameters (equipment geometric design and energy input), leading to a change in the physicochemical and micromeritic properties of the ingredient. As a result, a variation in oral product performance could be observed, e.g. to the drug dissolution profile or oral bioavailability, especially if the formulations contain relatively high quantity of the drug substance i.e. high-dose formulations (6,15,33,36). On the other hand, for low-dose formulations, pharmaceutical technologies are currently facing many challenges, especially in achieving a high content uniformity. This might lead to lower potency of the final product due to drug loss during the manufacturing process or inconsistent dosing from multiple units (37,38). The effect of changes in particle properties on drug efficacy and safety becomes even more noticeable and critical with highly potent active pharmaceutical ingredients (HPAPIs) such as hormones and anticancer compounds, which present significant pharmacological effects at low concentrations (39–41).

In recent years, several clinical problems were reported with commercial products due to variation in solubility and permeability. FDA acknowledged these issues whereby some solid dosage forms are recalled and removed from the market every month due to the clinical response's deficiency and variability. For example, when comparing different batches or sources of carbamazepine tablets, it was clear that changes in the crystal structure, particle size, or moisture content for raw drug powders led to a significant difference in the dissolution rate with unpredictable absorption and bioavailability (42,43). Furthermore, several batches from different generic drug products (venlafaxine hydrochloride extended-release tablets, nebivolol tablets and isoniazid tablets) were recalled in 2014 due to failure in dissolution specification during routine stability testing. In 2016, one company had to recall seven batches of hyoscyamine sulfate sublingual tablets as a precaution because the product did not meet the content uniformity specification, resulting in superpotent or subpotent therapeutic effects (44).

To improve the product quality and minimise variations in product specifications, there is a necessity to have pharmaceutical ingredients with optimal particle properties (e.g. morphology, particle size, porosity,

and density) and functionality (e.g. flowability, packing density and compressibility). As such, formulation and process development teams usually prefer using large spherical particles that are more favourable during formulation design and product development. These particle properties lead to better processability and lower failure risk, thus ensuring consistent quality throughout a product's life cycle (36,45).

Unfortunately, most pharmaceutical ingredients (drug substances and excipients) used these days are polydisperse powders with a wide range of particle size and shape distributions (1,3,9,34). In addition, most drug candidates have non-ideal properties for handling and processing, leading to failure in the critical quality attributes (CQAs) of the final dosage form, such as in weight uniformity, content uniformity, tensile strength and drug dissolution. Specifically, drug substances resulting from crystallisation processes usually have a small particle size (100 μm or less) and frequently exhibit elongated (needle-like) shape, which can result in unstable, poor powder flow with various unwanted technical problems (e.g. powder segregation and sticking to punches) during tableting unit operations such as feeding, blending, die-filling and compaction (2,29,46,47).

Generating pharmaceutical ingredients with uniform properties is not a trivial task. It is usually faced with a myriad of challenges due to the diversity in chemical entities and elementary molecular interactions, leading to difficulty in predicting what the particle properties and overall powder's attributes of any given ingredient will be (4,13–15,48). It was also found that using different manufacturing processes (i.e. synthesis routes, isolation, extraction, etc.) during API development could cause changes in physical material attributes that potentially affect the formulation manufacturability and process efficiency (1,3). As a result, most pharmaceutical ingredients generated from different sources, batches, or manufacturing processes usually exhibit some degree of variation in their properties. For example, small modifications in processing parameters (e.g. milling duration or spray drying temperature) were found to influence the physicochemical stability of cefditoren pivoxil as a consequence of changes in crystallinity degree and surface free energy of the particles (49,50). The effect of variability in raw material properties on the excipient’s functionality and its relevance for processability in pharmaceutical manufacturing has been extensively reported in many studies over the last few decades. For instance, microcrystalline cellulose (MCC) is commonly used as a filler/binder agent, especially in direct compression formulations. Nofrerias et al. illustrated that there was a significant difference in powder characteristics and functionality when comparing MCC powders of the same grade (101, 102, 301, 302 or 200) produced from four different manufacturers (51). According to experimental results based on SeDeM expert system, the variability in bulk powder properties, especially moisture content (%HR), inter-particle porosity (Ie) and particle homogeneity index (Iθ) had a great effect on MCC’s flowability and suitability for direct compression. Also, Landin et al. evaluated the properties of MCC (Avicel PH101) obtained from different sources (Finland, India, Ireland, and Japan). They found that there were significant differences in the chemical composition, crystal structure and particle size. All these critical material differences illustrated the observed differences in flow and compression properties (52). The variations in pharmaceutical excipient properties can alter the final dosage forms' physicochemical properties, which consequently affect the

biopharmaceutical performance (53–56). Bolhuis et al. evaluated the lot-to-lot variability in physicochemical properties of different batches of two brands of sodium starch glycolate (SSG). The study results showed significant changes in disintegration time of the tablet containing SSG as a disintegration agent. The differences in disintegration time and swelling rate were attributed to the differences in product purity (57). Also, it has been reported that lot-to-lot variation in the molecular structure, viscosity, and particle size of sodium starch glycolate significantly affects the disintegration behaviour of some tablet formulations. The results indicated that relatively small changes in material specifications can cause substantial modifications in disintegration and dissolution behaviour (58,59). The impact of the physical properties of magnesium stearates (MgSt) on lubrication efficacy has been presented previously. The results illustrated that the variability in particle size and shape distributions of the studied MgSt brands or batches had a prominent effect on tablet lubricity and drug release. Using MgSt with smaller particle sizes and larger specific surface area usually increases lubrication efficacy and decreases tensile strength as well as drug dissolution rate for different pharmaceutical tablets (60,61). On the other hand, the impact of active raw materials variability upon formulation manufacturability and eventually upon the final product specifications has also been well documented in the literature. For example, Stauffer et al. carried out a qualitative and quantitative analysis for a drug substance that was produced from eight different batches. The data obtained from the principal component analysis (PCA) illustrated that there were massive differences in particle and powder properties (crystal length, particle size distribution, flowability, electrostatic charges, etc.) when comparing between the batches. The authors hypothesised that lot-to-lot variation in drug substance properties should be considered during pharmaceutical product development as it can be significant, potentially causing process and product quality variation (9). By using a similar analysis approach, Hagsten et al. investigated the impact of raw material variability of 131 batches of 5-aminosalicylic acid on the granulation and extrusion processes. The results indicated that variations in the particle size and packing density led to differences in the powder processability when comparing the batches (62). Moreover, three comprehensive studies were performed to evaluate the variability in drug substance properties on the twin-screw granulation process and the resulting granule properties. The results indicated that the variability in powder properties has a significant impact on the twin-screw feeding and the final granule CQAs such as flowability and friability (10–12). Moreover, Zhao et al. evaluated three lots of the drug substance glipizide. Their results showed notable differences in the dissolution profiles and bioavailability of the prepared tablets when compared with the reference product (MINIDIAB®). These differences were related to particle size and size distribution, which varied between the different lots (63). For carbamazepine, Sehic et al. went even further in the analysis by studying the impact of variability in raw material properties on the intrinsic dissolution behaviour. It was shown that nine anhydrous commercial samples from three different sources exhibit the same polymorphic form but different particles morphology and size distribution. This led to different kinetics of conversion from the anhydrous to the dihydrate carbamazepine form, resulting in a variation in the intrinsic dissolution profile when comparing between the different samples (64).

According to the previous investigations, it is clear that the variations in raw material properties that may originate from using different material sources or manufacturing processes could lead to several challenges during formulation development. Any changes in these physical material properties can easily cause downstream problems during powder handling and processing, which ultimately affect the process efficiency, the final product quality attributes, and how the drug will eventually perform *in-vivo*, as seen in Figure 1.1.

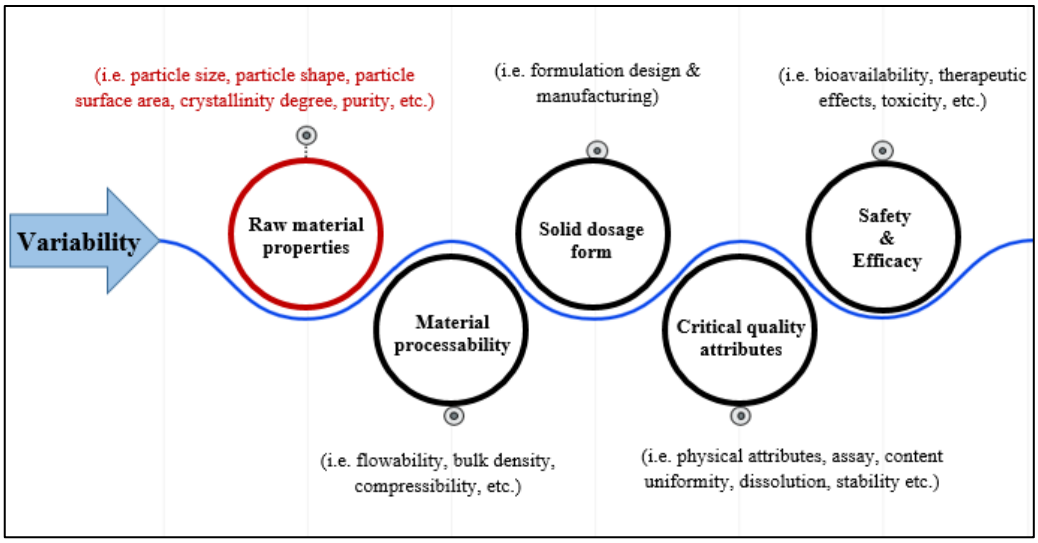

Figure 1.1: Summarising the impact of raw material variability on product development.

From a regulatory perspective, ICH guideline Q6A emphasised the importance of controlling particle properties through setting acceptance criteria for particle size and particle size distribution of drug substances. This is because these particle properties have a significant effect on product's critical quality attributes (CQAs) especially for poorly soluble/ low dose drugs due to concerns of variation in bioavailability and content uniformity, respectively (65). In the following sections, we will take a closer look at the impact of fundamental particle properties (particle size and morphology/shape) on material processability and how these properties significantly impact the CQAs of the final solid dosage form. This is followed by reviewing current technologies to generate multifunctional uniform particles and how monodisperse powder particles could play an essential role in enhancing formulation design, material processing, and final product performance.

1.3. Impact of fundamental particle properties on formulation design, process development and final product quality:

To understand the impact of raw material properties on the functionality of a solid dosage form during, it is vital to highlight the bulk solids' inherent nature first. Generally, solid properties can be classified into three levels (66), as depicted in Figure 1.2. The first one is a molecular level, which describes a specific arrangement of individual molecules in a crystal lattice. It is responsible for the solid-state structure (i.e.

crystal, co-crystal, amorphous and polymorphic forms) and substantial material properties such as melting point, intrinsic solubility, dissolution rate, thermodynamic stability, deformation properties, etc. The next one is a particulate level where every particle consists of many molecules, and it has a specific structure such as surface area, size, shape, and porosity. The last one is a bulk powder level that considers an assembly of particles together, and it describes powder behaviour (particle-particle interactions) at a macro scale such as flowability, compactability and packing density.

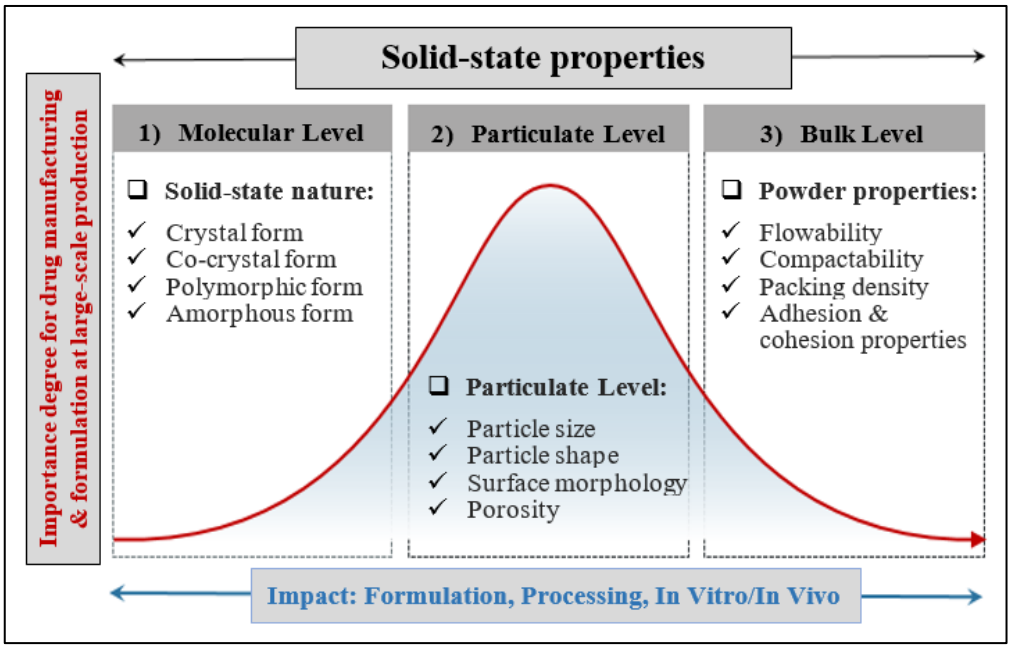

Figure 1.2: Classification of solid material properties at different levels.

These levels are critical for any solid ingredient and the change of properties at one level is closely linked to another (66). For example, changes in crystallisation conditions during production can significantly alter the physicochemical properties and physico-mechanical properties of drug substances, which ultimately affect manufacturability and biopharmaceutical performance of solid dosage form (15). In the pharmaceutical industry, the cost and time required to develop a new dosage form are significant and increase dramatically when the final product fails to meet the identified specifications according to regulatory agencies requirements (9).

For many pharmaceutical manufacturers, it is well known that powder blends with specific particle sizes and shapes are more amenable to handle than others, e.g. for tabletting it was demonstrated that regular shaped particles like spheres with size distribution of 100-200 μm are preferred due to better flow properties and compaction behaviour over a wide range of stress conditions (67,68). However, most pharmaceutical ingredients are polydisperse powders with different particle properties (i.e. size, morphology, agglomerates and surface flaws), as mentioned before. This fact presents various challenges in powder/formulation blend handling under highly accelerated timelines of the manufacturing process (36,46).

Therefore, obtaining detailed knowledge of fundamental particle properties helps manufacturers produce dosage forms with desired CQAs and enables them to maintain higher production stability (batch-to-batch consistency).

As mentioned previously, many researchers, industrialists and regulators have highlighted the importance of two fundamental particle properties, namely particle size and its shape, for many formulations. Below is a summary of the effects exerted by these material attributes:

1.3.1. Particle size effect:

Generally, particle size is one of the reliable indicators for bulk powder properties. It affects the powder's bulk density, flowability, packing properties and dissolution as well as adhesion and cohesion properties (5). These bulk properties significantly correlate with feeding/filling operations during tableting and encapsulation processes. Consistency of in-die filling and dosing powders' mechanisms are directly linked to the uniformity of drug dosage weight, which significantly affect other critical quality attributes such as tablet friability/tensile strength and dissolution rate (29,45). Specifically, particle size reduction tends to increase interactions and adhesion between neighbouring particles due to increasing the surface area per unit mass. This leads to numerous problems such as low bulk density and less powder flow, which is related to difficulty in powder handling and dispensing (69,70). Larger particle size results in a better flow behaviour for raw and in-process materials due to reduction in surface area per unit mass. Therefore, it is generally accepted that large-sized particles with mean particle size larger than 250 μm are usually free-flowing compared to particles smaller than 100 μm, which exhibit poor flow. Furthermore, when particle size falls below 50 and 10 μm, the particles become cohesive and remarkably cohesive, respectively (71,72). This is mostly due to strong interparticle interactions such as Van der Waals, capillary and electrostatic forces, which exceed the particle weight and become responsible for cohesiveness of the powder bed (2,73).

Not only particle size but also its size distribution (PSD) has a critical impact on powder flow. Many studies indicated that powders with narrow size distribution have better flow properties compared to those with wider size distribution (70,74). For example, Liu et al. found that when the finest size fraction of a needle-shaped ibuprofen powder (normally very cohesive) is separated from the bulk powder, the fine fraction flows better than the bulk powder due to its narrow size distribution (72). The majority of pharmaceutical products are blends of multiple components with different particle properties. This means the effect of particle size and its distribution on flowability/bulk powder properties of the multi-component mixture is more complex and depends on components proportion in the system as well as which particles are prevalent, the finest or the largest (75). For instance, Kojima and Elliott investigated packing and flow properties of binary mixtures of coarse and fine particles using a ring shear tester (RST). Their experimental results indicated that the contacts between coarse particles dominated the powder mixture's friction and packing properties when the fines content is small, while contacts between fine particles dominate when the fines content is high (76).

Usually, smaller amounts of powdered drug substances are blended with larger proportion of excipients. According to pharmacopoeia, obtaining a uniform mixing of the formulation components is essential for the final dosage form to meet the content uniformity's acceptance criteria (77). In the case of low-dose drugs, the impact of particle size on the blend uniformity is significantly more substantial due to the fact that segregation can be triggered even when the difference in particle diameters between drug and carrier (excipient) is quiet small. Some studies indicated that segregation can occur with a particle diameter ratio as low as 1.3-to-1 (78,79).

Segregation can occur when the formulation components have marked differences in size, density or shape, however, the dominant factor is the particle size (80). This issue can happen at any stage of blend handling and dosage form manufacturing e.g. mixing, granulation, tableting, bulk storage or flow in the hopper (81,82). For random mixing of polydisperse powder systems, the smaller particles in the core of bulk powder tend to percolate through the void spaces between larger particles and settle down at the bottom of the powder bed when the particle size distribution has a high span value. The span of a volume-based size distribution is defined as D_{90}-D_{10}/D_{50} and gives an indication of how far the 10^{th} and 90^{th} percentile points are apart, normalised with a midpoint (D_{50}). The segregation issue is further exacerbated when the powder bed is vibrated e.g. during transport and/or when the smaller particles are much denser. This could result in reduced blend uniformity and flowability, leading to poor content uniformity with variation in the drug dissolution rate of the final dosage unit (83).

Segregation could be minimised when the particle size of the powders in the blend is less than 100 μm (84). Furthermore, it becomes less important with particle sizes less than 30 μm (80). This could be explained by the fact that the fine particles are more prone to aggregate formation rather than segregation due to the significant impact of interparticle cohesion and friction. On the other hand, dealing with small particle sizes usually leads to unwanted flow problem during handling and processing.

Consequently, controlling the particle size of all formulation components within a narrow size range between 100-150 μm could help to minimise the risk of segregation in a random (non-interacting) mix (77). Many of the leading excipients (fillers and binder agents) used in solid dosage forms tend to be manufactured with particle size distribution in this range. However, for many drug substances which are processed by milling to improve their dissolution performance, the drug particle size distribution usually exhibits some degree of positive skewness due to aggregation of the fine cohesive particles (32,85). Therefore, the principle of size-matching drug substances to the excipients for minimising segregation is often challenging due to extra processing requirements e.g. for low-dose or low solubility drugs.

When working with low-dose products e.g. < 1% w/w of drug in the formulation blend, even few agglomerates of fine particles can alter the final dosage units' content uniformity and dissolution profile (86). Therefore, the achievement of homogenous and segregation resistant powder mixtures especially for use in direct compression is still challenging (66,68). In the last couple of decades, researchers have

attempted to predict the relationship between particle size distribution for drug substances, target dose and content uniformity of the dosage unit using different theoretical approaches and mathematical models (40,85,87,88). For instance, Huang and Ku demonstrated that the lowest possible dose of drug substances in the solid dosage form that could pass the acceptance criteria of USP <905> content uniformity test with 99% certainty can be estimated as a function of the particle size distribution of drug substances (85), as seen in Figure 1.3 below:

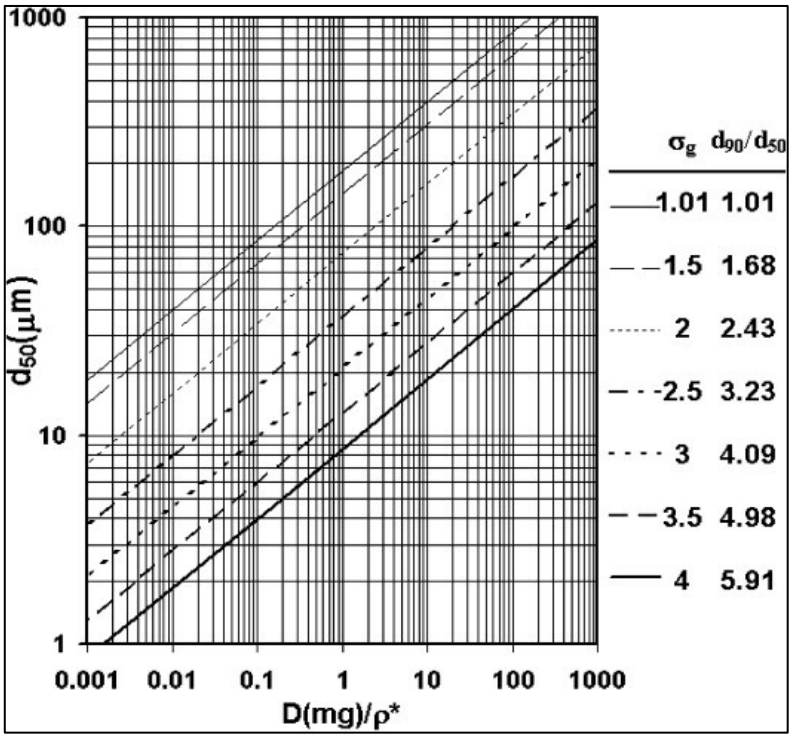

Figure 1.3: Nomograph presenting the maximum particle diameter (d_{50}) predicted for drug substances to pass USP Content Uniformity Test (Stages 1 and 2 of USP monograph 905) with 99% confidence as a function of various geometric standard deviation (σ_g) and dose limit (D/ρ^*). Where: the size distribution for drug substances follows a log-normal distribution; D and ρ refer to the target dose and true density of the drug substances. Reprinted with permission from (85); copyright 2009 Elsevier B.V.

According to the above model, when the drug substance has d_{50} and geometrical standard deviation (σ_g) of 20 μm and 3, respectively, the lowest dose limit which could be selected to achieve a uniform blend is 0.94 mg. However, when narrowing the size distribution with σ_g of 2, the lowest dose limit can be decreased to 0.02 mg (by 47-fold). Accordingly, designing and customising drug substances to have a very narrow size distribution helps to improve the content uniformity for the final dosage form with no need for additional processing steps such as milling or sieving. This could lead to substantial savings for the pharmaceutical industry through cutting down the number of downstream processes and achieving the goals of formulation development by design.

The effect of particle size and size distribution on powder compressibility and internal tablet structure has been documented in many studies. For instance, it is well known that powders with a wide size distribution or fine cohesive particles tend to have a higher ability to consolidate (higher compressibility index) when

subjected to a normal stress (89). This is due to increasing the likelihood of finer particles migrating into the voids that are formed between the larger ones. Also, Fu et al. reported that Spherolac®100 powder which has larger particles exhibits lower consolidation behaviour during compression (51% less consolidation) than Inhalac®230 powder, even if the two lactose samples have the most identical particle shapes (67). Generally, smaller particles form a tablet with greater tensile strength than the larger ones (70). Decreasing particle size leads to an increase in surface area and contact points between particles in a given volume of components, which in turn enhances mechanical interlocking/bonding between particles. For 1 g of spherical particles with a density of 1 g/cm^3, it is expected that decreasing particle diameter from 100 to 10 μm would lead to 1000 times more contact points between particles and much higher interparticle friction (90). Using micronised or milled pharmaceutical ingredients during solid dosage form manufacturing increases the propensity for punch sticking problems compared to non-micronised or unmilled form. This results in tablets with surface defects as noted for Ibuprofen tablets where the sticking risk increases by decreasing the particle size (91). Hence, any change in particle size distributions for raw materials and formulation components could affect the final product quality attributes.

The link between drug particle size and dissolution (which impacts bioavailability) has been explored widely previously mainly through models based upon the Noyes-Whitney equation (1.1 below). This equation describes the dissolution process of spherical drug particles as a function of time at a constant temperature, and sink conditions (92,93).

$$\frac{d_C}{d_t} = \frac{D\,.A}{\delta}\,(C_S - C) \qquad (1.1)$$

Where: d_C/d_t is the dissolution rate of the drug (Kg. s^{-1}), D is the diffusion rate constant of the drug molecules from particle surface (m. s^{-1}), A is the surface area of the undissolved solid particle exposed to solvent (m^2), which is directly linked to the particle size, δ is the thickness of the diffusion layer around each solid particle (m), which is also affected by particle size as expressed by the Prandtl equation (94), C_S is the saturation solubility of the drug in the stagnant layer (Kg or moles/L), and C is the drug concentration in the gastrointestinal medium (Kg or moles/L).

According to equation (1.1), solubility, surface area and hydrodynamics are the key parameters affecting the dissolution rate of powders. Therefore, the dissolution rate could be increased dramatically by decreasing the particle size. This leads to an increase in the effective surface area of the drug particle available for interaction with the dissolution medium and a decrease in the diffusion boundary layer around the particle. For instance, Hoag and Lim illustrated that particles with a diameter of 1 μm would yield a surface to volume ratio of 6 μm^{-1}, while particles with a diameter of 100 μm would only yield a surface to volume ratio of 0.06 μm^{-1} (90). Chu et al. investigated the dissolution behaviour of various drug substances and found that poorly soluble drugs' dissolution rate is strongly related to the primary particle size and specific surface area. The decrease in the particle size distribution from 250-600 μm to less than 45 μm led

to a significant increase in the dissolution rate (e.g. decreasing the particle size for ibuprofen powder led to an increase in dissolution rate constant approximately 25 folds) (95).

In addition, Liversidge et al. found that danazol's bioavailability is significantly increased by decreasing crystal particles' size to less than 200 nm (96). Furthermore, it was found that a decrease in the particle size to below 1 µm also brings about an increase in the drug-saturated solubility according to the Ostwald-Freundlich equation (97). This is because the reduction of particle size below 1 µm increases the solvation pressure, which leads to shifting in the equilibrium state (dissolution: recrystallization) to increase the saturation solubility of the solids (98).

Rohrs and Amidon carried out an interesting study on the effect of particle mono/polydispersity on dissolution. They found that it is possible to predict the dissolution rate of polydisperse drug powders as a function of solubility and particle size distribution (32,99).

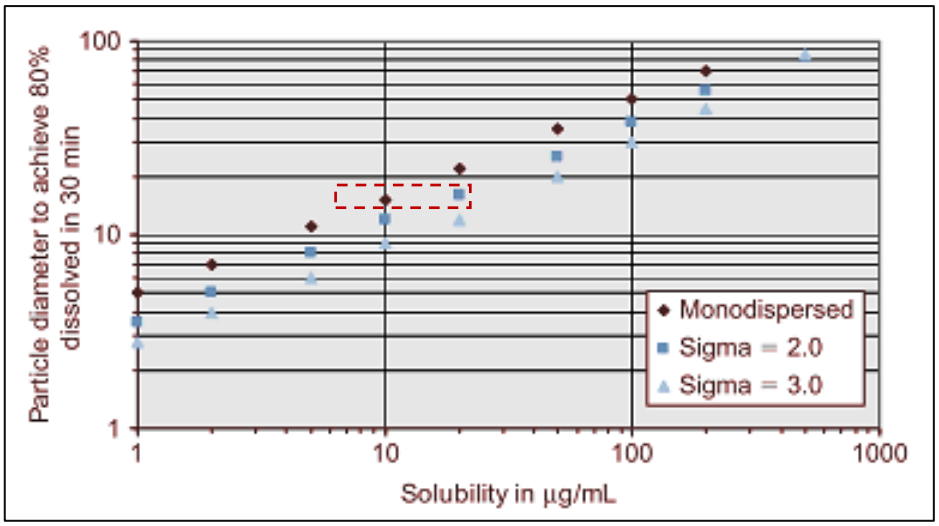

Figure 1.4: Relationship between drug solubility and drug powder parameters (predicted particle diameter and size distribution) necessary to achieve 80% dissolved in a USP dissolution tester in 30 min under sink conditions. Where Sigma value is a geometric standard deviation of a log-normal distribution.
Reprinted with permission from (32); copyright 2017 Elsevier Inc.

According to Figure 1.4, particles with similar average diameter but which are more polydisperse achieved substantially higher solubility (and potentially faster dissolution rate). For example, when comparing the square at 20 µg/mL (polydisperse with sigma 2) which has double the solubility of rhombus at 10 µg/mL (monodisperse) even though their average particle diameters are very similar (approx. 17-18 µm). The possible explanation for this is the fact that polydisperse powders, by definition, have a range of particle sizes which includes fine particles. These dissolve at a faster rate due to higher surface area as explained previously, thus the overall apparent solubility of polydisperse powder would be higher.

Furthermore, Xu et al. carried out an experimental investigation on the dissolution behaviour of different biodegradable PLGA polymer microparticles (20). As seen in Figure 1.5, they produced spherical

monodisperse particles with defined sizes ranging from 10 to 50 μm using a microfluidic emulsification technique. After loading bupivacaine (an amphiphilic drug), they found two significant drug release kinetic differences when comparing monodisperse and polydisperse particles. Firstly, the drug release from mono-sized particles was much slower than that observed from polydisperse particles, which have a similar average size. This confirms the above observations from the work by Rohrs and Amidon (Figure 1.4) although the key difference here is the dissolution/erosion of PLGA and drug solubility both control the drug release. Secondly, the initial burst release observed with monodisperse particles is significantly smaller than that observed with the corresponding conventional polydisperse particles. This difference might be explained due to less drug being adsorbed or trapped near the surface of monodisperse particles compared with conventional polydisperse particles. The SEM images in their paper showed no obvious change occurred on the surface of monodisperse particles, while several large pores formed on the surface of conventional polydisperse particles after treatment of the particles for one hour in dissolution medium. These results suggest that the mixing process between polymer/drug in a microfluidic device is more homogenous than the conventional emulsification method, leading to more uniform drug distribution in monodisperse microparticles (20).

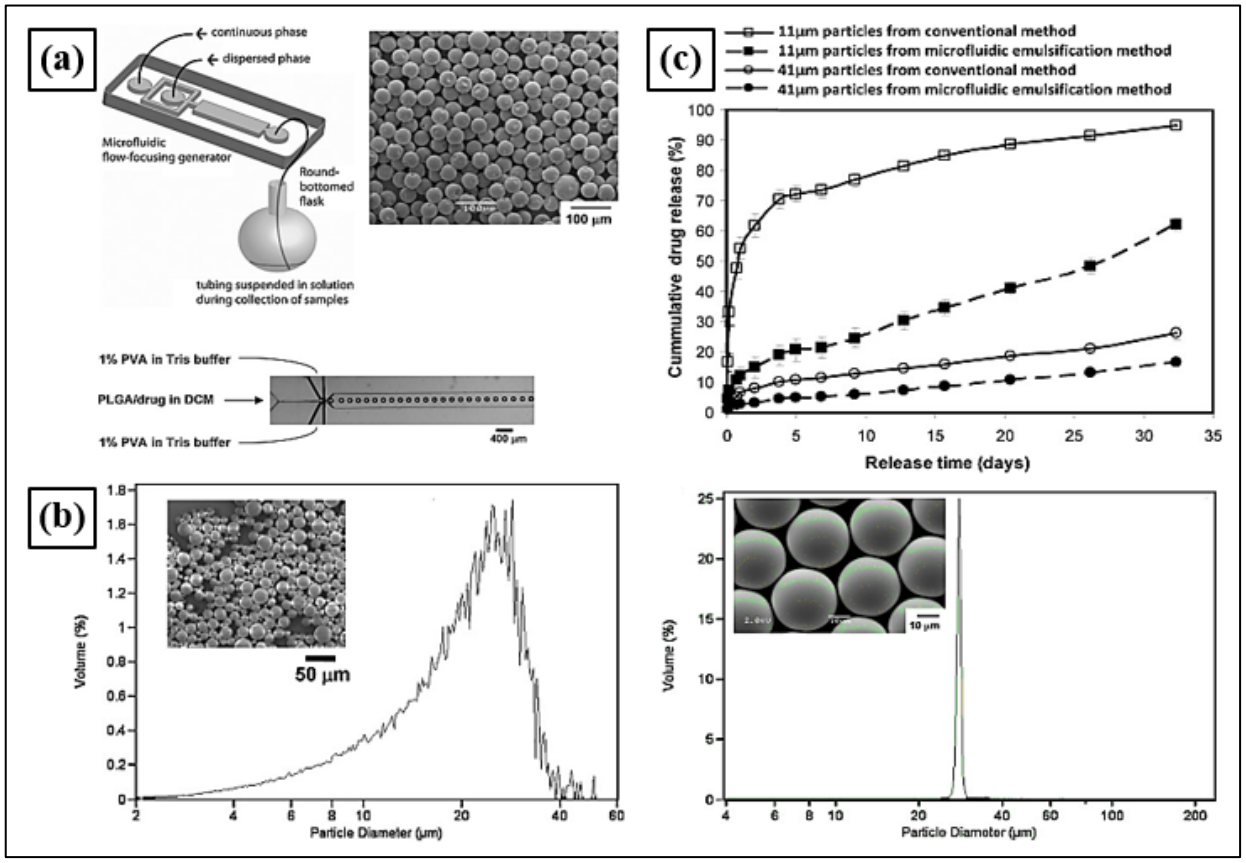

Figure 1.5: The fabrication method of PLGA microparticles and drug release profile from its:
a) schematic illustration of monodisperse PLGA microparticles fabricated using the microfluidic single emulsion method, b) SEM images and size distribution of different microparticles generated, and c) drug release profile from the microparticles as a function of preparation methods and particle size.
Reproduced with permission from (20); copyright 2009 Wiley-VCH.

Hence, controlling particle size for drug substances, especially for poorly soluble drugs, could have a great effect on dissolution/release and ultimately may help with controlling bioavailability (100,101). In addition, using monodisperse powder systems in formulation composition may facilitate optimisation of drug dissolution profile; achieve similarity of dissolution profile between generic and branded products; and ensure batch-to-batch consistency for solid pharmaceutical formulation (68).

1.3.2. Particle shape effect:

The shape of pharmaceutical particles, termed either as the crystal habit or morphology, is another critical material attribute to consider when designing and developing solid pharmaceutical dosage forms as it directly impacts material handling and processing (15,66,68). In physics, geometric particle shape is a dimensionless measure; however, it can be determined by the interrelationship between four critical parameters: length, breadth, thickness, and surface roughness. Due to the variety of these parameters, powdered materials often have different particle shapes e.g. acicular, angular, flaky, irregular, ellipsoidal, spherical, etc. (77). Particle morphology's effect on material handling and processing has been explored previously (4,68,102). Particles with different morphology and surface roughness can exhibit different flow characteristics even if they have similar size (103). In addition, many researchers agree that the departure from spherical-shaped particles with increasing surface irregularity/roughness usually leads to a fall in bulk powder density and flowability (104,105). For example, Šimek et al. illustrated that there is a significant difference in flow and compression behaviour between different particle shapes and sizes of paracetamol powders. It was demonstrated experimentally that spherical paracetamol particles have excellent flowability and compactability when compared with other particles e.g. irregular or plate-shaped particles (74). In another study, researchers investigated the bulk powder properties for two different lactose grades with similar particle size distribution using a universal shear cell tester. The experimental results indicated that irregular-shaped particles of SpheroLac®100 powder had lower flowability and packing properties when compared with spherical-shaped particles of FlowLac®100 powder (67). These results can be attributed to decreased mechanical interlocking and friction/cohesion forces between spherical particles, resulting in a better powder flow with uniform die arrangement during the tableting process (74).

The changes in packing characteristics can be related to different particle shapes in powdered materials. Zou and Yu found that the Hausner ratio for large non-cohesive mono-sized particles decreased with the increase of sphericity, as given by $HR = 1.478\times10^{-1.36\psi}$, where ψ is the sphericity value of the particle (106). Specifically, for mono-sized particles with identical spherical shape, it is well known that the maximum packing fraction that can be obtained in a cylindrical container is approximately 74%. This relatively high packing fraction is attained due to the low cohesion and better flow of the spherical particles past one another during the filling of the powder bed's void spaces. By contrast, for a binary mixture and for irregular powder particles that are cohesive, especially when the particle size distribution is wide, the ability of the powder to flow becomes less.

This results in decreasing the maximum packing fraction with more void spaces and less packed structure in the powder bed (75,89,107,108).This could affect the solid dosage form's weight uniformity, especially for high-dose drugs like needle-shaped ibuprofen, since the filling step is a volumetric process and weight uniformity is directly linked to the mass occupied in a constant volume. Therefore, generating and using monodisperse powder particles with spherical shape and smooth surface seems like a logical processing step to ensure that final product CQAs are met in comparison with using irregular or needle-shaped particles.

Particle shape also significantly affects the degree of blend uniformity and mixing performance of the final formulation powder (109). In general, powders with a high proportion of spherical particles are more straightforward to mix due to minimum interparticle contacts (i.e. minimal resistance to flow during mixing). However, they are more prone to segregate due to higher flowability, especially when there is a significant difference in size between the blend components. By contrast, using sharp-edged particles (e.g. acicular, flaky, angular) often impede free powder flow due to high mechanical interlocking and interparticle friction, resulting in prolonged mixing time due to aggregation issues (77). Woodle et al. studied the mixing behaviour of fifty coloured particles with the same shape but at different mixture ratios in a rotary kiln simulator experimentally. They found that particles with ovoid, shell and tube shapes significantly differ from each other in the time required for complete mixing, and some particles like ovoid may mix many times faster than others (110).

In addition, powders mixed from different particle shapes are more prone to segregation than those with similarly shaped particles. According to Tang et al., the most significant segregation occurs in the binary mixture when mixing irregular-shaped large particles (e.g. acicular, angular, etc.) with spherical-shaped fine particles. The possible reason for this finding could be related to using fine and large particles with high and low density, respectively (80). Specifically, the improper packing for the irregular-shaped large particles leads to large void spaces. As a result, this voidage prompts the small dense particles percolation to the lower zone of the powdered mixture when any slight vibration or shear motion is applied (80,111).

In the last few years, the effect of particle shape on mixing performance and segregation has been studied extensively via different Discrete Element Method (DEM) simulations. For instance, Pereira and Cleary evaluated a binary particles' mixture in a rotating drum. The key findings of their study were that (1) using particles with different shapes, but with the same size can induce segregation during the mixing process, (2) the spherical particles which have better flow and less interlocking properties tend to segregate from cubical particles during the mixing process and are more likely to accumulate in the periphery of the powder bed at the equilibrium state, and (3) segregation prompted by different particle shapes is a slower phenomenon compared with the size or density segregation (112). Similarly, He et al. illustrated that ellipsoidal particles often aggregate in the centre of the powder bed, whereas spherical particles tend to be distributed in the outer zone layer of the mixture (113). These results illustrated that improving the uniformity of mixing for any pharmaceutical formulation blend requires using non-cohesive ingredients

with very close particles' properties. Thus, one could proclaim that generating pharmaceutical ingredients as non-cohesive mono-sized spherical particles would provide an advantage in terms of powder handling and mixing process.

The previous studies provide valuable information regarding the importance of tailoring and optimising particles' shape to enhance mixing performance and blend uniformity. The other important aspect to discuss is the effect of particle shape on compression. Particle shape could have a significant impact on powder mechanical properties which is dependent on the particles' deformation mechanism during compression. For materials which consolidate by plastic deformation (e.g. starch 1500 and NaCl), increasing particle shape irregularity and surface roughness generally yields tablets with higher mechanical tensile strength due to increasing the total contact area and bonding points available between particles as they deform. By contrast, for materials which consolidate by fragmentation (e.g. lactose and Emcompress), the primary particle shape exhibits practically no effect on the above properties as it is lost during the compression process (114). In one report, ibuprofen crystals with different shapes exhibited different punch sticking propensities even when they had the same melting point. Plate-like crystals showed free-flowing behaviour, better compaction performance, and a lower sticking propensity when compared with a needle-shaped form (115). Also, Joiris et al. illustrated that improving the compression properties of paracetamol powder can be achieved via preparing particles with orthorhombic form (prismatic crystals) rather than monoclinic form or plate-like crystals (116). This is because the orthorhombic form can easily undergo plastic deformation upon compaction (116).

Because the dissolution rate is dependent on the surface area according to Eq. (1.1), particle shape can also influence biopharmaceutical behaviour (i.e. dissolution and oral bioavailability) of drug substances. In general, particles with different shapes have different surface to volume ratios, which ultimately affects the surface area's influence on drug dissolution and oral bioavailability. This impact of particle shape was considered by many researchers. For example, Lu et al. simulated the dissolution rate of hydrocortisone particles with cylindrical geometry. They observed that a better fit for experimental dissolution data was achieved by taking into account the particles' shape factor (117). Guo et al. compared the *in vitro* and *in vivo* performance of two different drug nanocrystals (NCs). They found that rod-shaped NCs for oral administration exhibit superior dissolution and bioavailability over spherical-shaped crystals even if they shared similar hydrodynamic diameter and crystalline state (118). Moreover, they recently carried out a comprehensive study to understand the impact of particle shapes (i.e. spherical, rod and flaky-shapes) on the transport of NCs across the intestinal barriers. The results showed that particle shapes greatly influence the *in vitro* dissolution and *in vivo* pharmacokinetics, where the mucus permeation, cellular uptake, and transmembrane transport of the rod-shaped NCs were higher than that observed with other crystals (119).

As mentioned above, many manufacturability aspects of solid dosage forms depend on fundamental particle properties, especially particle size, shape and their distributions, which play a key role in determining the final drug product attributes. The interplay between these properties is remarkably complicated and should

be considered when designing and manufacturing pharmaceutical formulations. Any subtle change in these properties due to the unintentional variability in raw materials (i.e. different supply chains, different batches, etc.) can easily cause problems in the powder handling, which ultimately affects the process efficiency and final product quality. As a result, variations in drug bioavailability, safety and efficacy could be observed.

The previous sections (1.3.1 and 1.3.2) emphasised the importance of controlling particle properties during pharmaceutical production. Monodisperse particles by default offer uniformity of properties (size and shape) of the individual particles which can be controlled to pre-defined specifications. Some of the potential benefits of using monodisperse particles for solid dosage form manufacturing may be summarised as: (1) improving the critical powder properties resulting in better material processability, (2) simplifying the formulation design and development and maintaining production consistency, (3) improving the dose uniformity and less batch-to-batch variability for low dose drugs and (4) controlling and modifying the dissolution rate especially for poorly soluble drugs.

1.4. Current methods for generating monodisperse particles:

There are two main options to produce pharmaceutical particles with uniform characteristics. The first one depends on controlling the conventional crystallisation process. However, achieving controlled solid forms and particle morphologies by this method is not a trivial task and depends on understanding many parameters such as molecular properties, molecular interactions, and crystallisation process conditions such as temperature, solution pH, impurities, etc. (15,24,120). The second option is based on improving the properties of existing ingredients using particle-engineering technologies. Spray drying is at the forefront of particle engineering techniques which gained significant interest in the last couple of decades in industry especially for drug bioavailability enhancement. The process does help in reducing particle size distribution and producing more uniform particle shapes in comparison with more traditional methods such as granulation. Nevertheless, there is still a significant room for improving those particle distributions leading to more monodisperse particles. Other methods for generating monodisperse micro- and nanoparticles were also developed by researchers over the years. The next few sections will provide an overview of previous attempts to create monodisperse powders/particles firstly based on non-spray drying methods (focus on microfluidics and micromoulding) followed by spray drying-based methods.

1.4.1. Methods not utilising a spray drying principle:

1.4.1.1. Segmented-flow (SF) microfluidics process for droplet generation:

- **Microfluidic Channels system:**

This system could be used to produce particles from different types of emulsions with precise control of composition and size. As seen in Figure 1.6, the basic principle of this system depends on focusing the flow

of two streams of immiscible fluids through narrow microfluidic channels. When these fluids meet at the micro T-junction, the inner fluid stream (called dispersed phase) becomes segmented into droplets due to the balance of its interfacial tension and exerted shear by the outer fluid stream (called continuous phase). Generally, droplets generation is influenced by a few parameters, including the feeds viscosities, polarities, flow rate of each fluid, and the geometry of channels used (121).

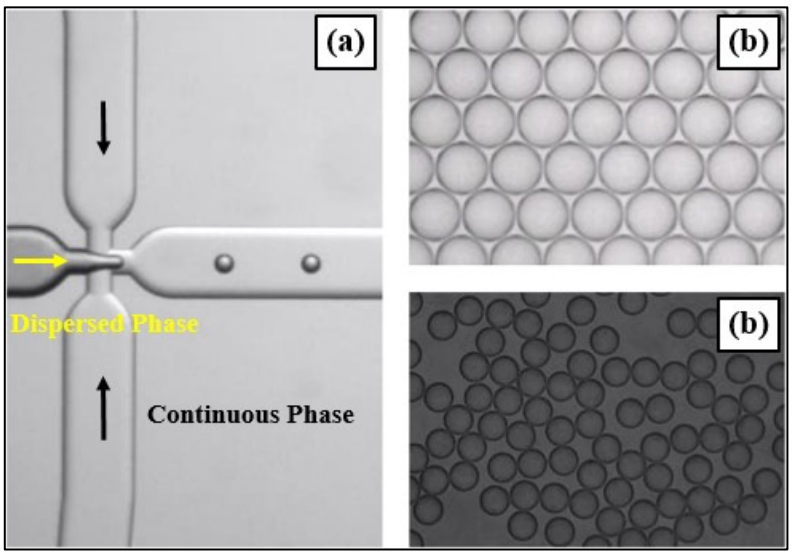

Figure 1.6: Schematic representation of the monodisperse particle generation using a microfluidic chip: a) droplets formation in a single emulsion system, b) monodisperse droplets emulsion (oil-in-water or water-in-oil droplets), and c) the resulted monodisperse particles after droplets solidification process. Adapted from (122).

The microfluidics system can produce uniform emulsion droplets with different size ranges, typically between 5 and 500 µm. The droplets are often stabilised using a suitable surfactant to avoid coagulation. After emulsion formation, the monodisperse droplets are solidified by polymerisation or gelation, resulting in the generation of uniform particles with identical shape (i.e. 1% coefficient of variation). The particle formation process is activated as a result of chemical, thermal or UV gelation process. The resulted particles are typically collected by solvent evaporation and/or filtration process. This method was used previously to generate different particle morphologies such as spherical, rod shape, ellipsoids and Janus particles (121), as seen in Figure 1.7.

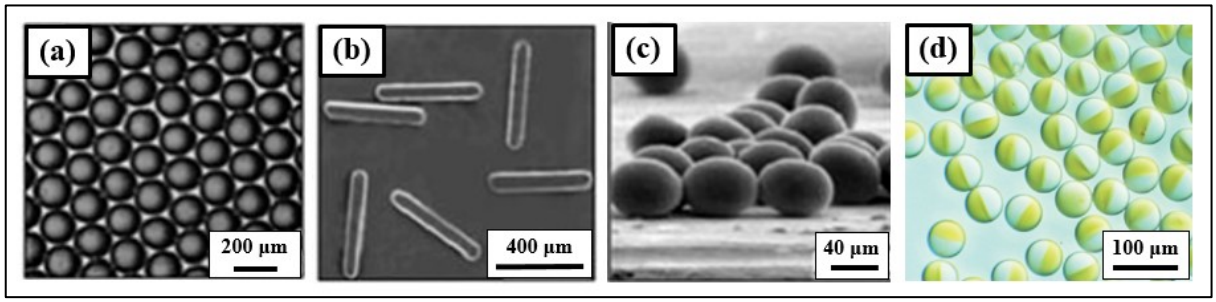

Figure 1.7: Optical microscope images of monodisperse microparticles generated by microfluidic channel systems: a) microspheres, b) rods, c) ellipsoids, and d) Janus particles. Images (a-c) and (d) were reprinted with permission from (21,123); copyright 2005 Wiley-VCH and 2010 American Chemical Society, respectively.

Although this method is applicable to various materials such as gels, metals, and polymers, it is not particularly adapted for active substances and biomaterials manufacturing yet. Currently, several researchers and companies have an interest in developing this technology under cGMP environment to design and generate uniform particles with various degree of complexity for several applications, including vaccine development, polymeric particle synthesis, drug solubilisation, improved drug encapsulation efficiency, controlled drug release, controlled drug delivery systems, cells encapsulation and taste masking (19,124,125).

- **Microfluidic droplet generator (MFDG) system:**

This is used to generate a single stream of monodisperse droplets with high reproducibility (22). The MFDG system depends on using continuous acoustic vibrations at high frequency in the KHz region to locally generate pressure fluctuations in a liquid feed, which in turn helps to disintegrate it into small droplets. Specifically, it is based on Rayleigh's breakup theory and ink-jet technology to break a laminar liquid stream and produce a chain of monodisperse droplets. Controlled vibrations are usually generated from a piezoelectric transducer unit attached to the nozzle body. During the atomisation process, spherical uniform droplets with almost any size from 40 to 2000 μm can be created by either adjusting the liquid flow rate, vibration frequency, and/or the nozzle orifice diameter (126).

The most common method to produce non-agglomerated uniform particles via the MFDG system was via precipitation of the stream of monodisperse droplets using a solvent extraction medium such as an aqueous PVA solution at 0.5-1%, w/v (Figure 1.8) (127).

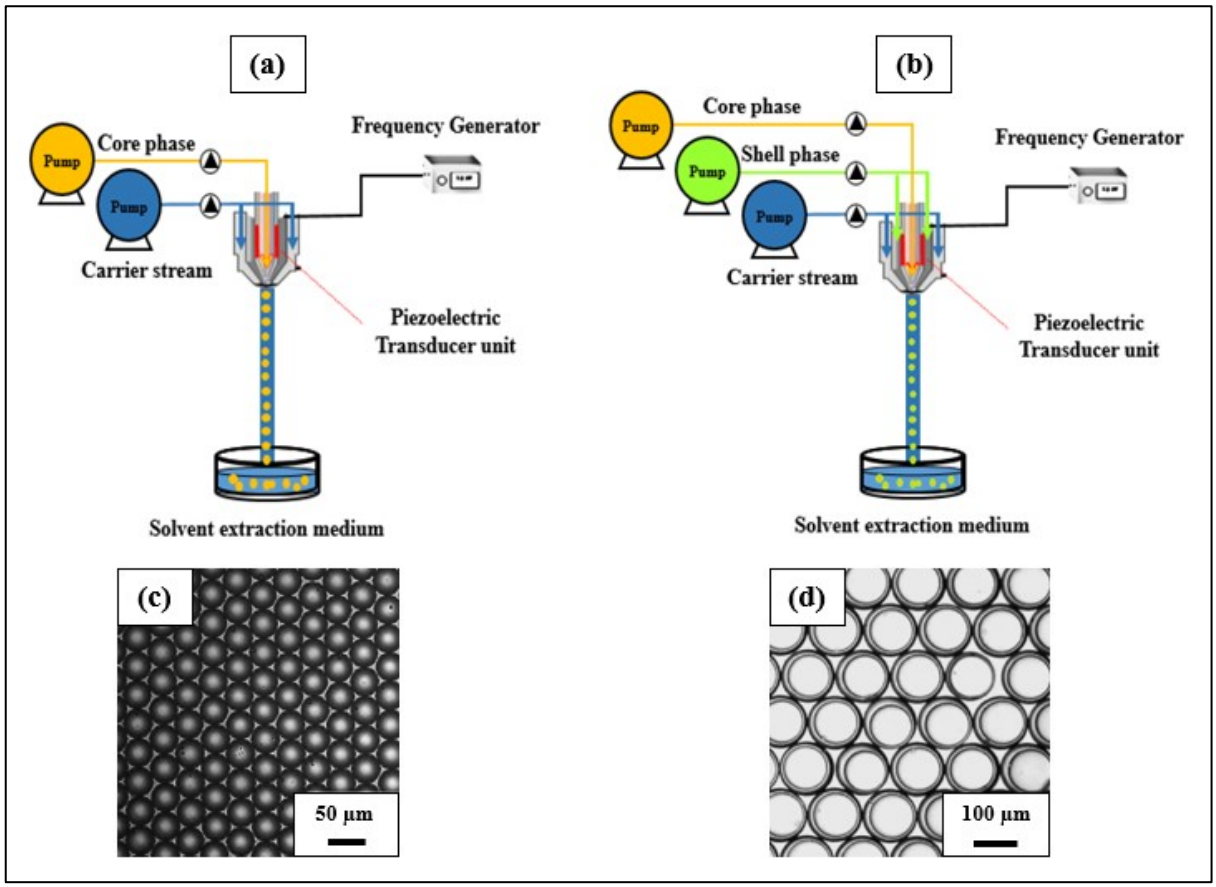

Figure 1.8: Schematic diagram of apparatus used for generating uniform particles by precipitation method: a) to create single-wall microspheres, b) to create double-wall microspheres/liquid-core microspheres, c) image of uniform PLG microspheres with diameter ~ 45 µm, and d) image of ~ 110 µm PLG microspheres with an aqueous core containing 100µg/ml dextran and 10µg/ml BSA. Optical microscopy images for monodisperse particles were reprinted from (128) and (129) with permission; copyright 2001 Elsevier B.V. and 2007 Springer , respectively.

Based on this approach, several biodegradable polymeric microparticles, including single-wall microsphere, double-wall microsphere with a core and shell composed of different materials, and microcapsules with liquid cores, have been generated with predefined size for controlled release of various drug substances (Figure 1.8) (127,130,131).

Even though the size uniformity of the generated particles is well controlled, this approach involves several steps such as repetitive washing, centrifugation, solvent evaporation and lyophilisation. These multiple operations could be considered time-consuming and affect the scalability of this approach.

Recently, researchers investigated 3D printing coupled with a piezoelectric nozzle system for fabricating drug-loaded polymer microparticles with controlled properties. For example, Lee et al. successfully used this technology to produce PLGA microparticles with various geometries such as circles, grids, honeycombs, and rings having different drug release rates (18). In their paper, the PLGA ink containing paclitaxel drug was loaded into a cartridge and then printed on the prepared glass slides. After the printing process, the resulting particles with different geometries were dried for 2 hours in a drying oven until it was completely solidified and the organic solvent was evaporated.

As seen in Figure 1.9, the resulting microparticles exhibited a fairly homogenous shape and size. However, this new approach has some limitations, such as higher product costs due to low process throughput, complex equipment setup and limited availability of biocompatible excipients (18,132).

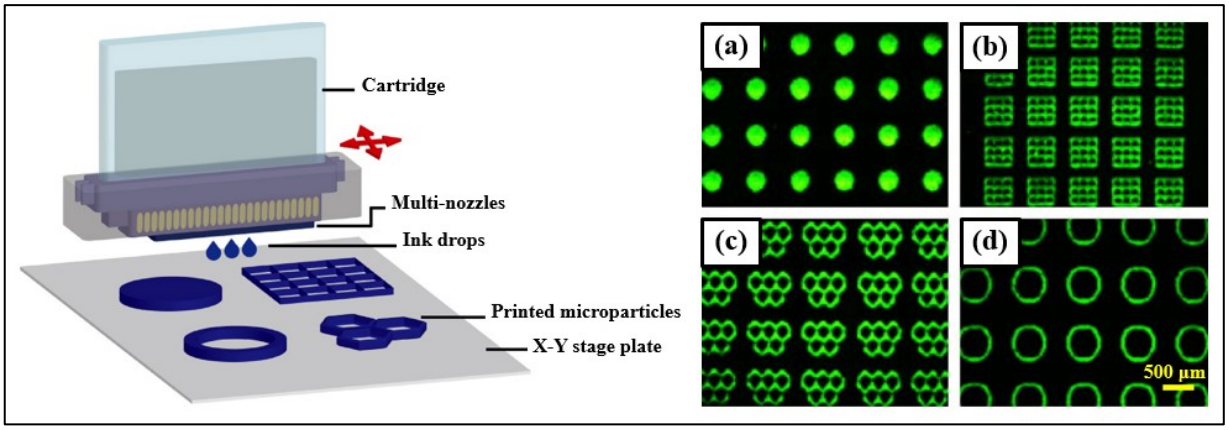

Figure 1.9: Schematic diagram for generating uniform particles using piezoelectric inkjet printing system with different geometries: the presented fluorescence microscopy images from (a) to (d) refer PLGA microparticles loaded with 10%(w/w) paclitaxel drug. Reprinted with permission from (18); copyright 2012 Elsevier B.V.

1.4.1.2. Particle replication in a non-wetting template (PRINT® technology):

This technology is based on a combination of micro-moulding approach with a roll-to-roll manufacturing process. It generates particles with precisely controlled size and shape according to the input micro-mould features. As seen in Figure 1.10, the technology depends on fabricating a non-wetting elastomeric template with precise cavities for the desired particle size and shape. Subsequently, a liquid solution of the target compound is confined in the cavities by applying pressure using the roll-to-roll technique. The capillary forces trap the liquid solution inside the template cavities and the rest of the solution is removed by sticking to the high-surface energy polymer sheet. The moulded solution is then solidified using methods such as crosslinking or solvent evaporation to form monodisperse particles (133,134). This is then followed by harvesting the solid particles.

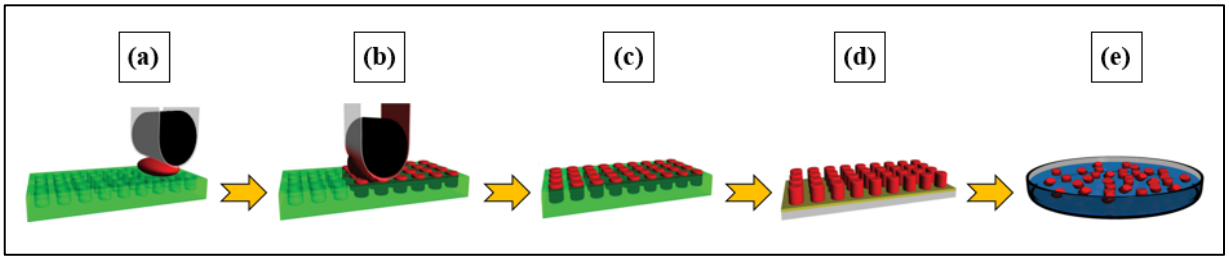

Figure 1.10: Schematic illustrations of the PRINT® process: a) empty elastomeric template with precise dimensional geometric cavities (green), high-surface energy polymer sheet (clear), roller (black) is brought into contact with pre-particles solution (red), b) roller evenly distributes pre-particles solution and pushed it into the template cavities; the excess pre-particle solution is moved away by sticking on the high-surface energy sheet, c) moulded solution is then solidified in the cavities using different methods, d) particles are isolated from the template cavities using adhesive tape, and e) particles removed by dissolving the harvesting tape to produce free particles dispersed in non-solvent solution which are then collected and purified via the appropriate procedure. Reproduced with permission from (135); copyright 2009 John Wiley & Sons, Inc.

Figure 1.11 shows examples of uniform particles with different sizes (80 nm to 20 μm) and morphologies (e.g. cylinder, cube, rod, cone, etc.) generated using the PRINT technology for several ingredients and applications (134–136). This technology can also be used to create particles for the pure drug without other additives (133).

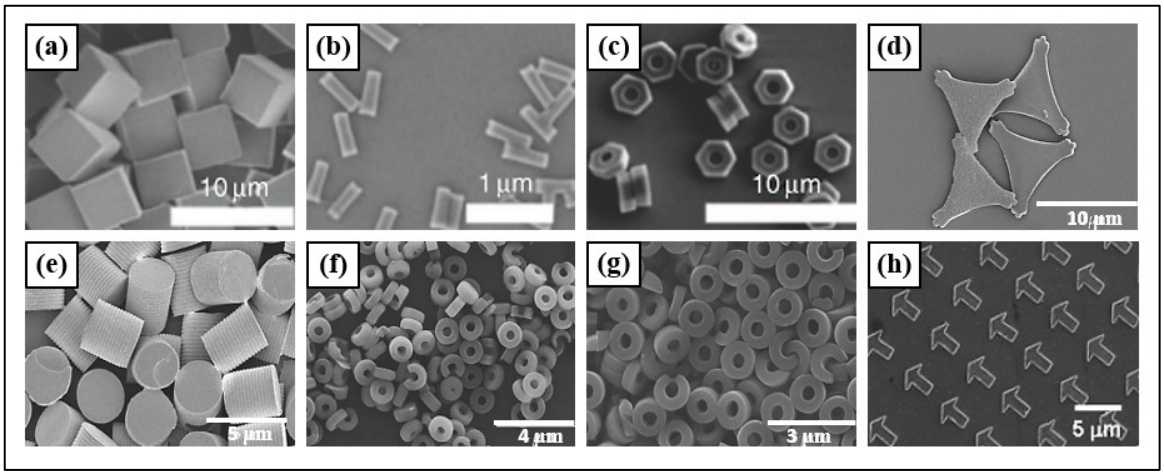

Figure 1.11: SEM images of PRINT particles with different size, shape and composition: a) 5μm cubed PEG particles, b) rod-like PEG particles with a diameter of 100 nm and height of 300 nm, c) 3μm " hex nut" PEG particles. Reprinted with permission from (137); copyright 2008 ACS, D) 10 μm "IgG/Lactose" pollen particles, e) 3μm PLGA cylindrical particles, f) 1.5 μm zanamivir toroidal particles, g) 1.5 μm siRNA toroidal particles. Reprinted with permission from (133); copyright 2008 Hindawi Publishing Corporation and h) 3μm arrow PEG particles. Reprinted with permission from (138); copyright 200 ACS publications.

The interest in PRINT® has increased recently as a strategy for formulating particle systems for several biotherapeutics such as proteins, oligonucleotides and antibodies, which usually present challenges in processing and administration, especially for pulmonary drug delivery (17). However, harvesting the particles prepared by this method is not simple as reported by the technology developers. Scientists are currently interested in fabricating nano/microparticles using hydrogel templates e.g. from gelatine or PVA as an alternative approach. These could easily be dissolved in an aqueous medium in order to collect the generated uniform particles (16).

1.4.2. Methods utilising a spray drying principle:

1.4.2.1. Overview of the spray drying process:

Spray drying is a rapid and continuous drying technique which depends on converting a liquid feed into solid particles by atomising it into a hot gas environment (139). This technique has mainly been utilised to prepare micro and nanoparticles for several pharmaceutical applications such as improving drug solubility, controlling drug release, optimising aerosolisation performance, and stabilising biopharmaceuticals (23,140). The technique can be used effectively to design complex particles with multifunctional properties and specified morphology (141).

Spray drying consists of three key stages: atomisation, droplet-to-particle conversion and product collection/recovery. As could be seen in Figure 1.12 below, the feed solution is atomised/sprayed into a continuous heated stream of drying air/gas leading to rapid solvent evaporation. Thus, the droplets dry into solid spherical particles that are separated/recovered from the drying gas using a cyclone (142). The process is very flexible because the used feed could be a solution, suspension or an emulsion, and the final product could take different forms e.g. powders, granules or agglomerates.

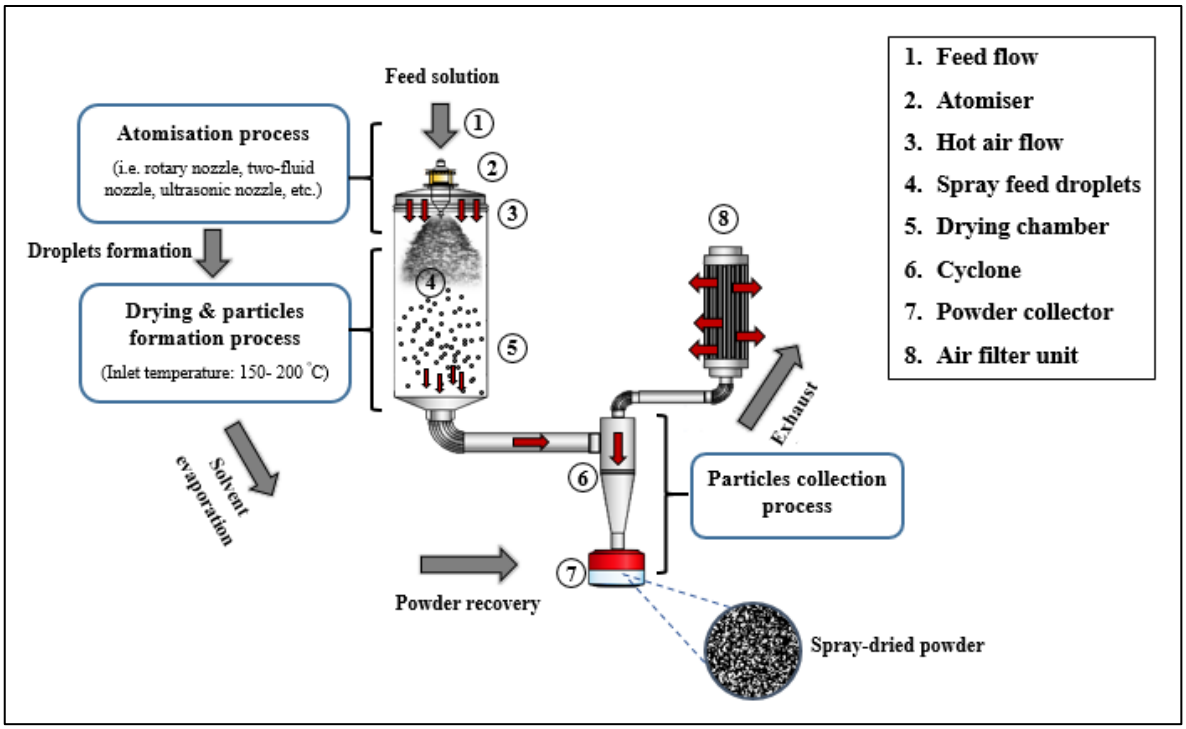

Figure 1.12: Schematic diagram showing the key spray drying stages.

Spray drying became a key industrial process for the generation of microparticles with controlled properties such as spherical morphology and uniform size distribution (22). Generally, there are three main factors which significantly affect the morphology of spray-dried particles: feed characteristics, spray dryer design specifications, and operation conditions. These factors were discussed previously in several review articles (23,140–143), however, Figure 1.13 below should help with summarising some of them. The interplay between these factors is important to generate particles with the desired morphology. For example, inlet temperature, feed flow rate and the dryer dimensions govern the drying kinetics within the process. High or low evaporation rates could lead to different particle sizes and shapes. Furthermore, the atomisation process largely influences the droplet size but also depends on the feed composition and rheology.

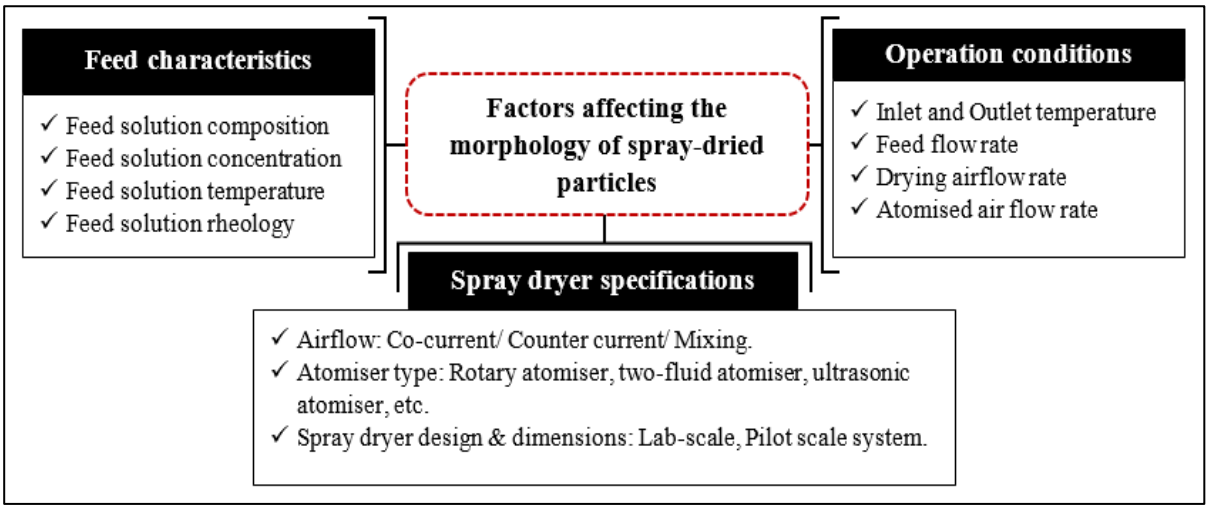

Figure 1.13: Schematic diagram of the factors affecting particle morphology.

One of the key concepts utilised for particle design is to control the liquid evaporation rate and the diffusion of droplet components during the spray drying process. This is often done based on Peclet number (*Pe*) which can be defined as the ratio between advection mass transport (solvent evaporation rate: K) and diffusion (D) mass transport of the solute, as shown in equation (1.2) below:

$$Pe = \frac{Evaporation\ rate}{Diffusion\ rate} = \frac{K}{8D} \tag{1.2}$$

During droplet drying, if the evaporation rate is low e.g. due to low inlet/outlet temperatures, the Peclet number would be less than one. This means that colloidal solids/solute have enough time to diffuse towards the droplet's centre to create dense particles. Conversely, if the evaporation rate is higher than the diffusion rate of solute, the Peclet number would be larger than one and the solids/solute start to accumulate at the surface of the droplets, producing a shell structure. This structure could represent a potential barrier to solvent evaporation depending on the type of shell formed e.g. thin permeable membrane or a thick crust. Therefore, according to the drying conditions, droplet size, and feed composition, the heat and mass transfer between the particles and drying air is expected to be different leading to various particle morphologies e.g. spherical, hollow, buckled or wrinkled (Figure 1.14) (140). The differences in particle shape usually influence the properties and functionality of the generated powder, as mentioned before (Section 1.3.2).

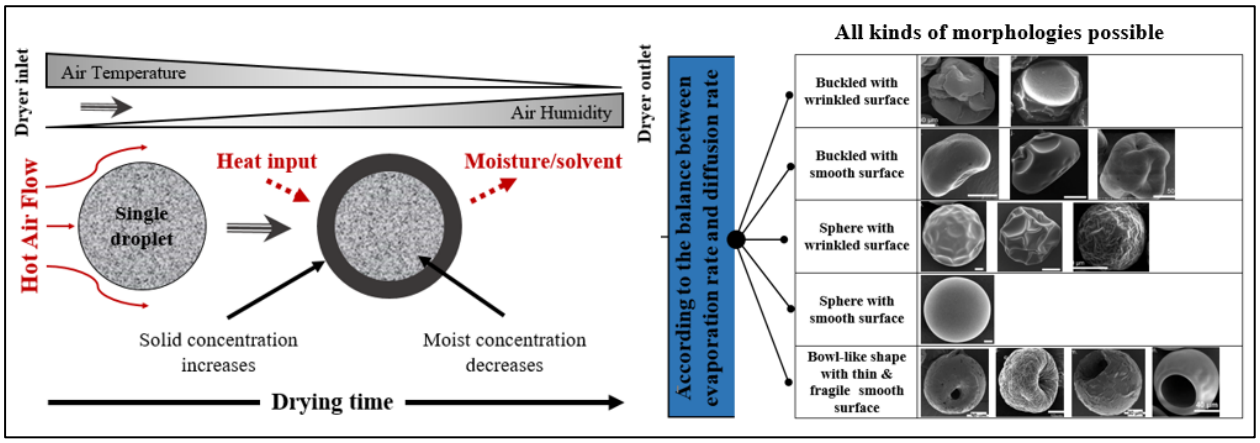

Figure 1.14: Schematic illustrating the proposed particle morphologies formation from the drying process for a single solid containing droplet. SEM images of the spray-dried particles were reprinted with permission from (144); copyright 2020 Taylor & Francis.

One of the main challenges in spray drying lies in the atomisation stage which affects the droplet size, drying behaviour and the entire spray dryer's performance (145). Conventional atomisers generally produce droplets with different sizes and trajectories (Table 1.1). These droplets then experience different drying profiles within the same environment, leading to significant variation in particle properties such as size, morphology, and moisture content even within the same batch.

Table 1.1: Typical ranges of droplet size during the atomisation process. Adapted from (146,147).

Nozzle type	Rotary	Two-fluid	Pressure	Ultrasonic
Scale	Pilot/Industrial	Laboratory/Pilot/Industrial	Pilot/Industrial	Laboratory
Atomisation energy	Centrifugal	Kinetic	Pressure	Ultrasonic vibrations
Atomisation parameters	Disc speed 10,000-30,000 rotations per minute	Compressed gas 250-10,000 Psi	Nozzle pressure 250-10,000 Psi.	High vibration frequency (>20 KHz)
Droplet size range (µm)	30-120 (148) 10-200 (149) 10-500 (146) 1-600 (142)	30-150 (148) 5-100 (149) 10-200 (139) 1-100 (146) 5-300 (142)	120-250 (148) 30-350 (149) 20-600 (139) 10-400 (146) 10-800 (142)	5-1000 (146)

The differences in particle properties could be problematic especially if the target formulation requires a specific particle size fraction or morphology to achieve the desired functionality. For instance, injectable suspensions require smaller particle size fraction preferably below 10 µm to avoid inflammation or irritation at injection site (150). Similarly, for direct compression a larger size fraction e.g. above 50 µm is necessary to avoid poor flow and dosage uniformity issues (33).

Within the same atomised spray, the smaller droplets eventually dry into fine particles which are cohesive and cause flowability and dusting issues while the larger droplets may not dry sufficiently causing stickiness issues. Therefore, scientists are currently interested in monodisperse droplet generation technology to control the atomisation process and create uniform droplets. Incorporating this technology within the spray drying process could facilitate the generation of spray-dried particles with highly consistent size distribution and morphology. In addition, using this technology could improve the spray drying process and reduce the changes in process conditions upon scaling up of production (23,151–153).

1.4.2.2. Previous works on producing uniform microparticles via spray route:

In the last two decades, researchers attempted to generate uniform spray-dried/spray freeze-dried powder particles based on using monodisperse droplet generators (MDGs) as atomisers. According to the desired droplet size and feed solution properties, different designs of spray dryers with several commercial monodisperse droplet generators have been used. For example, Lamprecht's group developed a spray freeze-drying set-up equipped with a piezo-actuated atomiser to produce microparticles of materials such as mannitol, maltodextrin, and lysozyme for inhalation applications (154–157). A single stream of monodisperse droplets was atomised inside a cold gas environment to produce microparticles. The final lyophilised powders generated from the process had a wide size distribution with span values up to 3 (Figure 1.15). This indicated that the initial droplet monodispersity was lost during the process probably due to the impact of aerodynamic braking, which leads to droplets collisions and coalescence before complete congealing (156,157).

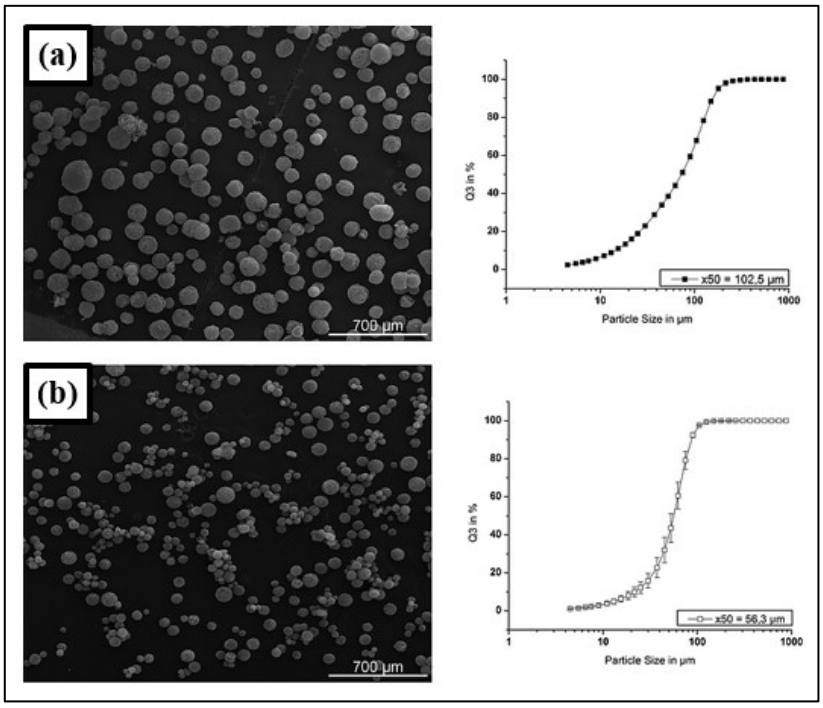

Figure 1.15: SEM images and cumulative size distribution for lyophilised powders produced by using the jet-vortex spray freeze dryer: a) large particles produced when using a low vortex velocity (0.8 m/s), and b) small particles produced when using a high vortex velocity (6.8 m/s). All powders were produced from the same stream of monodisperse droplets generated by 20 µm nozzle orifice. Reprinted with permission from (154); copyright 2017 Elsevier B.V.

Another example is from Vehring's group who used a custom-made droplet spray dryer provided with a droplet-on-demand piezo-actuated dispenser to study drying kinetics and particle formation processes. A single droplet falling in a gas flow has been used to mimic the drying conditions in spray dryers to some extent. In their studies, uniform particles with various sizes and morphologies were made from different ingredients such as proteins and trehalose. The findings from these studies helped elucidate the link between drying conditions and spray-dried particle morphology based on the Peclet number (Pe) (Figure 1.16) (151,158–162).

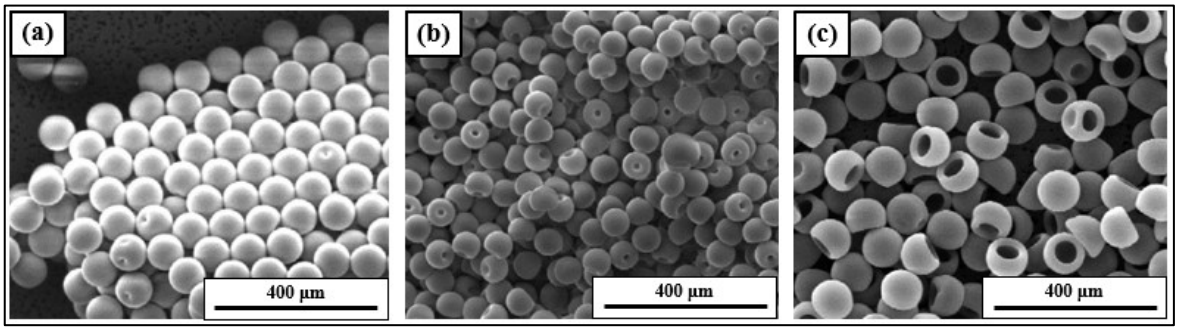

Figure 1.16: SEM images for uniform protein particles generated by using monodisperse droplets chain technique. Drying gas temperature from left to right: 25, 50, 125 ºC. As seen in the images, increasing the solvent evaporation rate by increasing the drying temperature degree leads to changing particle morphology from sphere to more hollow structure. Reproduced with permission from (151); copyright 2007 Elsevier B.V.

Furthermore, a new spray dryer referred to as the microfluidic jet spray dryer (MFJSD) was developed by Chen's group to produce non-agglomerated particles with uniform characteristics in a one-step process (163). Compared with traditional spray dryers, the MFJSD spray drying process depends on atomising the feed solution into a stream of monodisperse droplets using a custom-made piezo-actuated atomiser. The generated uniform droplets were dispersed in the main drying chamber and dried particles collected from the collection point at the device outlet.

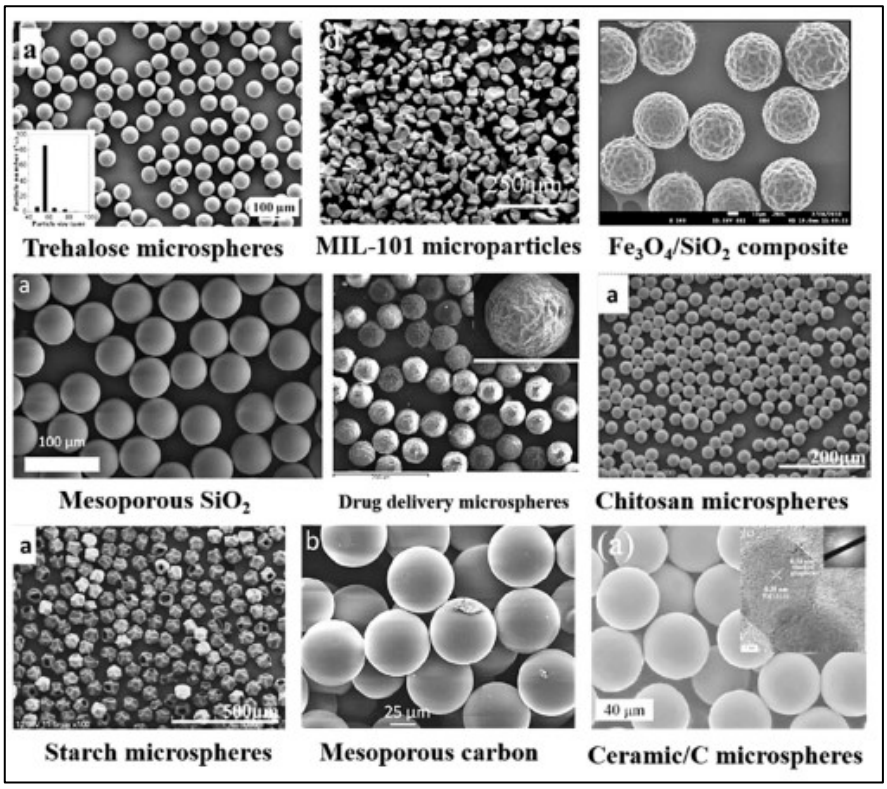

Figure 1.17: Spray-dried particles with uniform size produced using the MFJSD device. SEM images of the microparticles were reprinted with permission from (144); copyright 2020 Taylor & Francis.

As seen in Figure 1.17, the MFJSD was successfully used to produce uniform particles with adjustable size from different feed solutions. However, it is difficult to ascertain the production capability of this spray dryer currently due to limited information on industrial application, and the requirement for highly skilled operators to produce uniform particles with adjustable size (163,164).

In general, the production rate of many of the above processes is limited to a few milligrams/grams per hour, which is relatively very low with respect to bulk production. This could be explained by the nature of the atomisation mechanisms used e.g. droplet-on-demand atomisers produce lower number of droplets in comparison with continuous jet atomisers which provide higher throughput. There are other potential challenges with spray drying processes utilising monodisperse droplet atomisers including frequent nozzle blockages, droplets losing their monodispersity quite rapidly, insufficient drying due to high droplet velocity and the need for ancillary equipment to provide consistent atomiser operation. These challenges will be discussed in detail within chapters 2 and 3 of this thesis.

As discussed above, the implementation of monodisperse droplet generators within spray dryers is fraught with several challenges. To fully comprehend these, the following section (1.5) will provide will provide a mechanistic understanding of the atomisation process in detail, including monodisperse droplets generation.

1.5. Overview of the atomisation operation:

In general, atomisation is defined as the disintegration of a liquid jet into droplets by creating disturbances in a liquid film (165). As seen in Figure 1.18, atomisation in a spray can be classified into two broad types: primary atomisation which is close to atomiser orifice and based on the interaction between motive (impulse) forces, drag (cohesive) forces and friction forces; and secondary atomisation which is an extra disintegration of droplet plumes further downstream into smaller droplets. This secondary break-up results from the interaction between the dispersed phase (liquid medium) and the continuous phase (surrounding gas).

Primary atomisation can be categorised according to the energy (external force) used to produce the liquid jet's instability and form droplets. For instance, pressure atomisation, centrifugal atomisation, two-fluid atomisation and ultrasonic atomisation depend on pressure, centrifugal, gaseous/fluid interaction and acoustic vibration energies, respectively (166,167). For any liquid jet, the flow behaviour from the atomiser is affected by two kinds of forces. The first is motive forces (e.g. gravity and inertial forces) which pull the jet/droplet down, and the second is drag forces (e.g. surface tension and viscous force) which hold the liquid up (145). Basically, the goal of atomisation is to break the balance between these opposing forces through producing a disturbance in the liquid jet, leading to a dripping process (droplets formation).

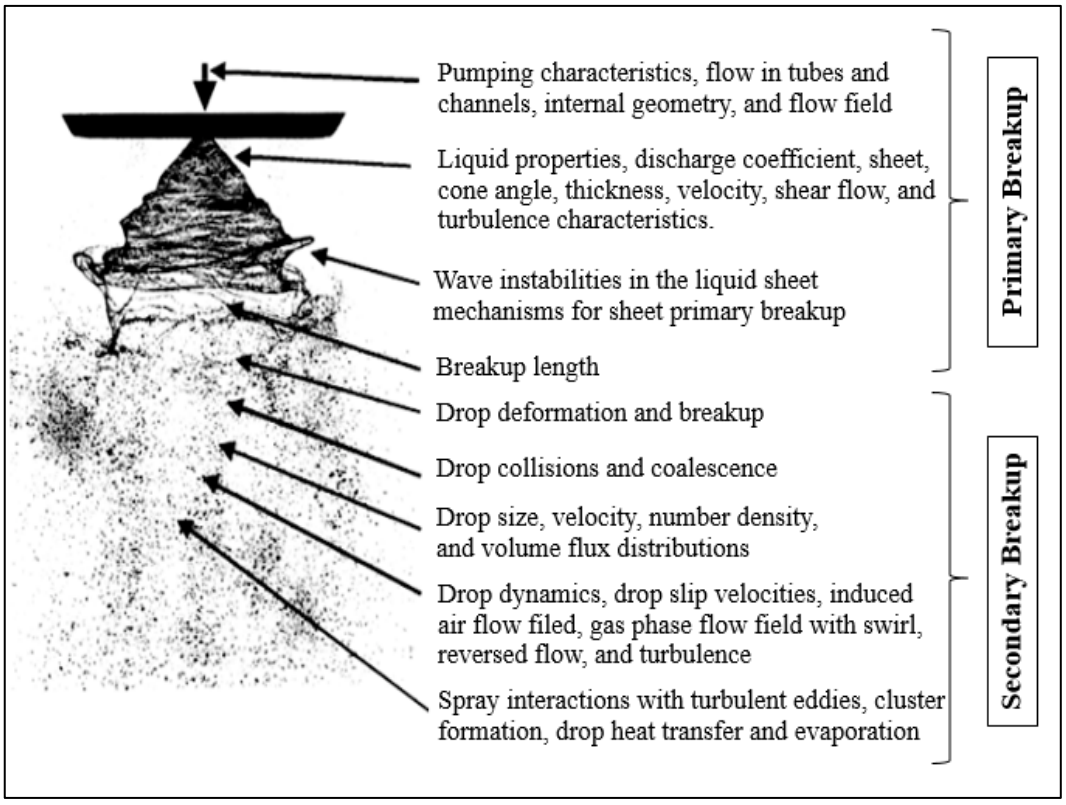

Figure 1.18: Example of a simple spray illustrating many features that need to be characterised. Reprinted with permission from (168); copyright 2000 Begell House, Inc.

1.5.1. Fundamentals of typical liquid breakup:

Generally, liquid properties and atomisation conditions are crucial factors affecting droplets formation from the nozzle tip. The main forces relating to the fluid properties during atomisation are an inertial force $\rho_L V_L^2$, viscous force $\mu_L V_L/D$, and surface tension σ/D (167,169). As seen in Figure 1.19, the jet breakup process at the atomiser tip can be classified into four main regimes or mechanisms. Each one is controlled by three dimensionless numbers which describe the liquid phase flow: Reynolds number (Re_L), Weber number (We_L) and Ohnesorge number (Oh) (167).

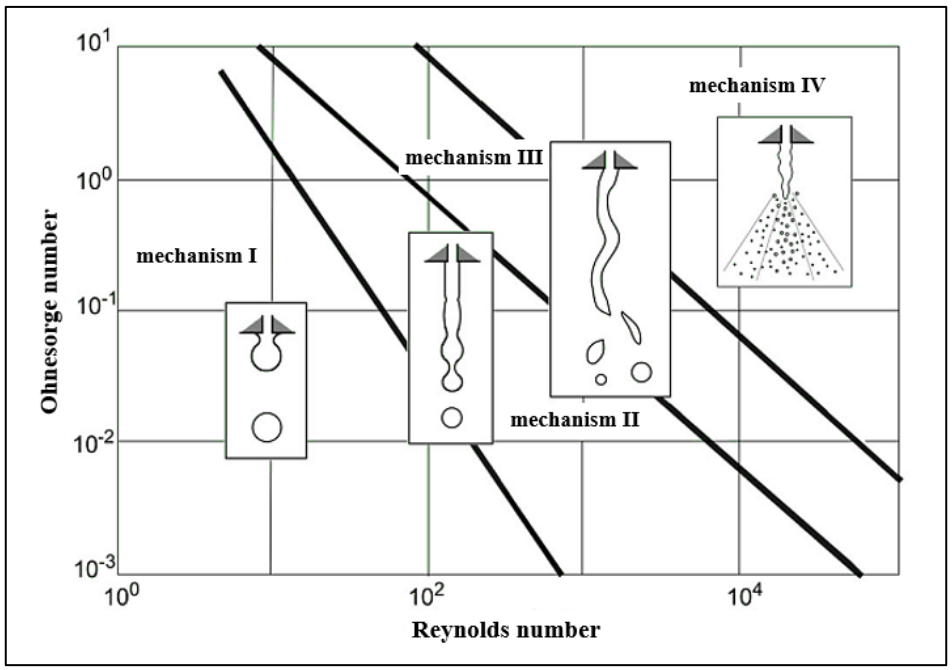

Figure 1.19: The mechanism of droplet formation as a function of operating conditions presented by Reynolds and Ohnesorge numbers. The controlled generation of monodisperse droplets is only possible via mechanisms I and II. Adapted with permission from (169); copyright 2004 Springer.

As presented in equations 1.3, 1.4, and 1.5 below, Reynolds number represents the inertial to viscous force ratio, Weber number represents the ratio of the inertial force to surface tension force. In contrast, the Ohnesorge number describes the balance between viscous force to surface tension force for the liquid.

$$Re_L = \rho_L V_L D/\mu_L = \frac{Inertial\ force}{Viscous\ force} \tag{1.3}$$

$$We_L = \frac{V_L^2 \rho_L D}{\sigma} = \frac{Inertial\ force}{Surface\ tension\ force} \tag{1.4}$$

$$Oh = We_L^{0.5} Re_L^{-1} = \frac{\mu_L}{(\rho_L \sigma D)^{0.5}} = \frac{Viscous\ force}{Surface\ tension\ force} \tag{1.5}$$

Where: V_L is the mean velocity of the liquid jet from the atomiser orifice (m/s), ρ_L is the liquid density (kg/m^3), μ_L is the dynamic liquid viscosity (kg/m.s), σ is the coefficient of surface tension (N/m), and D is the liquid jet diameter (m) (167).

As seen in Figure 1.19, higher velocity and therefore higher values of Reynolds (Re_L) and Weber (We_L) numbers lead to finer atomisation for any liquid jet (166). Furthermore, for a liquid with specific viscosity and surface tension, increasing jet velocity leads to an increase in aerodynamic effects and jet oscillation, resulting in a transfer of the fluid breakup regime from type I to type II, III or IV, which means the disintegration of liquid jet becomes unstable and chaotic (167).

1.5.2. Monodisperse droplet stream generation:

During the last decade, scientists have showed interest in the development of a new technology to produce monodisperse sprays for many industrial and research applications such as controlling liquid fuel combustion, improving the resolution in ink-jet printers, DNA arrays, spray coating, calibration of droplets measuring devices, etc.(145,170). A hybrid technology based on using a monodisperse droplets generator (MDG) with a spray dryer could be a useful contribution to produce spherical microparticles with high size and shape uniformity. Thus, it is essential to understand the technology of monodisperse droplets generation and determine the process parameters that have a significant effect on the formation of uniform droplets.

To create monodisperse droplets, a value of Reynolds number and Ohnesorge number for a specific liquid jet must be found in the range between the first and second regimes of jet formation. According to Rayleigh's instability theory, a non-viscous liquid jet with sufficient surface tension and low internal velocity can be disintegrated into uniform spherical droplets at uniform spacing under laminar flow conditions. The jet breakup mechanism depends on introducing symmetrical disturbances (vibrational forces), which have a wavelength (λ_{opt}) greater than the perimeter of the extruded liquid jet. These vibrations can be introduced mainly via ultrasonic sources. In other words, an appropriate balance between inertia and surface tension forces is required in the liquid to disintegrate the laminar jet into monodisperse droplets. (126).

More specifically, any extruded liquid stream has an equilibrium shape through the surrounding air phase. When mechanical vibrations are applied on it, the interface between the liquid jet and surrounding gas is deformed. Surface tension forces would try to regain the equilibrium shape and as a result a droplet is formed (165,171). In particular, the working mechanism for MDG atomiser depends on using controlled vibrations with a specific frequency which are propagated through the laminar liquid stream until they break-up the jet into a chain of droplets with high uniformity of size and spacing (172). An illustration of the disintegration of a liquid stream using the MDG atomiser is presented in Figure 1.20 (126,172).

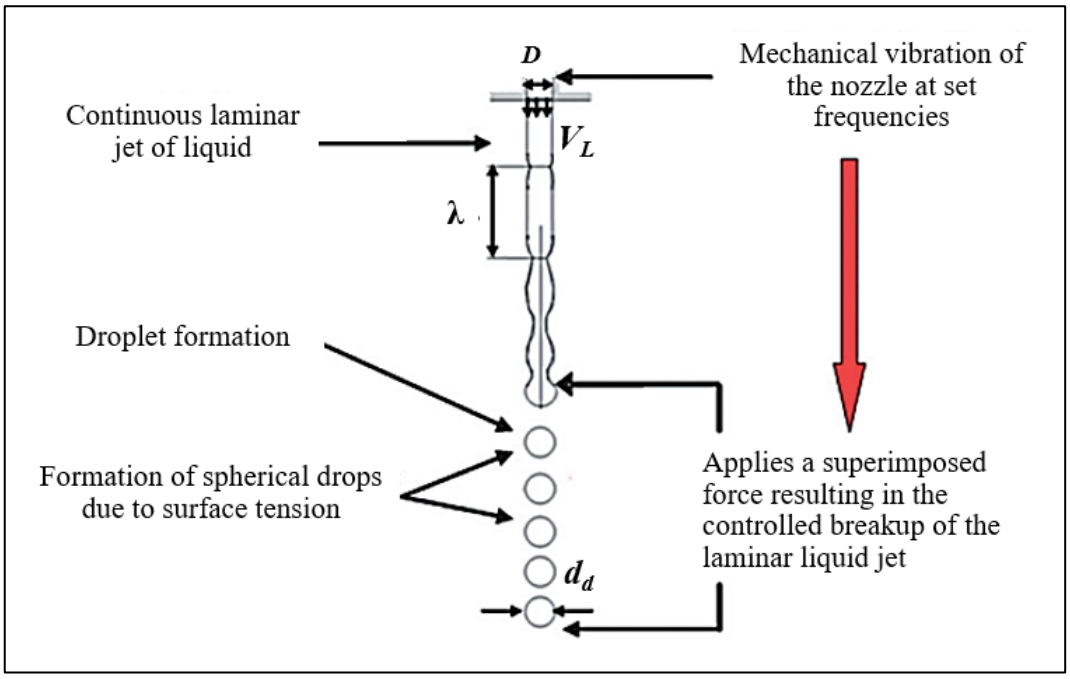

Figure 1.20: Schematic diagram of the disintegration of a liquid jet into monodisperse droplets. Reprinted with permission from (126); copyright 2011 Taylor & Francis.

Furthermore, a schematic diagram of the MDG atomiser is clarified in Figure 1.21. The central part of the MDG atomiser is a piezoelectric transducer which creates mechanical vibrations in the form of symmetric interface waves (Figure 1.22). It does this through applying a periodic voltage on the transducer so that the pulse frequency can be altered to produce and optimise monodisperse droplets (173–176). The size of the droplets is further determined via another important MDG component which is the pinhole diameter (shown in Figure 1.21).

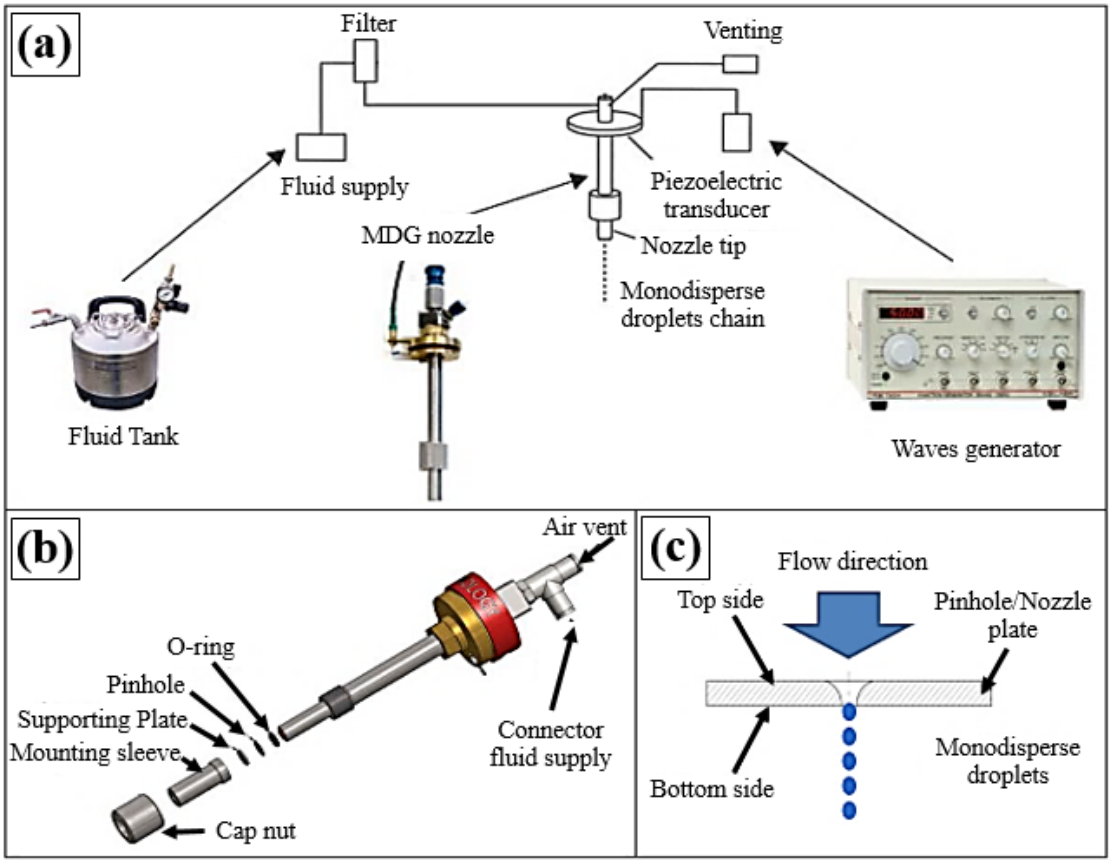

Figure 1.21: Setup for monodisperse droplets generator: a) construction of the overall system, b) construction of the monodisperse droplets generator (MDG), and c) mounting of the atomiser plate.

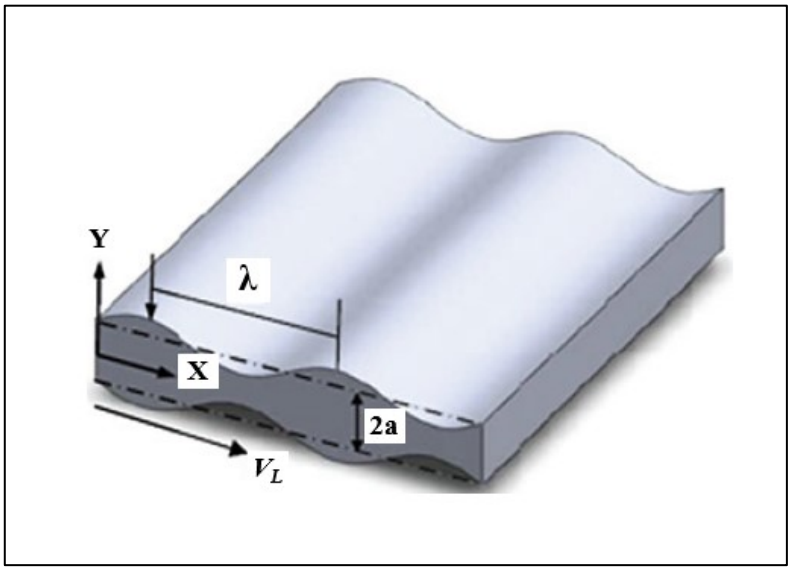

Figure 1.22: A brief description for symmetric disturbance applied to the unstable liquid stream. Where: V_L is a liquid velocity, λ is a wavelength, and 2a is a liquid sheet thickness. Reprinted with permission from (171); copyright 2011 Springer.

In addition, the wavelength (λ) and a non-dimensional wavenumber (*Ka*) of the disturbance waves (Figure 1.22) can be calculated using the following equations 1.6 and 1.7 (173,176):

$$\lambda = \frac{V_L}{f} \tag{1.6}$$

$$Ka = \frac{2\pi \,.\, D}{\lambda} = \frac{\pi \,.\, D.\, f}{V_L} \tag{1.7}$$

According to Schneider and Hendricks, and Rayleigh instability theory, to obtain unstable liquid jet with a maximum amplification rate of axisymmetric surface disturbance, the non-dimensional wavenumber (*Ka*) of a disturbance value must be between 0.45 and 0.95 (177). By contrast, Brenn et al. (2000) considered for MDG atomiser a slightly wider range for disturbance wavenumber to produce monodisperse droplets between 0.3 and 0.9 (175). The previous optimal ranges for wavenumbers were obtained empirically while the actual range depends on the atomiser pinhole morphology (171).

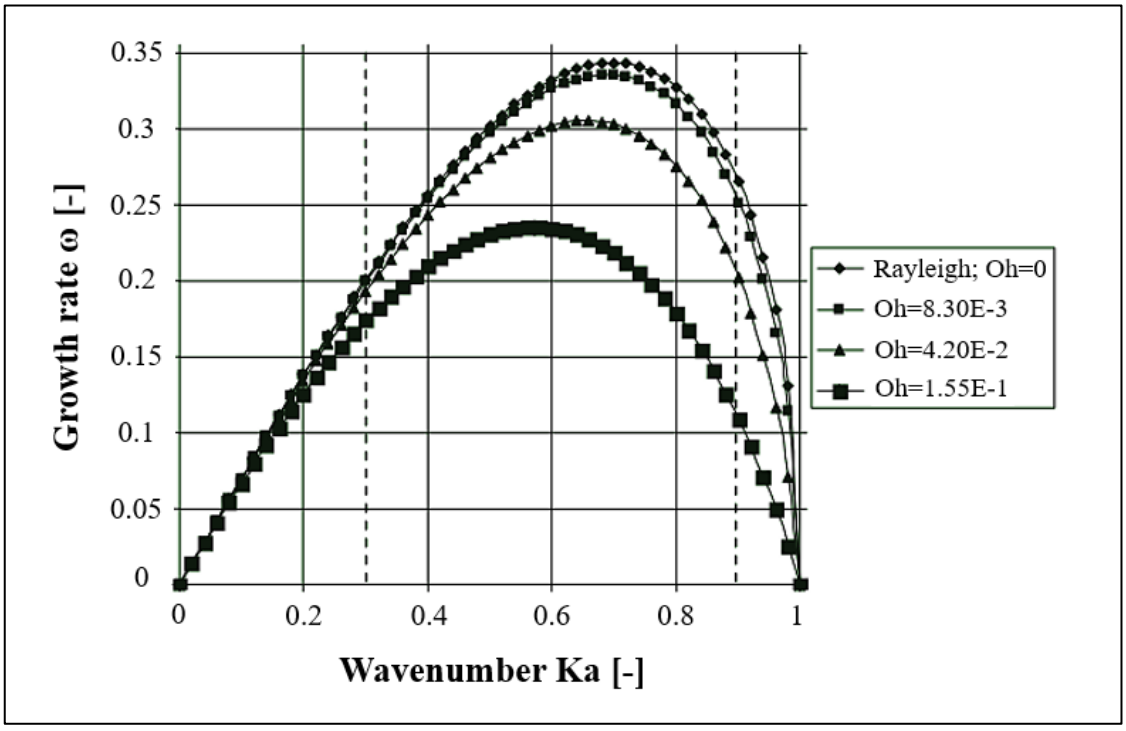

Figure 1.23: A relationship between wave growth rate and disturbance wavenumber (Ka) for different unstable liquid jets emerging from a 200 µm pinhole with different Ohnesorge numbers. Where Oh = 8.3 * 10^{-3}, 4.2 * 10^{-2}, and 0.155 is for water, propanol-2 and silicon oil at 20°C, respectively. The range (dashed lines) between 0.3 and 0.9 for Ka is used to produce monodisperse droplets. Reprinted with permission from (171); copyright 2011 Springer.

As seen in Figure 1.23, a wave growth rate which is a function of the initial wave amplitude depends on the fluid properties. The optimal range of wavenumber (*Ka*) to produce monodisperse droplets as a function of wave growth rate is between 0.3 and 0.9. If the wavenumber (*Ka*) is bigger than 0.9, unstable droplet generation occurs, and if the wavenumber (*Ka*) is smaller than 0.3, satellite droplets would form (169).

However, the preferable *Ka* value for optimal liquid jet disintegration depends on Ohnesorge number (*Oh*) and fluid properties such as surface tension and viscosity. For example, the optimal disintegration of water and silicone oil at 20°C happens when using waves with *Ka* values around 0.7 and 0.59, respectively. In addition, any increase in O*h* number for the atomised liquid leads to a decrease in the maximum growth rate as well as the disturbance wavenumber *Ka*. This indicates that liquid properties (viscosity and surface tension) have the main effect in damping or improving the liquid jet oscillation and disintegration (178).

Using the wavenumber's equation (1.7), the limits of vibration frequency (f_G) (shown as equation 1.8) for generating monodisperse droplets could also be estimated (175,176):

$$f_{G\,min} < f_{G\,opt} < f_{G\,max} \tag{1.8}$$

According to Schneider and Hendricks, and Rayleigh's instability theory, when combining equations 1.7 and 1.8, the f_G limits can be estimated using equation 1.9 below:

$$\frac{0.45\,.\,V_L}{\pi\,.\,D} < f_{G\,opt} < \frac{0.95\,.\,V_L}{\pi\,.\,D} \tag{1.9}$$

However, if considering the optimal (*Ka*) range from 0.3 to 0.9 as Brenn demonstrated (175), the previous equation becomes:

$$\frac{0.3\,.\,V_L}{\pi\,.\,D} < f_{G\,opt} < \frac{0.9\,.V_L}{\pi\,.\,D} \tag{1.10}$$

Thus, the optimal frequency value ($f_{G\,opt}$) which can be used to generate a chain of extremely monodisperse droplets is different for different atomiser orifice/pinhole diameter (*D*) and liquid jet velocity (V_L) (171,179). Furthermore, as can be seen in Figure 1.24 below, using too low or too high jet velocities results in no jet formation (dripping droplets) or a wavy jet, respectively. Moreover, using too low or too high vibration frequencies (outside the optimal frequency range) results in satellite (secondary) droplet formation or unstable droplet formation, respectively. Therefore, using a suitable jet velocity and selecting an optimal vibration frequency range is fundamental for generating a stable monodisperse droplet stream (169).

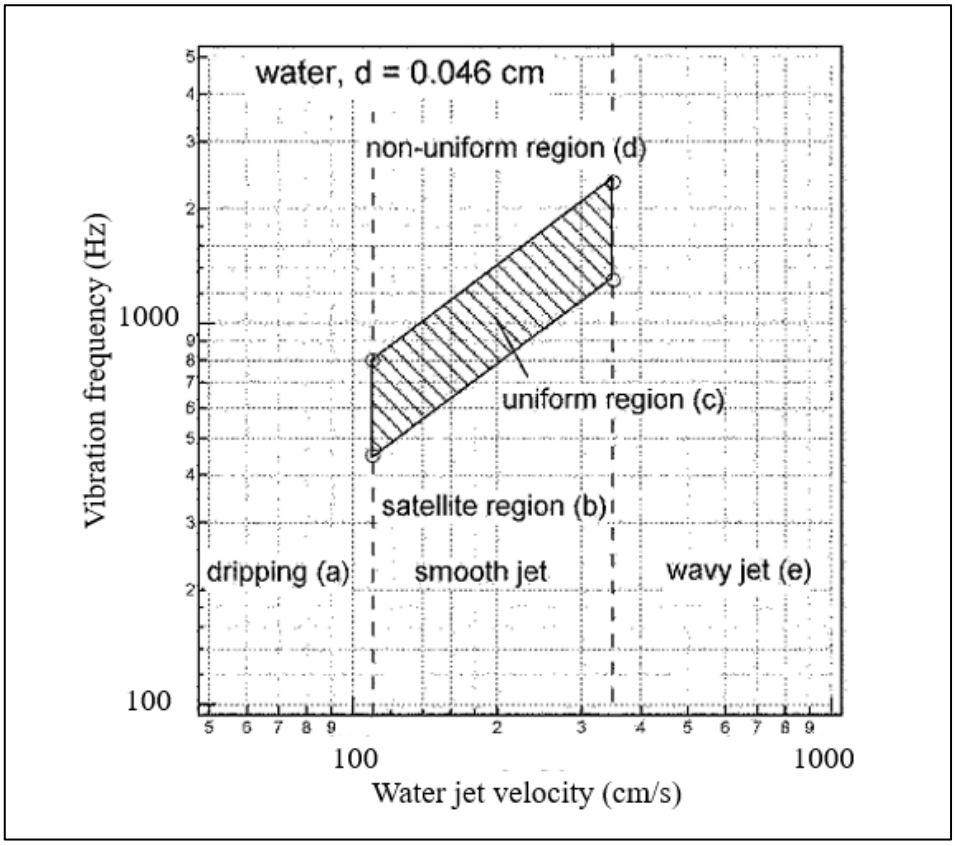

Figure 1.24: Mechanism of liquid jet disintegration as a function of vibration frequency and water jet velocity. Reproduced with permission from (169); copyright 2004 Springer.

On the other hand, the diameter and number of uniform droplets formed from the extruded jet rely on the MDG pinhole diameter, outlet liquid flow rate, and mechanical vibrations frequency. The droplet diameter and liquid flow rate can be calculated using the following equations (1.11 and 1.12) (176):

$$d_d = \sqrt[3]{\frac{6F}{\pi \,.\, f}} \tag{1.11}$$

$$F = \frac{\pi}{4} D^2 V_L \tag{1.12}$$

Where: d_d is the droplet diameter (m), F is the extruded liquid flow rate (m^3/s), f is the vibrational frequency (Hz), D is the atomiser orifice diameter (m), and V_L is the mean velocity of the liquid jet (m/s).

Accordingly, for each hertz through the optimal range of vibration frequency, one droplet is generated with a diameter roughly twice the orifice diameter ($d_d = 1.9D$), but it can also be changed slightly by modifying the frequency (179,180). The above equations 1.11 and 1.12 could be used to estimate the monodisperse droplet's diameter when the disintegration of the liquid jet is in continuous mode.

From the above discussion, it is clear that the atomisation operation could play a crucial role in the spray drying process. Conventional atomisation may be considered a random process, which usually leads to the

generation of droplets with wider size distribution and consequently less uniform powder after drying. This could have a significant impact on the CQAs of the final product as discussed in the previous sections. On the other hand, the disintegration of the liquid jet using MDG potentially helps to generate droplets with excellent size uniformity and would probably lead to better control over the spray-dried powder's properties if implemented within the spray drying process.

1.6. Summary:

Since most pharmaceutical formulations are solid dosage forms, it is not surprising that particle technology, physical material attributes and powder bed properties have attracted the attention of many scientists. Generally, it has long been recognised that the performance of pharmaceutical ingredients depends heavily on fundamental particle properties, especially size, shape and their distributions. However, due to the variability in these properties, it is difficult to predict the actual powder behaviour during handling and processing. This could lead to potential variation in the final product attributes such as for content or weight uniformity.

With the ongoing need to develop novel therapeutics and deliver them to the patients as quickly and safely as possible, the solid dosage form's quality must be sufficiently controlled during the manufacturing process to ensure that the drug presents the desired therapeutic effects as expected. However, this target cannot be achieved without a reliable control strategy for fundamental particle and raw material properties. Unfortunately, controlling particle size and morphology using conventional production methods is still very challenging. With the recent advances in particle engineering technologies, generating functional particles with uniform size and morphology could be the key to overcoming some of the existing formulation challenges and ensuring drug products with consistent CQAs in the future. Specifically, using monodisperse particles in solid dosage form manufacturing could ultimately support pharmaceutical companies in the development efforts of higher quality products.

Integrating monodisperse droplet generators into spray dryers has recently received much attention as a promising approach to fabricate uniform particles with adjustable size. In this project, the performance of an MDG atomiser for the generation of monodisperse droplets will be studied first (chapter 2). This is followed by designing and assembling a novel lab-scale spray dryer prototype for producing uniform microparticles with various properties and functionality (chapter 3); and finally, the impact of monodisperse spray-dried particles on powder manufacturability (chapter 4) and dosage form uniformity/performance (chapter 5) will be discussed.

1.7. Aim and objectives:

The research aims to develop a novel spray drying-based technology for producing monodisperse powders with controllable attributes (size and shape) to overcome processing issues and formulate solid dosage forms with optimal critical quality attributes (CQAs). Specifically, the proposed technology could improve the flowability of powders (even fine cohesive ones) without needing extra additives. This would enhance blend homogeneity/content uniformity and reduce variations in the quality of solid dosage forms.

In this context, the specific objectives of this work are to:

1) Investigate the effect of process parameters of a monodisperse droplet generator (MDG) on droplet size and other properties using a stroboscopic real-time imaging system.
2) Design and fabricate a new lab-scale spray dryer equipped with an MDG atomiser to produce monodisperse particles with size and morphological uniformity.
3) Generate monodisperse powders for several pharmaceutical ingredients and investigate their bulk properties compared to untreated and conventional spray-dried powders.
4) Investigate the effect of powder monodispersity on blend homogeneity and content uniformity for binary mixtures containing a drug at low doses (< 10%) compared to untreated and conventionally SD powders.

Chapter 2

CHAPTER 2

In-depth Look at the Monodisperse Droplets Generator (MDG) using a PAT Stroboscopic Imaging Technique

2.1. Introduction:

Many researchers have noted the importance of the atomisation process for successful spray drying (23,140–143,146,148,151,181,182). Atomiser type has a significant impact on the critical quality attributes of powdered materials, such as particle size uniformity and batch-to-batch reproducibility. This is because the atomiser type largely determines the droplet size, droplet size distribution, droplet velocity, and droplet trajectory (183–185). Monodisperse Droplet Generator (MDG) has a great promise as a potential atomiser for spray drying because it creates droplets which are uniform in size. It generates monodisperse droplets with the desired size from 40 to 1000 μm, depending on the MDG pinhole/orifice used, with the generated droplets' diameter roughly twice that of its pinhole diameter (179). This atomiser could provide several advantages (discussed earlier in chapter 1) such as designing and developing active ingredient particles with desired properties for better content uniformity, faster dissolution and less variability.

Theoretically, three parameters regulate MDG's performance including atomiser orifice diameter, liquid jet velocity and vibration frequency. However, the actual operational range of vibration frequency for generating uniform droplets is mainly dependent on the liquid jet velocity, liquid temperature or viscosity, atomiser orifice diameter, orifice geometry (e.g. cylindrical, conical) and total orifice quality (presence of cracks, erosion) (173,175,176). Changes to these parameters could lead to differences in the laminar jet properties and in turn adjustments to vibration frequency might be necessary. In addition, the MDG atomiser is very sensitive to particulate impurities in the liquid feed, therefore, clogging of its orifice could happen easily even after filtration of feed. Consequently, optimising the MDG's processing parameters and monitoring droplet formation/droplet stream stability without using process analytical technology (PAT) is practically challenging (155–157,186).

PAT enables the monitoring and control of pharmaceutical manufacturing processes with ultimate advantages such as rapid/online sample analysis, minimising the production cycle cost and time, preventing/reducing batch rejection, improving the product uniformity and reducing human errors (187–191). Specifically, process analytical technology tools such as stroboscopic imaging could play a vital role in understanding and monitoring droplet formation during the MDG operation (172).

Imaging systems have emerged as an essential tool in the pharmaceutical industry for observing spray formation and droplets' characteristics (i.e. size, size distribution, oscillation, trajectories, coalescence etc.)

during the atomisation process (166,192). Obtaining both qualitative and quantitative information via imaging is critical to understand how mono-sized droplets are formed and how the changes in processing parameters affect their size and uniformity. Imaging also helps to verify the theoretical droplet size calculations as discussed previously in chapter 1 under section 1.6.2 (173,175,176).

In this chapter, real-time stroboscopic imaging will be used to monitor the droplet generation process. This includes investigating the effect of vibration frequency and outlet feed pressure of MDG on droplet formation, droplet size distribution and the precision of producing monodisperse droplets. The outcome of this study should help the efforts in the subsequent chapters where MDG will be incorporated into a new spray drying system to generate monodisperse powder particles for various pharmaceutical ingredients. This study will help understand how the changes in the MDG processing parameters affect droplets' specifications e.g. size, monodispersity, the distance between subsequent droplets, and their collisions during atomisation. This investigation will ultimately help with selecting the optimal parameters required for the spray drying process to generate uniform particles with identical spherical shapes and adjustable sizes.

2.1.Materials and Methods:

2.1.1. Materials:

In all experiments, high-quality ultrapure water (UPW) produced from a Direct-Q® system (3UV version, Merckmillipore) was used to prepare all aqueous feed solutions.

2.1.2. Methods:

2.1.2.1. Monodisperse droplet generation:

Monodisperse Droplet Generator - MDG (MTG-05-G3) atomiser from FMP TECHNOLOGY (GMBH, Germany) equipped with 50 µm orifice was used for droplet generation. A function generator (TOELLNER 7404, GMBH, Germany) was utilised to generate a series of electrical square signals (amplitude of 15 V_{pp}) which, when transferred into the MDG piezoelectric transducer, resulted in vibrations that control the monodisperse droplets generation. Specifically, the square wave signals have been chosen because they are more effective in controlling the liquid jet's disintegration than other signals (i.e. sinusoidal, triangular, rectangular, etc.) according to literature (157,173,174,176).

The MDG atomiser can produce monodisperse droplets when using an optimal vibration frequency, which in turn depends on the MDG orifice diameter and feed flow rate/velocity. According to Raleigh's instability theory, this optimal frequency range falls between minimum and maximum frequency values ($f_{G\,min} < f_{G\,opt} < f_{G\,max}$) which can be estimated theoretically using the equation (2.1) below (173,175,176):

$$\frac{0.3 \cdot V_L}{\pi \cdot D} < f_{G\,opt} < \frac{0.9 \cdot V_L}{\pi \cdot D} \quad (2.1)$$

Where: $f_{G\,opt}$ is the optimal vibration frequency (Hz) used to generate monodisperse droplets, V_L is the mean liquid velocity (m/s), and D is the MDG orifice diameter or liquid jet diameter (m). In this study, D was 50 µm, corresponding to the orifice diameter used.

The theoretically expected droplet diameter (d_d) can also be calculated using the equation (2.2) below (126):

$$d_d = \sqrt[3]{\frac{6F}{\pi \cdot f}} \quad (2.2)$$

Where: d_d is the monodisperse droplet diameter (m), F is the extruded liquid flow rate (m^3/s) and f is the vibrational frequency (Hz).

The liquid velocity can be estimated from the feed flow rate by measuring the weight of water flowing from the atomiser tip for three minutes using an accurate and sensitive balance. In addition, the MDG feed pump pressure range is 0.5 - 4 bars, where laminar liquid flow is expected. However, preliminary trials indicated that only the lower pressures (0.5 and 1 bar) are suitable for use within a realistic spray drying set-up due to the extremely high droplet velocities at higher pressures (> 1 bar) preventing drying from happening. Accordingly, the theoretical values for processing parameters that can be used to generate monodisperse droplets with specific diameters are estimated using equations 2.1 and 2.2 above (Table 2.1).

Table 2.1: The characteristic parameters for a chain of monodisperse droplets as a function of outlet feed pressure and 50µm MDG orifice diameter.

Outlet feed pressure (bar)	[a] Liquid flow rate (ml/min)	Liquid flow rate (m^3/s)	Liquid jet velocity (m/s)	[b] Minimum frequency (KHz)	[b] Maximum frequency (KHz)	[c] Maximum droplet diameter (µm)	[c] Minimum droplet diameter (µm)
0.5	0.84	1.41×10^{-8}	7.18	13.72	41.17	125.22	86.82
1.0	1.24	2.06×10^{-8}	10.52	20.10	60.30	125.22	86.82

[a] All experiments for determining the liquid flow rate were made under normal ambient conditions and repeated three times.

[b] Vibration frequency values to generate monodisperse droplets were calculated theoretically using equation 2.1.

[c] Monodisperse droplet diameters were calculated theoretically using equation 2.2.

In line with the above, droplet chains were generated at the lower pressures of 0.5 and 1 bars whilst screening multiple frequencies in the range 0-85 kHz. These droplets were imaged using the procedure described below.

2.1.2.2. Real-time stroboscopic imaging system:

The set-up for the stroboscopic imaging system is outlined in Figure 2.1. The droplet chains generated at two pressures (0.5 and 1 bar) and multiple frequency ranges (0-85 kHz) were illuminated in pulse mode using backlight illumination by industrial BVS-II Wotan stroboscope (Polytec GmbH, Germany) with a pulse frequency of 25 Hz. A series of images were captured for each droplet chain at zero vertical distance between the camera (top lens edge) and the tip of MDG atomiser. Droplets' images were captured using OnSemi PYTHON industrial digital camera (Black/white camera USB 3.0 – 1.3 Megapixels, Ximea GmbH, Germany) at 25 frames per second. A precise lens (Precise Eye 1.33X, Navitar Inc. USA) was used to capture high-quality images with magnification of 2.39X. The resulting images were viewed using XIMEA CamTool software version 4.14.The droplet diameter and the distance between two droplet centres were measured using ImageJ 1.50i (NIH, USA). All measurements were determined in a pixel unit and were converted to micrometres using a scale (4.8/2.39=2.0083 pixels/µm). All measurements and calculations are repeated for three frames, and the results are recorded as (mean ± SD, ± CV%, n=3).

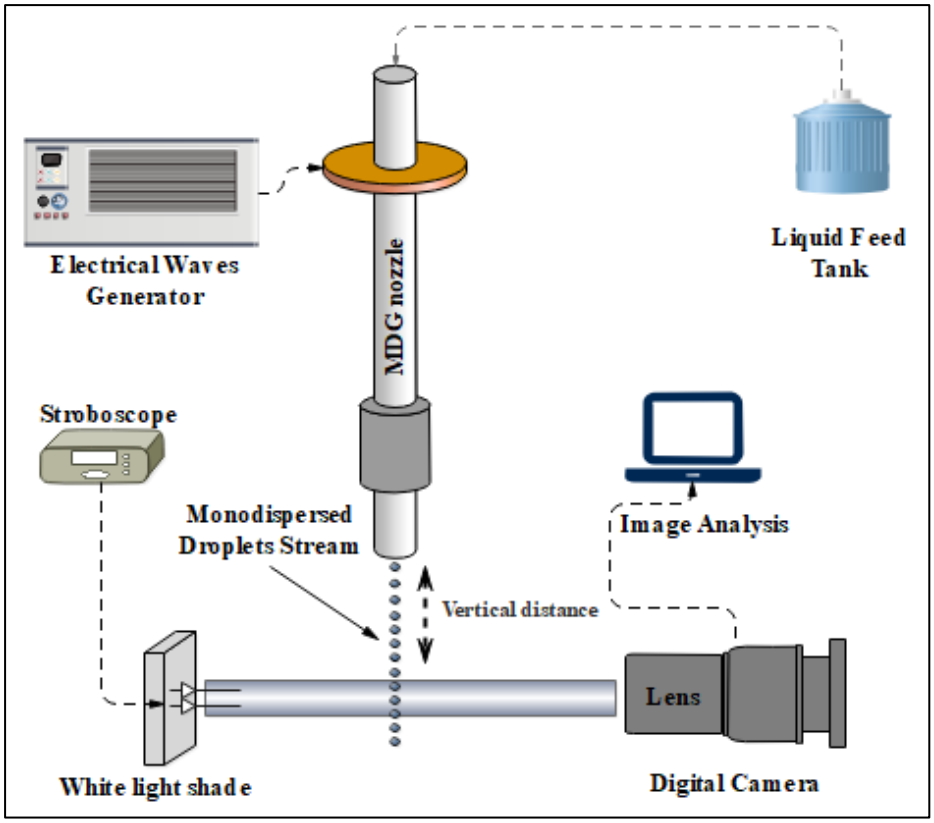

Figure 2.1: Schematic diagram of the setup used to control a liquid jet's disintegration emerged from the MDG atomiser using a real-time stroboscopic imaging system. The vertical distance between the camera (top lens edge) and the nozzle tip was adjusted to capture images for droplets at different downstream distances from 0 to 30 cm.

In addition to the previous microlens used, another lens with manual iris (2/3 type, C-Mount, focal length 50 mm, F 2.8, 5 megapixels, computar lens, CBC America LLC., USA) was utilised for imaging the droplets chain at different vertical distances (0, 2, 4, 6, 8, 10, 14, 18, 22, 26 and 30 cm) from the atomiser tip. Using this lens helped to investigate the collision and coalescence between subsequent droplets.

2.1.2.3. Statistical Analysis:

One-way analysis of variance (one-way ANOVA test) was used to compare the mean diameter for monodisperse droplets generated within the optimal vibration frequency range. When ANOVA indicated a significant difference ($P < 0.05$), Tukey's post hoc test was performed to confirm where the differences occurred between the groups. All statistical analysis was conducted using GraphPad Prism 7.03 software. In this study, all tests were conducted in triplicate and the results were presented as mean ± standard deviation (SD).

2.2.Results and Discussion:

In this study, real-time stroboscopic shadowgraph imaging was used to monitor the droplet generation process and measure droplet diameter. Figure 2.2 below presents the mean droplet diameter as a function of the vibration frequency (0-85 kHz) for 0.5 and 1.0 bar pressures, respectively (dashed lines). For comparison, the figure also shows the calculated droplet diameters within the theoretical minimum and maximum vibration frequency ranges (presented as solid lines).

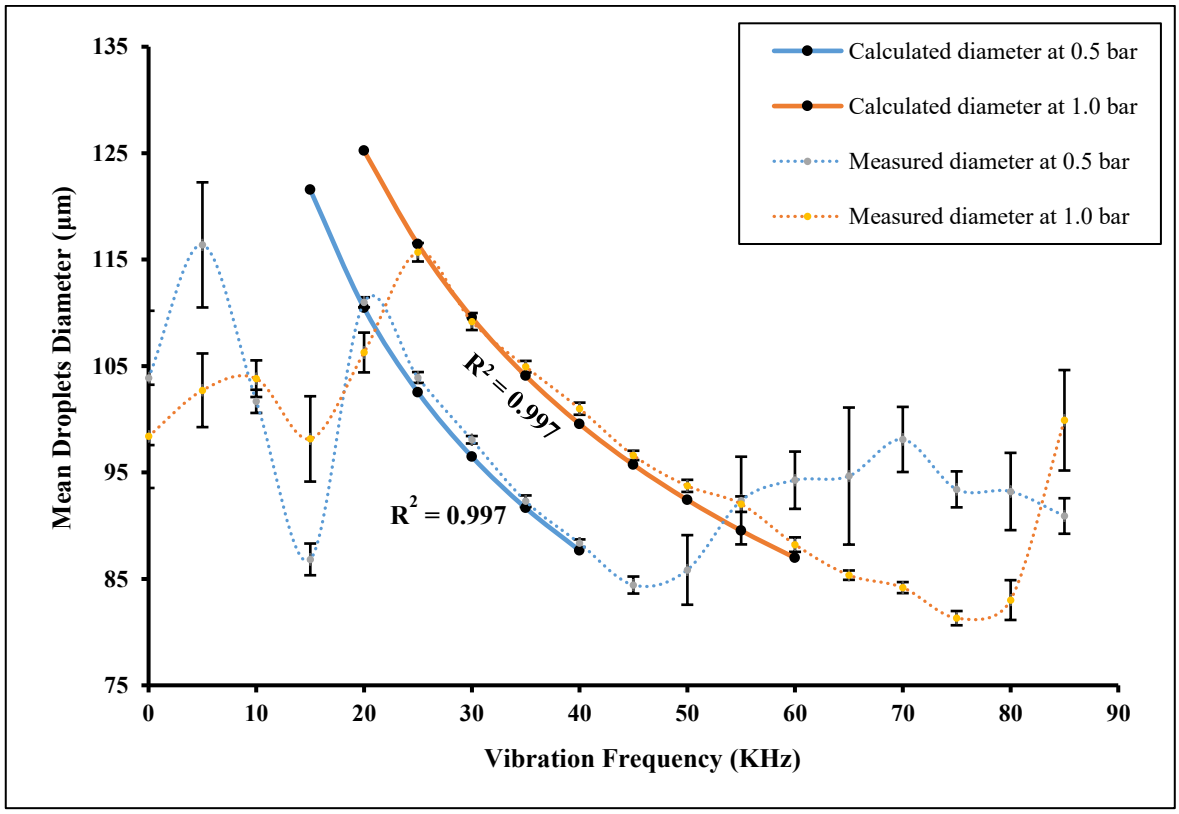

Figure 2.2: Mean droplets diameter as a function of the vibrational frequency for different feed pressure (mean ± SD, n= 3 frames). The actual operational range of optimal vibration frequency observed for generating uniform droplets was from 20 to 45 and from 25 to 75 KHz for feed pressure 0.5 and 1.0 bar, respectively. The large error bars reflected the droplets' varying diameters when it generated using frequency outside the optimal range. R^2 refers to the correlation coefficient for the relationship between the mean droplets diameters measured using the imaging technique and the calculated droplets diameters at each vibration frequency and feed pressure used.

As seen in Figure 2.2, the droplets that were generated using vibration frequencies between 20-45 KHz or between 25-75 KHz showed consistency in the size where the diameters of the droplets were stable with low standard deviations. Outside these optimal frequency ranges, the generated droplets exhibited varying diameters with high standard deviations. In addition, it can be seen that the droplet diameter decreases almost linearly when the vibration frequency is increased within the optimal frequency ranges. These results indicate that the MDG atomiser creates uniform droplets when using optimal processing parameters (i.e. jet velocity and vibration frequency). This is an important finding, as it will help with the selection of the optimal frequency value to achieve the desired droplet size for spray drying in the future.

Furthermore, high correlation coefficients (R^2) could be observed for the relationship between the droplet diameters measured using the imaging technique and the calculated droplet diameters at both pressures indicating predictability of the technique in estimating the droplet size when operating within the minimum and maximum frequency ranges. The imaging technique also helped ascertain the distance between two subsequent droplets which is crucial for droplet-droplet interactions, as will be seen in section 2.3.3. As a result, the images analysis system provided qualitative and quantitative data for better understanding of the liquid stream structure (193).

The next few sections will focus on interpreting the impact of vibration frequency on droplet diameter, the distance between subsequent droplets, and the stream's overall monodispersity.

2.2.1. The effect of vibration frequency on droplet diameter and distance between subsequent droplets:

The influence of vibration frequency on droplet size at different outlet feed pressures of 0.5 and 1 bar was investigated using the imaging system. As can be observed from stroboscopic images (Figures 2.3 and 2.4), droplets formed as a single chain rather than a spray plume, reflecting the mechanism for this technique based on Rayleigh's theory (126,169). For the 50 µm MDG pinhole, the optimal vibration frequency ranges for synchronised droplets formation are between 20-45 and 25-75 KHz for the outlet feed pressure 0.5 and 1.0 bar, respectively. Outside these frequency ranges, the fluid jet's disintegration was unpredictable with subsequent droplets merging into larger ones leading to polydisperse droplets. This is because generating equally sized and spaced droplets require creating an appropriate time scale between liquid jet velocity and vibration frequency. The physical reason for this lies in the fact that the laminar liquid jet can be broken up into uniform droplets when the wavenumber ($Ka = 2\pi. D.f/V_L$) of the applied disturbances is between 0.3 and 0.9. As a result, the propagated surface waves (disturbances) can grow exponentially along the liquid jet until they break it into uniform-sized droplets. Thus, when using vibration frequency outside the optimal range, the generated disturbances corresponded with a wavenumber either smaller than 0.3 or bigger than 0.9 which will lead to satellite droplets formation or unstable droplet formation, respectively (169,171). Furthermore, the results exhibit that the observed frequency ranges (20-45 and 25-75 KHz for 0.5 and 1 bar, respectively) used to produce monodisperse droplets by the MDG (Figures 2.3 - 2.4) are slightly shifted

towards higher frequencies than the theoretical ranges (13-41 and 20-60 KHz for 0.5 and 1 bar, respectively). This is because the actual range for monodisperse droplets formation depends on the nozzle hole geometry (171). The nozzle has a conical pinhole (as seen in Figure 1.21/ chapter 1/p: 45), which is desirable for better flow and directional stability. Brenn et al. confirmed that a pinhole with conical geometry inhibits the flow turbulence inside the liquid jet when it emerges from it. Using this pinhole effectively extends the operational range of the Reynolds number for a laminar liquid flow and thus leads to extending the driving frequencies necessary to generate a uniform droplet stream (176).

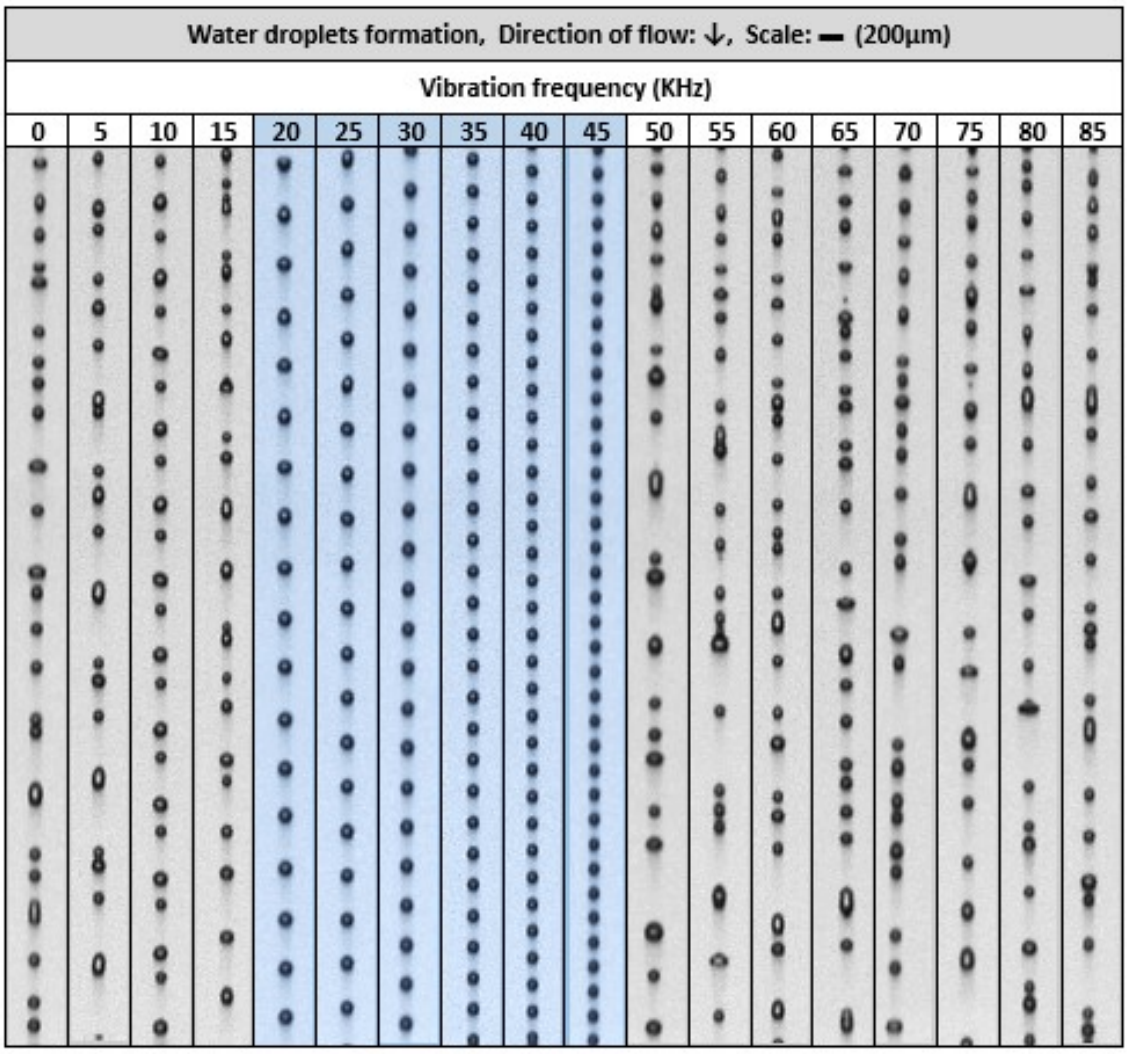

Figure 2.3: Images of droplets formation from MDG nozzle using different excitation frequencies with feed pressure at 0.5 bar, feed flow rate at 0.84 ml/min, and droplets velocity 7.18 m/s. All images were taken using a Computar lens with a resolution of 5 megapixels. All images were taken within the first centimeter of the vertical distance from the nozzle tip.

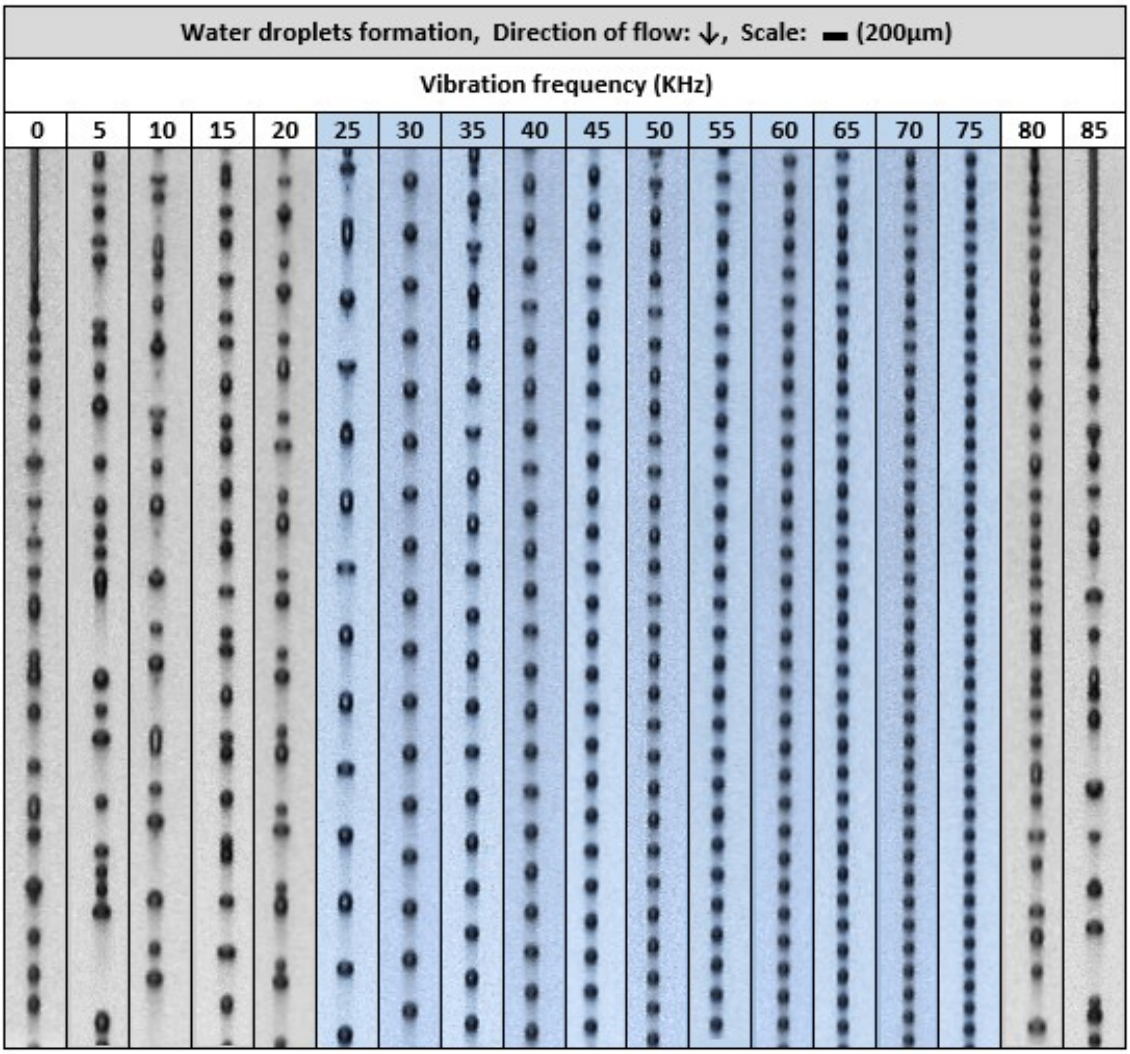

Figure 2.4: Images of droplets formation from MDG nozzle using different excitation frequencies with feed pressure at 1.0 bar, feed flow rate at 1.24 ml/min, and droplets velocity 10.52 m/s. All images were taken using a Computar lens with a resolution of 5 megapixels. All images were taken within the first centimeter of the vertical distance from the nozzle tip.

Looking at the above data in Figures 2.2 - 2.4, the droplet diameter seems to significantly decrease (ANOVA, $P < 0.05$) upon increasing the vibration frequency at both feed pressures. For example, at 0.5 bar the droplet diameter decreased from 110.99 µm to 84.42 µm when vibration frequency was increased from 20 to 45 KHz. This can be explained by the fact that increasing the vibration frequency (*f*) leads to a decrease in the surface wavelength (λ) and an increase in the surface wavenumber (*Ka*) per surface area unit for the propagated disturbances along the liquid jet (as clarified before in Figure 1.22 and Equations 1.6 and 1.7; chapter 1/ p: 45-46) (171,173,176). Thus, the number of uniform droplets generated from the nozzle tip increases, with a corresponding decrease in droplet size and distances between subsequent droplets, as seen in Figures (2.3 and 2.4). These results were in good agreement with the data reported in literature (194), where the net effect of increasing vibration frequency is a reduction in droplet size and an increase in droplet ejection rate (number of droplets per unit time) from the nozzle when it is operated using optimal conditions.

The influence of vibration frequency on the uniformity of droplets' spacing (droplet-to-droplet distance) in the single stream was also assessed at different outlet feed pressures of 0.5 and 1 bar. Figures 2.5 and 2.6 show that the uniformity in droplets' spacing depends on the vibration frequency used. When generating droplets using the optimal vibration frequency ranges, the droplets' spacing was consistent. Outside these ranges, the distances became inconsistent due to unstable droplet formation. This leads to an increase in droplets' collisions and coalescence, which translates into an increase in droplets' polydispersity in an unpredictable way. Furthermore, the spacing between droplets and the vibration frequency were inversely proportional. Increasing the vibration frequency led to a decrease in the distance between droplets. These results can be explained by the fact that increasing the optimal vibration frequency leads to an increase in droplet formation per unit of time (194). These results indicate that generating monodisperse droplets depends on producing droplets with uniform sizes and spacing. Slight variations in operating parameters could have a great impact on the stability and monodispersity of the stream.

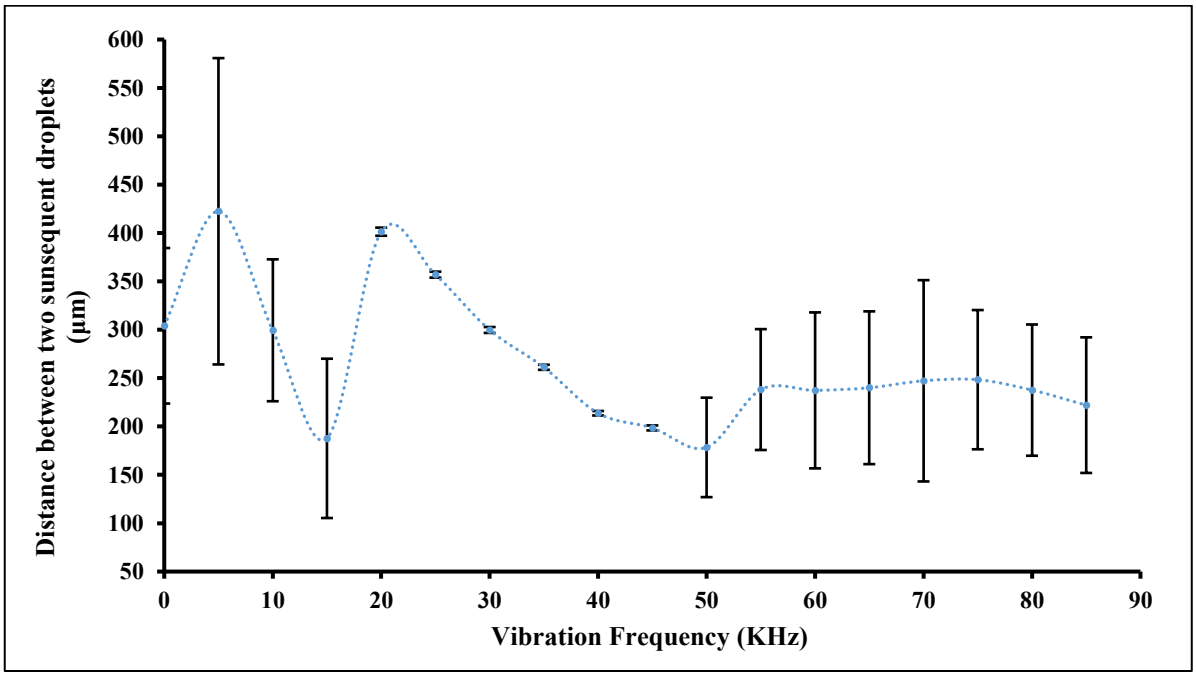

Figure 2.5: A distance between two subsequent droplets as a function of the vibrational frequency with feed pressure 0.5 bar, (mean ± SD, n=3 frames). The range of optimal vibration frequency observed for generating uniform droplets was from 20 to 45 KHz. The large error bars reflected inconsistency in droplets spacing when generated using frequency outside the optimal range.

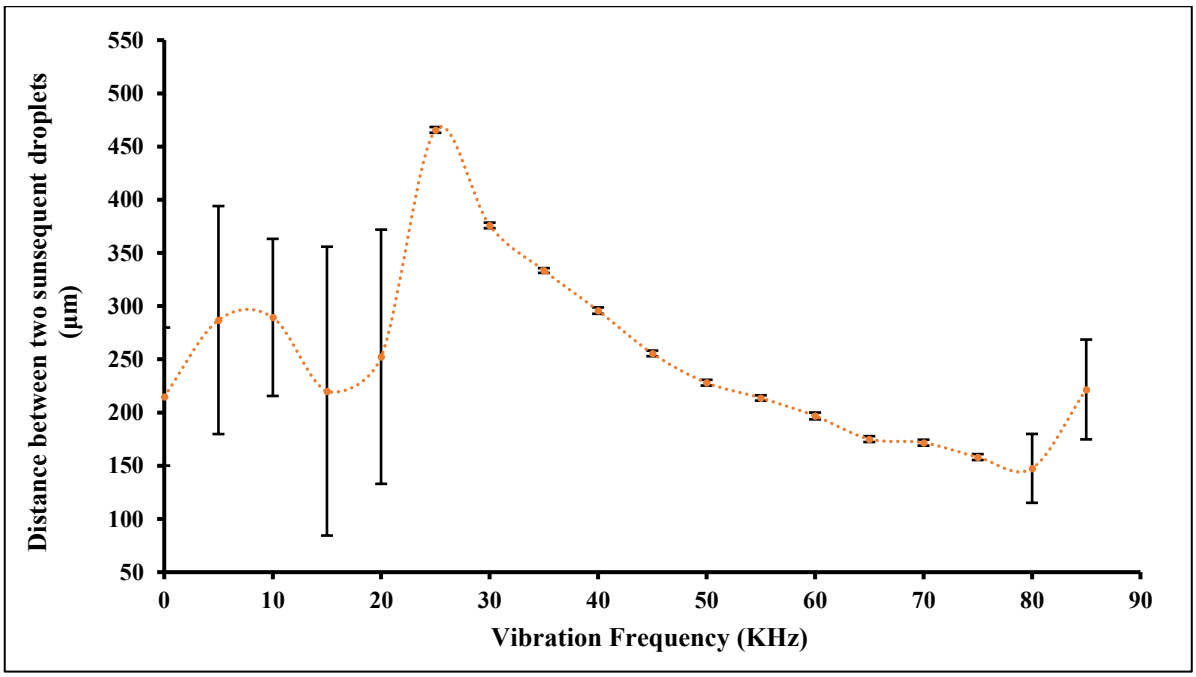

Figure 2.6: A distance between two subsequent droplets as a function of the vibrational frequency with feed pressure 1.0 bar, (mean ± SD, n=3 frames). The range of optimal vibration frequency observed for generating uniform droplets was from 25 to 75 KHz. The large error bars reflected inconsistency in droplets spacing when generated using frequency outside the optimal range.

2.2.2. Assessment of repeatability (precision) of monodisperse droplets generation:

The droplet images were analysed further to estimate the precision of the droplet generation process. Specifically, the precision of droplet diameter and in maintaining a uniform distance between subsequent droplets was investigated. This was necessary to ensure that the process was repeatable and provided further confidence to proceed to the device development activities in the next chapters. As seen in Table 2.2, the coefficient of variation (CV%) for droplet diameter was less than 0.94 and 0.83% at vibration frequency ranges of 20-45 and 25-75 KHz with outlet feed pressure 0.5 and 1.0 bar, respectively. Similarly, the CV% for droplet-to-droplet distance was less than 2% (Table 2.2). These results indicate a high precision of micrometre-sized droplet generation can be achieved by the MDG atomiser when used at the optimal frequencies. On the other hand, the precision level falls significantly as demonstrated by high CV% when the droplets were generated at vibration frequencies higher or lower than the optimal range. This confirms the importance of selecting the optimal frequency for operation of the MDG atomiser. However, it is worth noting that the droplets may start behaving differently, and monodispersity could be lost depending on the distance of the droplet from the atomiser tip.

Table 2.2: Droplets stream specifications as a function of different vibration frequencies and feed flow pressures.

Vibration frequency (KHz)	d_d (µm), 0.5 bar	d_d (µm), 1.0 bar	Mean droplet diameter (µm)						Droplet-to-droplet distance (µm)					
			Flow pressure 0.5 bar			Flow pressure 1.0 bar			Flow pressure 0.5 bar			Flow pressure 1.0 bar		
			Mean	*± SD.*	*± CV%*	*Mean*	*± SD.*	*± CV%*	*Mean*	*± SD.*	*± CV%*	*Mean*	*± SD.*	*± CV%*
0	-	-	103.88	6.31	6.07	98.39	4.85	4.92	304.10	80.39	26.43	215.01	64.88	30.17
5	-	-	116.38	5.88	5.05	102.72	3.46	3.37	422.47	158.34	37.48	286.92	107.14	37.34
10	-	-	101.68	1.09	1.07	103.81	1.72	1.66	299.43	73.34	24.49	289.41	73.83	25.51
15	121.56	-	86.83	1.49	1.72	98.15	4.01	4.09	187.70	82.36	43.87	220.13	135.74	61.66
20	110.45	125.43	**110.99**	**0.47**	**0.42**	106.27	1.87	1.76	**401.39**	**4.19**	**1.04**	252.45	119.46	47.31
25	102.53	116.44	**103.92**	**0.51**	**0.49**	**115.69**	**0.87**	**0.75**	**356.99**	**3.09**	**0.86**	**465.64**	**2.70**	**0.58**
30	96.48	109.57	**98.07**	**0.35**	**0.36**	**109.18**	**0.80**	**0.73**	**299.77**	**3.06**	**1.02**	**375.87**	**2.62**	**0.69**
35	91.65	104.08	**92.30**	**0.54**	**0.59**	**104.94**	**0.54**	**0.52**	**261.20**	**2.63**	**1.01**	**333.49**	**2.23**	**0.67**
40	87.66	99.55	**88.35**	**0.36**	**0.41**	**100.99**	**0.57**	**0.57**	**213.69**	**2.32**	**1.08**	**295.80**	**2.98**	**1.01**
45	-	95.72	**84.42**	**0.80**	**0.94**	**96.60**	**0.44**	**0.45**	**198.52**	**2.57**	**1.29**	**255.58**	**2.66**	**1.04**
50	-	92.42	85.84	3.27	3.81	**93.74**	**0.57**	**0.61**	178.36	51.42	28.82	**228.05**	**2.68**	**1.17**
55	-	89.53	92.36	4.12	4.46	**92.02**	**0.73**	**0.79**	238.16	62.48	26.23	**213.72**	**2.51**	**1.17**
60	-	86.97	94.27	2.69	2.86	**88.22**	**0.68**	**0.78**	237.30	80.62	33.97	**196.81**	**3.2**	**1.64**
65	-	-	94.66	6.44	6.80	**85.35**	**0.44**	**0.51**	240.03	78.97	32.90	**175.06**	**2.73**	**1.56**
70	-	-	98.10	3.06	3.12	**84.18**	**0.52**	**0.62**	247.21	104.05	42.09	**171.69**	**2.79**	**1.63**
75	-	-	93.41	1.69	1.81	**81.31**	**0.67**	**0.83**	248.38	71.97	28.97	**158.17**	**2.78**	**1.76**
80	-	-	93.21	3.63	3.89	83.01	1.87	2.26	237.59	67.85	28.55	147.53	32.38	21.94
85	-	-	90.91	1.67	1.84	99.90	4.72	4.72	222.05	70.10	31.57	221.69	46.90	21.15

- Numerical values presented in **bold** refer to droplet stream specification when generating mono-sized droplets.
- **d_d** is a diameter of mono-sized droplets according to **theoretical calculations** (equations 2.1. and 2.2/ p: 54). The water flow rate from 50 µm MDG pinhole was 1.41×10^{-8} and 2.06×10^{-8} m^3/s when using feed flow pressure of 0.5 and 1.0 bar, respectively.

2.2.3. Droplet behaviour at longer vertical distances from the MDG atomiser tip:

It has been reported previously that droplets can start colliding with each other after a specific vertical distance leading to loss of droplet monodispersity (156,157). This is critical for our study as the intention would be to limit the droplet collisions and coalescence until droplets can be converted to solid particles via drying (see chapter 3). The droplet stream was imaged at longer vertical distances from the atomiser tip to understand the droplet behaviour. The vibration frequency selected for this study was 30 KHz for feed pressure of 0.5 bar and 45 KHz for feed pressure of 1.0 bar. The overall behaviour of the monodisperse droplets stream for different distances from the MDG tip is presented in Figures 2.7 and 2.8. It can be observed that the coherent structure of the uniform stream is completely lost after 4 - 6 cm from the MDG tip for both outlet feed pressures. The droplets started to collide with each other after this distance leading to coalescence into bigger droplets, and eventually these changed their trajectories and left the stream.

The droplets' tendency to collide is probably due to aerodynamic effects around the falling droplets. When increasing the downstream distance from the MDG tip, the interaction between the boundary air layers and the droplets makes the initial droplets' velocity much lower than the velocity of other subsequent droplets in the chain, resulting in losing the uniform spacing between the subsequent droplets. This aerodynamic braking leads to collisions and coalescence between the successive droplets (157).

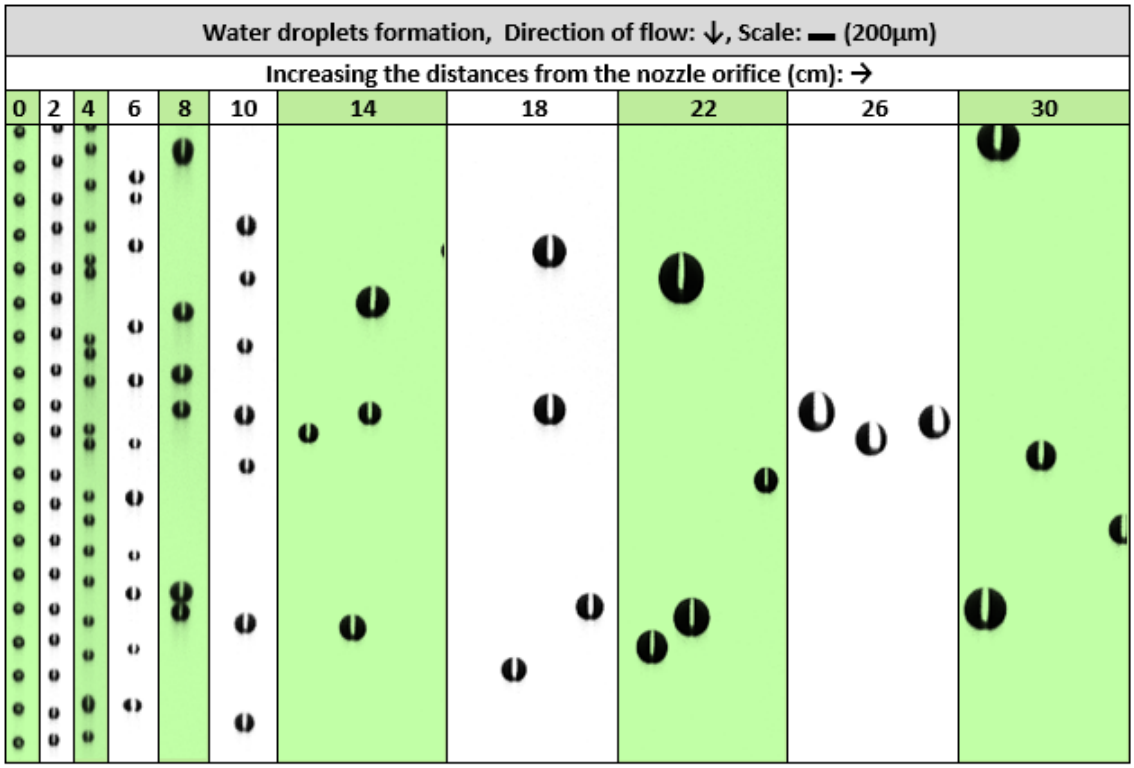

Figure 2.7: Images of a single monodisperse droplets stream generated from 50 µm MDG pinhole with feed pressure at 0.5 bar and vibration frequency at 30 KHz. All images were taken using a Computar lens with a resolution of 5 megapixels.

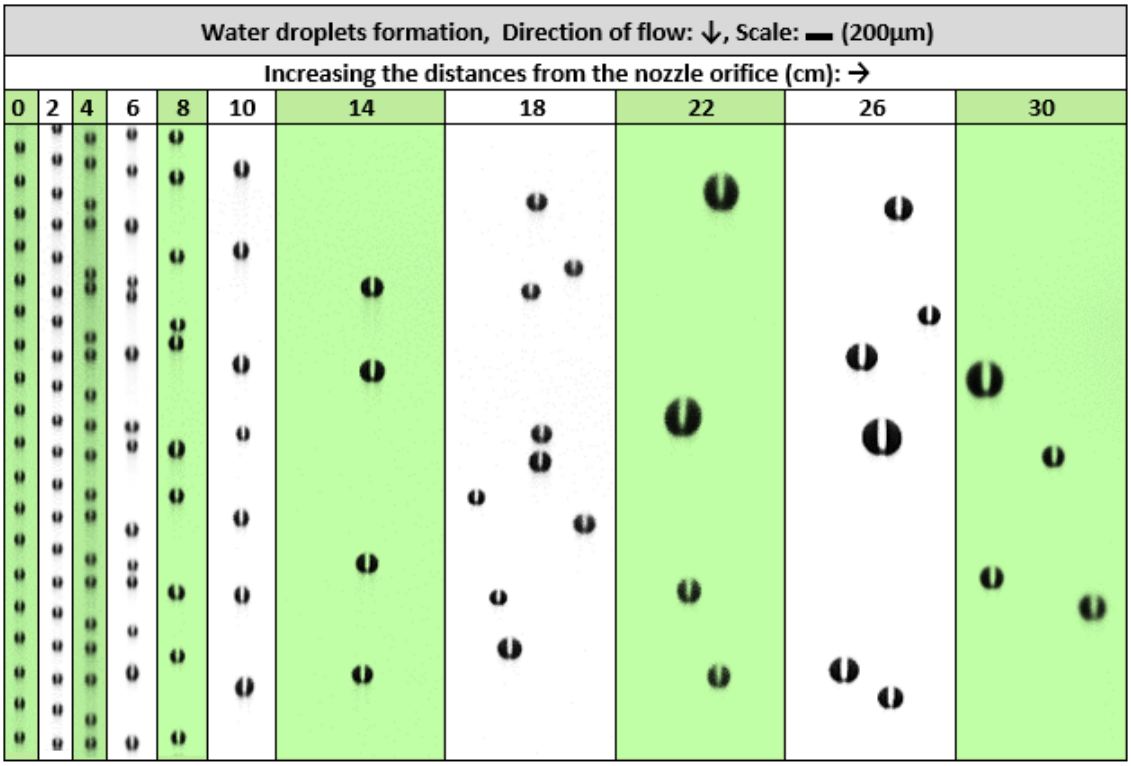

Figure 2.8: Images of a single monodisperse droplets stream generated from 50 µm MDG pinhole with feed pressure at 1.0 bar and vibration frequency at 45 KHz. All images were taken using a Computar lens with a resolution of 5 megapixels.

As the downstream distance from the atomiser tip increases, droplets tend to lose their monodispersity and instead create a polydisperse droplet population. This result is compatible with findings from previous studies (156,157,172). For example, previous researchers mentioned that the coalescence phenomenon affects the uniformity of the droplets' spacing after a downstream distance of 500-1000 jet diameters for a single uniform droplets stream (173). Considering this, the jet diameter that emerged from the MDG pinhole should be approximately 50 µm, therefore, the expected distance for starting of coalescence would be around 2.5-5 cm from the nozzle tip. This is in line with what has been observed in the imaging study reported above (Figures 2.7 and 2.8).

2.3. Conclusion:

Generating monodisperse droplets by the MDG atomiser requires using optimal processing parameters. The diameter of droplets produced from a given pinhole size can be modulated through controlling the vibration frequency and feed flow rate/pressure of the MDG atomiser. Those factors were studied using a PAT stroboscopic imaging technique, which enabled direct visualisation of the produced droplets and subsequent quantification of droplet parameters. Specifically, using an imaging technique helped with identifying a practical vibration frequency range, which is necessary to generate monodisperse droplets. Increasing the vibration frequency led to an increase in the number of droplets generated but decreased their size. The generation process for monodisperse droplets is precise when operating within the observed range. However, the behaviour of the droplets becomes different at longer distances probably due to aerodynamic resistance in the surrounding environment. This led to a loss of monodispersity through collisions and subsequently coalescence of the droplets. Overall, the PAT tool utilised in this investigation helped optimise the parameters necessary for generating monodisperse droplets and will serve an essential role in the next chapter, where the MDG atomiser will be incorporated into a novel spray-drying device for the fabrication of monodisperse pharmaceutical particles.

Chapter 3

CHAPTER 3

Design and Fabrication of a Single-Stream Spray Dryer

3.1. Introduction:

During the last few decades, the interest in designing pharmaceutical powders with specific characteristics has increased dramatically to improve the properties of various dosage forms, including solid dosage forms, inhalable products and parenteral preparations (7,141,195–199). To produce powders with the desired critical quality attributes (CQAs), specific fundamental particle properties need to be obtained. For instance, the particle size and morphology characteristics are often the primary attributes to be investigated in a powder-based formulation. The uniformity of these characteristics (e.g. unimodal or uniform distribution of particle size or spherical shape) is often sought after since dealing with polydisperse powders or less homogenous powders could lead to manufacturability issues (34,200).

As mentioned before in the first chapter, spray drying is a continuous dehydration process that converts atomised liquid droplets into dry micro-/nano-particles in a one-step operation. Due to its scalability and capability of engineering particles, the technique has become one of the most common pharmaceutical methods to produce powdered ingredients with tailored particle properties and functionality. The structure and morphology of particles could be manipulated by changing the spray drying process conditions and feed solution properties (23,141,201). However, controlling the conventional spray dryers to produce particles with highly uniform characteristics is still a big challenge to date (152,172). The heterogeneous nature of powders produced using conventional spray dryers is mainly attributed to the atomised droplets' polydispersity and turbulent airflow patterns in the drying chamber, which make the droplets experience different drying profiles and several droplet-droplet, droplet-particle, and droplet-wall collisions within the same drying process. This usually leads to producing fine powders with wide distribution of particle properties and agglomerates. Sometimes, these properties affect the final powder manufacturability and have been noted in several sources (140,172,202). For example, it is well understood that larger rounded particles with narrow size distributions express better flow properties than smaller, finer particles, which usually exhibit high cohesive properties due to their large surface area (74,203). Therefore, using spray-dried powders in solid dosage form manufacturing without extra processing (e.g. granulation or blending with glidants) could affect blend homogeneity and die-filling uniformity due to poor powder flowability (29,204). As a result, a variation in dosage uniformity can be observed during tableting and encapsulation processes, leading to variation in final product quality.

To minimise the previous issues, replacing the conventional atomisers usually used within spray drying with monodisperse droplet generators seems like an attractive option because it potentially offers control over the droplets' trajectories, their size distribution and drying kinetics. Specifically, this combination between monodisperse droplets atomisation and spray drying has a great promise for reaching the goal of manufacturing powders with controlled particle properties (i.e. controlled size, size distribution, morphology, moisture content, etc.) and functionality (i.e. flowability, dissolution, hygroscopicity, etc.) (3,33,34,100,102,141,205). This uniformity of powder properties paves the way for controlling the mechanical properties of solid dosage forms and may support implementing the Quality by Design (QbD) approach into manufacturing processes (7,34,206,207). The uniformity of powder properties could become critical and perhaps a prerequisite for manufacturing of high-value medicines with stringent quality attributes. Different groups are working towards incorporating monodisperse droplet generators (MDGs) within spray drying to produce uniform particles (151,163). However, thus far the commercial adoption of this technique by the pharmaceutical industry is very limited potentially due to reasons such as complexity of the process, low productivity, collision and coalescence between uniform droplets and high vulnerability to blockages.

Therefore, it is believed that developing a spray dryer with the capability to produce monodisperse non-agglomerated particles will allow manufacturers to create new pharmaceutical products with added value and functionality by design. A new lab-scale spray dryer equipped with an MDG atomiser was designed and built in our laboratories at Aston University to achieve this goal. This included testing different designs and overcoming the process challenges, e.g. chamber length, airflow patterns, atomiser requirements such as cooling jacket, and most importantly the reduction of droplet-droplet interactions to ensure a non-agglomerated, highly flowable powder production. Details of hardware design and fabrication procedures will be presented in the following sections of this chapter.

3.2. Experimental set-up and methodology:

3.2.1. Single-stream spray dryer design:

The single-stream spray drying system was designed based on atomising a uniform stream of droplets into a co-current laminar airflow environment. Generally, using a laminar airflow helps to control droplets' trajectories and ensures stream stability, leading to less interactions between droplets and of droplets with the chamber wall during the spray drying process. The outcome of this would be to improve the final powder monodispersity. For this purpose, a new spray dryer enclosure 'the crown' suitable for holding the MDG atomiser in place has been fabricated and provided with an air diffuser unit (perforated plate) for generating co-current laminar airflow directed vertically downwards onto the drying chamber. The chamber itself consisted of two parts: a top cylindrical glass chamber (OD 165 mm × L 1500 mm) made from borosilicate glass 3.3 (Duran®, Dixon Glass Ltd, Kent, UK) connected with a bottom stainless steel 316 L conical part

of approximately 356 mm in height (Concentric reducer, Tri-Clamp connections with sizes: 6 × 1.5 in. and with length: 14 in., Advanced Couplings Ltd, West Yorkshire, UK) (Figure 3.1).

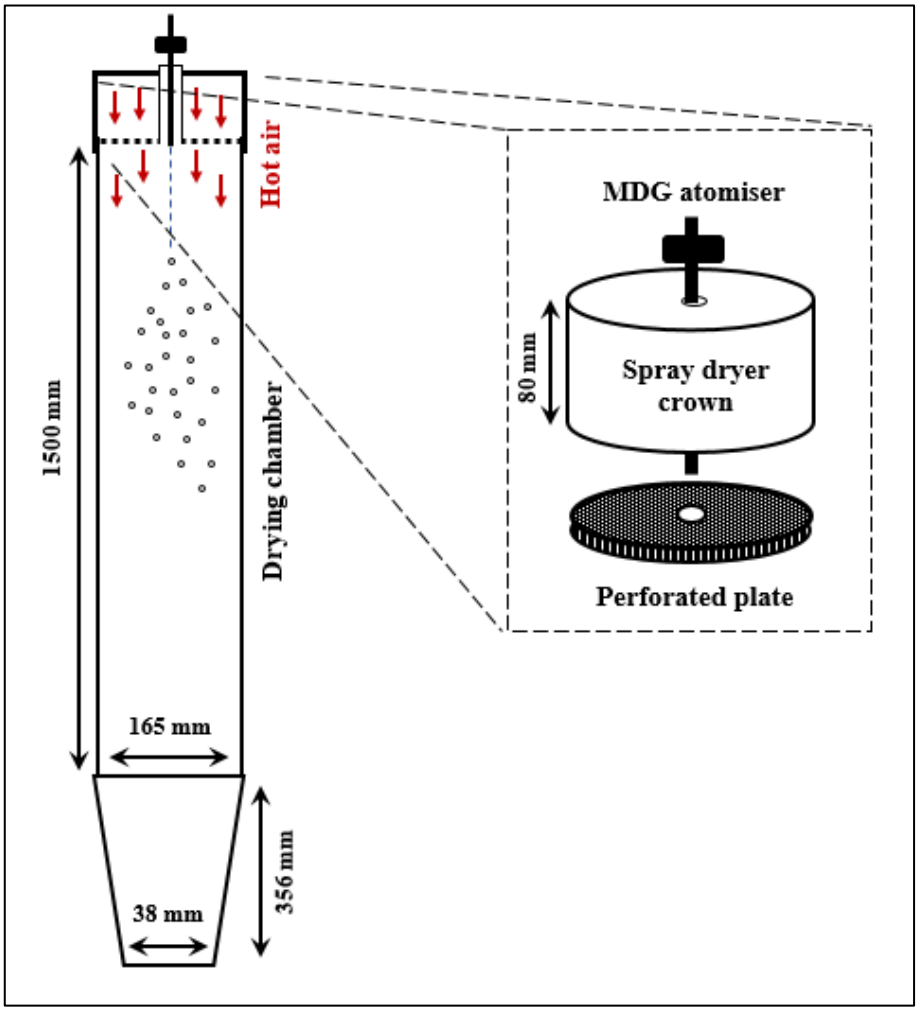

Figure 3.1: Schematic diagram of the single-stream spray drying system (the initial prototype).

This initial prototype has been constructed in the laboratory as follows. The lower metal part of the MDG atomiser was inserted in the centre of the air diffuser unit at the top of the drying chamber so that the MDG tip and the lower part of the perforated plate are centred on matching the vertical axis of the drying chamber, as seen in Figure 3.2. The heater and air blower (aspirator) of a BUCHI B-190 mini spray dryer (Labortechnik AG, Flawil, Switzerland) were used to pump hot drying air to the crown's air diffuser unit and then to the rest of the drying chamber using an aluminium heat-resistant hose. The drying process parameters such as drying airflow rate (approximately 30 to 60 m^3/h) and inlet temperature (50 to 220 ºC) were adjusted using the control panel of the Buchi device. The powder was collected through a standard Buchi cyclone. Further information about the cyclone dimensions is available in the literature (208).

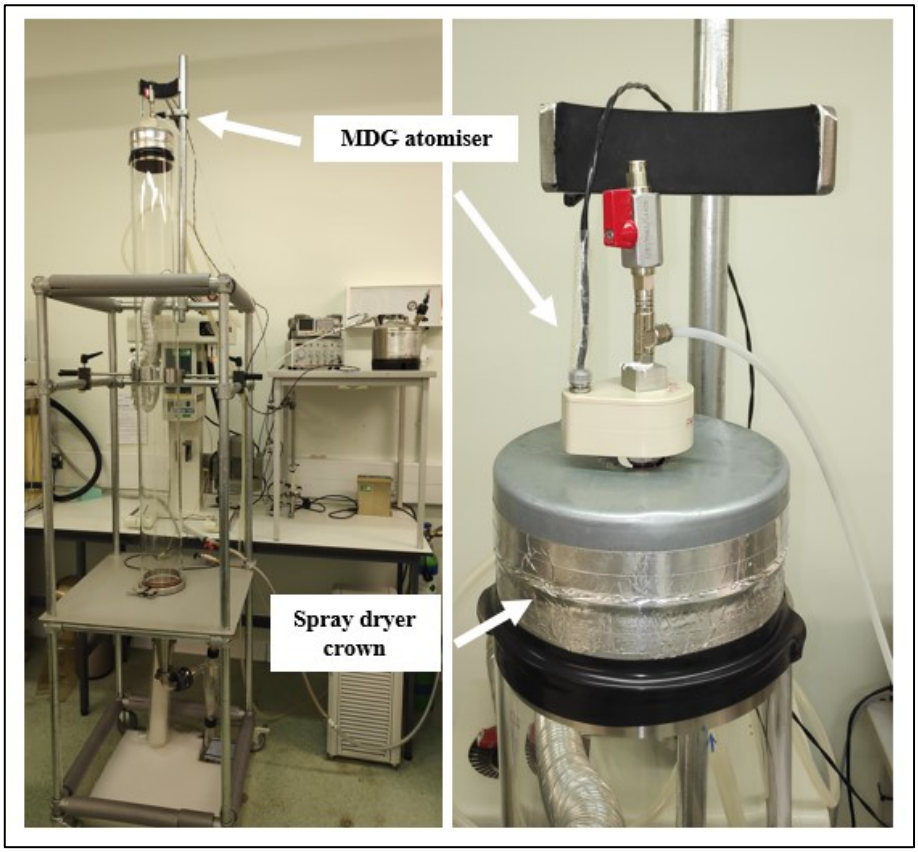

Figure 3.2: Photographs for the initial prototype of the single-stream spray dryer.

In this work, the initial prototype's capacity for generating spray-dried (SD) particles with high monodispersity and good powder recovery was investigated using different processing conditions. Subsequently, the final single-stream spray drying system has been designed and constructed after several iterations and sequential updates of the initial prototype. The following factors were considered for successful spray-dried monodisperse particles production: 1) the dimensions of the drying chamber to ensure that atomised uniform droplets have sufficient residence time for drying with no deposition on the chamber wall, 2) stability of MDG performance in generating monodisperse droplets without any potential clogging when it is operated in a hot drying air environment, 3) interaction among uniform droplets (i.e. through collisions and coalescence) and 4) generating uniform spray-dried particles with good powder recovery. A schematic diagram and photographs of the final single-stream spray dryer prototype are shown in Figures 3.3-3.5.

The new apparatus comprises of several parts that are highlighted in Figure 3.3. However, there are five key elements that were crucial for the successful operation of this prototype. These were the MDG atomiser (component 2 in Fig 3.3), MDG accessories (dispersion air tube and cooling jacket, components 11 and 12), spray dryer crown with perforated plate (components 3 and 13), drying chamber (component 4), and particle collection cyclone (component 5). All MDG accessories for atomiser cooling and droplet dispersing purposes were assembled within the spray dryer crown. In this design, the main body of the MDG atomiser can be inserted safely into the cooling jacket and placed in the centre of the spray dryer crown in such a

way that the orifice of the MDG and the centre of the perforated plate (air distribution plate) matched with the centre vertical axis of the drying chamber. The cooling jacket (also shown in Figure 3.17) is equipped with two ports, one for the input of cooling water and one for output. A recirculating cooler (FL601, Julabo GmbH, Seelbach, Germany) was used to pump the water to the cooling jacket. During all spray drying experiments, the water was circulated into the jacket body at a flow rate of 23 L/min and a temperature of 25ºC.

For dispersing the monodisperse droplets stream generated by MDG, pulsating air is introduced through a bent copper tube (ED: 3mm, ID: 2mm; bend angle of 90º) constructed around the cooling jacket i.e. 'dispersion air tube' (component 11 in Figure 3.3 and bottom view of Figure 3.4), so the tube's outlet is fitted very close to the MDG tip.

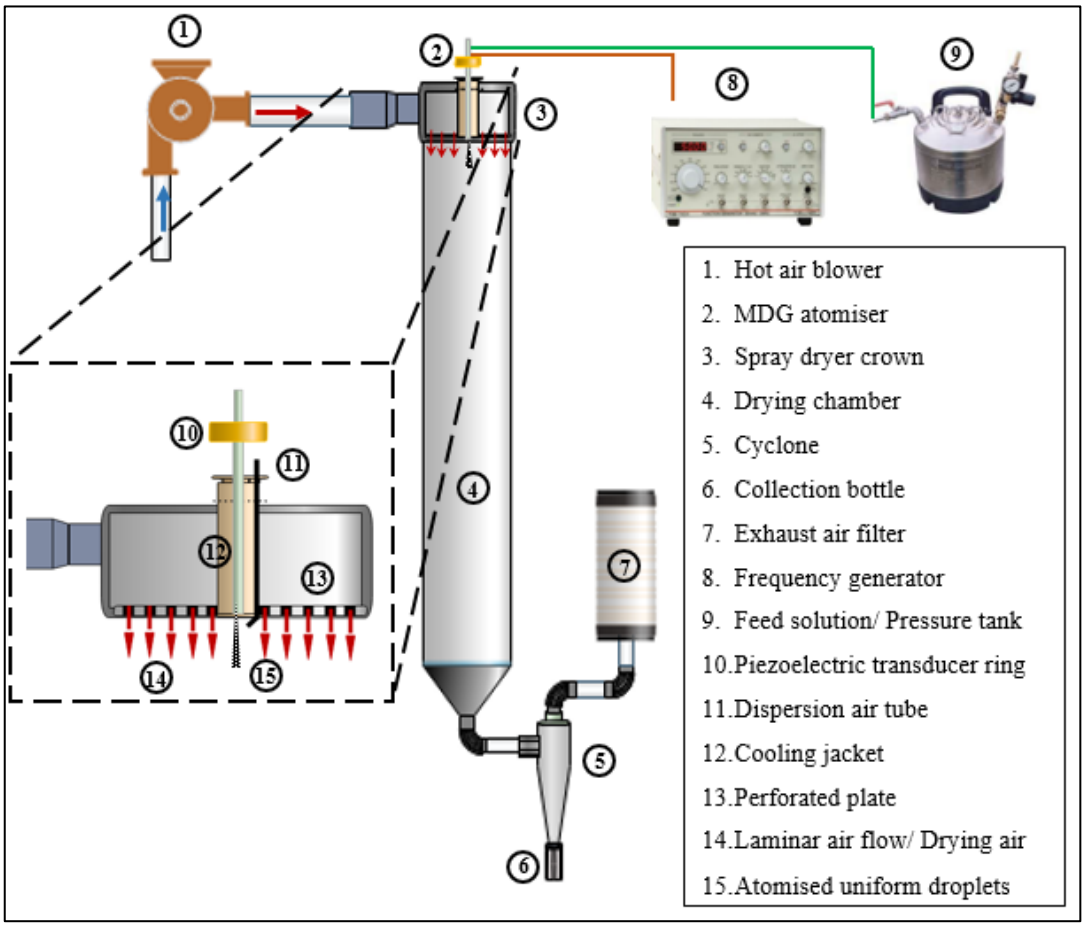

Figure 3.3: Schematic diagram of a new single-stream spray drying system.

The crown unit is made from galvanised steel and contains the cooling jacket, dispersion air tube and perforated plate. The laminar airflow tubes making the perforated plate are made from stainless steel and have the following dimensions: 2 mm (ID), 3 mm (ED), and 30 mm in height. They help to reduce the velocity of the incoming drying air and produce laminar airflow streams. The crown is symmetrically mounted onto the top of the drying chamber, as seen in Figures 3.3 and 3.4.

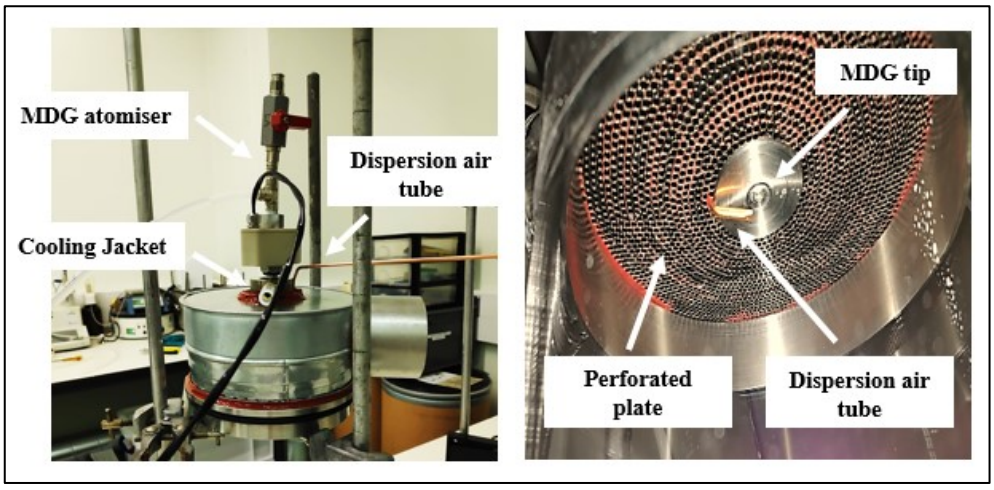

Figure 3.4: Photographs of newly fabricated crown for single-stream spray dryer apparatus: left image and right image show the crown's side view and bottom view, respectively. The new crown was provided with a cooling jacket, dispersion air tube and perforated plate to enhance the conversion of the monodisperse droplets generated by MDG atomiser into uniform particles through reduction of droplet collisions and coalescence.

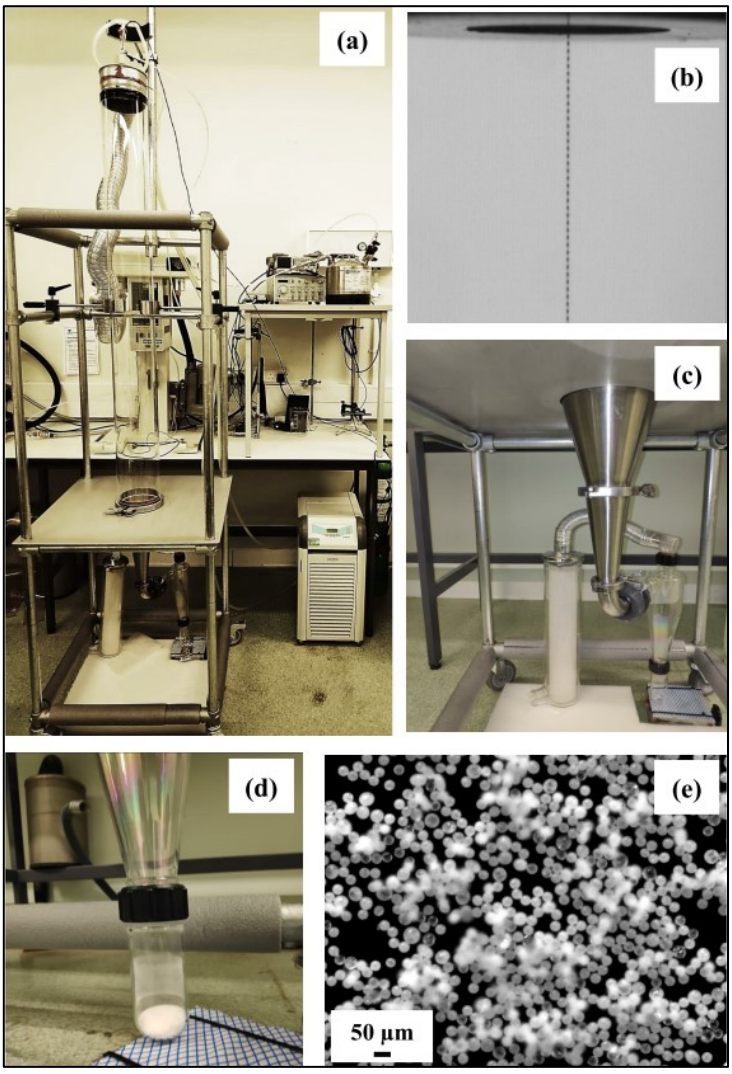

Figure 3.5: Photographs of a new single-stream spray drying system: a) the whole mounting system, b) single stream of monodisperse droplets generated by 35µm MDG orifice, c) Conical part, standard cyclone, and filter, d) collection bottle contained monodisperse powder particles, and e) SEM images for monodisperse spray-dried particles.

The drying chamber dimensions were the same as that of the initial prototype (Figure 3.1). The bottom of the conical reducer is connected to a standard Buchi cyclone with a collection bottle for spray-dried particle recovery via an elbow connection (Figure 3.5). During the spray drying process, the droplet size generated from the MDG could be controlled by tuning the operation parameters (e.g. frequency, feed flow rate, etc., as depicted previously in more detail in chapter 2). The blower's drying air was introduced horizontally through an annular hose connection into the crown. The air flowed inside the crown surrounding the MDG cooling jacket before being distributed into multiple laminar flow streams to the drying chamber through the perforated plates. The drying airflow rate is controlled and recorded digitally by a flow meter (drying airflow capacity can be set from 30 to 60 m^3/h). The new single-stream spray dryer is provided with two thermocouples (K-type, 6mm in diameter) to measure the inlet and outlet temperatures during the spray drying process. One is placed inside the dryer crown for measuring inlet temperature, and another is inserted in the drying chamber elbow fitting for measuring the outlet temperature. The heating temperature range can be controlled from 50 to 220ºC.

The initial and final prototypes were assembled using various components designed in the laboratory and several parts purchased from the market. Most materials used for the construction of this prototype were of pharma grade e.g. stainless steel 316 L, borosilicate glass 3.3. The experimental setup is constructed on a portable stainless-steel frame at Aston University.

3.2.2. Testing of the designed prototypes:

3.2.2.1. Spray-drying experiments and microparticles formation:

Aqueous solutions of metformin HCl at high concentrations (20% and 15%, w/v) were used for testing the prototypes. Streams of mono-sized droplets were ejected from 35 and 50 µm MDG pinholes using different feed pressures (feed flow rate ml/min) with optimal vibration frequencies (KHz). The mechanical vibrations applied on the MDG liquid jet were generated using square wave signals from a function generator (TOELLNER 7404, GmbH, Germany). The spray drying process was performed under a laminar airflow with a co-current set-up. The performance of the initial prototype for generating monodisperse spray-dried particles was tested using different drying conditions, including aspiration/airflow rates (30 to 60 m^3/h) and inlet temperatures (200 to 220ºC). Before starting the atomisation process, the system was preheated with hot air to the desired drying temperature. Subsequently, liquid solution was fed into the MDG at different flow rates (up to 2 ml/min). Finally, the powder in the collection bottle was weighed to evaluate the percent powder recovery/yield using the equation below:

$$\text{Process yield (\%)} = \frac{\text{Mass of solids after spray drying}}{\text{Mass of solids before spray drying}} \times 100 \qquad (3.1)$$

3.2.2.2. Droplets monitoring during the spray drying process:

MDG atomiser can generate a stream of uniform droplets with adjustable size and droplet spacing when used at optimal operation conditions (feeding pressure, atomiser orifice/pinhole diameter, and vibration frequency). To select the optimal parameters, the droplets had to be monitored using an imaging system assembled for this purpose (see chapter 2). In this study, droplet formation and stream stability under the laminar airflow conditions were assessed using this imaging system.

3.2.2.3. Spray-dried particles observation:

The morphology of all spray-dried particles was examined using Zeiss Axio Scope A1 optical microscope (Carl-Zeiss, Oberkochen, Germany). A small powder sample was sprinkled onto a glass microscope slide and examined using an X10 magnification lens. Then, optical microscopy images of different powders were taken using a Zeiss Axio camera interfaced with the Zeiss Axio Vision imaging software.

3.3. Results and Discussion:

Producing spray-dried powders with high monodispersity is based on the concept of generating a stream of monodisperse droplets and drying it into particles under controlled gas conditions. In our preliminary studies, integration of a monodisperse droplet generator (MDG) with a benchtop mini spray dryer (BUCHI B-290, Labortechnik AG, Flawil, Switzerland) to generate uniform-sized droplets/particles was investigated. Numerous trials have been conducted using different process conditions with several feed solutions. However, many challenges have been identified with this proposed approach, such as small drying chamber and high droplet velocity not allowing sufficient drying time, turbulent airflow patterns causing droplet interactions, and unstable atomiser performance with frequent blockages. As a result, no spray-dried powders were produced in those initial trials. Therefore, it can be said that generating spray-dried powders by this combination was practically difficult, if not impossible. This led to a conclusion that using the MDG atomiser to produce uniform SD particles requires designing and building of a new spray drying system with unique specifications. An initial prototype of this new spray drying system was fabricated and evaluated as described in the next section.

3.3.1. Creation and evaluation of the initial spray dryer prototype for generating monodisperse particles:

3.3.1.1. Selecting the drying chamber for the new system:

During the spray drying process, successful drying and particle formation depend on understanding the interplay between many parameters, such as drying air temperature, drying airflow rate, droplets size, droplets velocity and feed concentration. This is because these parameters have a critical impact on the evaporation rate of the solvent and ultimately on the performance of the resulting particles (141,209). However, the behaviour of the spray drying process is also affected by the drying chamber geometry, which

should be selected appropriately to minimise droplet-wall collisions and provide adequate residence time for droplets to dry completely (210). For example, the droplet residence time decreases significantly with increasing its size and velocity. The short residence time leads to incomplete evaporation of the solvent/droplet due to a low heat exchange between the drying air and atomised droplets. Thus, if the drying chamber does not have an appropriate length, the atomised droplets sprayed into the drying chamber may not have sufficient residence time for drying, which ultimately affects the final powder recovery and product quality (211). Therefore, obtaining information regarding the atomisation characteristics and drying conditions is essential to design and fabricate a spray drying system with good powder recovery.

When comparing MDG to conventional atomisers, it is clear that there is a massive difference in specifications of the generated droplets. For example, the polydisperse droplets generated by a two-fluid nozzle have an initial velocity of 0.1 and 5.0 m/s for laboratory and industrial-scale spray dryers, respectively (212). In contrast, the initial velocity of the monodisperse droplets generated by the MDG atomiser provided with a 50 μm pinhole is around 8 to 10 m/s, as clarified previously in chapter 2. Thus, when designing a single-stream spray dryer, a large enough distance is needed between the MDG tip and the bottom of the drying chamber to enhance the drying process for the monodisperse droplets. In the new fabricated spray dryer, a cylindrical glass chamber (165 ×1500 mm) connected with a stainless-steel conical part of 356 mm in height has been used as a drying chamber. This set-up is also used in the final prototype design of the single-stream spray dryer as particles were dry at the end of the chamber, and its dimensions allowed relatively easy handling and cleaning.

3.3.1.2. Design of air diffuser:

Turbulent airflow during the spray drying process usually leads to some issues, including unsteady (oscillation) flow of the droplets stream, unpredictable droplet trajectory, more droplet collisions, and more droplet-wall deposition. To avoid these issues, a new spray dryer crown provided with an air diffuser unit has been designed to ensure a laminar airflow is directed vertically downward into the drying chamber. Generally, the behaviour of a gas flowing inside any pipe depends fundamentally on understanding the dynamic gas properties, especially its Reynolds number (Re), which helps in estimating whether the airflow is laminar or not, as seen in Figure 3.6 below. If the Re number is equal to or below 2300, the airflow pattern is laminar, whereas if the Re is equal to or above 4000, the airflow pattern will be turbulent.

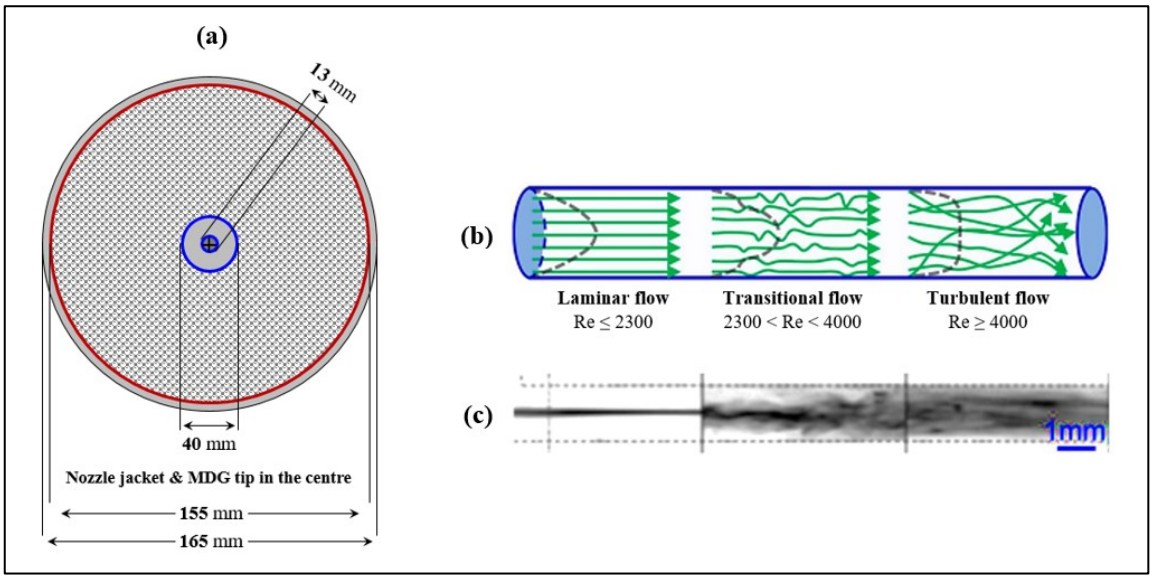

Figure 3.6: a) Structure of a perforated plate made from 2208 small stainless-steel tubes with the following dimensions: 2 mm (ID), 3 mm (ED) and 30 mm in height, b) Schematic presentation of the transition from laminar to turbulent airflow according to Reynolds number (Re) calculations, and c) Macroscopic images of flow pattern alteration obtained by increasing Re number value. (b-c) Reproduced with permission from (213); copyright 2019 MDPI.

In light of this, a perforated plate made from small tubes (2 mm internal diameter) has been fabricated and tested in order for droplets to fall in the central vertical axis of the chamber and achieve a uniform drying profile inside the chamber (Figure 3.6 above). According to the calculated Reynolds number at different drying air velocities, the airflow pattern inside the drying chamber was laminar even when increasing the aspiration/airflow rate from 50 to 100% (approximately 30 to 60 m^3/h) (Table 3.1).

Table 3.1: Characteristics of airflow generated from the perforated plate with 2208 small holes.

Aspirator	Airflow velocity	Re	Flow type*
50 %	1.14 m/s	28.02	Laminar
75 %	1.76 m/s	43.27	Laminar
100 %	2.38 m/s	58.51	Laminar

Note: The airflow rate values were provided by the manufacturer (BUCHI). The diameter of the air diffuser plate and spray dryer chamber is 165 mm. At 200ºC inlet temperature, air density and dynamic air viscosity are 0.3163 kg/m^3, 25.73×10^{-6} kg/m.s, respectively. So, the Reynolds number (Re) values can be calculated using the equation: $Re = \rho.V.D/\mu$, where ρ, V, D and μ are the air density, the airflow velocity, the holes diameter (2 mm), and the dynamic air viscosity, respectively. The flow is laminar when Reynolds number (Re) ≤ 2300, transient when 2300 < (Re) <4000, and turbulent when (Re) ≥ 4000.

3.3.1.3. Investigating the effect of laminar airflow on the stability of the monodisperse droplets stream:

The droplets' behaviour under different airflow rates (0, 30, 45, and 60 m^3/h) was tested to identify the most suitable conditions for spray drying. Several images for the droplet stream were taken at different distances from the MDG atomiser tip. As seen in figures (3.7-3.14) below, increasing the airflow rate for the drying air from 0 to 60 m^3/h did not negatively impact on the stability of the monodisperse droplet stream at both feed pressures of 0.5 and 1.0 bar. This could be attributed to the nature of the laminar drying air streamlines (air columns) surrounding the uniform droplets. However, as seen in Figures (3.7 – 3.14), the monodisperse droplets started to collide 2 to 4 cm along the stream and thus created larger droplets through coalescence. This is the case even when using an increasing airflow rate from 30 to 60 m^3/h.

Although there is less collision and coalescence with laminar airflow as compared to turbulent airflow, there is a threshold past which colliding and coalescence behaviour of droplets seems to be independent of airflow. In other words, laminar airflow substantially decreased the collision and calescence behaviour to a level but did not entirely mitigate it. This is likely because apart from airflow, there are other factors at play which collision and coalescence are dependent upon, including the kinetic energy of droplets as a function of droplet size and velocity. To elaborate, as the first droplet leaves the nozzle, it faces maximum friction against the air through which it moves in. This droplet would also shield any droplets that follow. Thus, the droplets ejected first move slower than those which follow, allowing the latter to catch up, potentially resulting in collisions and coalescence of droplets. These results are consistent with previous reports (171,214), where the researchers illustrated that a vertical monodisperse droplets catch-up usually starts after a distance from the atomiser tip of 500-1000 jet diameters (173). However, to minimise the effect of droplet collision and coalescence on monodisperse particle formation during the drying spray process, some solutions could be implemented.

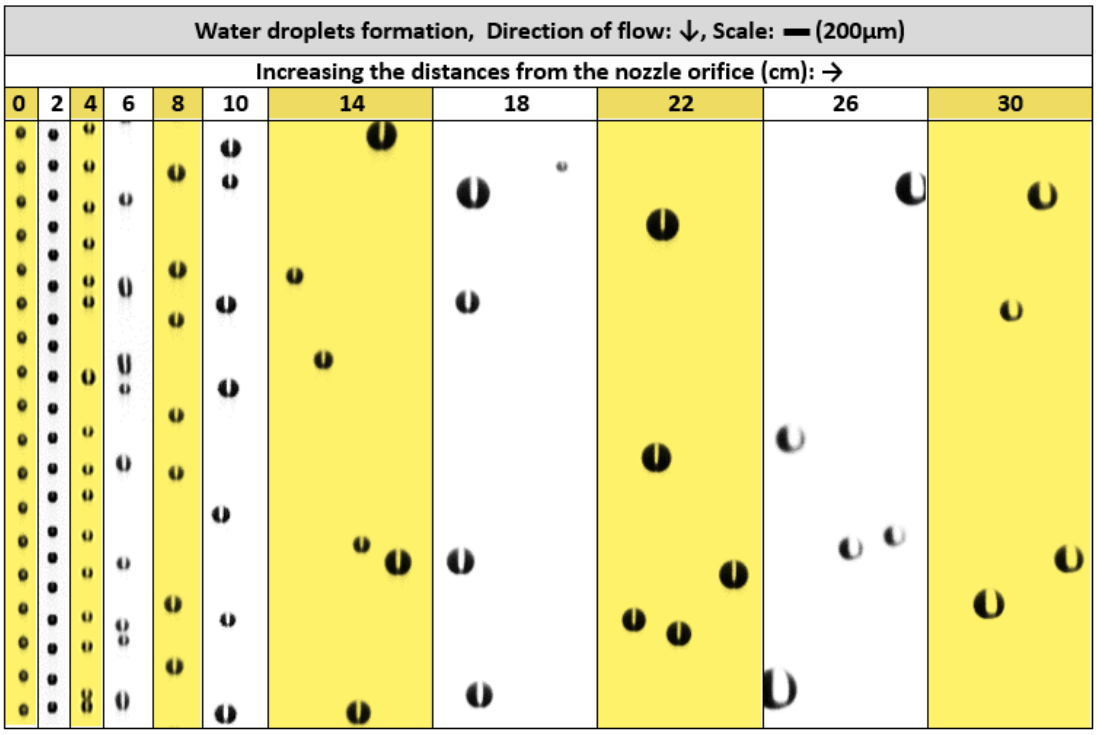

Figure 3.7: Images of a single monodisperse droplets stream generated from 50 µm MDG orifice with feed pressure at 0.5 bar and vibration frequency at 30 KHz. Water droplets were generated during the spray drying process with no airflow rate (i.e. 0 m^3/ h or aspiration rate of 0%). The larger droplets seen after 2 to 4 cm distance from the nozzle tip are an indication that smaller droplets have coalesced into larger ones. All images were taken using a Computar lens with a resolution of 5 megapixels.

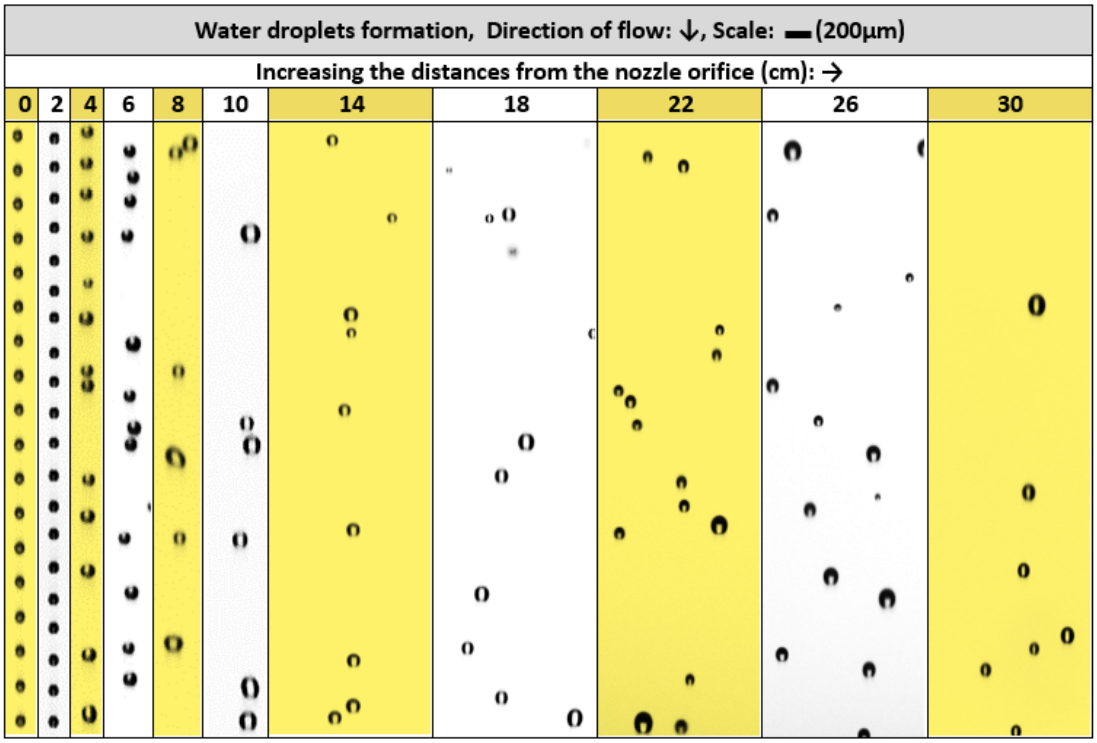

Figure 3.8: Images of a single monodisperse droplets stream generated from 50 µm MDG orifice with feed pressure at 0.5 bar and vibration frequency at 30 KHz. Water droplets were generated during the spray drying process with a co-current laminar airflow rate of 30 m^3/h (aspiration rate of 50%). The larger droplets seen after 2 to 4 cm distance from the nozzle tip are an indication that smaller droplets have coalesced into larger ones. All images were taken using a Computar lens with a resolution of 5 megapixels.

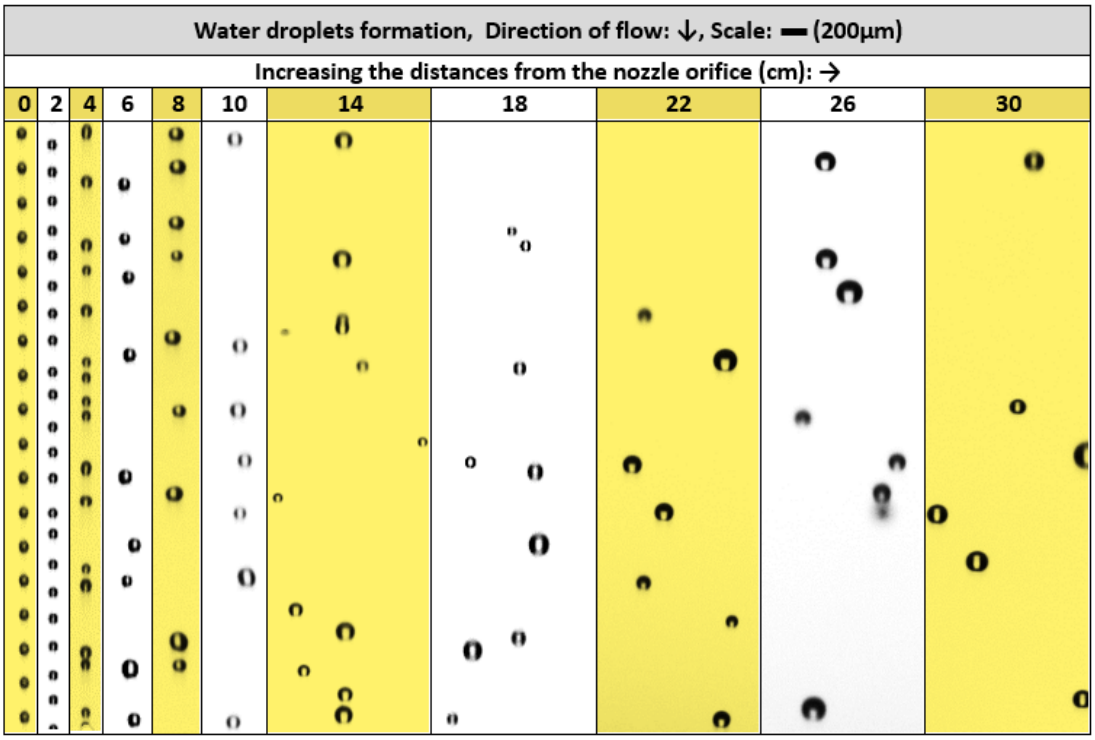

Figure 3.9: Images of a single monodisperse droplets stream generated from 50 µm MDG orifice with feed pressure at 0.5 bar and vibration frequency at 30 KHz. Water droplets were generated during the spray drying process with a co-current laminar airflow rate of 45 m^3/h (aspiration rate of 75%). The larger droplets seen after 2 to 4 cm distance from the nozzle tip are an indication that smaller droplets have coalesced into larger ones. All images were taken using a Computar lens with a resolution of 5 megapixels.

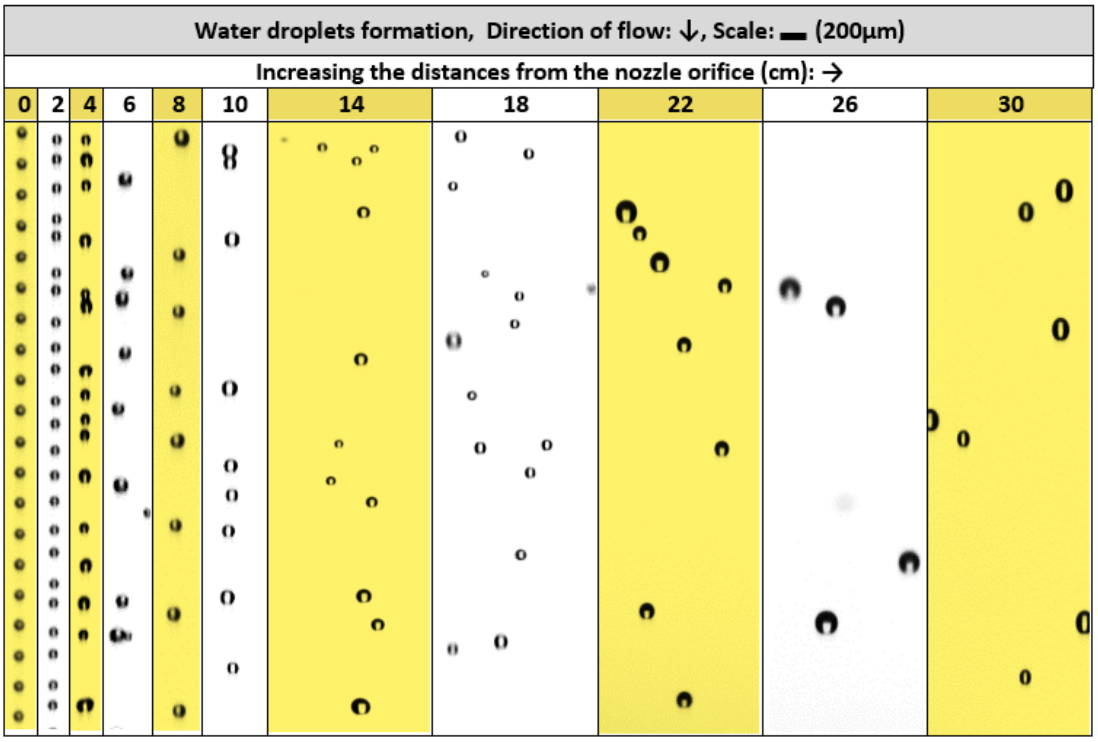

Figure 3.10: Images of a single monodisperse droplets stream generated from 50 µm MDG orifice with feed pressure at 0.5 bar and vibration frequency at 30 KHz. Water droplets were generated during the spray drying process with a co-current laminar airflow rate of 60 m^3/h (aspiration rate of 100%). The larger droplets seen after 2 to 4 cm distance from the nozzle tip are an indication that smaller droplets have coalesced into larger ones. All images were taken using a Computar lens with a resolution of 5 megapixels.

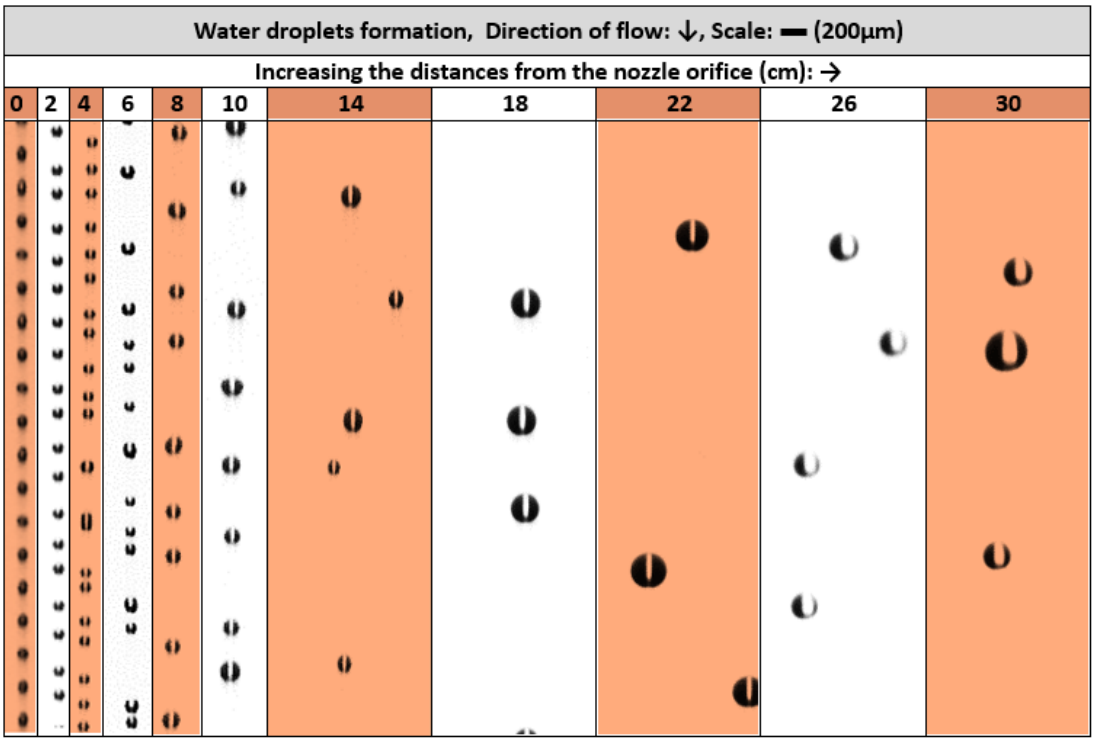

Figure 3.11: Images of a single monodisperse droplets stream generated from 50 µm MDG orifice with feed pressure at 1.0 bar and vibration frequency at 45 KHz. Water droplets were generated during the spray drying process with a co-current laminar airflow rate (0 m^3/h) and aspiration rate of 0%. The larger droplets seen after 2 to 4 cm distance from the nozzle tip are an indication that smaller droplets have coalesced into larger ones. All images were taken using a Computar lens with a resolution of 5 megapixels.

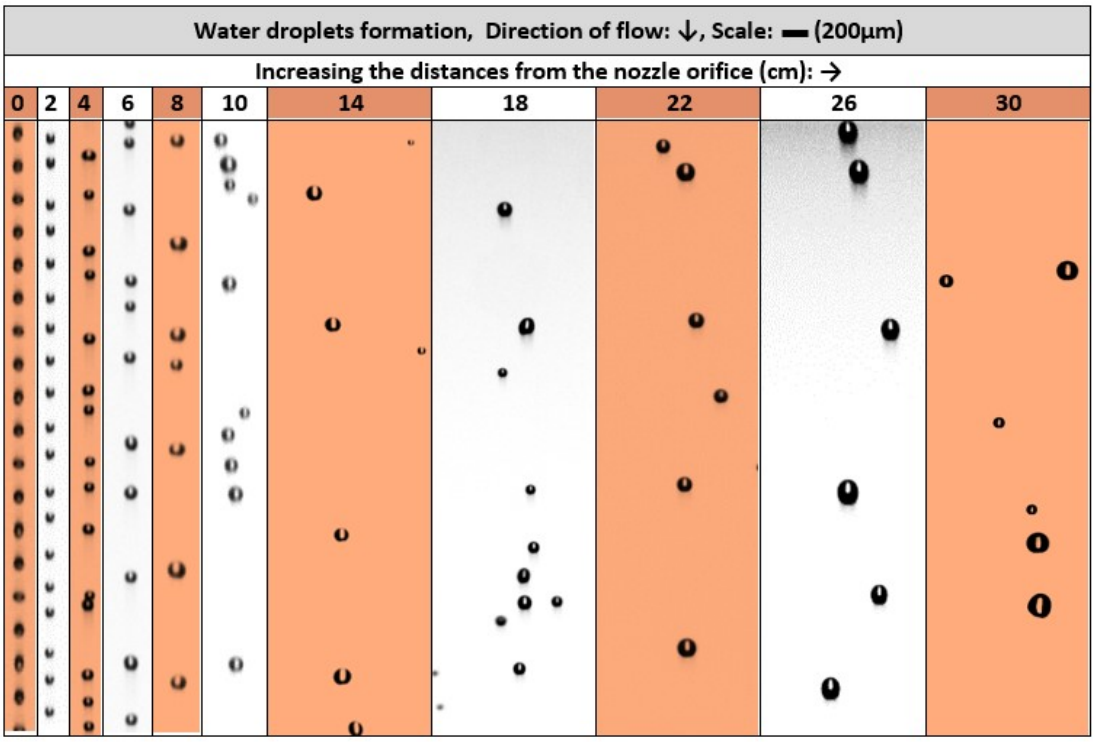

Figure 3.12: Images of a single monodisperse droplets stream generated from 50 µm MDG orifice with feed pressure at 1.0 bar and vibration frequency at 45 KHz. Water droplets were generated during the spray drying process with a co-current laminar airflow rate of 30 m^3/h (aspiration rate of 50%). The larger droplets seen after 2 to 4 cm distance from the nozzle tip are an indication that smaller droplets have coalesced into larger ones. All images were taken using a Computar lens with a resolution of 5 megapixels.

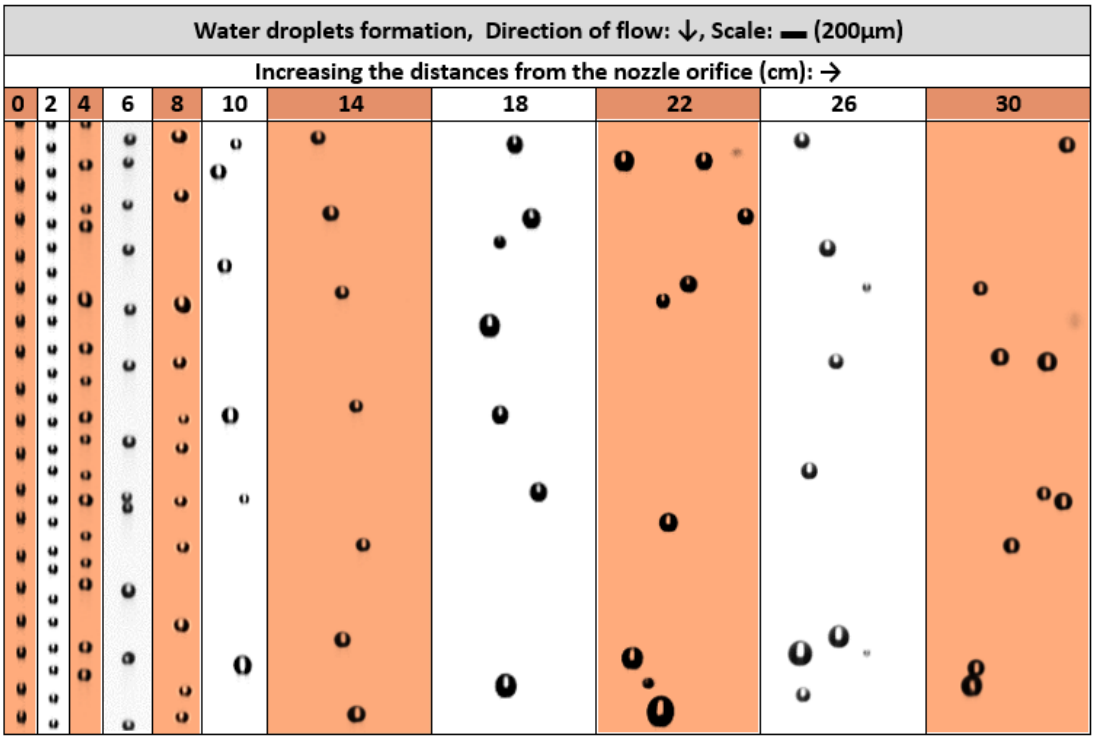

Figure 3.13: Images of a single monodisperse droplets stream generated from 50 µm MDG orifice with feed pressure at 1.0 bar and vibration frequency at 45 KHz. Water droplets were generated during the spray drying process with a co-current laminar airflow rate of 45 m^3/h (aspiration rate of 75%). The larger droplets seen after 2 to 4 cm distance from the nozzle tip are an indication that smaller droplets have coalesced into larger ones. All images were taken using a Computar lens with a resolution of 5 megapixels.

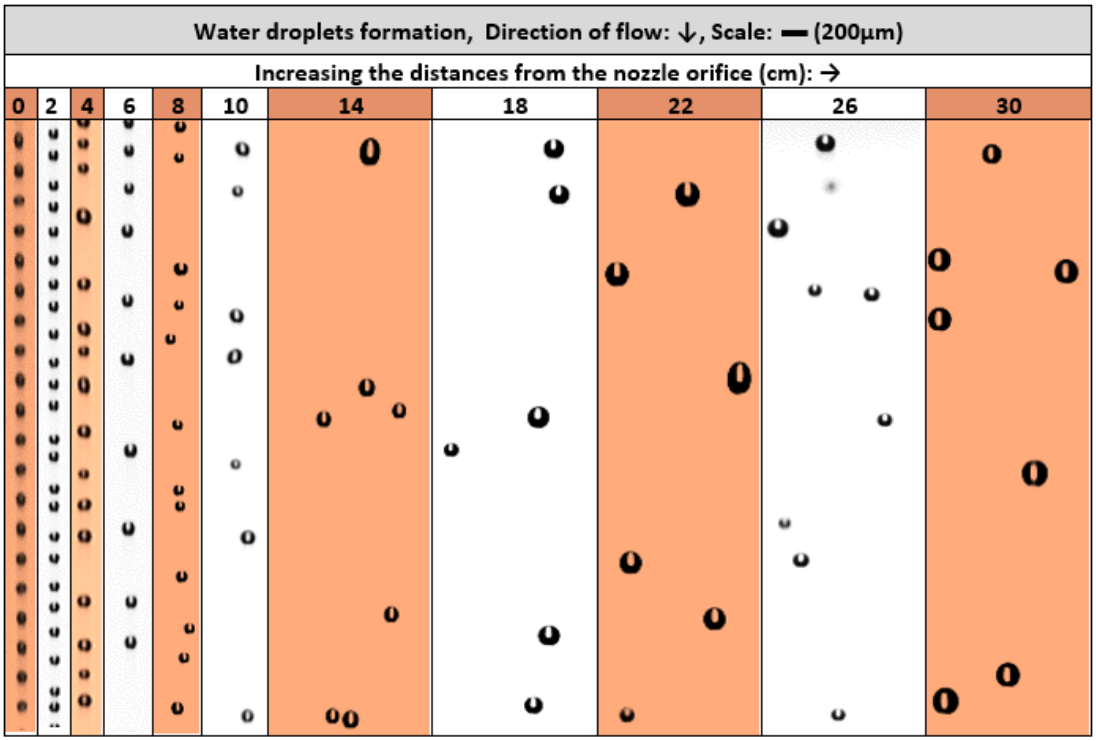

Figure 3.14: Images of a single monodisperse droplets stream generated from 50 µm MDG orifice with feed pressure at 1.0 bar and vibration frequency at 45 KHz. Water droplets were generated during the spray drying process with a co-current laminar airflow rate of 60 m^3/h (aspiration rate of 100%). The larger droplets seen after 2 to 4 cm distance from the nozzle tip are an indication that smaller droplets have coalesced into larger ones. All images were taken using a Computar lens with a resolution of 5 megapixels.

For instance, using very high inlet air temperatures could accelerate the evaporation process to create semi-dried or fully dried particles such that droplets coalescence is minimised when they reach the critical distance for collisions mentioned above (172). Other possible solutions including using a monodisperse droplets generator working with a drop-on-demand mechanism. This mode mechanism can control the number of generated droplets per second, which helps in modifying the droplet-to-droplet distance as required. However, this has the shortfall of very low droplet numbers generated per second and ultimately very low throughput (214). Using a smaller atomiser pinhole to create smaller monodisperse droplets would also be helpful to reduce the droplet-air friction and to improve the drying process. Furthermore, utilising an electrostatic charging probe to neutralize the uniform droplets immediately after being ejected could help to keep the same vertical distance between droplets and prevent them from coalescing (178,215).

3.3.1.4. Investigating the performance of initial prototype in producing monodisperse particles:

The performance of the initial prototype in producing mono-sized particles was investigated whilst using different MDG feed pressures and vibration frequencies. Metformin HCl was chosen as a solute component to prepare a feed solution in this work due to its higher aqueous solubility (216). This would enhance the drying process and generate spray-dried particles with high powder recovery because the amount of water in the generated droplets could be decreased (high initial solid fraction in the droplet). For this, initially 15% (w/v) aqueous metformin HCl solution was used as a feed liquid. According to a preliminary investigation, generating monodisperse droplets using a 20 μm pinhole (the smallest pinhole used for the MDG atomiser) was not possible as no droplet stream was observed using it. The smallest pinhole suitable to produce a stable stream of monodisperse droplets was the 35 μm pinhole and was used for the spray drying process in this work. In these spray drying experiments, even though the drying air heater and aspirator were operated at high inlet temperature (200 to 220ºC) and airflow rate (30 to 60 m^3/h), respectively, most of the droplets were not dried sufficiently by the time they reached the lower part of the drying chamber, leading to deposit formation. As a result, the powder production rate was limited to a few milligrams per hour. Thus, the powder recovery was less than 1%, which is very low when considering bulk production. In addition, the resultant spray-dried (SD) particles exhibited non-uniformity in size and shape. This was the case even when different optimal vibration frequencies and feed flow rates were tested for the atomisation process. For example, monodisperse droplets were ejected from the 35 μm MDG pinhole using the outlet feed pressure of 0.5 or 1.0 bar with different optimal frequency range 15-55 KHz or 25-80 KHz, respectively. However, the microscope images of the collected particles showed that the particle population consisted of polydisperse spherical particles with agglomerates due to droplet-droplet interactions (Figure 3.15).

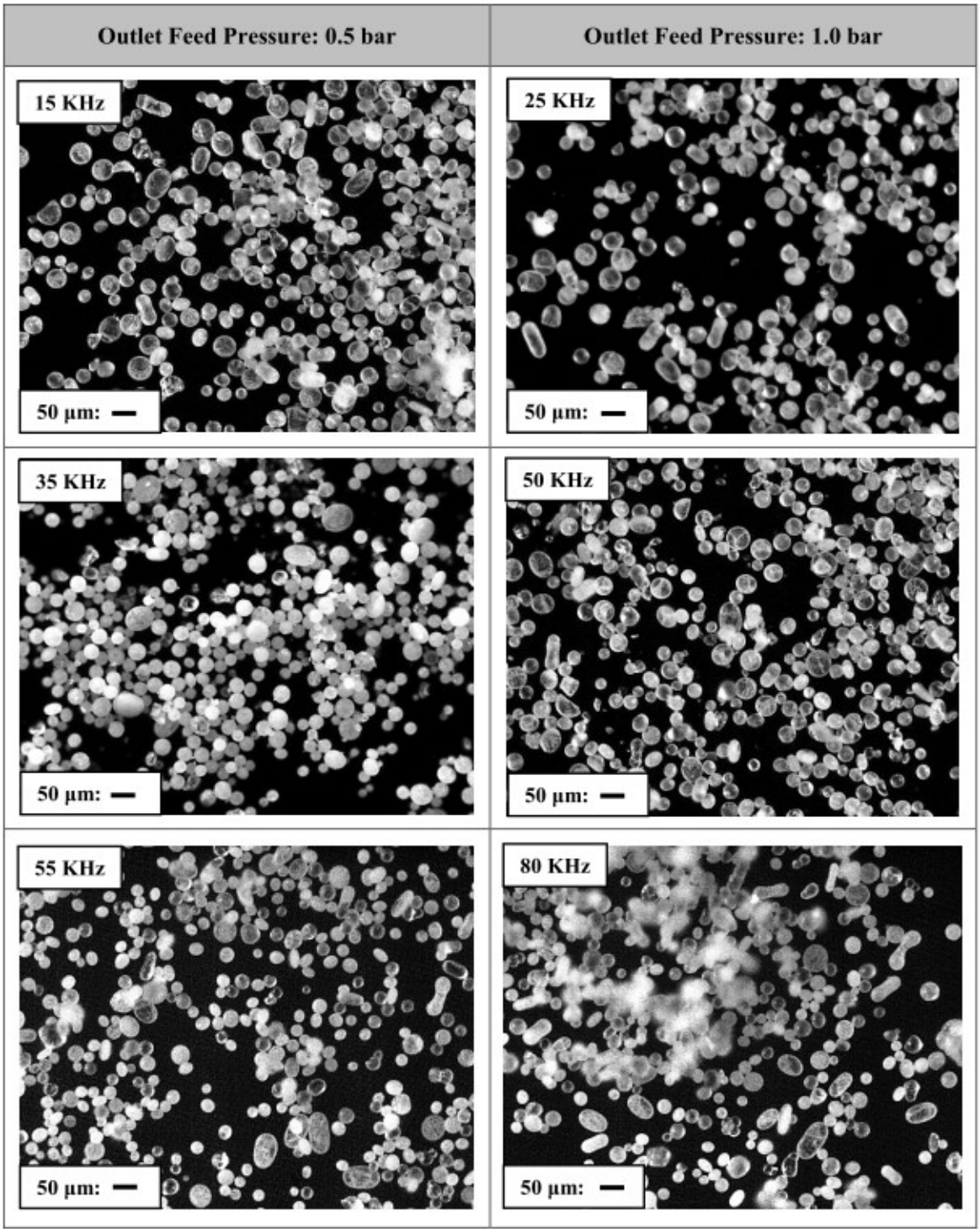

Figure 3.15: Microscope images for the spray-dried metformin HCl particles generated using a 35 µm MDG pinhole with optimal processing conditions. The ejected velocity for the monodisperse droplets generated with the outlet feed pressure of 0.5 and 1.0 bar was around 7 and 9 m/s, respectively. The spray drying process was conducted at the highest inlet and outlet temperatures: 220 and 85ºC, respectively.

In these experiments, even though the initial prototype was operated with the highest inlet and outlet temperatures to improve the drying efficiency (220 and 85 ºC, respectively), the process yield was very low. In addition, when increasing the concentration of the atomised feed solution from 15 to 20% (w/v), the drying efficiency and powder recovery were not enhanced significantly. This was due to a frequent blockage of the nozzle pinhole when a higher feed concentration (20%) was used, and the drying process

was conducted at such high surrounding temperatures which exacerbated the blockages. Even when atomisation of the 20% (w/v) aqueous metformin HCl solution was performed again using a 50 µm MDG pinhole with optimal processing conditions, no powder could be collected in these experiments. This is because monodisperse droplets generated from 50 µm MDG pinhole have a bigger diameter than droplets generated from 35 µm MDG pinhole and were unable to dry over the length of the drying chamber thus accumulating as a solution at the elbow connection section. Three main reasons could explain the previous results. The first is the high velocity of the ejected droplets from the nozzle tip, which reduces residence time for drying and could explain the presence of agglomerates at the lower part of drying chamber. The second is the collision and coalescence phenomena between droplets during falling into the drying chamber, as discussed earlier in this chapter and in chapter two. The third one is the instability of the MDG in generating monodisperse droplets as it was affected negatively by the high inlet temperature. For example, it was found that operating the MDG with a high surrounding temperature (i.e. ~ 200ºC) usually led to several interruptions in the formation of uniform droplets and in many cases, flash-boiling (chaotic) atomisation was noted. This improper atomisation of the feed solution led to fine polydisperse particles but with a high powder recovery of ~ 65%, as seen in Figure 3.16.

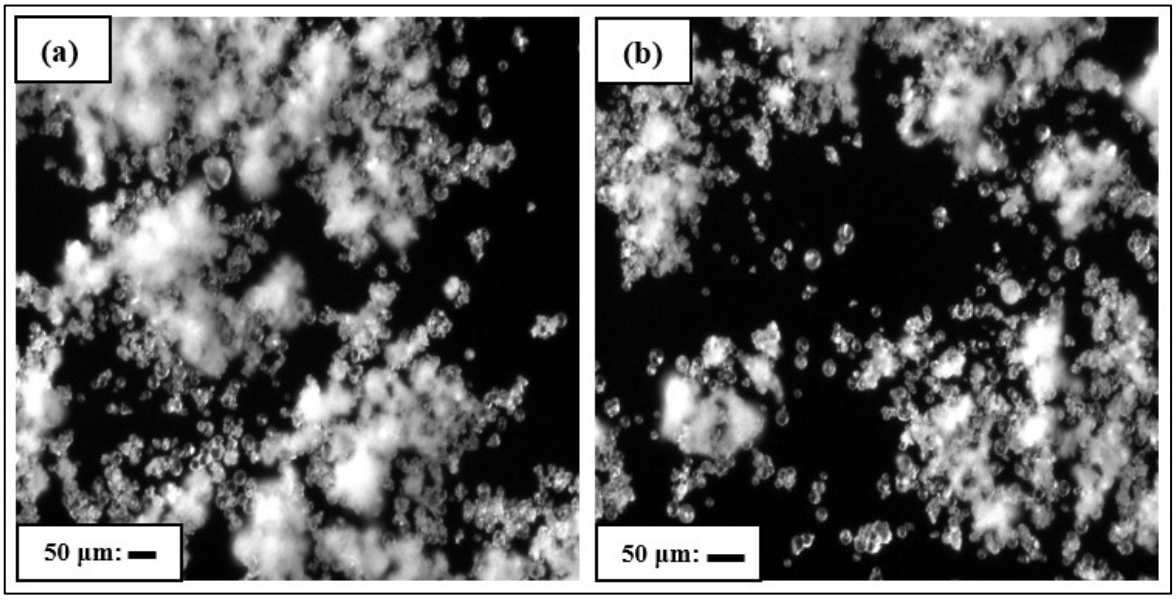

Figure 3.16: Spray-dried metformin HCl particles generated using a 35 µm MDG pinhole with an outlet feed pressure of 0.5 (a) and 1.0 (b), respectively. Atomisation caused by a flashing mechanism when the inlet drying temperature was 220 ºC.

The effect of high temperature on the performance of MDG in generating monodisperse droplets has been cited many times in literature as a critical challenge. Butt and Pasha illustrated that increasing the MDG's piezoceramic transducer's temperature above a critical temperature called 'Curie temperature' decreases its electro-mechanical properties due to depolarisation caused by heat (217). The inception of flashing strongly depends on the level of superheating and bubble formation within the pressurised liquid in the atomiser column (218–220). As a result, using the initial prototype was unsuitable to produce monodisperse

spray-dried particles due to two main challenges: a failure to control monodispersity of the generated droplets and the lack of sufficient residence time required for evaporation. Therefore, to improve the drying operation, maintain monodispersity and minimise the collision behaviour during droplet falling, the atomiser required adjustments to enhance its performance. These enhancements are presented in the next section.

3.3.1.5. MDG atomiser accessories design and fabrication:

After evaluating the MDG performance during the actual spray drying process, it was found that the MDG needs to be assembled with a few accessories to make it more suitable as a spray dryer atomiser. These accessories are a cooling water jacket and a pulsating air system.

- **Cooling water jacket:**

To overcome the flashing atomisation issue and ensure a sustainable performance of the MDG, the surrounding temperature of the atomiser must be constant and controlled during the whole process of spray drying. For this purpose, a cooling stainless steel jacket was designed and fabricated to fulfil this requirement. As seen in Figure 3.17, the lower part of the MDG can be safely inserted into a heated spray dryer crown using this cooling jacket. The upper jacket body was outfitted with cooling ports that allowed cooling water to circulate inside it and keep the MDG atomiser operating at an ambient temperature (25ºC). During practical testing, using the cooling jacket improved the stability of MDG performance through less interruption to atomisation, but also helped to reduce the clogging risk and facilitated the atomiser cleaning.

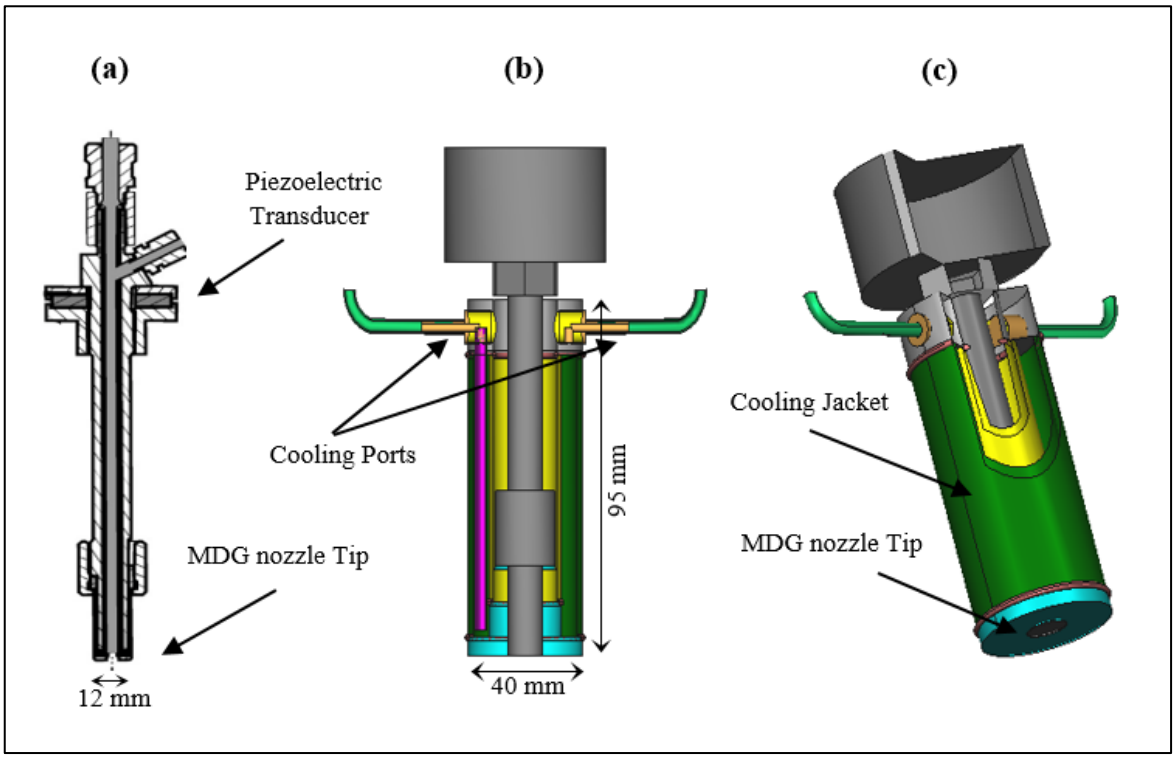

Figure 3.17: a) Schematic structure of the MDG atomiser, b and c) Solidworks CAD drawing of the initial design for the MDG atomiser inserted into the cooling jacket. 3D CAD models were designed using the ABViewer 14 software (https://cadsofttools.com/products/abviewer/).

- **Pulsating air system to disperse the uniform droplets:**

As mentioned before, the uniform droplets usually start to collide after a downstream distance of 500-1000 jet diameters from the MDG tip and thus create larger droplets which are difficult to dry (Figures 3.7 and 3.14). This phenomenon has been noted in several studies regardless of the initial droplet characteristics as long as the droplets have been generated in a continuous mode (173). Therefore, to minimise this problem which affects monodispersity, a stream of pulsating air provided by a dispersion air tube located beside the MDG tip has been used to disperse the uniform droplets ejected from the tip, as seen in Figure 3.18. The pulsating air system produces pulses of air at a frequency of 50 pulses/second. The concept behind this is that each pulse of the produced air will push a group of droplets outside of the stream, helping to minimise the collisions of the droplets with each other whilst increasing the interaction of droplets with the hot air laminar streams to enhance their drying. Continuous dispersion air was trialled prior to selecting pulsating air and was found to have a negative impact on droplet dispersion as it led to droplets gaining significant momentum and hitting the chamber walls.

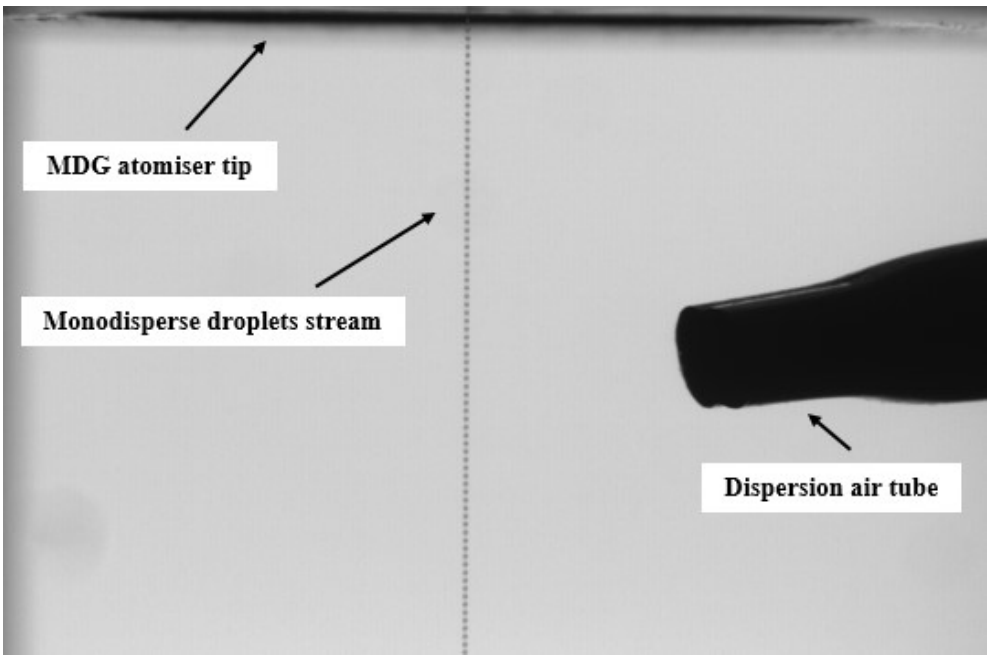

Figure 3.18: A representative photograph showing a stream of uniform droplets before being dispersed by pulsating air. A stream of pulsating air was provided using a small copper tube with an internal diameter of 2 mm and an outer diameter of 3 mm.

Several images for the atomised uniform droplets were also taken using the imaging system to investigate how pulsating air helps to avoid droplet collisions during spray drying. Figures (3.19-3.23) show that using pulsating air during the spray drying process effectively disperses the uniform droplets during their fall into the drying chamber. However, creating ideal dispersion conditions of the falling droplets depends mainly on selecting the dispersion air's flow rate to overcome the droplets kinetic energy and deviate the droplets from their path. For example, dispersing uniform droplets generated with different velocities (feed pressures) requires different dispersion airflow rates. In this project, it was found that using pulsating air with a velocity of 20 m/s was suitable for creating an optimal dispersion in the aqueous stream of uniform droplets generated using 35 μm MDG pinhole with the outlet feed pressure of 0.5 bar (droplets velocity ~ 7 m/s). This could be noticed in Figure 3.23, where the droplets maintained their original size, whereas when other pulsating air velocities were used, e.g. 5-15 m/s, coalesced larger droplets could still be seen (Figures 3.20-3.22).

Similarly, when the droplets were generated with a feed pressure 1.0 bar (droplets velocity ~ 9 m/s), the pulsating airflow velocity should be increased to 25 m/s to have an optimal dispersion in the stream of uniform droplets. Thus, as a general rule a higher droplet velocity means higher pulsating airflow velocity is necessary to ensure the droplet leaves the stream and overcome its initial kinetic energy.

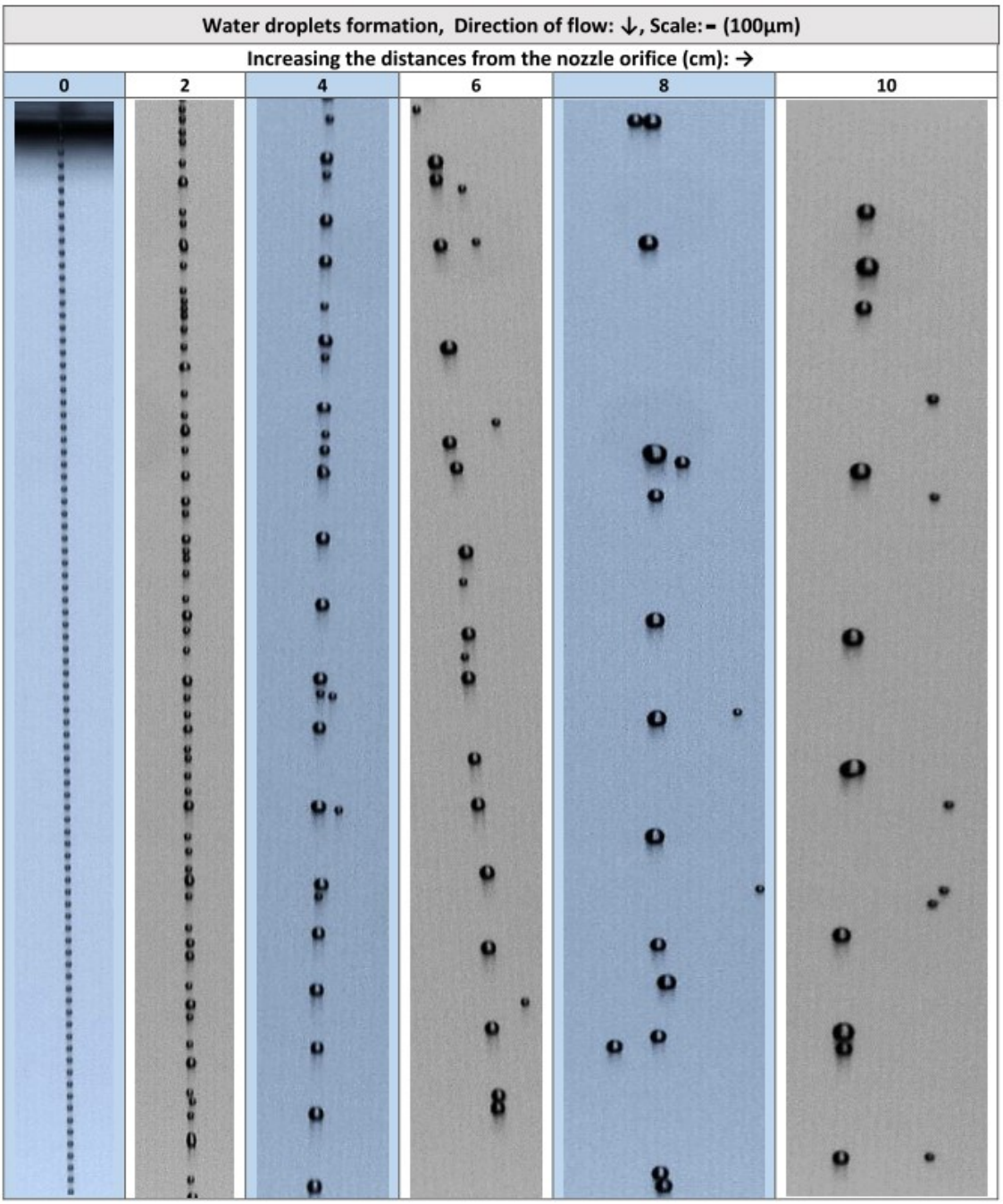

Figure 3.19: Images of the effect of the dispersion air with flow velocity 0 m/s on the stability of monodisperse droplets produced by 35µm MDG orifice with feed pressure at 0.5 bar and vibration frequency 50 KHz. Water droplets were generated during the spray drying process with a co-current laminar flow and aspiration rate of 50%. All images were taken using a Computar lens with a resolution of 5 megapixels.

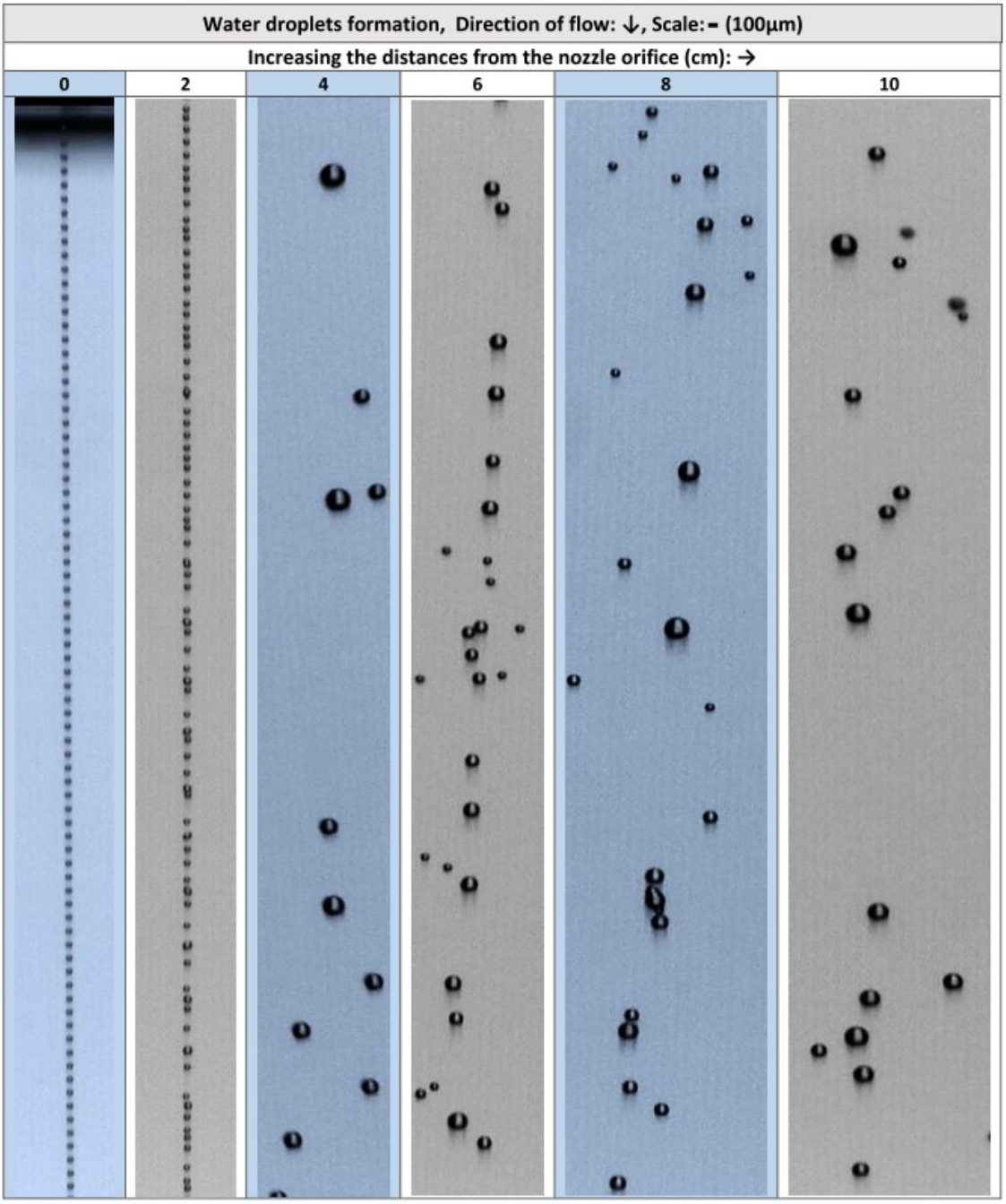

Figure 3.20: Images of the effect of the dispersion air with flow velocity 5 m/s on the stability of monodisperse droplets produced by 35µm MDG orifice with feed pressure at 0.5 bar and vibration frequency 50 KHz. Water droplets were generated during the spray drying process with a co-current laminar flow and aspiration rate of 50%. All images were taken using a Computar lens with a resolution of 5 megapixels.

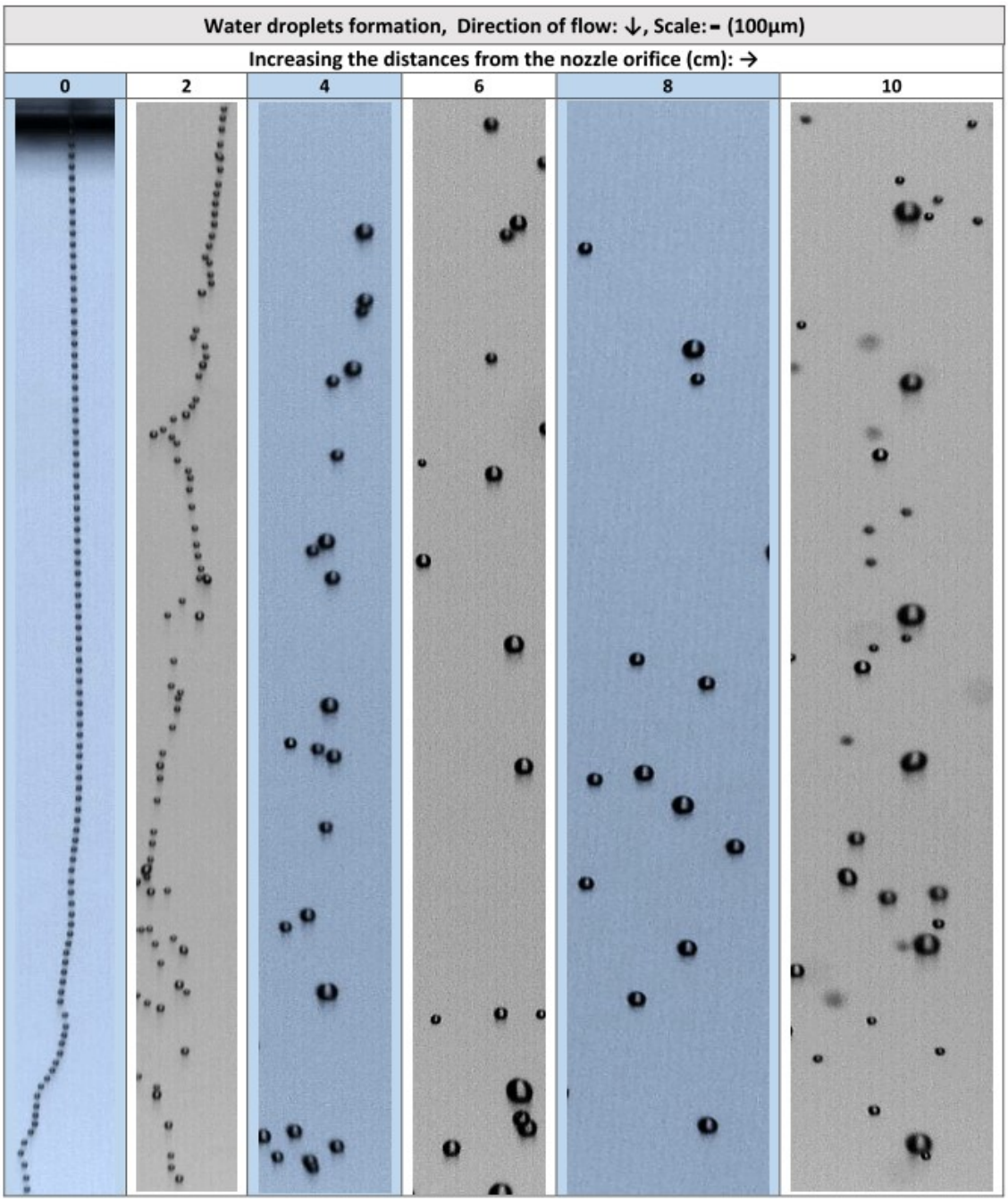

Figure 3.21: Images of the effect of the dispersion air with flow velocity 10 m/s on the stability of monodisperse droplets produced by 35µm MDG orifice with feed pressure at 0.5 bar and vibration frequency 50 KHz. Water droplets were generated during the spray drying process with a co-current laminar flow and aspiration rate of 50%. All images were taken using a Computar lens with a resolution of 5 megapixels.

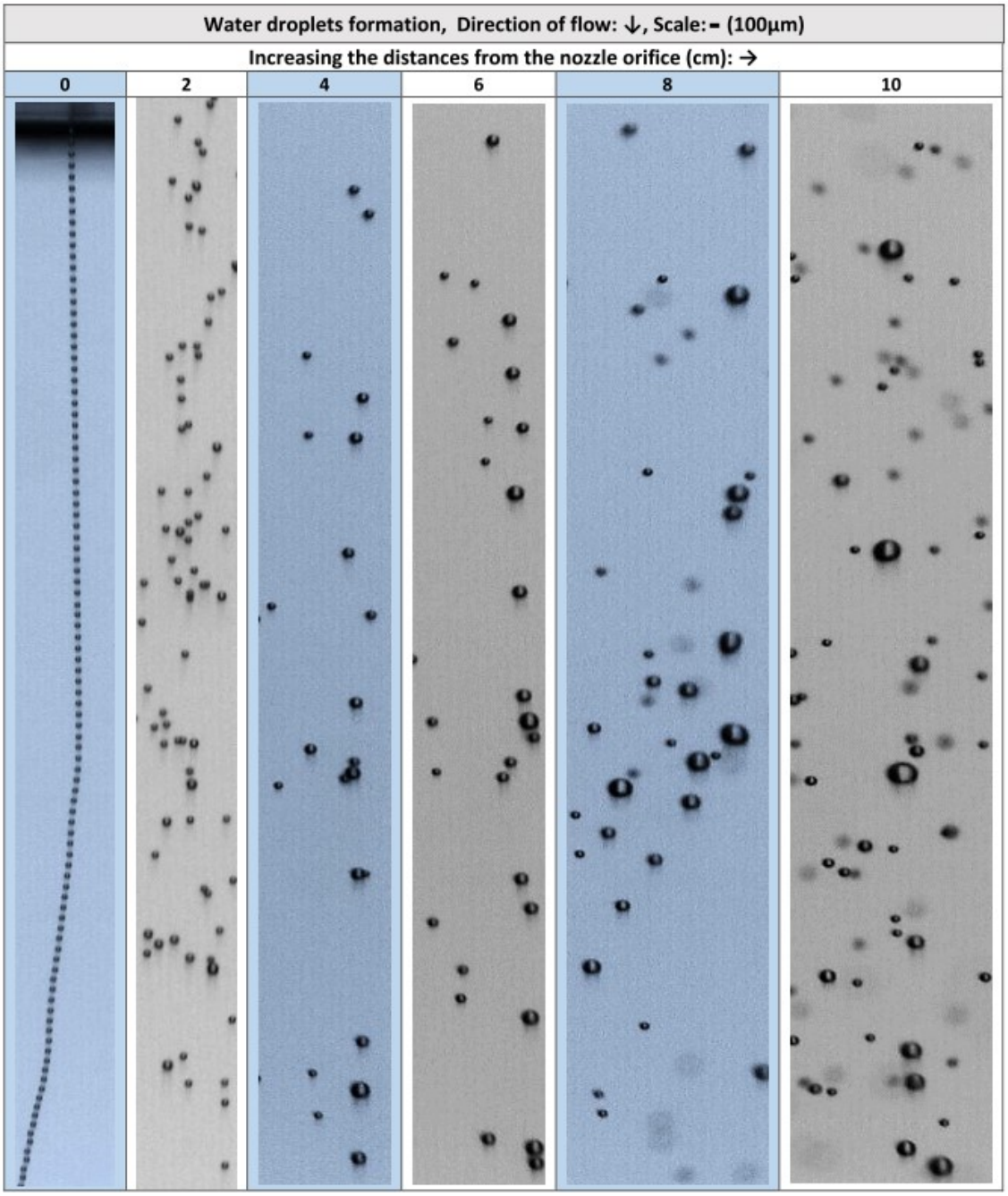

Figure 3.22: Images of the effect of the dispersion air with flow velocity 15 m/s on the stability of monodisperse droplets produced by 35µm MDG orifice with feed pressure at 0.5 bar and vibration frequency 50 KHz. Water droplets were generated during the spray drying process with a co-current laminar flow and aspiration rate of 50%. All images were taken using a Computar lens with a resolution of 5 megapixels.

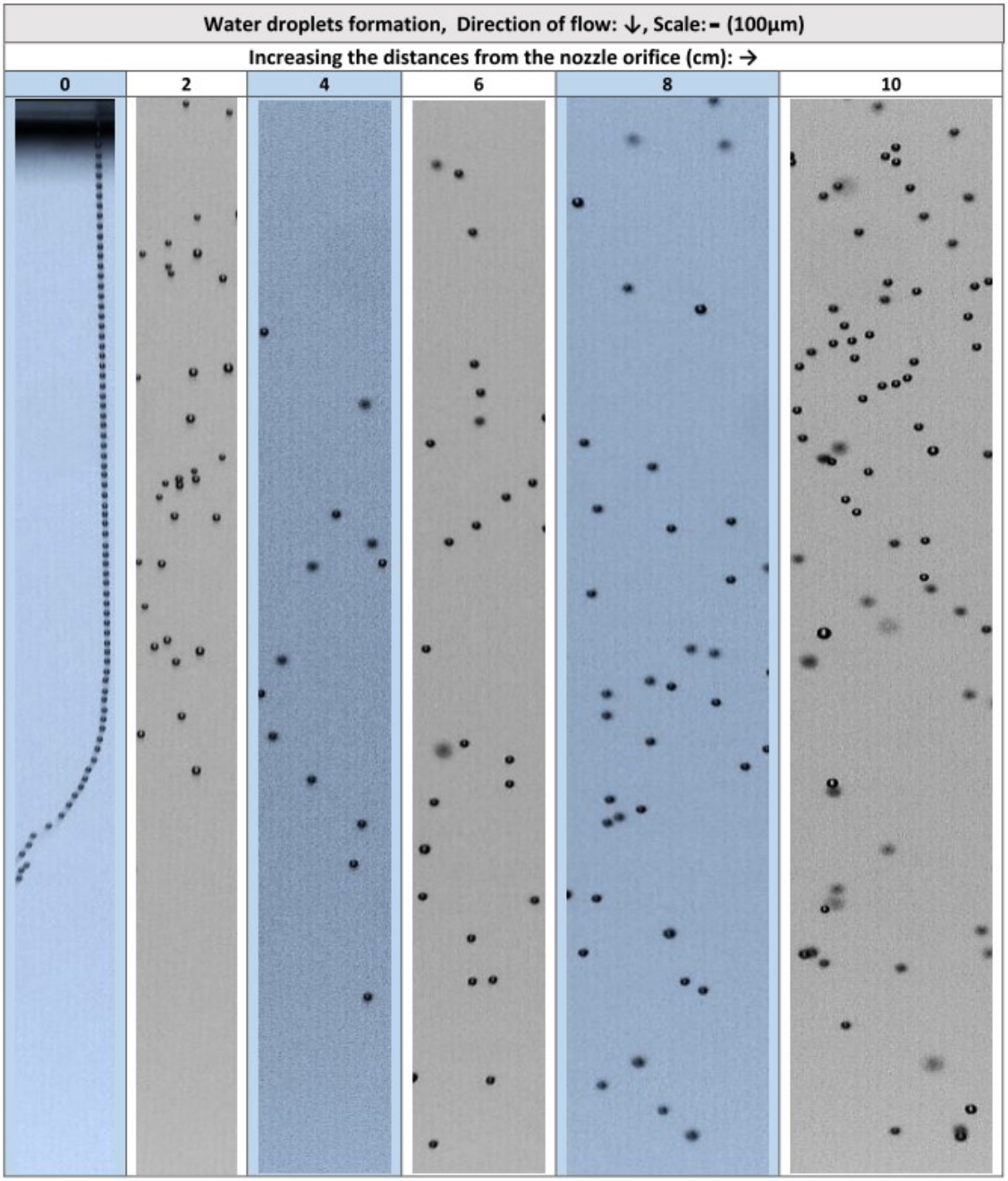

Figure 3.23: Images of the effect of the dispersion air with flow velocity 20 m/s on the stability of monodisperse droplets produced by 35µm MDG orifice with feed pressure at 0.5 bar and vibration frequency 50 KHz. Water droplets were generated during the spray drying process with a co-current laminar flow and aspiration rate of 50%. All images were taken using a Computar lens with a resolution of 5 megapixels.

3.3.2. Investigating the performance of single-stream spray dryer in producing monodisperse particles:

The spray drying system was operated at the highest inlet temperature of 220ºC, and the drying air was flowing at the lowest flow rate of 30 m^3/ h. Using this flow rate alongside the presence of a perforated plate led to generation of a co-current laminar airflow with a velocity of 1.14 m/s. Here, monodisperse droplets were generated using optimal MDG processing parameters (i.e. frequency and feed flow rate) with a feed

concentration of 15% (w/v). Operating the MDG with a cooling water jacket at 25ºC led to the generation of a stable and undisrupted monodisperse droplet stream without any pinhole blockage. In addition, the droplet stream was dispersed using a pulsating air tube, which resulted in minimal inter-droplet collisions and coalescence. This resulted in the droplets moving into different laminar airflow streams within the drying chamber. When uniform droplets were generated with a diameter of ~ 60-70 µm and initial velocity of ~ 7 m/s, this new single-stream drying approach successfully produced highly uniform spherical particles for metformin HCl. As can be seen in Figure 3.24 below, the spray-dried powders consisted of mono-sized particles with identical spherical shape and mean diameter around 35 µm. The powder yield was around 50%, which is a significant improvement in comparison with the few milligrams obtained in the previous initial prototype set-up. Stickiness of the dispersed uniform droplets and some semi-dried particles happened at the conical part of the drying chamber, but this is not unexpected in spray drying, especially at a small scale. Further improvements to yield are expected upon scale-up to pilot or large scale as the chamber dimensions will further enhance the residence time.

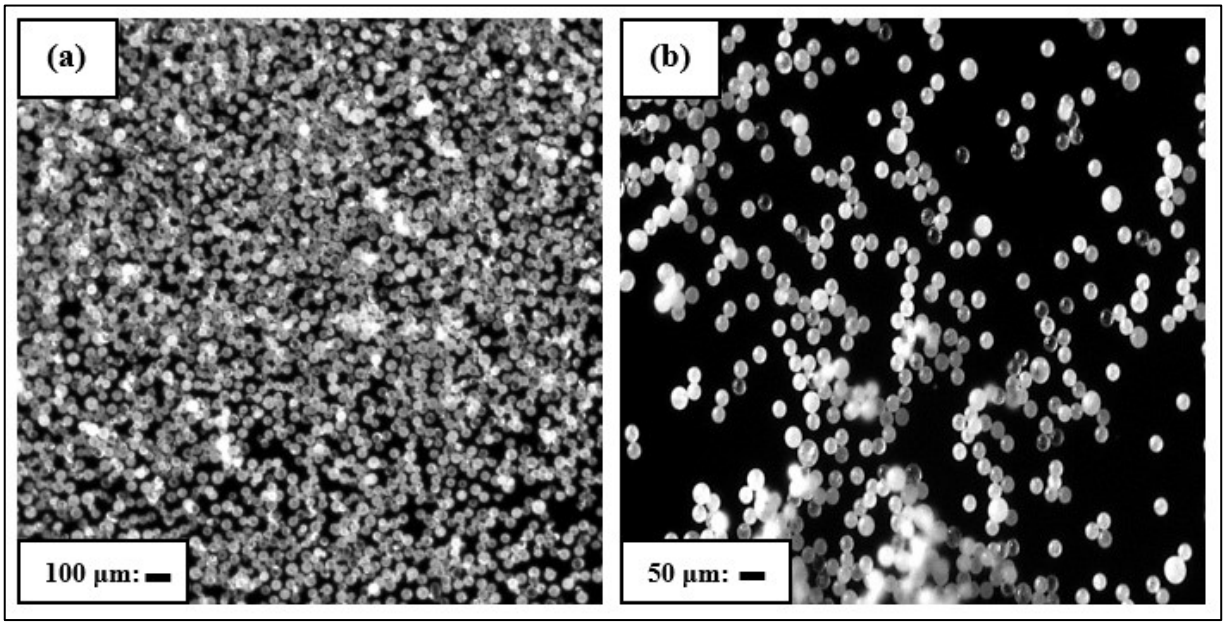

Figure 3.24: Microscope images for the spray-dried metformin HCl particles generated using a 35 µm MDG pinhole with optimal processing conditions. The ejected velocity for the monodisperse droplets generated with the outlet feed pressure of 0.5 and vibration frequency 46 KHz. The spray drying process was conducted at the highest inlet and outlet temperatures: 220 and 85 ºC, respectively. Images (a) and (b) are for the same sample at different magnifications.

These results indicate that the single-stream spray dryer (the final prototype) can be used to generate monodisperse particles with a good yield when using an MDG atomiser with a 35 µm pinhole. When using 50 µm MDG pinhole with aqueous feed solutions, no powder could be collected. This is because the generated monodisperse droplets do not have enough residence time for drying to occur due to their bigger size and higher velocity.

3.4. Conclusion:

Product non-uniformity and several potential problems during the spray drying process can be surpassed by achieving better control over atomisation process characteristics such as droplet size distribution and droplet trajectories. In this chapter, a new type of spray dryer, referred to as a single-stream spray dryer, has been designed and constructed based on the idea of atomising monodisperse droplets and drying them under a laminar airflow pattern to produce particles with uniform characteristics and quality. For effective drying, the design considerations and engineering requirements were described in detail. In this new design, the MDG atomiser was successfully used to produce uniform particles with high repeatability when operating it with few accessories. The spray-dried particles' size in every batch can be predetermined and controlled by adjusting the MDG operation parameters and feed solution properties. This could have future implications on the design and engineering of particle size to achieve the goal of building quality into products by design (QbD). Generating monodisperse and polydisperse powders using a single-stream spray dryer and a Buchi B-290 mini spray dryer will be conducted, respectively, in the following chapter using various ingredients. The generated powders will be characterised using various techniques to investigate the impact of uniform particles on the bulk powder properties and manufacturability of solid dosage forms.

Chapter 4

CHAPTER 4

Monodisperse versus Polydisperse Powders: The impact of material attributes on powder flow and compaction properties

4.1. Introduction:

Handling and processing of powders are essential steps in pharmaceutical operations, which requires using free-flowing formulations for efficient manufacturing. Correlation between particle properties and powder's manufacturability has been well documented previously (3,4,7,9,33,34,74,195,205). For example, particle size and size distribution significantly affect the powder flow behaviour, where the reduction in particle size usually leads to decreased flowability (69,70,102). This is due to increasing interactions and mechanical contact between neighbouring particles. As particle size falls below 100 μm, powders become more cohesive and resistant to flow (71,72,221). Also, it has been noted that the departure from spherical particle morphology reduces flow properties (104,105). In addition, many studies indicated that the tendency of particles to segregate or agglomerate during mixing is increased dramatically when increasing the variation in particle properties of the mixture's ingredients, especially size, density, and morphology (77,78,80). On the other hand, the effect of particle properties on the compaction process and tensile strength of pharmaceutical powders have also been investigated. Generally, smaller particles increase tablet tensile strength due to a higher number of contact points between particles. Smaller particles tend to aggregate under compaction, whereas larger particles are fractured, and the propensity of fragmentation under the load is usually increased with increasing particle size (222,223). For this reason, a change in the mean particle size of the final pharmaceutical formulation may alter the blend's homogeneity, the die filling process and/or the consolidation mechanism during tableting, leading to variation in the final product's quality.

Most pharmaceutical ingredients are polydisperse powders with undesired micromeritic properties (3,4,7,9,33,34,74,195,205). In many cases, this could lead to manufacturing issues during different pharmaceutical operations (e.g. mixing, tableting, sampling and dispensing) with poor product quality and batch rejection risk (3). Specifically, powders with uncontrolled particle size and shape distributions usually exhibit poor flowability with various costly technical problems during the tableting process (3,29).

Therefore, the more and earlier understanding of the bulk powder behaviour, the easier it is to overcome any potential challenges in subsequent drug product manufacturability. Accordingly, Leane et al. recently developed a four-box platform for solid dosage form production, termed the manufacturing classification

system MCS (33). This system classifies solid dosage form manufacturing processes into four routes according to the properties of active pharmaceutical ingredients (APIs). These are direct compression (DC-MCS1), dry granulation (DG-MCS2), wet granulation (WG-MCS3) and other technologies (MCS4). Direct compression (DC) is cheaper, faster, and less complicated than other approaches. However, the DC method is reliant mainly on the API particle properties. The API particle size and distribution, together with particle morphology, are critical for the DC process as there are no additional processing steps to mitigate these unfavourable properties (33,34). Hence, manufacturers would require pharmaceutical ingredients with controlled properties suitable for the DC process in order to decrease the variability in product quality. This is especially important when dealing with highly potent active pharmaceutical ingredients (HPAPIs) or low-dose formulations (33,224).

In particular, using uniform particles during solid dosage form development helps to minimise manufacturing issues such as poor weight/content uniformity and variations in disintegration time/dissolution rate which ultimately affect the drug bioavailability in the body (3,68,81). This concept of controlling particle properties was highlighted in regulatory documentation, e.g. in ICH Q6A, as one of the critical solutions to enhance the consistency in drug dissolution and bioavailability, especially when comparing between different batches for generic/branded products (65,200).

The main aim of this chapter was to generate monodisperse powders using the single stream-spray dryer developed in our laboratories at Aston University (see chapter 3), followed by systematic characterisation of the bulk powder properties using several techniques. The studies will elucidate the impact of monodispersity on bulk powder behaviour during packing, flowing and compaction process. For the first time, this study offers an evaluation of the powder behaviour for monodisperse spray-dried particles compared to other untreated and conventional spray-dried particles. The outcome of this study should help with understanding the effect of monodispersity on powder properties when the particles are less than 50 µm (i.e. fine powders) compared to polydisperse powders (with smaller or larger particle sizes). Specifically, two pharmaceutical ingredients with different particle characteristics were selected as model ingredients to create microparticles using different spray drying systems: traditional spray dryer (BUCHI B-290) and single-stream spray dryer. D-mannitol is widely used in tablet formulations as a filler (225) while metformin HCl is an oral antihyperglycemic drug (226). Both model ingredients are cohesive crystalline powders which present unfavourable flowability and compressibility during tableting (226–228). Therefore, creating uniform spherical particles using the new single-stream spray dryer might improve the materials' suitability for direct compression without the need for extra processing (i.e. granulation or recrystallisation) and/or the addition of flow-aids.

4.1. Material and methods:

4.2.1. Materials:

D-mannitol (>98.0% pure) was purchased from Sigma-Aldrich (Pool, UK), while Metformin HCl (>99.9% pure) was obtained from Discovery Fine Chemicals (Dorset, UK). Both ingredients were of pharmaceutical grade and used without further purification to prepare the feed solutions. Deionised water from a Milli-Q Integral system (Hertfordshire, UK) was used as a solvent to prepare feed solutions.

4.2.2. Spray-drying experiments and microparticles formation:

4.2.2.1. Feed solutions preparation:

D-mannitol and metformin HCl powders were each dissolved in deionised water to achieve a feed concentration of 15% (w/v). The solutions were sonicated for 10 minutes at room temperature for complete dissolution and then filtered using 7 μm filters. All feed solutions were prepared freshly before use in the spray drying process.

4.2.2.2. Conventional spray-drying system:

Conventional spray-dried powder for each model ingredient was prepared using a mini spray dryer BUCHI B-290 (Labortechnik AG, Flawil, Switzerland) operating in suction mode, where the feed solution with a flow rate of 3.6 ml/min was atomised using a two-fluid nozzle (inner tip 0.7 mm and cap 1.5 mm). The atomising airflow rate was 55% (approximately 601 L/h) and aspiration rate was 90% (approximately 30-35 m^3/h). The dryer inlet temperature was set at 220 and 150ºC, while the outlet temperature was 154 and 101ºC for metformin HCl and D-mannitol, respectively.

4.2.2.3. Single-stream spray drying system:

Generating spray-dried particles with high uniformity in size and morphology was conducted using a newly developed single-stream spray drying system, where the feed solution was atomised into uniform microdroplets using the MDG atomiser. The design and structure of this system were described previously in chapter 3. Several atomisation parameters and drying conditions were investigated using the above feed solutions. The MDG atomiser was provided with a 35 μm orifice and operated with a feed flow rate of 0.4 ml/min as well as vibrations frequency of 46 KHz. These parameters were selected by monitoring droplet atomisation using a real-time stroboscopic imaging system (detailed specifications in the next section and chapter 2). The generated uniform microdroplets were then dispersed using pulsating air with a velocity of around 20 m/s. A co-current laminar airflow with a constant velocity of 1.14 m/s was used for drying (air flow rate was set at 30 m^3/h). The inlet temperature of drying air was maintained at 220ºC, whereas the outlet temperature was found to be 85ºC. The same procedure and drying conditions were used to generate spray-dried (Mono-SD) particles for both model ingredients. All the generated powders were stored in desiccators at room temperature before characterisation.

4.2.3. Characterisation of the generated monodisperse droplets:

The optimal MDG parameters were selected using the stroboscopic imaging system discussed previously in chapter 2. The camera used had a resolution of 1280 X 1024 Pixels (OnSemi PYTHON USB 3.0/1.3 MP, XIMEA GmbH, Germany) and was equipped with a micro lens (2/3" 50 mm F/2.8 C-Mount manual iris, Computar lens, CBC America LLC., USA). The droplet stream was illuminated using backlight illumination controlled by a BVS-II Wotan stroboscope (Polytec GmbH, Germany). Images of droplet stream were captured at 25 frames per second and recorded using XIMEA CamTool software (version 4.14). The exposure length of the strobe light was approximately 0.8 µs which was necessary to freeze the motion of the falling droplets. From the captured images, the size of droplets and the distance between each subsequent two droplets were analysed using the ImageJ 1.50i software (NIH, USA) for image processing and analysis. For each spray drying experiment, at least 30 droplets were measured, and the results were presented as a mean ± standard deviation.

4.2.4. Characterisation of the powder particles properties:

4.2.4.1. Particle morphology and size analysis:

- ***Static imaging analysis:***

An automated microscopic image analysis system Morphologi 4 (Malvern Panalytical Ltd, Malvern, UK), was used for measuring particle size and shape parameters. The powder sample was dispersed onto a glass plate using the integrated sample dispersion unit (SDU) with a low energy setting (1.0 bar air pressure) to minimise particle breakage. Approximately 10,000 particles for each sample were imaged and analysed. For better comparison between the samples, while ensuring the largest particles present were imaged, spray-dried powders and unprocessed powders were imaged using the 5x and 2.5x objective lens, respectively. Post-analysis shape filters have been applied for each tested sample to exclude images of any touching particles. For each individual tested particle, the size and shape parameters were calculated from 2-dimensional images using Morphologi software. These parameters are listed below:

a) ***Circular equivalent diameter (CED)*****:**

A volume-weighted circular equivalent diameter (CED) is the main parameter used to determine the particle size and size distribution of the powdered materials. This expression can be defined as the diameter of the obtained particle based on its volume, and it can be calculated by identifying the diameter of the circle that has the same volume of the analysed particle, followed by a cubic transformation process. This enables the particle size distributions to be viewed by volume, not by number (229).

b) ***High sensitivity circularity (HSC):***

It is a measure of the closeness of the particle shape to a circle and is calculated by the following equation:

$$HS\ Circularity = (4\pi \times Area)/ (actual\ perimeter\ of\ particle)^2 \quad (4.1)$$

The value ranges from 0, where the particle has an extremely narrow rod shape, to near 1 where the particle has a perfect circle shape.

c) *Elongation:*

It is a measure of the length-width relationship, and this shape parameter is unaffected by surface roughness. The following equation calculates it:

$$Elongation = 1 - (Particle\ width/particle\ length) \quad (4.2)$$

The value ranges from 0 to 1. Particles with a regular square or circle shape have an elongation value close to 0, whereas particles with a large aspect ratio (i.e. rod-like particle) have an elongation value close to 1.

d) *Convexity:*

It describes the surface roughness of the particle, and it is the expression of irregularities. The following equation is used to calculate it:

$$Convexity = (perimeter\ of\ the\ convex\ hull\ of\ the\ particle/\ actual\ particle\ perimeter) \quad (4.3)$$

The value ranges from 0 to 1. Particles with a smooth surface have convexity values close to 1, whereas irregularly shaped (spiky) particles have convexity values close to 0.

e) *Polydispersity:*

The polydispersity of the powders was identified by the span value, which is defined as:

$$Span = (D_{90} - D_{10})/D_{50} \quad (4.4)$$

D_{90}, D_{50}, and D_{10} are the equivalent volume-based CED diameters at 90, 50, and 10% of the cumulative particle size distribution curve, respectively. Generally, increasing the span value, for example, leads to an increase in the polydispersity nature for powder.

Furthermore, the homogeneity of the powder was expressed by the homogeneity index (HI), which measures the relationship between $D_{90} - D_{50}$ and $D_{50} - D_{10}$, and can be calculated by dividing the smaller value over the larger one. Homogeneity values range from 0 to 1. Symmetrical particle size distribution, for example, has a homogeneity value equal to 1, whereas this value becomes closer to 0 when the distribution is asymmetric.

- ***Optical microscope observations:***

For closer morphology observation, images of different powders were taken by optical microscopy (Zeiss Axio Scope A1, Carl-Zeiss, Oberkochen, Germany). A small amount of powder sample was sprinkled onto

a glass plate and examined using an X10 magnification lens. The particles were captured using a Zeiss Axio camera interfaced with the Zeiss Axio Vision imaging software.

- ***Scanning electron microscope (SEM) observations:***

The surface morphology and microstructure of the different powders were characterised by the SEM technique. Several images were taken using Zeiss Supra 55VP FE SEM (Zeiss, Oberkochen, Germany) operated at 2 and 10KV in variable pressure mode. The powder sample was sprinkled onto a metal stub covered with an adhesive conductive carbon tape and then it was observed at the different magnifications without coating.

4.2.4.2. Solid-state analysis:

The solid-state properties for metformin HCl and D-mannitol powders were characterised using two different methods as follows:

- ***Differential scanning calorimetry (DSC):***

The thermal properties of powders were characterised by differential scanning calorimetry Q200 (TA instrument – Waters LLC, New Castle, DE, USA). Approximately 2 mg of powder sample was accurately weighed and hermetically sealed in an aluminium Tzero pan with a vented lid. DSC measurements were performed at a temperature range of 50-300°C with a heating rate of 10°C/min under a nitrogen flow rate of 50 mL/min. The enthalpy of fusion, onset temperature, and melting point for all phase transition peaks in the DSC profile were recorded with TA Advantage software for Q series and interpreted using TA universal analysis 2000 software (version 4.5, TA Instruments-Waters LLC, Milford, MA, USA).

- ***X-ray diffraction (XRD):***

The XRD measurements of all mannitol and metformin powders were made on an Empyrean third generation powder diffractometer (Malvern Panalytical Ltd., Malvern, UK) equipped with multicore (iCore/dCore) optics and a Pixcel3D detector operating in 1D scanning mode. A Cu tube was used, giving *Kα* radiation (λ = 1.5419 Å), and a beam knife was used to reduce air scatter at the low angles. The powder was scanned in the range 4 – 60° 2θ with a step size of 0.0131° and a counting time of ~ 200 s/step. The diffraction patterns were recorded with the Malvern diffractometer's software and combined using OriginPro software (version 2021, OriginLab Corporation, Northampton, MA, USA). The polymorphic phase quantification for percentage of α, β, and δ of D-mannitol and A and B of metformin HCl was performed through the Rietveld refinement method (HighScore plus software, Malvern Panalytical Ltd, Malvern, UK) (230). All refinements were done based on fitting the complete experimental diffraction patterns with the calculated polymorphic profiles for mannitol and metformin powders which were obtained from the Cambridge Crystallographic Data Centre.

4.2.4.3. Loss on drying assessment:

A thermogravimetric analyser (Pyris 1TGA) from Perkin-Elmer (Massachusetts, USA) was used to measure moisture content for unprocessed and spray dried powders (231). In each experiment, a platinum pan was used to hold 10 mg of powder sample. Subsequently, weight loss was measured by heating the sample from 50 to 120ºC and holding it at this temperature for 5 min under a nitrogen gas stream (purge rate of 20 ml/min). Moisture content (%) was calculated using Pyris Manager Software (version 5.00.02).

4.2.4.4. Hygroscopicity assessment:

About 3 g of each powder was transferred into a dry Petri dish and kept in a humidity chamber for 24 h with the following conditions: temperature at 25ºC and relative humidity at 75%. After that, the percentage of water uptake for each powder sample was determined following the previous procedure used for loss on drying assessment by TGA.

4.2.5. Characterisation of the powders flowability:

4.2.5.1. Packing properties determination:

Bulk densities (ρ_{bulk}) and tapped densities (ρ_{tapped}) for all powders were tested according to the methods outlined in USP monograph ⟨616⟩(232). Approximately 50 g of each powder sample was poured through a funnel into a pre-weighed 100 ml graduated cylinder readable to 0.5 ml, and the bulk volume (Va) was recorded. After that, the cylinder was tapped with a nominal rate of 250 taps per minute using a Sotax TD2 tapped density tester (Allschwil, Switzerland). The tapped volume (Vc) was recorded every minute until a constant volume was reached (after 1750 taps). The bulk and tapped densities were calculated as mass of powder/initial powder volume and as mass of powder/final powder volume, respectively. All measurements were carried out in triplicate and presented as mean ± standard deviation.

Carr's compressibility index (CI%), and Hausner ratio (HR) were calculated using the measured values for bulk and tapped densities as follows:

$$Compressibility\ Index = 100 \times [(\rho_{tapped} - \rho_{bulk})/\rho_{tapped}] \quad (4.5)$$

$$Hausner\ Ratio = (\rho_{tapped}/\rho_{bulk}) \quad (4.6)$$

The generally accepted scale of flowability is given in Table 4.1 below, where lower CI% or lower HR is indicative of better flow properties than higher ones (233,234).

Table 4.1: Relationship of compressibility index, Hausner ratio and flowability levels.

Compressibility index (%)	Flow character	Hausner ratio
≤ 10	Excellent	1.00 – 1.11
11-15	Good	1.12 – 1.18
16-20	Fair	1.19 – 1.25
21-25	Passable	1.26 – 1.34

26-31	Poor	1.35 – 1.45
32-37	Very poor	1.46 – 1.59
> 38	Very, very poor	> 1.60

In addition, inter-particle porosity (*P*) for each powder sample was calculated (235) as follows:

$$P = [(\rho_{tapped} - \rho_{bulk}) / (\rho_{tapped} \times \rho_{bulk})] \quad (4.7)$$

4.2.5.2. The angle of repose determination:

The angle of repose (θ), which is another standard method to describe the powder flow, was calculated using a fixed height method described in USP monograph ⟨1174⟩ (236). A stainless-steel funnel with 12 mm orifice diameter was used in this experiment. About 10 g of powder sample was allowed to flow freely from the funnel at a fixed height of 100 mm over a millimetre-grid sheet. After forming the cone, the diameter (d) and height (h) of the powder pile were measured. Calculating the angle of repose (θ) value was achieved using the following equation:

$$\theta = tan^{-1}(2h/d) \quad (4.8)$$

All experiments were only considered valid when a symmetrical uniform cone was formed. The determination of the angle of repose was conducted in triplicate using new powder samples each time, and the results were presented as mean ± standard deviation. Based on the obtained repose angle values, the flow behaviour could be considered as excellent flow (θ: 25-30º), good flow (θ: 31-35º), fair flow (θ: 36-40º), passable flow (θ: 41-45º), poor flow (θ: 46-55º), and very poor flow (θ >56º) (236).

4.2.5.3. Mechanical flow function testing:

Powder flowability was evaluated in an automated powder flow tester (PFT; Brookfield Engineering, Middleboro, Massachusetts, USA) using a small volume shear cell (43 cc, 5 inches). The working principle of the PFT tester depends on Jenike's methodology, where a standard flow function test was implemented using five normal uniaxial stresses: 0.795, 1.607, 3.246, 6.559 and 13.252 KPa. Under each known normal stress, the powder was first consolidated, and then the shear stress needed to create a steady-state flow was measured while the powder was subjected to consolidating stress itself. Then, a yield locus was constructed by plotting the failure shear stress against normal stress at each consolidating stress. The previous procedure was repeated five times to create another yield locus for each consolidating stress. Values for unconfined failure strength (UFS), major principal consolidating stress (MPCS), the effective angle of internal friction (δ_e) and flow index were calculated using the Powder Flow Pro software (version 1.3) based on Mohr circles and yield loci. Powder flow was characterised mainly by its flow function (FF) curve, which was a plot of

unconfined yield strength (UYS) values of the powder against major principal consolidating stress MPCS values calculated for five yield loci.

Usually, the flow index (f_i), which is obtained from the inverse slope of the flow function line, is used to characterise flowability numerically as follows (237,238):

Non-flowing ($f_i > 1$), very cohesive ($1 > f_i > 0.5$), cohesive ($0.5 > f_i > 0.25$), easy flowing ($0.25 > f_i > 0.1$), and free flowing ($f_i < 0.1$). All the tests for powder flow determination were carried out at room temperature and ambient relative humidity.

4.2.6. Characterisation of the powder tableting performance:

A hydraulic compaction simulator system was used to compact mannitol and metformin powders for the determination of their Heckel profiles and strain rate sensitivity (SRS) index values. Each compact was prepared by weighing 300 mg of powder into a 10 mm stainless-steel cylindrical die. A 5% w/v suspension of magnesium stearate in acetone was used to apply a lubricating film to the punch/die set before each compression cycle. Each powdered material was compacted at two different compression speeds (0.1 and 300 mm/s) to a maximum pressure of 500 MPa measured using a 50 KN load cell. Powders were tested in triplicate at each compression speed and the data analysed by the compaction analysis software.

The impact of bulk powder properties on materials deformability was investigated using the Heckel equation as follows:

$$ln\,[1 / (1-D)] = KP + A \qquad (4.9)$$

Where D is the relative density of the compact in the die at pressure P and is given by the ratio between the apparent density of the compact at applied pressure P and the true density (ρ_{true}) of the powdered material. ($1-D$) denotes the pore fraction or compact's porosity. The constant K is the slope of the straight line portion of the Heckel plot. The constant A is the intercept of the straight line and it is a function of particles' rearrangement. A plot of $ln\,[1 / (1-D)]$ vs P is referred to as Heckel plot and is a useful tool to describe the structure of the powder bed changes e.g. particle rearrangement, plastic deformation, and fragmentation during the compression process (239,240). More details about the Heckel profiles were presented in the Appendix A1.

From the Heckel equation, the powder's deformability could be predicted by calculating the mean yield pressure (P_y), which is given by the reciprocal of the slope (K) value (241). The lower P_y values refer to materials that are mainly consolidated by the plastic deformation, while the higher P_y values refer to materials that are consolidated primarily by fragmentation (70). In particular, materials with P_y values lower than 40 MPa are classified with high plastic deformability, while materials with P_y values higher than 200

MPa are classified with very low plastic deformability, such as fragmenting and viscoelastic materials (242,243).

The effect of compaction speed on material's deformability and particle fragmentation was evaluated by calculating the strain-rate sensitivity (SRS) (244) using the following equation:

$$SRS = [(P_{y2} - P_{y1}) / P_{y2}] \cdot 100 \quad (4.10)$$

Where P_{y1} and P_{y2} are the mean yield pressures from the Heckel plots obtained at 0.1 mm/s (low compression speed) and 300 mm/s (high compression speed). Materials which are more strain-rate sensitive are those materials which plastically deform (244).

In addition, the tensile strength (TS) for each compacted powder was calculated using the following equation:

$$TS = 2F / (\pi.D.T) \quad (4.11)$$

Where F is the breaking force or hardness, and D and T are the diameter and thickness of the compact, respectively. Specifically, F is a measurement of the load at which the compact breaks under diametrical compression between two flat platens, while TS is a fundamental measurement of the compact's resistance to fracture (245,246).

Moreover, the solid fraction (SF) for each compacted powder, which is defined as the proportion of solid materials contained in the compact body was calculated using the equation below:

$$SF = \text{density of the tablet / true density of material} = m / (\rho_{true} .v) \quad (4.12)$$

Where m and v are the mass and volume of the compact prepared, respectively.

Prior to solid fraction calculation, the true density (ρ_{true}) for all powders was measured using a helium multipycnometer from Quantachrome Instruments (Syosset, NY, USA). Approximately 2 g of each powder was placed into a micro-sample cell and assessed for the true volume and, in turn, true density values. Detailed information about this experimental methodology has been reported previously in the literature (247).

Furthermore, the percentage of elastic recovery in the die for each compacted powder system was calculated using the equation below:

$$\% \text{ Elastic recovery} = [(H-H_c)/H_c] \cdot 100 \quad (4.13)$$

Where H_c and H are the thickness of compact in the die under maximum pressure and after the compression force was removed, respectively (248).

All testing for Heckel profile analysis was carried out at Merlin Powder Characterisation Ltd. (Brierley Hill, UK).

4.2.7. Powder properties evaluation based on a modified SeDeM expert system:

The SeDeM expert system is a novel preformulation tool based on characterising the physical properties of powdered materials (APIs and excipients) in order to predict the suitability of the powders to be used in tablet production by direct compression (235,249). This innovative tool has been used effectively for powders' evaluation in order to design and manufacture solid dosage forms with high quality and less cost/time consumption (51,250–252).

The system methodology is based on the experimental study and quantitative determination of the twelve input parameters presenting the most common physical properties that significantly affect powder flowability and compressibility behaviour. These parameters include bulk density (ρ_{bulk}), tapped density (ρ_{tapped}), inter-particle porosity (IP), Carr's compressibility index (CI), cohesion index (Icd), Hausner ratio (HR), angle of repose (θ), powder flow rate (t''), loss on drying (%LOD), hygroscopicity (%H), percentage of particles measuring < 50 μm (%Pf) and powder homogeneity index (HI). The input parameters' resulting values are converted into four outputs: three comprehensive indices and the SeDeM diagram. The resulting output parameters help to evaluate and classify different pharmaceutical ingredients according to powder's suitability for successful processing by direct compression technique. Detailed information about the SeDeM methodology and calculation of input/output parameters were reported in the literature (249).

In this study, the concept of the SeDeM expert system was used as visual presentation tool to summarise the previous results (bulk powder properties) of the materials in a holistic manner. The SeDeM expert system was modified to include mean yield pressure, tablet tensile strength and powder flow index which play a significant role in powder flowability and compressibility assessment. As seen in Table 4.2, the numerical values of the input parameters for powder substances, which were obtained experimentally as described in the above sections, were converted to radius values (r) by applying specific factors and then presented using a radar chart. The polygon diagram was formed by connecting radius values with linear segments. All radius values had the same scale: 0 is a minimum value, 10 is a maximum value, and 5 is a minimum accepted value for robust powder processing by direct compression, as seen in Figure 4.1. The exceptional values that appear below 0 were considered 0, and those above 10 were considered 10. The converted data that was generated makes the powders more comparable because all tested parameters were presented at the same general numerical scale from 0 to 10.

Table 4.2: Summary of modified SeDeM diagram input parameters and limit values.

Parameter	Symbol	Limit value (V)	Unit	Equation to convert actual (V) values to SeDeM radius (r) values
Bulk density	ρ_{bulk}	0 - 1	g/cm^3	10V
Tapped density	ρ_{tapped}	0 - 1	g/cm^3	10V
Mean yield pressure [a]	P_y	200 - 0	MPa	(200 – V)/20
Tensile strength [b]	TS	0 - 5	MPa	2V
Carr's index*	CI	50 - 0	%	10 - (V/5)
Hausner ratio*	HR	2 - 1	-	(20 -10V)
Angle of repose	θ	50 - 0	(º)	10 - (V/5)
Flow index [c]	f_i	1 - 0	-	10 - (10V)
Loss on drying	%LOD	10 - 0	%	10 - V
Hygroscopicity*	%H	10 - 0	%	10 - V
Particles > 50µm*	%Pf	0 - 100	%	V/10
Homogeneity index*	HI	0 - 1	-	10V

* Equation used to convert the input parameter's actual (v) value to SeDeM radius (r) was modified for better comparison when assessing the powder flowability.

[a] Mean yield pressure (P_y) was used instead of the original parameter (inter-particle porosity) to assess powder compressibility. The range of the P_y parameter was set between 0 and 200 MPa. The range was selected based on the values reported in the literature for various powder materials. A lower value indicates that the tested material has better compressibility behaviour (242,243). The P_y was determined by Heckel analysis using a high compression speed of 300 mm/s.

[b] Tensile strength (TS) was used instead of the original parameter (cohesion index: N), and it was calculated from the crushing strength measurement for 300 mg powder compressed in 10 mm die using compression pressure of 500 MPa and high compression speed of 300 mm/s. The range of the TS parameter was set between 0 and 5 MPa. The range was selected based on the values reported in the literature for various powder materials and the fact that 2 MPa is considered the minimum tensile strength needed for the tablets to withstand stresses in their life-time (253).

[c] Flow index (f_i) was used instead of the original parameter (powder flow rate: g/s).

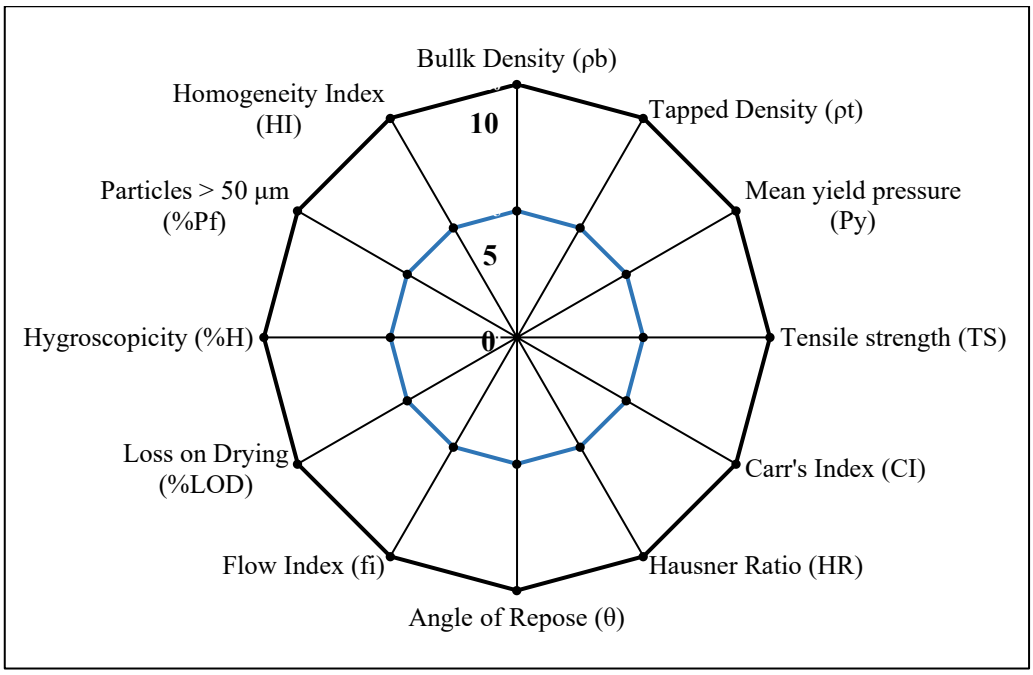

Figure 4.1: A typical modified SeDeM diagram with 12 parameters.

4.2.8. Statistical analysis:

The statistical analysis of the data was carried out using GraphPad Prism 7.03 software. One-way ANOVA followed by post-hoc Tukey's test was used for comparison between the different powders. Statistical significance was considered when the P-value was less than 0.05. In all powder characterisation methods, the measurements were performed using a fresh new sample from the studied powder, and the results were presented as mean ± standard deviation of three repeats. However, for Heckel profile analysis, the measurements were only taken for three compacts per powder sample, and the results were also presented as mean ± standard deviation.

4.2. Results and discussion:

4.3.1. Morphology and size distribution comparison:

Monodisperse droplets were converted to spray-dried microparticles using the single-stream spray drying process detailed in chapter 3 (details of the relationship between atomisation and monodisperse droplets diameter presented in Appendix A2). The morphology and size distributions for these powders were then compared with conventionally spray-dried and unprocessed starting materials. As observed in Figure 4.2 below, there is a noticeable difference in particle morphology when comparing the images for the different powders. The Mono-SD powders of D-mannitol or metformin HCl that were generated by the new spray drying system exhibited a high uniformity in particle morphology, unlike the unprocessed (pure) and conventionally spray-dried powders.

The unprocessed powders exhibited elongated or prismatic rod shapes while the fabricated particles from conventional spray drying showed a broader range of fine particles with irregular aggregates. In contrast, Mono-SD particles generated by the single-stream spray drying system showed mainly a highly spherical shape with uniform size and smooth surface. No aggregates could be observed for Mono-SD particles in comparison with unprocessed and conventional SD powders which showed significant aggregation, as seen in Figure 4.2. Based on these observations, the Mono-SD particles are expected to have better bulk powder properties (discussed later).

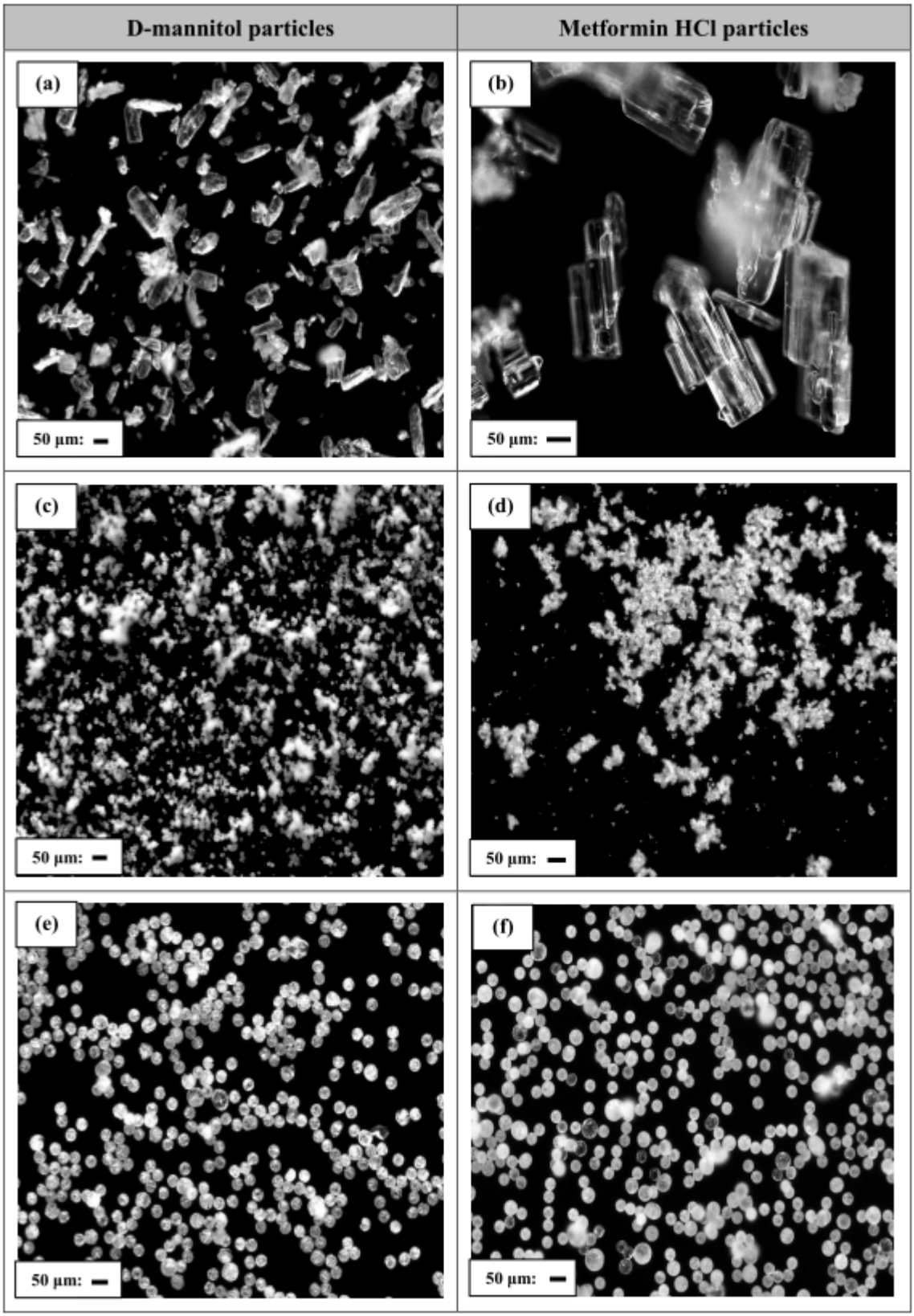

Figure 4.2: Optical microscope images for powders produced using different approaches: (a, b) unprocessed particles, (c, d) SD particles, and (e, f) Mono-SD particles for D-mannitol and Metformin HCl, respectively.

The powder samples generated via both conventional SD and the single-stream spray drying process had an overall size range smaller than the unprocessed powders (ANOVA, $P < 0.05$). This confirms the utility of spray drying as a technique capable of reducing the particle size of pharmaceutical materials regardless of the specific type of instrument (254,255).

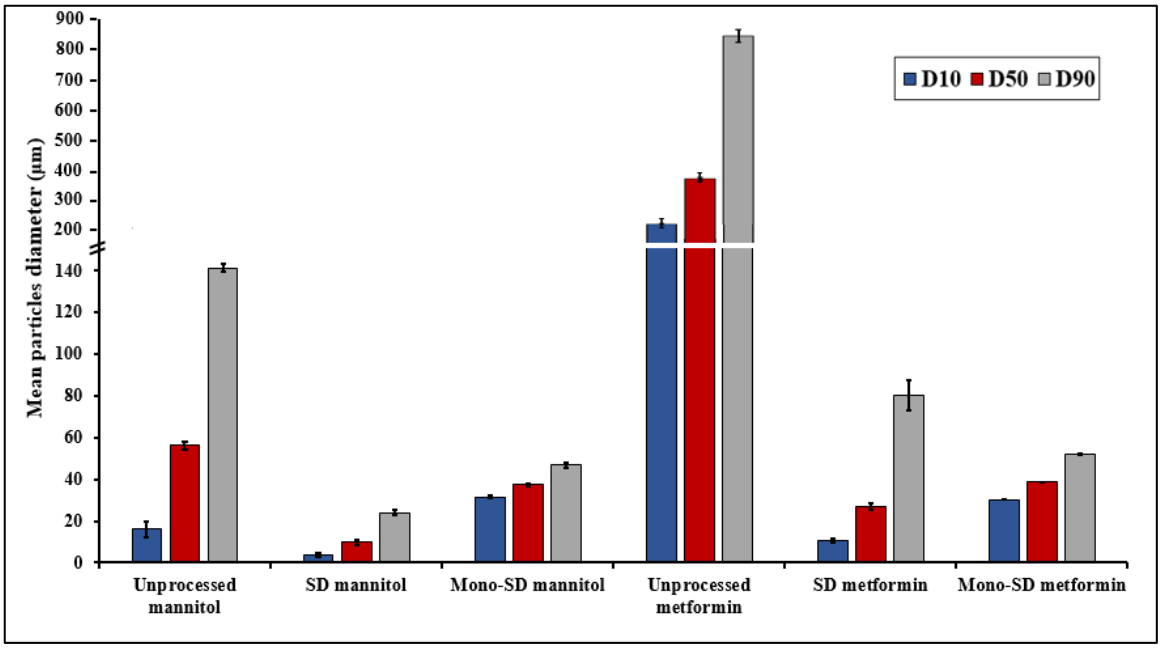

Figure 4.3: Particle size distribution for different untreated and spray-dried powders based on calculating the volume-based CED diameters at 10, 50 and 90% of the cumulative size distribution; (mean ± SD, n=3).

By comparing the Mono-SD powders together, it is clear that the fabricated D- mannitol and metformin HCl particles exhibited roughly the same size distribution. As seen in Table 4.3, the average particle (CED, D_{50}) diameter was 37.40 ± 0.62 and 38.56 ± 0.05 µm for Mono-SD mannitol and Mono-SD metformin, respectively. The same initial droplet diameter and solid content were used for both materials, resulting in a similar size range (256).

Among the three D-mannitol powders, the particle size distribution for Mono-SD mannitol (span of 0.41) was much narrower (ANOVA, $P < 0.05$) than the unprocessed mannitol with a span of 2.22 and SD mannitol with a span of 2.12. In addition, the SD mannitol powder showed less homogeneity in particle distribution (homogeneity index: 0.44), whereas Mono-SD powder displayed higher uniformity in size distribution (homogeneity index: 0.66), as seen in Figure 4.3 and Table 4.3.

Table 4.3: Summary of fundamental particle properties for different unprocessed and fabricated powders.

Size-Shape parameters	D-mannitol powders			Metformin HCl powders		
	Unprocessed	***SD***	***Mono-SD***	***Unprocessed***	***SD***	***Mono-SD***
Volume-based CED[1]						
D_{10} (µm)	16.18 ± 3.78	3.48 ± 0.94	31.36 ± 0.68	206.96 ± 7.88	10.46 ± 0.85	30.30 ± 0.00
D_{50} (µm)	56.11 ± 1.72	9.80 ± 1.07	37.40 ± 0.62	379.46 ± 9.13	26.90 ± 1.30	38.56 ± 0.05
D_{90} (µm)	141.12 ± 1.96	24.02 ± 1.45	46.80 ± 1.39	847.83 ± 26.31	80.03 ± 7.12	52.16 ± 0.37
Span	2.22 ± 0.06	2.12 ± 0.29	0.41 ± 0.04	1.68 ± 0.01	2.58 ± 0.25	0.56 ± 0.00
Homogeneity index (HI)	0.46 ± 0.05	0.44 ± 0.03	0.66 ± 0.22	0.36 ± 0.01	0.31 ± 0.02	0.60 ± 0.01
Particles (%) < 50 µm	43.46 ± 0.63	98.72 ± 0.95	95.01 ± 0.84	0.5 ± 0.15	77.2 ± 0.10	90.1 ± 0.02
HS circularity (HSC)[2]						
D_{10}	0.63 ± 0.01	0.68 ± 0.02	0.89 ± 0.01	0.46 ± 0.01	0.72 ± 0.01	0.98 ± 0.00
D_{50}	0.87 ± 0.01	0.91 ± 0.01	0.95 ± 0.00	0.73 ± 0.01	0.89 ± 0.01	0.99 ± 0.00
D_{90}	0.94 ± 0.01	0.96 ± 0.01	0.99 ± 0.00	0.91 ± 0.00	0.96 ± 0.00	1.00 ± 0.00
Elongation[3]						
D_{10}	0.10 ± 0.01	0.08 ± 0.08	0.00 ± 0.00	0.17 ± 0.00	0.09 ± 0.00	0.00 ± 0.00
D_{50}	0.28 ± 0.02	0.16 ± 0.00	0.04 ± 0.00	0.42 ± 0.01	0.24 ± 0.00	0.01 ± 0.00
D_{90}	0.60 ± 0.06	0.38 ± 0.01	0.10 ± 0.00	0.66 ± 0.01	0.43 ± 0.01	0.10 ± 0.00
Convexity[4]						
D_{10}	0.93 ± 0.01	0.94 ± 0.00	0.97 ± 0.03	0.89 ± 0.01	0.91 ± 0.00	0.99 ± 0.00
D_{50}	0.98 ± 0.00	0.98 ± 0.00	0.99 ± 0.02	0.98 ± 0.00	0.95 ± 0.00	1.00 ± 0.00
D_{90}	0.99 ± 0.00	1.00 ± 0.00	1.00 ± 0.00	1.00 ± 0.00	0.99± 0.00	1.00 ± 0.00
Loss on drying						
(%)	0.02 ± 0.00	0.03 ± 0.00	0.03 ± 0.00	0.04 ± 0.00	0.04 ± 0.00	0.04 ± 0.00
Hygroscopicity						
(%)	0.04 ± 0.00	0.04 ± 0.00	0.03 ± 0.00	0.06 ± 0.00	0.05 ± 0.00	0.06 ± 0.00

Results reported as mean ± standard deviation (n = 3).

[1] Volume –weighted circular equivalent diameter (CED).

[2] High sensitivity circularity or HSC (range 0-1; a particle with perfect circle has circularity value of 1, whereas extremely narrow rod particle has circularity value closer to 0).

[3] Elongation (range 0-1; shape with large aspect ratio has elongation value closer to 1, whereas a circle or square-shaped particle has elongation value of 0).

[4] Convexity (range 0-1; a smooth-shaped particle has convexity of 1, whereas an irregular-shaped particle has convexity value closer to 0) (257).

Similar results were found when comparing the different metformin HCl powders. The Mono-SD powder generated via the new single-stream spray drying system has a very narrow and symmetrical size distribution (span: 0.56, homogeneity index: 0.60) compared with the unprocessed and conventionally spray-dried samples where the size distribution was much broader and less homogeneous (Figure 4.3 and Table 4.3).

Geometrical particle shape parameters of the different powder samples were also quantified in this study. Upon comparing the mean values of D_{10}, D_{50}, and D_{90} for shape parameters, namely, HS circularity, convexity and elongation, it seems evident that Mono-SD powders have the highest HSC and convexity values close to 1 (Table 4.3). Furthermore, the mono-SD powders approached elongation values of 0 meaning the particles have a uniform spherical shape. Conversely, unprocessed powders and SD powders presented variations in particle dimensions and morphology demonstrated by the wider HSC, elongation, and convexity (D_{10}, D_{50}, and D_{90}) distributions, as seen in Table 4.3.

The particles' surface morphology was investigated using SEM. Figures 4.4 and 4.5 below show good agreement with the above morphological analysis results. The particles of unprocessed powders were irregular in shape with crystals exhibiting an elongated/prismatic shape and sharp edges. This agrees with previous studies, which confirmed that crystals of pure unprocessed mannitol and metformin mainly reveal an elongated habit (228,258–260). On the other hand, the fabricated SD powders consisted of irregularly shaped particles with different levels of fines and agglomerates, while the particles of Mono-SD powders showed a spherical shape and relatively smooth surface.

Mono-SD mannitol particles generally exhibited spherical shape with some irregularities e.g. some particles are shrivelled or collapsed. On the other hand, Mono-SD metformin particles were observed to have a relatively smooth surface structure with no distortion (i.e. no folds or wrinkles). The irregularities in Mono-SD mannitol particles are probably due to droplet inflation and deflation behaviour during the spray drying process. The morphology of spray-dried particles is dependent upon the drying kinetics but also on the diffusion properties which vary between materials. The balance between drying kinetics/evaporation rate and diffusion rate influences the final particle morphology as described previously according to Peclet number concept in Chapter 1 (141,261).

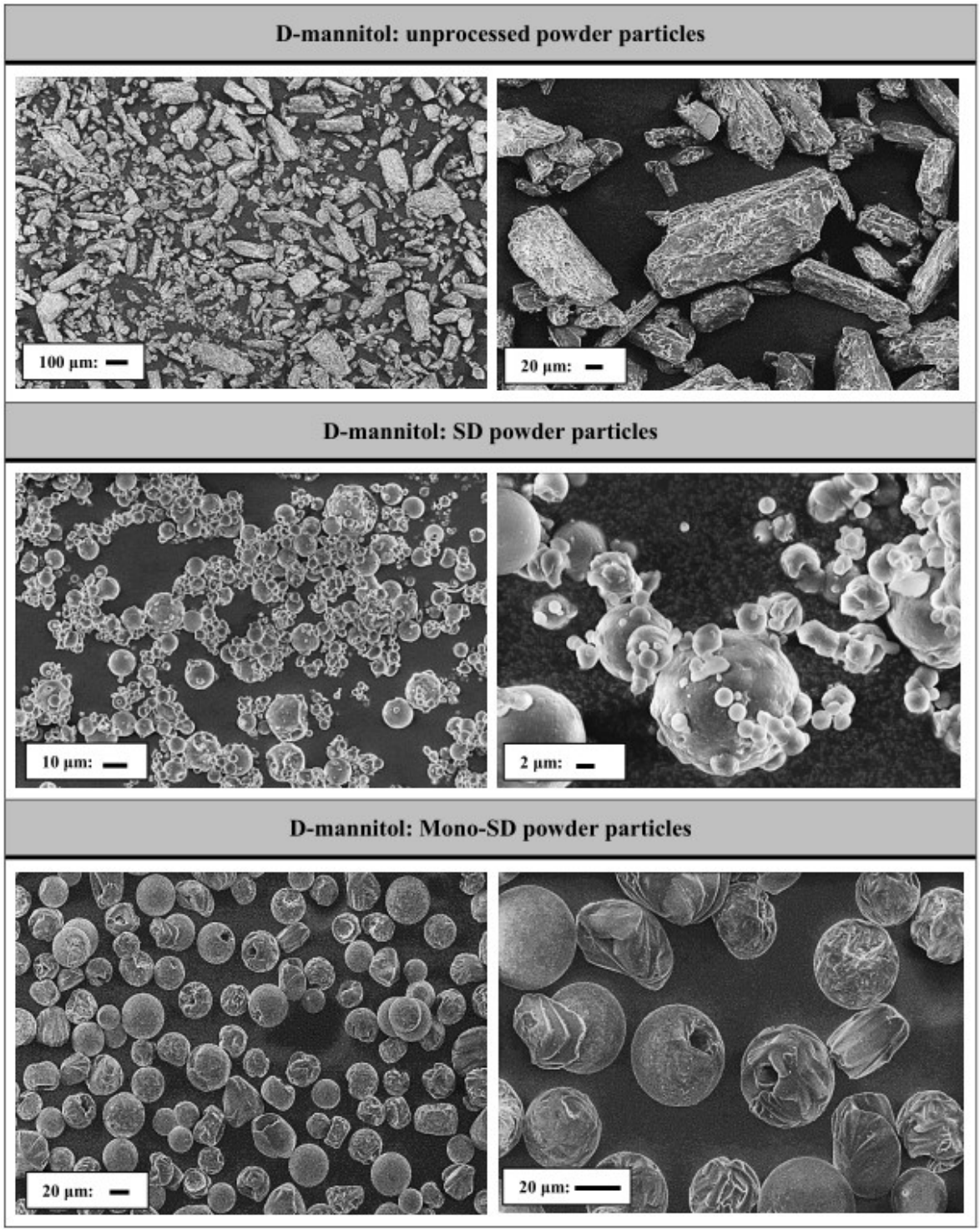

Figure 4.4: SEM images at different magnifications of some D-mannitol particles prepared using two different spray-drying systems in comparison to unprocessed powder particles.

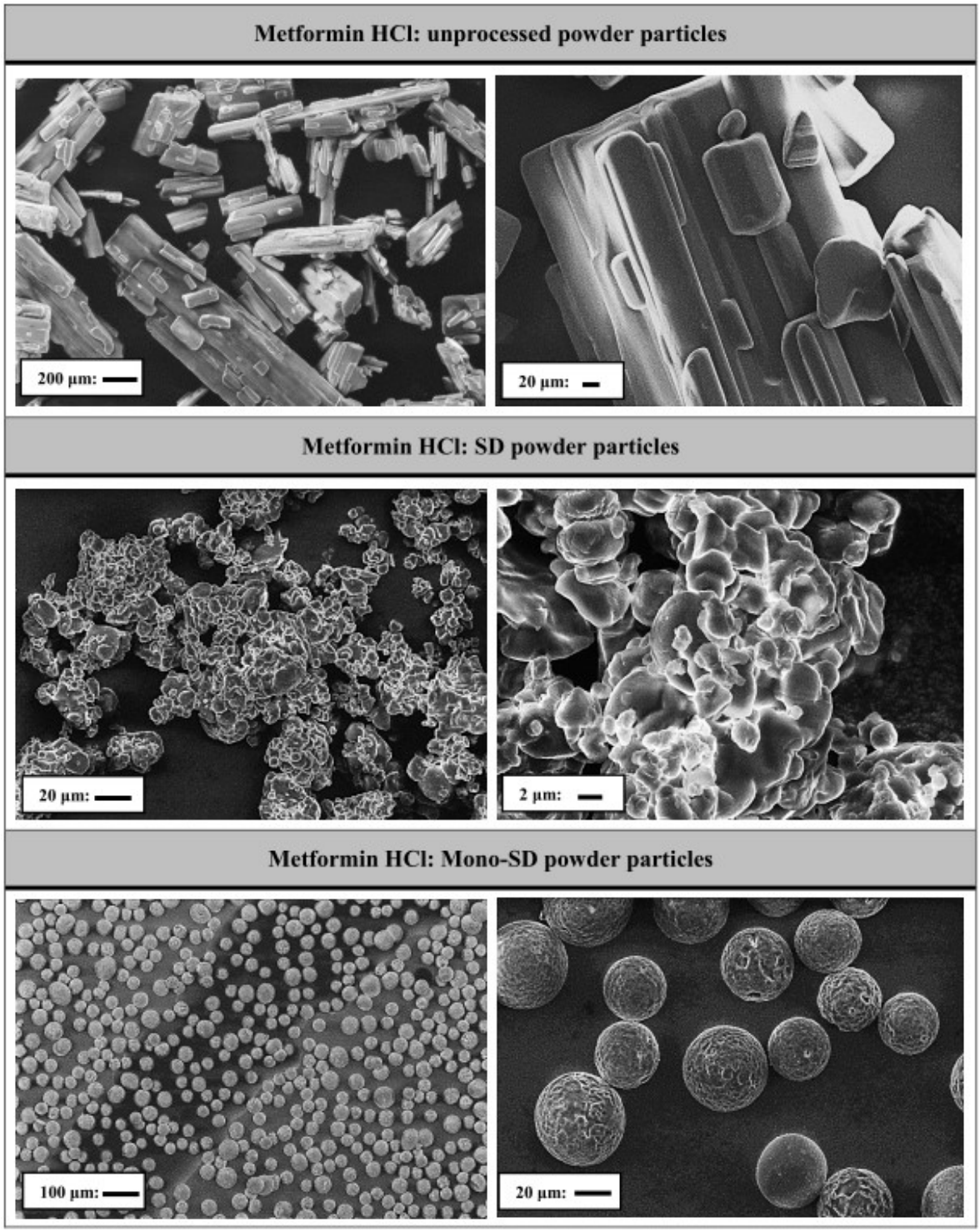

Figure 4.5: SEM images at different magnifications of some metformin HCl particles prepared using two different spray-drying systems in comparison to unprocessed powder particles.

Specifically, the differences in particle size and shape properties for the different studied powders could be explained by the principles of processing routes that were used to make them. The crystallisation technique generally produces particles with wider size and morphological distributions due to difficulty to control nucleation and crystal growth steps, as seen in the unprocessed powder samples (4,13–15,48). In addition, microparticles obtained from the two spray drying systems exhibited a significant difference (ANOVA, P

< 0.05) in morphology and size, indicating that the atomisation mechanism employed in the new single-stream spray drying system significantly affected the powder properties. The conventional spray drying process depends on atomising polydisperse droplets with different trajectories, and each droplet experiences different drying kinetics depending on its size. As a result, SD powder particles usually have a wider size distribution and can agglomerate (165). Conversely, the monodisperse droplets generated by the MDG atomiser typically have similar drying profile during the Mono-SD process, leading to spherical and uniform-sized particles, as anticipated. Controlling particle properties by generating Mono-SD powders may improve bulk powder properties such as flowability and mechanical properties (72,204,262). Thus, the impact of shape and size monodispersity on flowability and compaction will be discussed in sections 4.3.3 and 4.3.4, respectively, after investigating the crystallinity/thermal properties of those powders, which could also play a key role.

4.3.2. Particle crystallinity investigations:

According to literature, mannitol powders can be crystalline in three main polymorphic forms; alpha (α), beta (β) and delta (δ) or a mixture of them. Specifically, β- form is the most thermodynamically stable form at ambient temperature, δ- form is the least stable one, and α- form exhibits intermediate stability between the other two forms (263,264). Also, metformin HCl is observed to crystallise into two conformational polymorphs; a stable phase (form A) and a metastable phase (form B) (265).

Solid-state characteristics of the powdered ingredients were investigated using DSC and XRD. According to the obtained DSC profiles, all powders were crystalline with no fundamental changes in solid-state structure observed after processing (Table 4.4 and Figure 4.6). No endothermic transitions for moisture were noticed below 100ºC which was in good agreement with TGA results, where the moisture content for the studied powders was less than 0.04%, as seen in Table 4.3 above.

Table 4.4: Average melting temperature and enthalpy of the different powdered ingredients.

Powdered ingredient	Thermal parameters		
	Melting onset (ºC)	Melting point (ºC)	Enthalpy of fusion (J/g)
Unprocessed mannitol	165.80 ± 0.21	167.32 ± 0.40	315.46 ± 3.22
SD mannitol	165.34 ± 0.31	167.24 ± 0.30	313.66 ± 2.47
Mono-SD mannitol	165.49 ± 0.16	166.96 ± 0.20	317.96 ± 1.68
Unprocessed metformin	228.68 ± 0.74	231.16 ± 0.30	334.83 ± 2.37
SD metformin	232.03 ± 0.67	233.10 ± 0.50	336.63 ± 3.22
Mono-SD metformin	230.30 ± 0.21	231.92 ± 0.29	336.70 ± 3.44

Results reported as mean ± standard deviation (n = 3).

The DSC curves of all D-mannitol powders presented sharp endothermic transitions at approximately 166 – 167ºC corresponding to the melting points of α or β polymorphs (Table 4.4 and Figure 4.6). All mannitol powders did not display any endothermic transitions at 155ºC, suggesting no δ polymorphic crystals were formed (263). Furthermore, the DSC results indicated no notable differences (ANOVA, $P > 0.05$) in the melting onset and melting enthalpy values, indicating that unprocessed and SD mannitol powders might have similar polymorphic forms. This is consistent with results reported by Hulse et al. for D-mannitol crystals, where they found no significant difference could be observed when comparing the thermal properties of α and β polymorphs (266).

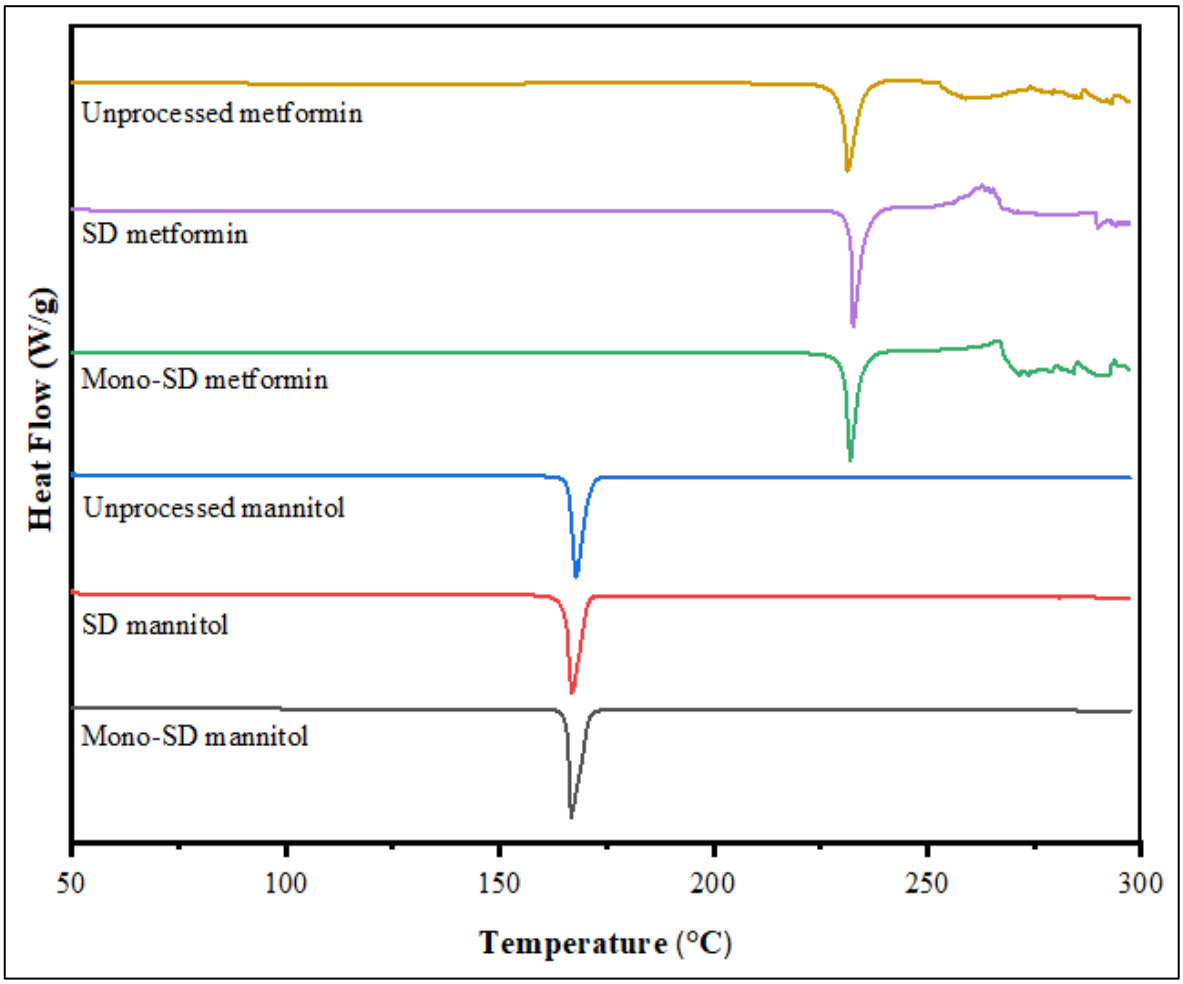

Figure 4.6: Differential scanning calorimetry (DSC) thermograms of different unprocessed and spray-dried powders.

The DSC thermograms of metformin HCl powders showed an initially flat profile, followed by a single sharp endothermic peak transition at approximately 231-233ºC, representing the substance's melting peak. Following this peak, the changes observed were related to the substance's decomposition (Figure 4.6). The DSC results also indicated that the metformin HCl used was in the anhydrous form (267,268). The slight differences observed in the onset of melting between the different powder samples might be attributed to the variation in crystallinity degree or conformational arrangement (polymorphic form) of metformin molecules (Table 4.4). However, no significant difference (ANOVA, $P > 0.05$) in the melting enthalpies

was observed when comparing metformin powders, i.e. the energy required to melt the samples was almost the same even if crystal disruption existed.

XRD was utilised to obtain a more complete picture of the crystalline polymorphic forms of the materials. The summary of the specific XRD polymorphic peaks for each ingredient is presented in Table 4.5 below.

Table 4.5: Unique XRD peaks for polymorphic forms of D-mannitol and metformin HCl materials.

Ingredient	**Polymorphic form**	**Position of peak (*2-theta degree)***
D-mannitol (263,266,269,270)	Polymorph α (metastable form)	Significant scatter at 9.6, 13.8 and 17.2 degrees.
	Polymorph β (most stable form)	Significant scatter at 10.6, 14.7, 23.4 and 29.5 degrees.
	Polymorph δ (less stable form)	An extremely intense peak at 9.74 degrees, then no significant scatters until 19.50 degree.
Metformin HCl (265)	Polymorph A (most stable form)	A significant scatter at 12.21, 12.74 and 17.73 degrees, followed by a subsidiary scatter between 22.40 and 23.82 degrees (3 peaks).
	Polymorph B (metastable form)	Significant scatter at 14.12, 16.61 and 18.57 degrees, followed by subsidiary scatter between 19.86 and 22.62 degrees (4 peaks) and between 27.56 and 34.51 degrees (5-6 peaks).

Furthermore, Figures 4.7 and 4.8 show the XRD patterns which confirm the highly crystalline nature of all mannitol and metformin powders and agree with the previous DSC results. One may expect that XRD peaks of spray-dried powders should exhibit similar intensities to the same peaks of unprocessed materials. However, there was a significant difference in those intensities. This was attributed to the XRD analysis process which is usually affected by particle size and shape. The unprocessed mannitol and metformin HCl powders were made of elongated particles which usually exhibit a preferred orientation during packing in the XRD sample holder and this could have led to distortions in the peak intensities (271,272). The findings from literature also supports this observation, where the variation in the intensity of XRD patterns may be explained due to variations in crystallite size and shape for the material (273–275). For instance, reducing the crystallite size was reported to cause a decrease in the observed peaks' intensity (276). Holder and Schaak also illustrated that decreasing the crystallite size from micro to nanoscale is accompanied with a decrease in XRD peak intensities (271). In addition, Sain et al. confirmed that pyramid-shaped crystals had a much higher resolution and intensity compared to others shapes (277).

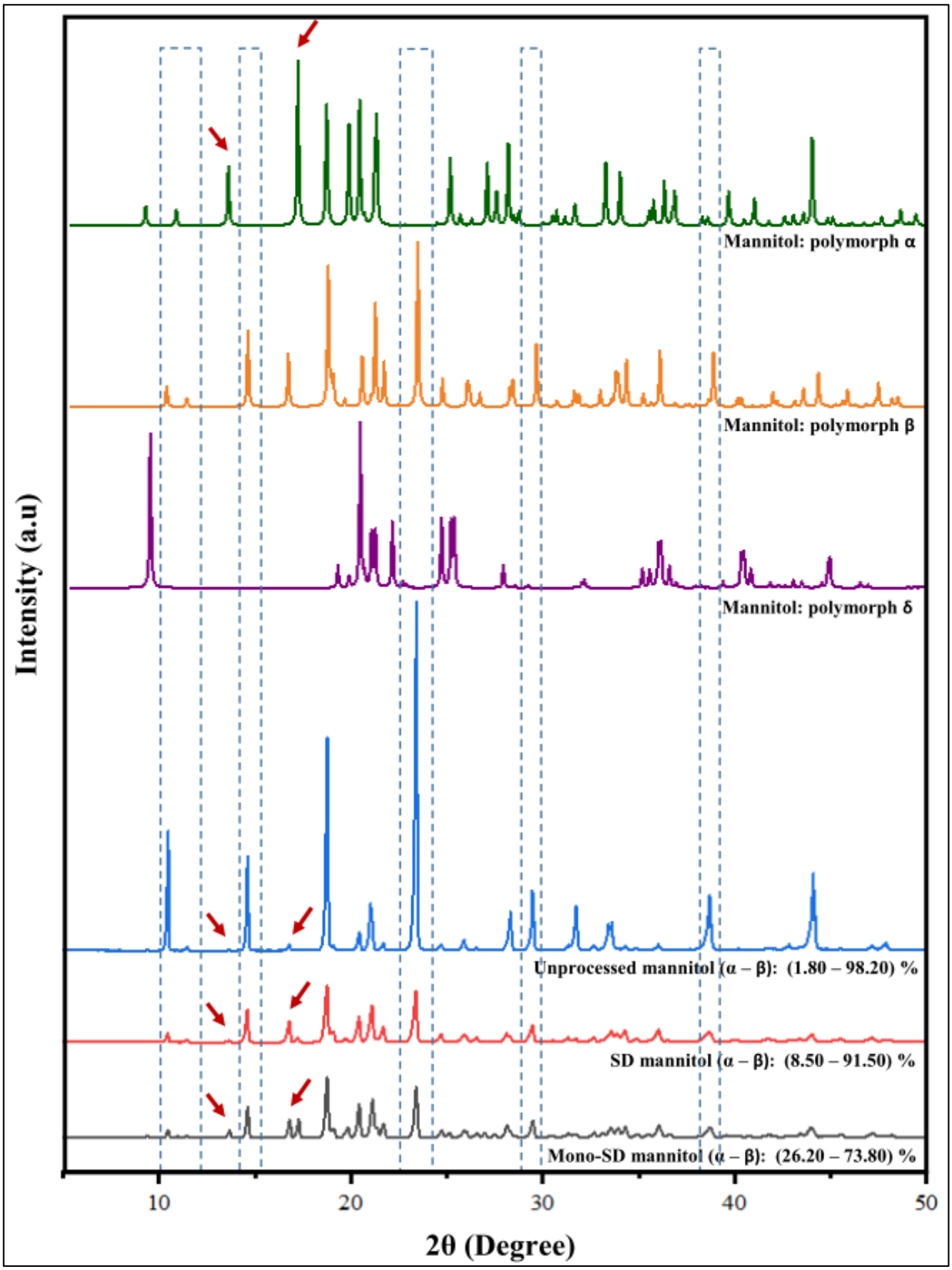

Figure 4.7: Combined plots of XRD for D-mannitol powders and polymorphic forms. The dashed rectangles show the unique scattering peak for β polymorph at 2θ 10.46º, 14.62º, 23.39º, 29.46º and 38.69º. The arrows indicate to the unique scattering peak for α polymorph at 2θ 13.72º and 17.29º. The first three XRD patterns from the top refer to the theoretical patterns of the native mannitol polymorphic forms, while the last three below are for the actual experimental XRD patterns of the mannitol powders that have been analysed. The theoretical patterns of the native mannitol polymorphic forms were obtained from the Cambridge Crystallographic Data Centre (278).

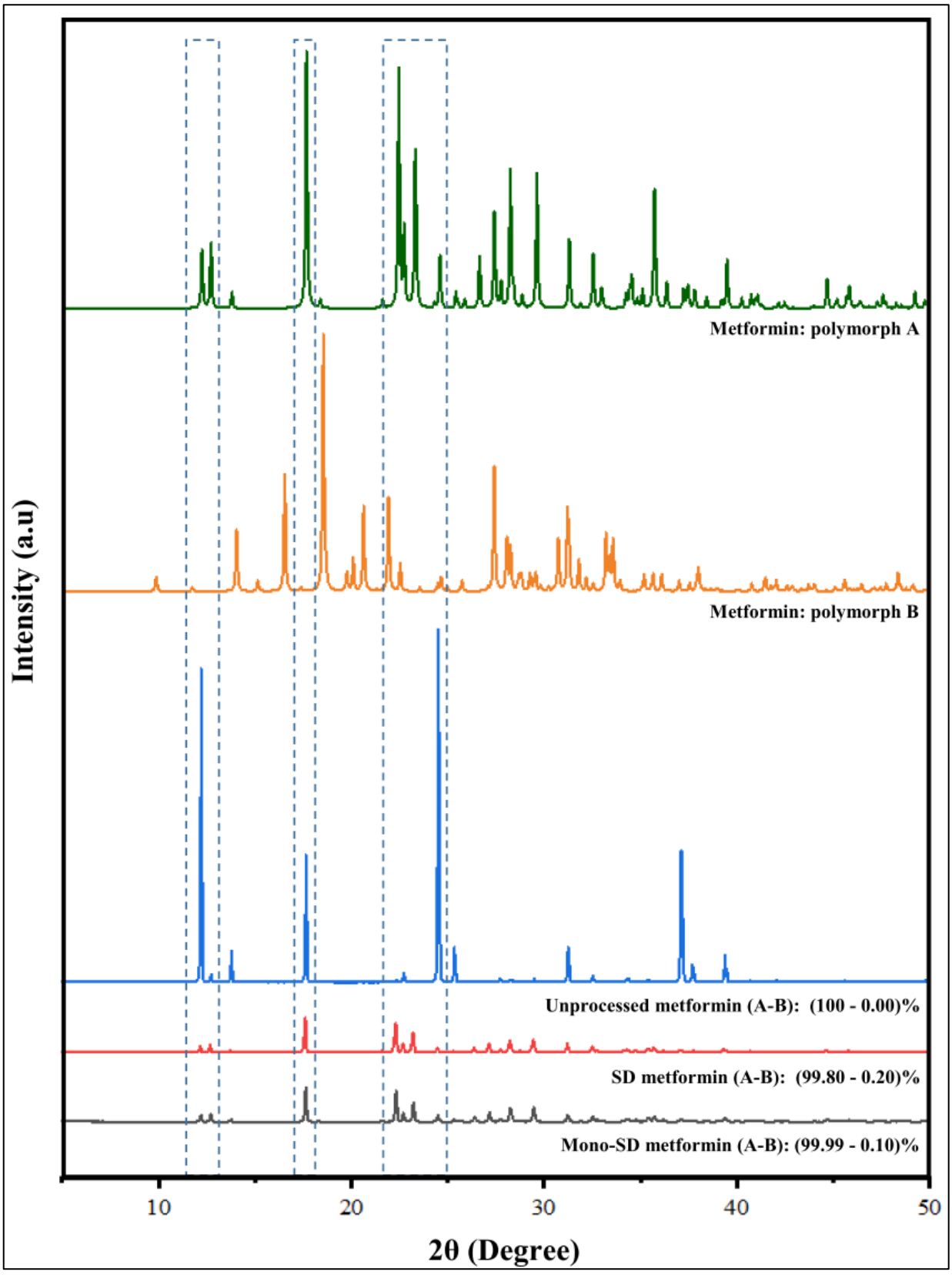

Figure 4.8: Combined plots of XRD for metformin HCl powders and polymorphic forms. The dashed rectangles show the unique scattering peak for polymorph A at 2θ 12.21º, 12.68º, 17.65º, 22.34º and 23.83º. The first two XRD patterns from the top refer to the theoretical patterns of the native metformin HCl polymorphic forms, while the last three below are for the actual experimental XRD patterns of the metformin HCl powders that have been analysed. The theoretical patterns of the native mannitol polymorphic forms were obtained from the Cambridge Crystallographic Data Centre (278).

Furthermore, according to the quantitative Rietveld refinement analysis, unprocessed mannitol is crystalline made mainly from 98.20% w/w of β- crystal form, and a much smaller amount (1.8% w/w) of α-form (Figure 4.7). The SD mannitol had slightly more α form than unprocessed powder of around 8.50 % w/w while β- form is the major component at 91.50 % w/w. Mono-SD mannitol had the highest α- proportion between the three powders of around 26.20% w/w while β- made 73.80% w/w. No δ-polymorph (thermodynamically unstable form) could be observed in all mannitol powders, consistent with the DSC results (no melting peak at 155ºC). Our findings were in good agreement with the literature data where the powders of spray-dried mannitol usually contain α-polymorph alongside β-polymorph, and the amount of α-polymorph significantly increases with the increase in the spray-drying temperature (227,279). Comparing the spray-dried mannitol powders (Figure 4.7), the crystal fractions of α-polymorph rose from 8.50% to 26.20% w/w upon increasing the inlet temperature for spray drying process from 150 to 220ºC. Concomitantly, the crystal fraction of β-polymorph decreased from 91.50% to 73.80% w/w under the same conditions. This higher temperature was necessary to ensure drying of the high velocity droplets emerging from the MDG atomiser.

Unlike mannitol powders, the Rietveld refinement analysis for metformin showed that all diffractograms corresponded to the polymorph A structure (which is considered the most thermodynamically stable form) with only traces of the metastable B form (265). However, as seen in Figure 4.8, there is a significant variation in XRD peaks intensity when comparing SD powders with the unprocessed sample. Furthermore, the XRD patterns of the spray-dried powders look similar. This result indicates that Mono-SD and SD metformin powders may contain similar crystallite sizes compared to unprocessed metformin powder, which contains crystals of relatively large size (271,277,280).

Such polymorphic forms of the same pharmaceutical ingredient are essential to detect it as it is known that different polymorphic forms could have different physical properties and may lead to pharmaceutical formulations with different manufacturability and critical attributes (281).

4.3.3. Effect of monodispersity on powder packing and flowability:

It is well recognised that bulk powder properties are directly related to particle size and shape distributions and thus to processing routes and spray drying conditions (282). Bulk density (ρ_{bulk}) and tapped density (ρ_{tapped}) for different mannitol and metformin powders were measured (Table 4.6). The difference between ρ_{bulk} and ρ_{tapped} for the different powders could be used as an indication of how efficiently the powder packs, which in turn depends on its particle morphological characteristics. The difference between ρ_{bulk} and ρ_{tapped} for Mono-SD powders was significantly (ANOVA, $P < 0.05$) lower than that of the other powders. This is because the change in powder bed volume for the monodisperse particles during tapping is minimal when compared with polydisperse powders (unprocessed and SD powders). The latter two powders have smaller particles that can fill the voids between larger ones, leading to a significant decrease in the powder bed volume upon tapping. This is an indication that Mono-SD powders efficiently pack without any assistance,

therefore little difference in density can be seen upon tapping the powder. However, for the other powders their initial state of packing is affected by the arrangement/rearrangement in the bulk powder bed (74). A departure from spherical particle morphology for the unprocessed and SD powders led to decreased initial packing density and increased the difference between untapped and tapped density (74,283). Prismatic shaped particles (unprocessed) and those that form agglomerates (SD) have the capacity to form bridges and create interparticle pores and large void structure, leading to powder beds with low bulk density and high permeability. On the other hand, the mono-SD powder had a better initial packing due to ease of movement of particles past each other (ball bearing effect), less agglomeration and less formation of bridges between particles i.e. less interparticle porosity.

Table 4.6: Summary of powder packing properties and flow analysis for different unprocessed and fabricated powders.

Packing Parameters	**D-mannitol powders**			**Metformin HCl powders**		
	Unprocessed	***SD***	***Mono-SD***	***Unprocessed***	***SD***	***Mono-SD***
Bulk density (g/cm^3)	0.49 ± 0.01	0.39 ± 0.02	0.66 ± 0.01	0.42 ± 0.01	0.31 ± 0.01	0.74 ± 0.01
Tapped density (g/cm^3)	0.75 ± 0.01	0.66 ± 0.01	0.77 ± 0.01	0.68 ± 0.00	0.54 ± 0.01	0.86 ± 0.00
Inter-particles porosity	0.68 ± 0.02	1.08 ± 0.09	0.22 ± 0.01	0.89 ± 0.06	1.38 ± 0.07	0.19 ± 0.01
Flow parameters						
Carr's index (%)	33.74 ± 0.89	41.40 ± 2.29	14.36 ± 0.73	37.63 ± 1.62	42.77 ± 1.38	13.69 ± 0.84
Hausner ratio	1.51 ±0.02	1.71 ± 0.06	1.17 ± 0.01	1.60 ± 0.04	1.75 ± 0.04	1.16 ± 0.01
Angle of repose (º)	42.00 ± 1.38*	51.54 ± 1.08*	15.82 ± 0.56	44.35 ± 1.07*	46.06 ± 1.13*	13.27 ± 0.71
Flow index (f_i)	0.16 ± 0.01	0.34 ± 0.00	0.07 ± 0.00	0.12 ± 0.00	0.54 ± 0.04	0.08 ± 0.00
Angle of internal friction (º)	42.86 ± 0.37	47.76 ± 0.41	30.56 ± 0.23	36.63 ± 0.55	52.50 ± 0.79	25.86 ± 0.81

Results reported as mean ± standard deviation (n = 3). *Note: powder flow through the funnel with assisted tapping.

In order to estimate flowability for the different mannitol and metformin powders, Carr's compressibility index (CI%), Hausner ratio (HR) and repose angle (θ) for all powder samples were measured (Table 4.6 and Figure 4.9). It was found that Mono-SD powders had significantly (ANOVA, $P < 0.05$) smaller CI, HR and θ values compared with the unprocessed and SD powders. Based on the obtained results, Mono-SD powders' flow was rated as excellent, whereas the flow of unprocessed and SD powders was mainly rated as very poor.

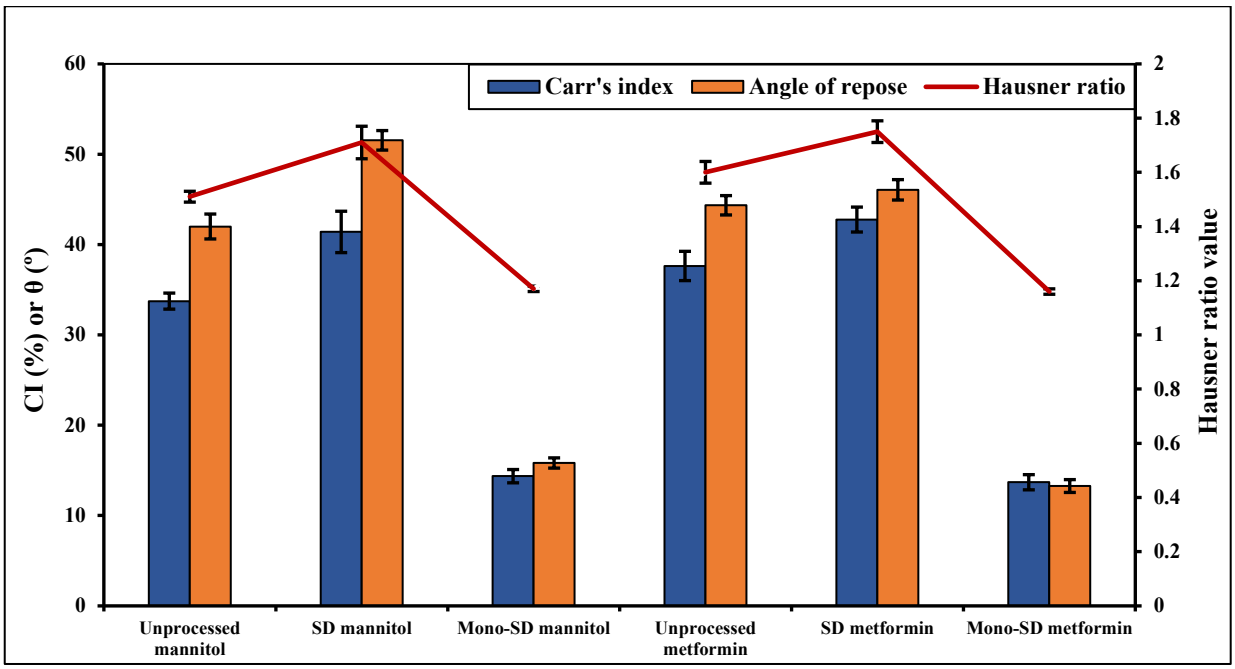

Figure 4.9: Values of Carr's index (CI), angle of repose (θ) and Hausner ratio for different D-mannitol and metformin HCl powders determined following pharmacopoeial methods; (mean ± SD, n=3). The angle of repose for unprocessed and SD powders was determined with assisted tapping.

According to literature, powder flow is significantly affected by both particle size and particle shape distributions (72,284,285). It is typically confirmed that the larger particles have significantly better flow. Particles larger than 250 µm exhibit free-flowing behaviour, whereas particles smaller than 100 µm tend to be more cohesive (72,286). This is because smaller particles correspond to larger specific surface areas (m^2/g), leading to increased interparticle interactions (284). However, even with large particles (e.g. unprocessed metformin particles), a departure from spherical shape has been shown to reduce powder flowability due to increased mechanical interlocking tendency and interparticle friction (103,287).

In this study, unprocessed powders for mannitol and metformin exhibited a cohesive flow despite their relatively larger size (D_{50} > 56 and 379 µm, respectively) (227,288). This could be attributed to their irregular shape (low HSC and high elongation values), resulting in poor packing structure of the powder bed. On the other hand, conventional SD powders for mannitol and metformin had higher HSC and lower elongation values which in theory should help flowability. However, their small particle size (D_{50} < 9.80 and 27 µm, respectively) created more chance for particle-particle interactions, and therefore, powders showed an extremely poor flowability. Compared to the previous results, Mono-SD powders' particles for mannitol and metformin had small size (D_{50} < 39 µm), but unlike conventionally spray dried powders they exhibited better packing density with superior flow due to much tighter CED distribution, higher HSC value and much lower elongation value (Table 4.3). These shape factors may have led to reduced particle interlocking and resistance to flow thereby resulted in the superior flow behaviour.

Furthermore, even though both Mono-SD powders have roughly the same size distribution (i.e. D_{10}, D_{50} and D_{90}), as seen in Figure 4.3 and Table 4.3, it was noticed that Mono-SD metformin powder presented

slightly better flow in comparison with Mono-SD mannitol powder (Figure 4.9 and Table 4.6), especially when investigating the angle of repose. This result mainly exhibits the effect of particles' surface habit on the powder flow, where the particles of Mono-SD metformin showed smoother surface with no folds or wrinkles (Figures 4.5). This could lead to fewer interactions between neighbouring particles and better flowability. In contrast, Mono-SD mannitol particles generally presented a rougher surface and microstructure (Figure 4.4), leading to a powder with a higher angle of repose and inter-particles porosity.

The flow behaviour was further investigated using an automated powder flow tester (PFT) for better understanding of the impact of particle properties on flowability. The results indicated that the powders with different particle size and shape distributions had significantly different shear stress values over a wide range of major principal consolidating stress applied (Figure 4.10). The flow index (fi) values were used for powder flow classification. Statistically, fi values for different mannitol and metformin powders were in the following rank order (Table 4.6): Mono-SD powders > Unprocessed powders > SD powders. For D-mannitol, conventional SD powder showed very cohesive behaviour with fi value of 0.34 while unprocessed and Mono-SD powders showed to be easy flowing and free flowing with fi values of 0.16 and 0.07, respectively. Similar results were observed for metformin HCl powders, where SD powder exhibited cohesive behaviour with fi value of 0.54, while unprocessed and Mono-SD powders showed to be easy flowing and free flowing powders with fi value of 0.12 and 0.08, respectively. Regarding the values of effective angle of internal friction (Table 4.6), the conventional SD powders for metformin and mannitol exhibited significantly (ANOVA, $P < 0.05$) the highest values. However, Mono-SD powder of the same ingredient showed the lowest values (ANOVA, $P < 0.05$), indicating that more cohesive interactions occurred between particles that were produced using the conventional method of spray drying.

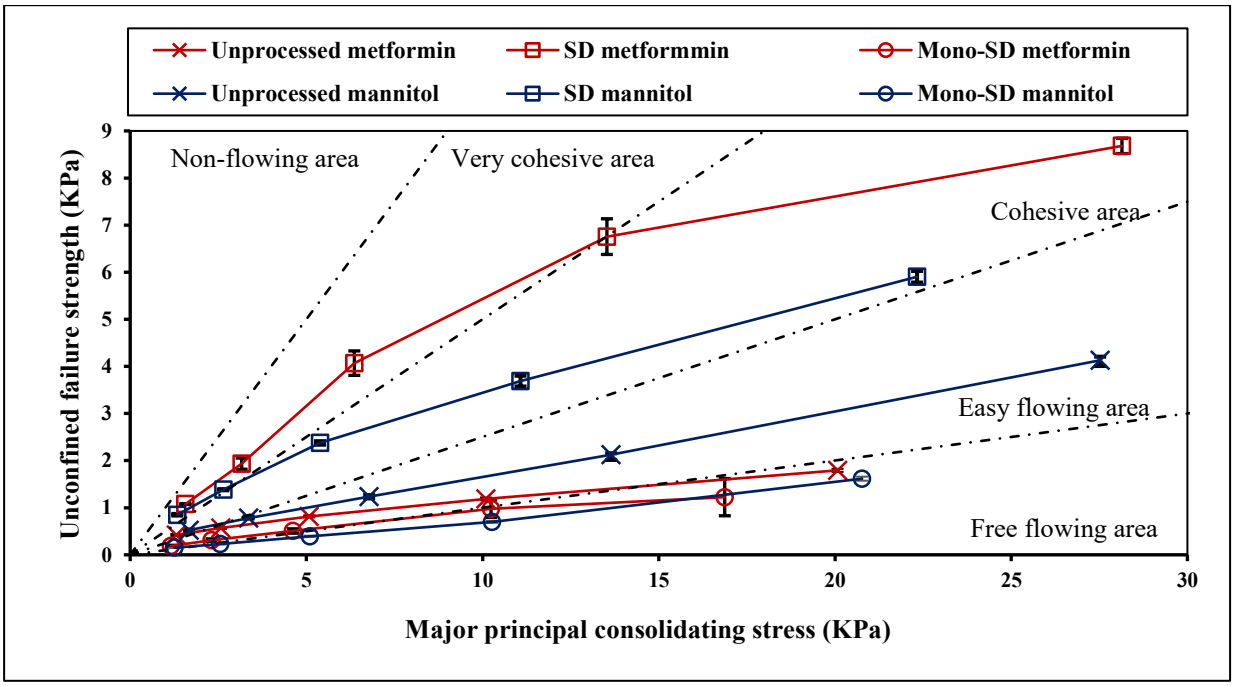

Figure 4.10: Flow function (FF) curves showing unconfined failure strength as a function of major principal stress for different D-mannitol and metformin HCl powders; (mean ± SD, n=3).

The observed flow capacity obtained from the PFT tester for each powder was in agreement with the results reported previously. However, it was found that unprocessed powders for mannitol and metformin were rated as easy flowing by PFT tester, whereas the same powders showed very poor flow by using conventional flowability measurements (i.e. Carr's index, Hausner ratio and angle of repose). This finding can be explained by appreciating the differences between the flow function test (PFT) and the conventional flowability tests. The powder flowability assessment in PFT depends on estimating the cohesion strength that remained in the powder bed after a major principal consolidating stress is applied and removed. Because the unprocessed powders consist of large elongated particles with prismatic/rod shapes, the powder bed's remaining stress is low because the applied consolidating stress has worked only on rearranging the particles in the powder bed by removing the interstitial spaces between them. Thus, the powder flow properties could change when determined by its own weight (i.e. with traditional methods) compared with applying stress. However, it is well known that elongated particles exhibit low bulk density and the flow energy required for agitating the powder bed is much larger than that required for spherical particles (289).

In this study, the differences in bulk powders properties (i.e. packing density and flow behaviour) reflect only the differences in particle size and shape distributions, and it could not be attributed to moisture content effect as all powders were tested in a dry state and they had moisture content less than 0.04%, as seen before in Table 4.3.

4.3.4. Mechanical properties of powders:

Particle size and shape is well known to influence powder tableting performance by affecting the bonding strength, bonding area, and/or particles rearrangement and deformation behaviour (70,74,223). However, the effect of distribution of these properties is less well known. In this section, the effect of powder monodispersity on compaction properties was investigated.

4.3.4.1. Mannitol powders assessment:

Mannitol is a brittle material with relatively poor binding properties. Due to its brittle nature, mannitol commonly generates compacts with poor mechanical properties (i.e. low tensile strength and high friability), especially when using the β- polymorphic form (the most stable form) (290). However, it has been shown that mannitol with α- or δ- polymorphic forms has a better tabletting behaviour than β- form. This is because α- and δ- forms have a lower propensity to fragmentation and lower elastic recovery in comparison with the β-form. As a result, α- and δ- forms can generate a robust tablets with low die wall friction even at a high compression pressures (227,263).

Heckel profile analysis (Table 4.7) showed that all mannitol powders displayed high mean yield pressures (P_y) when they were compressed using low or high compaction speed. These results illustrated that the consolidation mechanism for all compressed mannitol powders was mainly brittle fracture (fragmentation). In addition, it was noted that the propensity for fragmentation increases (increased P_y values) when

increasing the compression speed from 0.1 to 300 mm/s. This is because particles have less time available for rearrangement and slippage at higher compression speed, leading to fewer contact points between particles and/or higher air content in the powder bulk during the compression process (244,291,292). As a result, the compacts produced at the higher compression speed had significantly lower tensile strength, lower solid fraction, and a higher percentage of elastic recovery than the compacts made at low compression speed.

Table 4.7: Compaction parameters of the mannitol powders obtained at low- and high- compression speeds [a].

D-mannitol powders						
Compression speed (mm/s)	***Unprocessed***		***SD***		***Mono-SD***	
	0.1	***300***	***0.1***	***300***	***0.1***	***300***
Tensile strength (MPa)	1.92 ± 0.09	0.39 ± 0.01	3.09 ± 0.10	1.88 ± 0.20	1.79 ± 0.09	0.37 ± 0.02
Out of die solid fraction	0.91 ± 0.00	0.79 ± 0.00	0.93 ± 0.00	0.85 ± 0.00	0.92 ± 0.00	0.84 ± 0.00
Elastic recovery (%)	2.54 ± 0.23	13.35 ± 1.03	1.03 ± 0.27	3.11 ± 0.17	1.95 ± 0.20	5.11 ± 0.93
Mean yield pressure (MPa)[b]	174.70 ± 3.04	189.45 ± 0.32	156.34 ± 5.97	182.62 ± 4.17	177.29 ± 2.63	189.08 ± 4.92
SRS (%)	7.78 ± 1.50		14.41 ± 1.67		6.17 ± 2.73	
Powder true density (g/cm^3)	1.49 ± 0.00		1.50 ± 0.00		1.50 ± 0.00	

[a] All values were determined from the compaction simulator displacement system. Results reported as mean ± standard deviation (n = 3).

[b] Mean yield pressure (P_y) was calculated from the straight-line portion of the Heckel plot (25-150 MPa) with a correlation coefficient (R^2) ≥ 0.984.

When comparing the different mannitol powders, SD powder which contains the highest percentage of fines (D_{50} < 9.80 μm), exhibited significantly (ANOVA, P < 0.05) the lowest P_y and the highest SRS. These results indicated that SD mannitol had slightly better plasticity than the other powders, leading to compacts with significantly higher tensile strength, higher solid fraction, and lower elastic recovery (Table 4.7). By contrast, P_y values for the unprocessed and Mono-SD powders were much higher with no significant difference between them (ANOVA, P > 0.05), leading to compacts with lower tensile strength and higher elastic recovery. These findings suggested that the inter-particulate bond structure of the three mannitol powders was significantly different (223). Powders with smaller particle size usually exhibit better particles rearrangement at the initial stage of the compaction process, leading to a lower P_y (221). For example, Katikaneni et al. investigated the effect of particle size on the tableting properties of ethylcellulose, and found that decreasing the particle size from 420-840 to 105-149 μm led to a significant decrease in the yield pressure (P_y) from 83 to 58 MPa (291). In addition, for materials with a high tendency to fragment such as

mannitol powders, a reduction in primary particle size could give an increase in the tensile strength and decrease in the elastic recovery of the compacts, probably due to the increased number of contact points between particles (222). These results indicate that mannitol powders with smaller particle sizes (D_{50} < 18 μm) can be compacted more firmly than the larger particles. This leads to compacts with higher tensile strength even though it contains a slightly lower percentage of α- polymorph (~ 8.50%) i.e. the one with better compaction properties. By contrast, the Mono-SD powder, which contains spherical particles with narrow distribution (D_{50} ~ 37 μm), generated compacts with the lowest tensile strength even though it has a higher percentage of α- polymorph (~ 26.20%). In addition, compared with unprocessed mannitol powder which contains bigger particle size but with the lowest percentage of α- polymorph (~ 1.80%), the Mono-SD powder exhibits roughly the same poor compaction properties. This is probably due to fragmentation of the large particles of unprocessed mannitol leading to similar bonding behaviour to that of the fine powder of Mono-SD. In other words, even though Mono-SD powder contains a smaller particle size than the unprocessed mannitol and a higher percentage of α- polymorph (~ 26.20%), the high monodispersity of the powder led to compacts with poor mechanical properties. This is probably because the monodisperse particles with identical spherical shape displayed very low adhesion and interaction during the compaction process (Appendix A3).

These results agree with the previous studies, where the primary particle size and specific surface area were identified beside the polymorphic forms as the major contributing factors affecting the mannitol powders' compaction properties and tableting performance (293,294). For example, Tarlier et al. found that the compacts of mannitol powder (Pearlitol®) with particles size (D_{50}) of around 25 μm exhibited tensile strength 2 times higher than the compacts with particle size of around 160 μm (295). Al-Khattawi et al. investigated the effect of polymorphism on the compaction properties and behaviour of the spray-dried mannitol powders generated with different polymorphic ratios (α- and β-) forms. They showed that increasing α-polymorph in the powder content from 2.23% to 84.1% led to 2.5 times increase in the tensile strength of the compacts, even though the powders had roughly similar particle size distributions (227). Also, as expected, they found that the mean yield pressure was reduced from 233.48 to 34.67 MPa as the percentage of α-polymorph increased. This was attributed to better powders' plasticity.

4.3.4.2. Metformin HCl powders assessment:

Metformin HCl is considered a viscoelastic material with poor compressibility, resulting in weak tablets with a high tendency to cap or laminate (226,228,267,296). From the Heckel profile analysis (Table 4.8), it can be noted that all metformin powders display high values of mean yield pressure (P_y). However, the unprocessed powder significantly exhibited the lowest P_y values, while the P_y values for SD and Mono-SD powders were much higher, with no significant difference between them (ANOVA, P > 0.05). Furthermore, it is clear that increasing the compression speed from 0.1 to 300 mm/s led to a decrease in the P_y values. As a result, the SRS had negative values with no significant difference between metformin powders. This finding confirms that all metformin powders exhibit time-dependent viscoelastic properties, resulting in

compacts with deficient strength and a high tendency to cap and laminate even when using low compression speed.

Table 4.8: Compaction parameters of the metformin powders obtained at low- and high- compression speeds[a].

Metformin HCl powders						
Compression speed (mm/s)	***Unprocessed***		***SD***		***Mono-SD***	
	0.1	***300***	***0.1***	***300***	***0.1***	***300***
Tensile strength (MPa)	0.20 ± 0.06	0.02 ± 0.01	0.04 ± 0.04	0.03 ± 0.02	0.07 ± 0.00	0.04 ± 0.01
Ejection force (N)	97.00 ± 11.31	300.33 ± 10.65	49.66 ± 3.68	269.66 ± 11.08	53.00 ± 6.68	282.66 ± 4.71
Out of die Solid fraction	0.90 ± 0.00	0.90 ± 0.00	0.79 ± 0.00	0.79 ± 0.00	0.83 ± 0.00	0.84 ± 0.00
Elastic recovery (%)	7.81 ± 0.25	1.63 ± 0.15	17.51 ± 0.45	10.65 ± 1.05	12.06 ± 1.03	4.99 ± 0.94
Mean yield pressure (MPa)[b]	171.66 ± 11.55	165.15 ± 7.81	200.55 ± 8.92	196.54 ± 2.42	205.72 ± 5.24	195.64 ± 8.33
SRS (%)	-3.98 ± 5.70		-2.09 ± 5.51		-5.45 ± 7.12	
Powder true density (g/cm^3)	1.36 ± 0.00		1.36 ± 0.00		1.36 ± 0.00	

[a] All values were determined from the compaction simulator displacement system. Results reported as mean ± standard deviation (n = 3).

[b] Mean yield pressure (P_y) was calculated from the straight-line portion of the Heckel plot (25-150 MPa) with a correlation coefficient (R^2) ≥ 0.984.

It was observed that the compacts of unprocessed metformin exhibited slightly higher tensile strength than that of the compacts made from SD/Mono-SD powders. This finding could be attributed to the relatively large particle size of the unprocessed raw powder where a bigger particle size with a prismatic shape likely to fragment more at the initial stage of compression than smaller particles. This leads to creating new clean and uncontaminated surfaces, which helps to increase inter-particulate bonding in the powder bed. This finding may explain why the compacts of unprocessed metformin powder showed significantly lower elastic recovery than the spray-dried powders, which exhibited higher resistance to fracture under compaction due to their small particle sizes (297,298). As a result, spray-drying process of metformin powder did not enhance its mechanical properties and tableting performance even though it formed particles with smaller size, which theoretically should increase the inter-particulate bonding in the resulted compacts.

For metformin HCl, according to the above discussion, it can be concluded that the impact of particles monodispersity and/ or polydispersity on material compaction properties can be considered negligible due to the viscoelastic properties of the metformin HCl. As a result, improving compaction properties of metformin powders depends mainly on increasing material's plasticity and bonding strength between particles.

4.3.5. Holistic understanding of the powders direct compression properties using a modified SeDeM expert system:

Direct compression (DC) technology is the most preferred route for tablet preparation due to its simplicity and cost-effectiveness (299). However, this technology can be applied only if the powder blend presents optimum characteristics with respect to the flow, packing density, and compaction behaviour. In recent years, the interest in the SeDeM expert system has been increasing dramatically as an effective holistic tool to predict powder's suitability for direct compression based on its physical properties.

The principle of this method depends on quantifying twelve input parameters that have a critical impact on flowability and compressibility for any powder substance. However, this system is currently used for multiple applications, such as evaluating materials quality and manufacturability, controlling lot-to-lot variability in raw material properties, optimising formulation composition and process conditions, developing direct compression formulations with a minimum number of experiments, and selecting the most suitable excipients to use in formulation development for direct compression, etc. (250).

In the conventional SeDeM expert system, the compressibility of the powders is determined by empirical methods, i.e. Carr's compressibility index and inter-particle porosity. These methods are based on the volume reduction of powder when subjected to lower mechanical stress, such as the tapping process. However, in the pharmaceutical industry, these parameters might not help to predict the powder compressibility during the typical process of direct compression where the powder undergoes high compression pressure to form a compact with appropriate mechanical properties (236). Also, in this conventional system, the ability of materials to form compacts is determined by their cohesion index, which represents the hardness of tablets formed after compression. However, this value (tablet hardness) depends on the material properties, the compression pressure applied, and the dimensions of the tablet (300). Moreover, in this conventional system, monitoring the rate of material flow through an orifice has been proposed to predict powder flowability. However, this method is only suitable for relatively free-flowing powder. In addition, the variability in packing density, container geometry, orifice diameter, orifice height and the volume of the powder bed leads to significant variability in the test results (236,301). Therefore, the repeatability of this method can be relatively poor and null results are usually obtained with cohesive powders that do not flow easily.

Based on these scientific principles, the previous conventional parameters, such as Carr's compressibility index, inter-particle porosity, cohesion index and powder flow rate, could be replaced with more representative parameters for material flowability and compressibility. For example, the mean yield pressure (P_y) determined by Heckel analysis has been widely used to assess the deformability of powdered materials (239,240). However, for highly compressible materials, the mean yield pressure (P_y) will be much lower compared to poorly compressible materials (242,243). The tablet tensile strength, which depends only on material properties, is scientifically a more appropriate parameter to represent the ability of powdered material to form a tablet rather than the cohesion index (300). The shear cell analysis is another

pharmacopeial method to estimate powder flowability by measuring the powder flow index (fi). Recently, this technique is widely used in the pharmaceutical industry to assess powder flow behaviour because it is automated and offers a greater degree of experimental control when compared with other manual pharmacopeial methods (236,238).

Therefore, the conventional SeDeM expert system was modified to include mean yield pressure, tablet tensile strength and powder flow index, which are essential to investigate when the powders manufacturability need to be determined. In this study, a modified SeDeM system with 12 input parameters was used to capture the overall picture of the powders used.

As seen in Table 4.9, Mono-SD powders for both mannitol and metformin generally had the highest score for each input parameter except P_y, TS, and %Pf, leading to creating modified SeDeM diagram with a better profile (i.e. symmetrical structure and closer to the optimal outside polygonal limits). The modified SeDeM diagram for unprocessed and SD powders exhibits a relatively smaller area with a less symmetrical structure, as seen in Figure 4.11.

Table 4.9: Test results of untreated and spray-dried powders proposed by the modified SeDeM expert system.

Powders assessment by modified SeDeM expert system						
SeDeM system Input parameters (r)	***D-mannitol powders***			***Metformin HCl powders***		
	Unprocessed	***SD***	***Mono-SD***	***Unprocessed***	***SD***	***Mono-SD***
Bulk density (ρb)	4.90	3.90	6.60	4.20	3.10	7.40
Tapped density (ρt)	7.50	6.60	7.70	6.80	5.40	8.60
Mean yield pressure (P_y)	0.52	0.86	0.54	1.74	0.17	0.21
Tensile strength (TS)	0.78	3.76	0.74	0.04	0.06	0.08
Carr's index (CI)	3.25	1.72	7.12	2.47	1.44	7.26
Hausner ratio (HR)	4.90	2.90	8.30	4.00	2.50	8.40
Angle of repose (θ)	1.60	0.00	6.83	1.13	0.78	7.34
Powder flow index (f_i)	8.40	6.60	9.30	8.80	4.60	9.20
Loss on Drying (%LOD)	9.98	9.97	9.97	9.96	9.96	9.96
Hygroscopicity (%H)	9.96	9.96	9.97	9.94	9.95	9.94
Particles >50µm (%Pf)	5.65	0.12	0.49	9.95	2.28	0.99
Homogeneity index (HI)	4.60	4.40	6.60	3.60	3.10	6.00

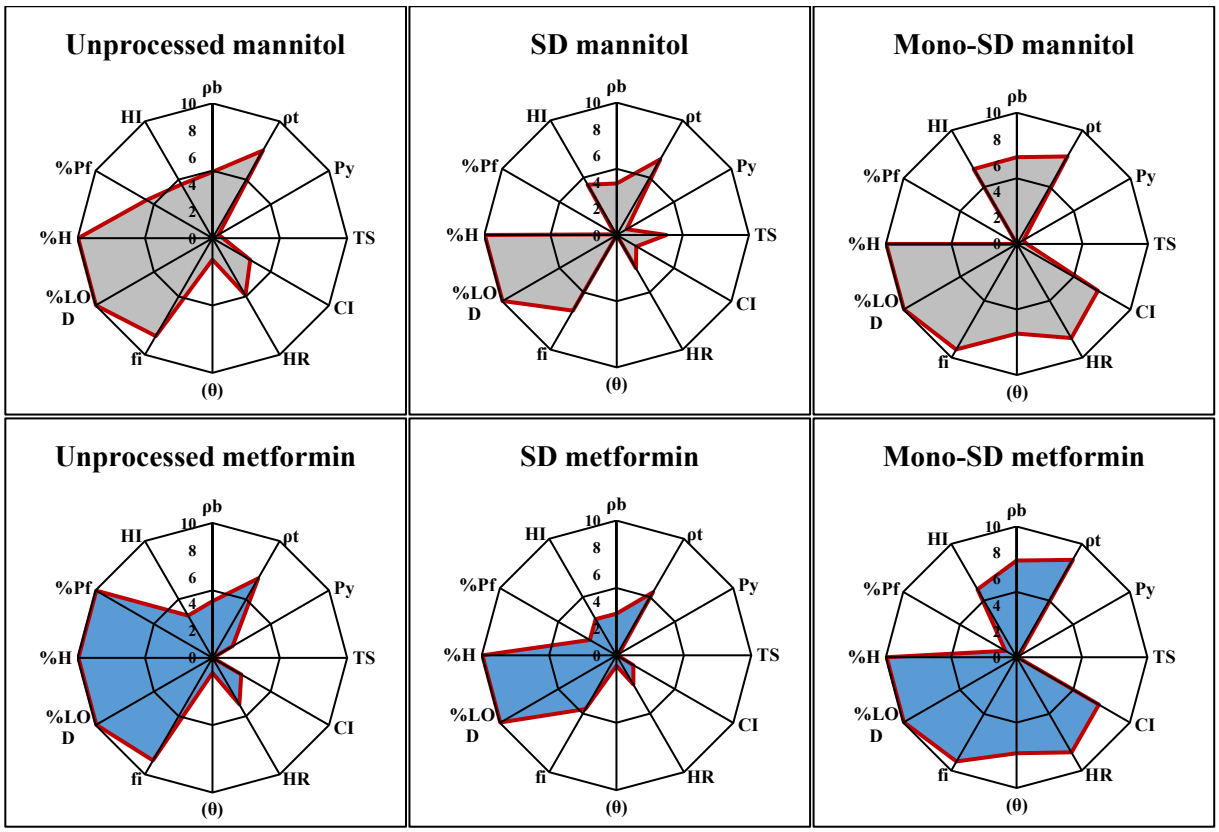

Figure 4.11: The modified SeDeM diagram for different mannitol and metformin powders.

As seen in Figure 4.11 and Table 4.9, even though the powder's compressibility was undesirable due to the nature of materials used in this study, it can be concluded that controlling particle size and morphology has made a drastic improvement to the bulk powder flowability component of the diagram. Expressly, our results indicated that spherical particle powders with uniform size < 50µm have better flow and packing properties than other conventional powders containing particles with wider size and shape distributions. This phenomenon could be attributed to a decrease friction and adhesion forces between uniform spherical particles. This result was in good agreement with a previous report where spherical crystals < 62 µm of paracetamol powder showed significantly better flowability and compression properties than other powders having different geometrical particle properties (74).

Based on the obtained results, it can be concluded that the D-mannitol and metformin HCl powders which were investigated in this study are not suitable for direct compression due to their poor compression properties. However, the Mono-SD mannitol and metformin's high powder flowability reduces the need to use functional excipients and/or further production steps to improve flowability and content uniformity of the powdered pharmaceutical formulations. Therefore, using these Mono-SD powders could be appropriate for developing pharmaceutical formulations ideal for capsule filling, leading to solid dosage forms with optimal CQAs (i.e. weight and content uniformity).

4.3. Conclusion:

Achieving the desired powder flow and packing properties of pharmaceutical ingredients is essential for manufacturers, especially within chemical development teams, to enhance the solid dosage forms' critical quality attributes (CQAs). Unfortunately, most pharmaceutical ingredients are polydisperse powders containing fine particles with uncontrolled morphologies and agglomerates. Powders with small particles less than 100 μm usually exhibit poor flowability. This is due to their high specific surface area that leads to increased interactions between neighbouring particles. In this study, Mono-SD powders that were generated using a single-stream spray drying technology with particle sizes less than 50 μm exhibited significantly better bulk powder properties (e.g. flowability and packing density) compared with other untreated and conventional spray-dried powders. This could lead to the conclusion that controlling fundamental particles properties by creating uniform spherical particles during material manufacturing not only enhances powders flowability but also helps to minimise the variations in critical material attributes during powders handling and processing, leading to producing pharmaceutical products with higher quality.

Specifically, the impact of using Mono-SD powders in the pharmaceutical industry could become more apparent when producing pharmaceutical dosage forms as low-dose units for oral and inhalation applications. This is because the high monodispersity and free flowability of the powder could help in dispensing small amounts (5 μg to 5 mg) of pure APIs into capsules with accurate weight and content uniformity, resulting in decreasing the variations in clinical response, especially if the drug is highly potent and has a very narrow therapeutic window. Furthermore, relying on using monodisperse particles in solid dosage forms production could be critical to ensure good dispersibility and uniformity in dissolution, especially for micronised drugs that may tend to aggregate in blends due to their increased surface area. In other words, monodispersity could help in achieving high dissolution profiles similarity between generic and branded products and/or high consistency between batches for solid dosage formulations.

Chapter 5

CHAPTER 5

Using Monodisperse Spherical Carrier Particles to Improve the Content Uniformity of Low-Dose Binary Blends

5.1. Introduction:

Processing of Highly Potent Active Pharmaceutical Ingredients (HPAPIs) usually presents a number of challenges e.g. high manufacturing cost and poor content uniformity, especially if the active is a low dose one that requires uniform blending with a larger amount of excipient (filler/carrier) before tableting/capsule filling (38,41,302). Content uniformity (CU) of solid dosage forms is one of the critical quality attributes directly linked to the patient (224). Hence, inadequate uniformity is unacceptable as it leads to fluctuations in the delivered dose. Some of these problems can be manifested in medicine ineffectiveness that result from under dosing, while an overdose can cause remarkable side effects. Both situations are harmful to the patient and could lead to serious health issues (303,304). For example, patients with congestive cardiac failure (CCF) usually take digitoxin tablets (50 to 200 μg) daily where under-dosing causes therapeutic failure and can lead to death from CCF, while overdosing causes toxicity and chances of death due to development of arrhythmia (303). Therefore, achieving a uniform distribution of the drug substances for these low dose highly potent drugs throughout the formulation blend is critical to obtain the correct effect in the final product.

However, producing formulations with high blend homogeneity is not a trivial task due to agglomeration and segregation issues, leading to non-uniformity in the mixing process, especially when the drug substances are poorly flowing (cohesive) and used in small concentrations (38,39,302). This is because of the mismatch in fundamental particle properties (i.e. size, shape, density, surface morphology, etc.) between the different ingredients used in the formulation. This variation in particle properties leads to problems such as particle segregation due to difference in size and density between the active and excipients or failure to generate random/ordered mixtures which ultimately negatively impacts the blend uniformity (77,85). Unsatisfactory content uniformity often leads to batch rejection and recalls. For example, even though many pharmaceutical manufacturers have successfully developed low-dose formulations for the levothyroxine compound, several batches have still been recalled every year because they do not meet the content uniformity specifications (44).

According to the literature, several approaches have been utilised to improve blend homogeneity and content uniformity, mainly when producing low-dose solid dosage forms. These approaches include: (a) geometrical drug blending with excipients, (b) ordered mixing of micronised drug with appropriate carrier

excipient to form interactive mixtures in which the micronised drug particles are adsorbed onto the carrier particles (305,306), (c) dissolving or dispersing the drug substances in a liquid vehicle and spraying the resulting solution onto the powder bed, (d) dissolving or dispersing drugs into either liquid or semi-solid vehicles followed by encapsulating them into capsules (307), and (e) using microdroplets dispensing technology to disperse the drug/polymer solution onto the surface of the carrier tablets (308). Although the previous approaches have shown some successes, they are considered costly and time consuming for many manufacturers. In addition, in many cases, these approaches are not preferred for use in the early stages of drug development where prototype formulations need to move to Phase I clinical studies quickly without heavy capital investment in the above technologies. Therefore, formulation scientists are currently interested in using automated powder dispensing systems for formulating low-dose solid dosage forms (309–311). The performance of these dosing systems and capsule machines depends significantly on the blend's bulk properties to be fed to the system. Specifically, the flowability of the blend affects its content uniformity, and for a low-dose drug this becomes of critical importance (307,312). As discussed previously in chapter 1, bulk powder properties, including flow behaviour and packing properties, are usually related to fundamental particle properties such as particle size, size distribution, and shape (6,16,17).

As discussed in the previous chapter, monodisperse spray-dried powders have better flowability and packing properties than conventional unprocessed and spray-dried powders. Therefore, it can be supposed that using monodisperse powders in the pharmaceutical industry may help to improve the homogeneity and flowability of low-dose powder blends. Consequently, this can lead to enhancing their filling processes into capsules using automated or conventional systems and enabling capsules with high content uniformity for HPAPIs.

This study aims to investigate the impact of particle size and shape of the formulation ingredients, powder monodispersity/polydispersity and dilution potential of the excipient on the homogeneity and content uniformity of a binary mixture system containing a low-dose drug. Felodipine and mannitol were used as a model drug and carrier excipient, respectively. In this investigation, different binary mixtures of felodipine and mannitol were prepared using powders with varying bulk properties: unprocessed powders, spray-dried (SD) powders and monodisperse (Mono-SD) powders. Specifically, the experimental approach consisted of preparing mixtures of each of the carrier samples (unprocessed, SD, and Mono-SD mannitol powders) with different concentrations of each drug samples (unprocessed, SD, and Mono-SD felodipine powders), followed by measuring their content uniformity after 10 and 30 minutes of the mixing process. In order to understand the impact of powder properties on the mixing behaviour and blend homogeneity, all powdered materials were characterised using particle size analysis, angle of repose method, and optical/scanning electron microscopy technique.

5.2. Material and methods:

5.2.1. Materials:

D-mannitol and felodipine with high purity >98.0% were purchased from Sigma-Aldrich (Pool, UK) and Discovery Fine Chemicals (Dorset, UK), respectively. Both ingredients were of pharmaceutical grade and used without any further purifications to prepare feed solutions for spray-dried powder production. Sodium phosphate monobasic and phosphoric acid 85% were purchased from Sigma-Aldrich (Dorset, UK). HPLC-grade organic solvents (ethanol, methanol, acetonitrile) were all supplied by Fisher Scientific (Loughborough, UK).

For HPLC analysis, the buffer solution was prepared according to the official felodipine monograph presented in the US Pharmacopoeia by dissolving 6.9 g/L of monobasic sodium phosphate monohydrate in water adjusting with phosphoric acid to a pH of 3.0 ± 0.05 (313).

All aqueous solutions were prepared using ultra-purified water produced by Milli-Q Integral system (Hertfordshire, UK).

5.2.2. Spray-drying experiments and microparticles formation:

Conventional spray-dried powder for felodipine was fabricated using a mini spray dryer Büchi B-290 (Büchi Labortechnik AG, Flawil, Switzerland) equipped with an inert loop B-295 for safe operation and organic solvent condensation. A feed solution composed of felodipine in ethanol at 15% (w/v) was atomised using a two-fluid nozzle with an inner tip of 0.7 mm and a cap of 1.5 mm. The co-current spray drying process was conducted under the following conditions: feed solution flow rate at 3.5 ml/min; atomising nitrogen flow rate at 300 L/h; drying gas (nitrogen) flow rate at approximately 30-35 m^3/h (90% of aspirator rate); inlet temperature at 115ºC and outlet temperature at 88ºC.

Monodisperse spray-dried powder for felodipine was fabricated using the single-stream spray drying system built in our laboratories (see chapter 3 for more details). The system was equipped with a 35 µm pinhole MDG atomiser. A feed solution composed of felodipine in ethanol at 15% (w/v) was pumped through to the MDG atomiser at 0.4 ml/min and was disintegrated into monodisperse droplets using a vibration frequency of 46 KHz. The generated droplets were dispersed using pulsating air with a velocity of around 20 m/s. All previous operation parameters were selected by monitoring the droplet atomisation using a real-time stroboscopic imaging system (the detailed specification for this system have been presented in chapter 2). During the spray-drying process, a co-current laminar airflow with a constant velocity of 1.14 m/s was used, and the inlet temperature of drying air was maintained at 200ºC, whereas the outlet temperature was recorded at 79ºC. All feed solutions were prepared fresh before use in the spray drying process.

For spray-dried mannitol samples, the operation conditions and processing parameters used to generate monodisperse and polydisperse powder particles were explained previously in detail in chapter 4.

All the spray-dried powders were stored in desiccators at room temperature before characterisation or further analysis.

5.2.3. Characterisation of the powders particle properties:

5.2.3.1. Particle morphology analysis:

For morphology observation, powder samples were imaged using:

- ***Optical microscope observations:***

Optical microscopy (Zeiss Axio Scope A1, Carl-Zeiss, Oberkochen, Germany) was used to study the morphology of the particles in each sample. A small powder sample was sprinkled onto a glass plate in this analytical approach and examined using an X10 magnification lens. The particles were imaged using a Zeiss Axio camera interface provided with the Zeiss Axio Vision imaging software.

- ***Scanning electron microscope (SEM) observations:***

SEM was used to study the morphological structure of the particles. The samples were observed using Zeiss Supra 55VP FE SEM (Zeiss, Oberkochen, Germany) operated at 2 and 10 KV in variable pressure mode. Each powder sample was first sprinkled on a double adhesive tape over an aluminium stub. Subsequently, the sample was observed directly by the SEM without gold coating to avoid any change in particles' surface morphology and spurious results.

5.2.3.2. Particle size analysis:

Particle size distributions (PSDs) for all D-mannitol and felodipine powders (both unprocessed and processed) were determined using laser diffraction, Sympatec HELOS/ RODOS (Sympatec GmbH, Clausthal-Zellerfeld, Germany). Approximately 0.5 g of each powder was dispersed through the laser path using 1.0 bar dispersion air pressure and 70% feed flow rate. All measurements were conducted in triplicate and were set to record for 10 sec each when the optical concentration ($C_{opt.}$) was > 2%. All powder samples were analysed using an R5 lens which provides a feasible operating range for particle size measurement between 0.45 and 875 µm. PSDs (D_{10}, D_{50}, and D_{90}), particles volume fractions (%) less than 10 µm and less than 25 µm for each sample were calculated based on Fraunhofer theory and analysed using the Sympatec PAQXOS 5.0 software. The size distribution width of the powder samples was also determined by calculating the span value using the equation below:

$$\text{Span of distribution} = (D_{90} - D_{10})/D_{50} \quad (5.1)$$

D_{90}, D_{50}, and D_{10} values represent the particle diameters, respectively, when 90, 50, and 10% of the total powder particles have diameters less than these values, according to the cumulative size distribution curve. Generally, increasing the span value, for example, refers to an increase in the polydispersity nature for powder size distribution (314).

5.2.3.3. Particle flowability assessment:

The flow behaviour of the powders was evaluated using the angle of repose method outlined in the US Pharmacopoeia <1174> monograph (236). A stainless-steel funnel with 12 mm orifice diameter was used in this experiment. About 5 g of powder sample was allowed to flow freely from the funnel at a fixed height of 50 mm over a millimetre-grid sheet. The height (h) and diameter (d) of the powder pile was measured, and the angle of repose (θ) was calculated using the following equation:

$$\theta = tan^{-1}(2h/d) \quad (5.2)$$

Measurements were carried out in triplicate and presented as mean ± standard deviation. Results were only considered valid when a symmetrical cone of powder was formed. Based on the obtained repose angle values, the flow behaviour can be described as excellent flowing (θ: 25-30º), good flowing (θ: 31-35º), fair flowing (θ: 36-40º), passable flowing (θ: 41-45º), poor flowing (θ: 46-55º), and very poor flowing (θ >56º) (236).

5.2.4. Physical mixtures preparation:

The investigation focussed on developing binary drug:carrier formulation blends of felodipine:mannitol at three different drug strengths/concentrations: 1, 5 and 10 % (w/w). The different blends are summarised in Figure 5.1 below.

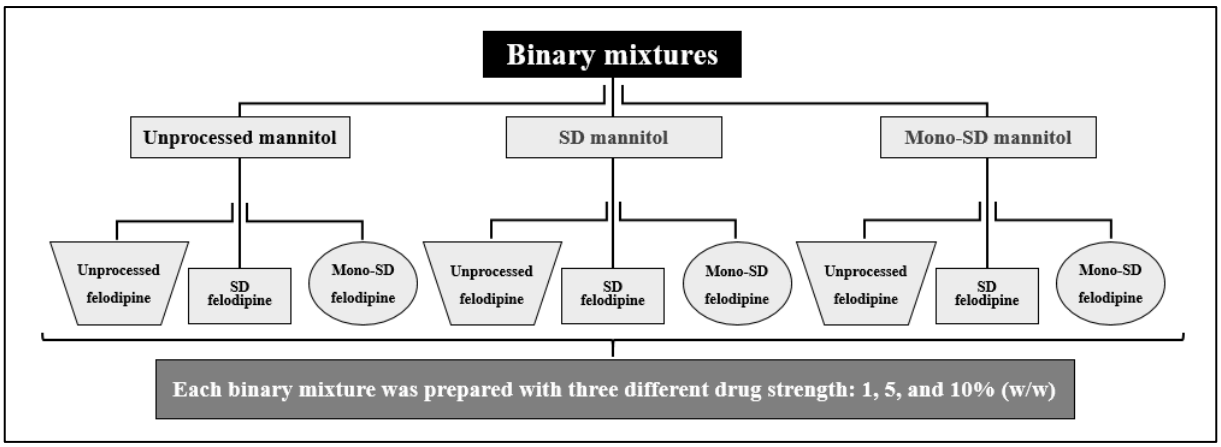

Figure 5.1: Schematic structure presents the binary mixtures required to prepare.

The binary powder blends were prepared in 1 g batches each. The ingredients of each formulation blend according to Figure 5.1 were added into a 5 ml plastic bottle at three different drug:carrier concentrations 1, 5 and 10% w/w and shaken manually for 10 and 30 minutes to mix the ingredients together. For example, unprocessed felodipine was mixed with unprocessed mannitol at three different ratios 1:99, 5:95 and 10:90 reflecting a concentration of 1, 5 and 10% w/w, respectively. The same procedure was applied to the rest of the 9 different combinations at 3 concentrations for each (i.e. 27 different blends in total).

It is worth noting here that the original (unprocessed) felodipine powder was sieved manually prior to use in this study to remove the larger irregular aggregates. Thus, the fraction of powder with particle size less than 53 μm was used in this study to prepare the binary blends.

5.2.5. Analytical method used for drug assay:

The drug amount in each binary mixture prepared was quantified using the HPLC analytical method for felodipine described in the US Pharmacopoeia (313). Waters Alliance® e2695 HPLC system (Waters Corp, Milford, USA) equipped with UV detector at wavelength 362 nm and column C18 (15cm × 4.6 mm, 5μm, Phenomenex®, USA) was used in this study. The system was operated under isocratic mode with a 1 ml/min flow rate using a degassed mobile phase of phosphate buffer:acetonitrile:methanol (30:45:25; v/v). The injection volume of the samples was 40 μL, and the retention time of felodipine was approximately 5 min. The data were collected and analysed using Empower®3 software.

Before the blend uniformity investigation, the HPLC analytical method was verified according to the published acceptance criteria for linearity, precision and recovery (accuracy) based on the International Conference on Harmonisation guidelines for validation of analytical procedures [ICH: Q2(R1)] (315). Linearity experiment was performed to check the detector's response was linear at the selected concentration range, which typically covered 25, 50, 75, 100, 150 and 200% of the target felodipine concentration (40 μg/ml). Three individually prepared replicates at each concentration were prepared and analysed. The calibration curves were constructed by plotting peak area versus concentrations of felodipine, and the regression equations were calculated. The precision and relative recovery were assessed using spiked samples at three different concentrations over the range of 50 to 150% of the target felodipine concentration. The method's precision was expressed in terms of percent relative standard deviation (%RSD), and accuracy was expressed as a percentage of the theoretical concentration (observed concentration × 100/ theoretical concentration).

5.2.6. Blend homogeneity analysis:

Drug content uniformity was assessed using a random sampling technique at time intervals of 10 and 30 minutes, where six samples of 40 ± 1 mg were taken out from different locations of the powder blend. This small sample size was used as it provides better reliability when investigating the blend homogeneity and

content uniformity, assuming the mean weight of the powder blend used for filling the capsules is 40 mg (71). To determine the drug content within these samples, the samples of binary mixtures at 1, 5 and 10% w/w drug concentration were dissolved in 10, 50 and 100 ml of ethanol, respectively and sonicated for 5 minutes. After sonication, 5 ml of each sample was filtered through 0.45 μm syringe filter into HPLC vial, discarding the first 3 ml of the filtrate. The drug concentration in each solution was determined according to the previous HPLC method. The drug content in each sample was calculated as a percentage (%) of the sample weight. Content uniformity was assessed by determining the deviation of the experimental drug content compared to the theoretical drug content. The results were presented as a mean ± relative standard deviation (n=6). The powder blend homogeneity was evaluated according to the acceptance criteria provided by the FDA draft guidance, where the powder blend is considered uniform when all of the tested samples are within ±10% range of the content claim on the label and the relative standard deviation (RSD) of these is ≤ 5% (316).

5.2.7. Statistical analysis:

Statistical analysis studies were performed using GraphPad Prism software (version 7.03, San Diego, California, USA). For content uniformity investigation, a one-way analysis of variance (one-way ANOVA) test followed by Tukey's multiple comparisons test was used to compare the data groups. The results were considered significantly different when the probability (P) value was less than 0.05.

5.3. Results and discussion:

5.3.1. Particle size distribution and morphology of individual powders:

Understanding the fundamental particle properties (i.e. size and shape distributions) for the powdered materials is critical to determine or predict their aggregation, agglomeration, and motion during the mixing process, where non-ideal mixing usually leads to non-uniformity in dosing, particularly for low dose drugs (77,80,109,110,113,317). As seen in Figures 5.2, 5.3 and 5.4, there is a noticeable difference in particle morphology when comparing the different powders. Among all felodipine and D-mannitol powders, it is clear that the unprocessed powder particles are less uniform in terms of shape and size since several elongated or irregular particles (e.g. subangular and prismatic crystals with sharp edges) and a large number of fractured structures could be detected. However, unprocessed felodipine particles exhibited relatively smoother surfaces (Figure 5.3) compared with unprocessed mannitol, where its particles presented with rough surface structures (Figure 5.4). Compared with unprocessed crystals, powders generated by a conventional spray drying system showed a spherical shape and relatively small size with a wide range of irregular aggregates. In contrast, Mono-SD particles generated by the single-stream spray drying system showed mainly spherical shapes with uniform size and aggregate-free surface. The surfaces of Mono-SD powders were free from aggregates due to less contact points between monodisperse spherical particles during their formation from individual droplets (see chapter 3 for a detailed description of the mechanism

of droplet dispersion using pulsating air). However, some of the Mono-SD particles exhibited blowholes, which are varied in size and shape depending on the drying temperature used during the production process (261).

When comparing all four spray-dried powders, a variation in particles' surface topography has also been observed. SD and Mono-SD felodipine particles formed surface structures, covered with multiple crystalline nucleation sites, which gave the particles a rough "furry" appearance (Figure 5.3), whereas the surface structures of SD and Mono-SD mannitol particles were relatively smoother (Figure 5.4). This variation in particle morphology when comparing spray-dried particles for felodipine and mannitol can be explained by the fact that different materials exhibit different crystallisation behaviour and drying kinetics during the spray drying process. In addition, there are also few Mono-SD mannitol particles with folds and wrinkles. These varied morphologies of the Mono-SD mannitol particles are mainly due to droplets inflation and deflation behaviour during the spray drying process when using high inlet temperature for drying (141,261).

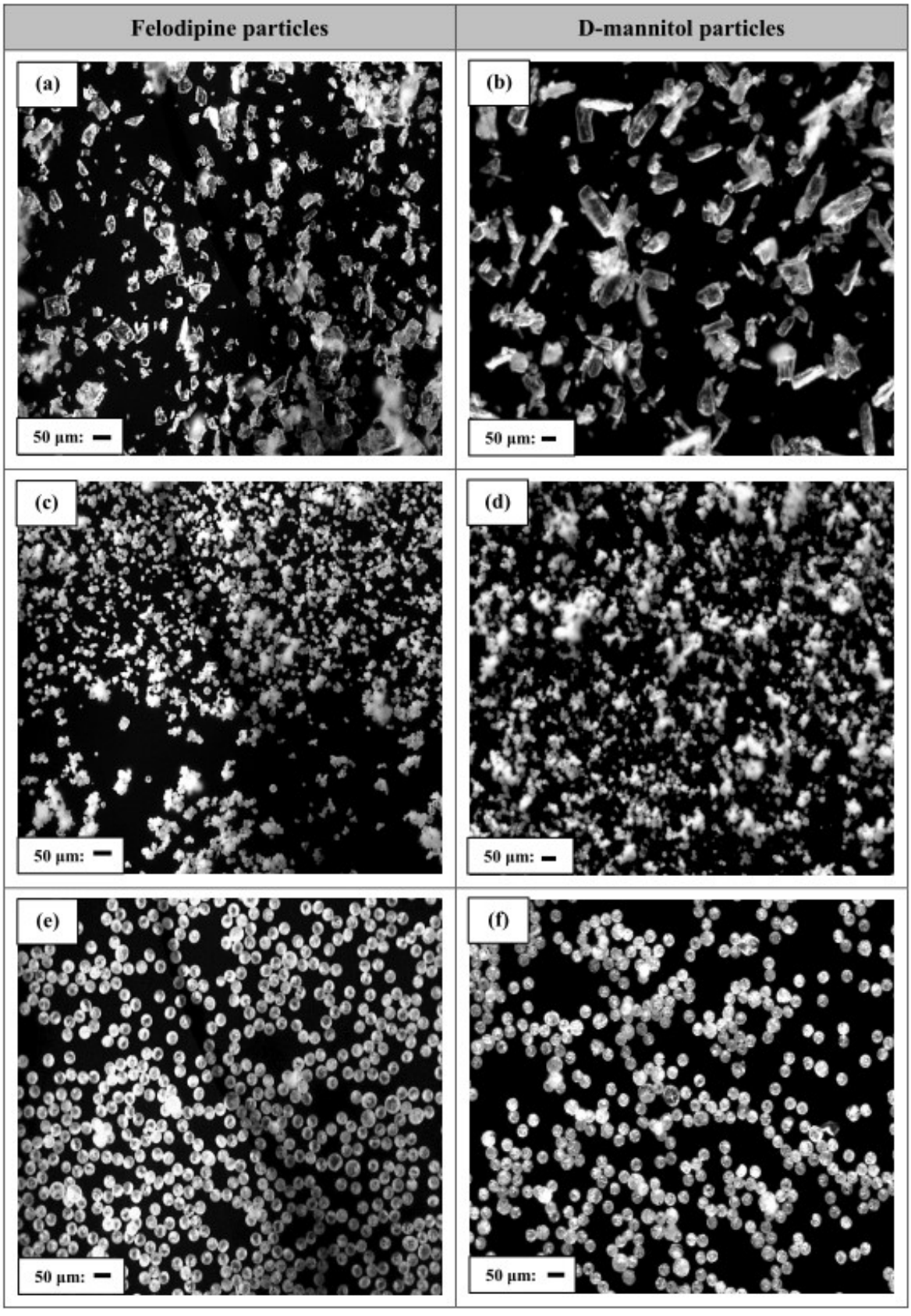

Figure 5.2: Optical microscope images of various felodipine and D-mannitol particles produced using different approaches: (a, b) unprocessed particles, (c, d) SD particles, and (e, f) Mono-SD particles. The optical microscopy provides a good particle population perspective and is complemented by the detail of particle surface and structure observed in the SEM images below. D-mannitol images shown here are a repeat of Figure 4.2 on the page 110.

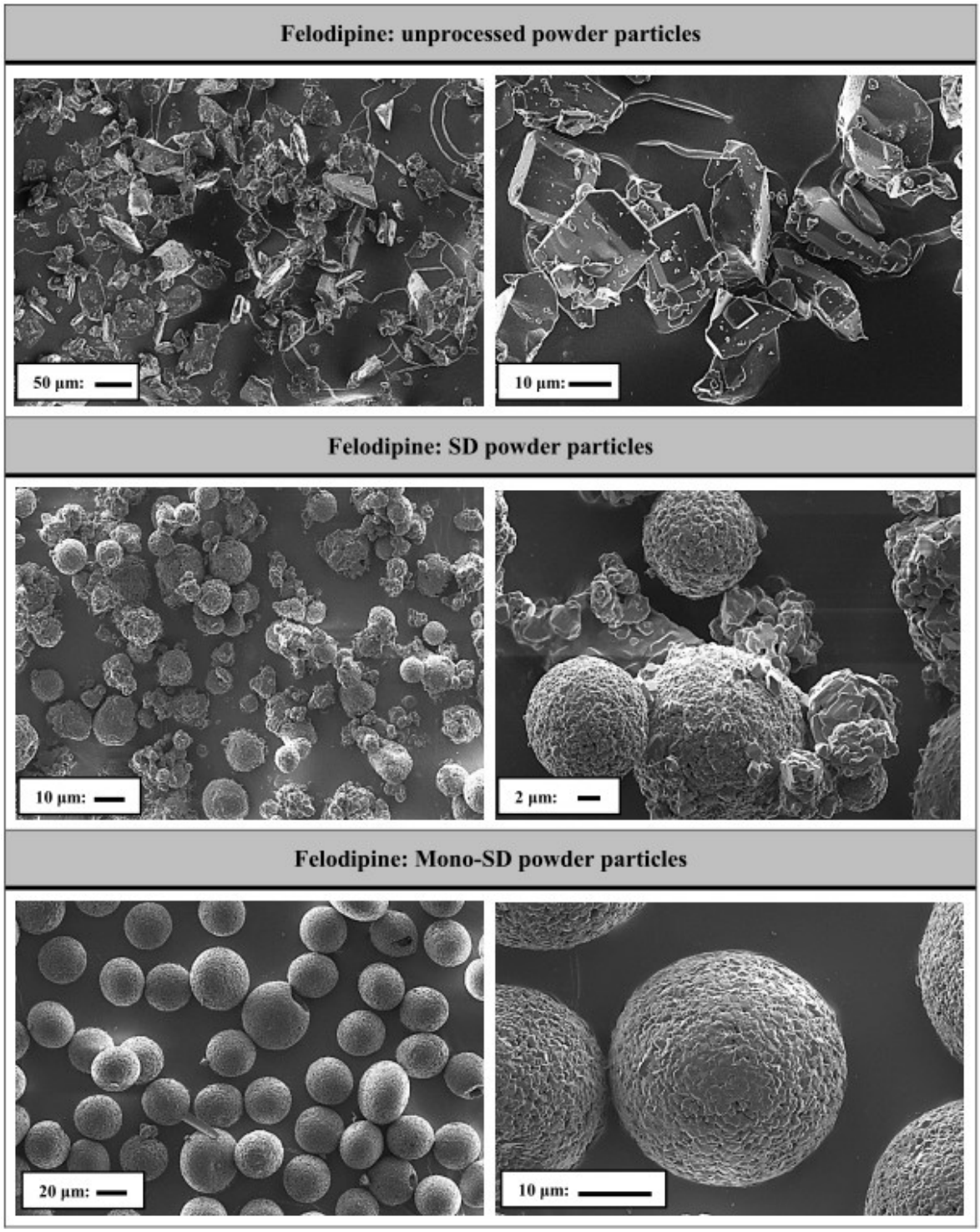

Figure 5.3: SEM images at different magnifications of some felodipine particles prepared using two different spray-drying systems in comparison to unprocessed powder particles.

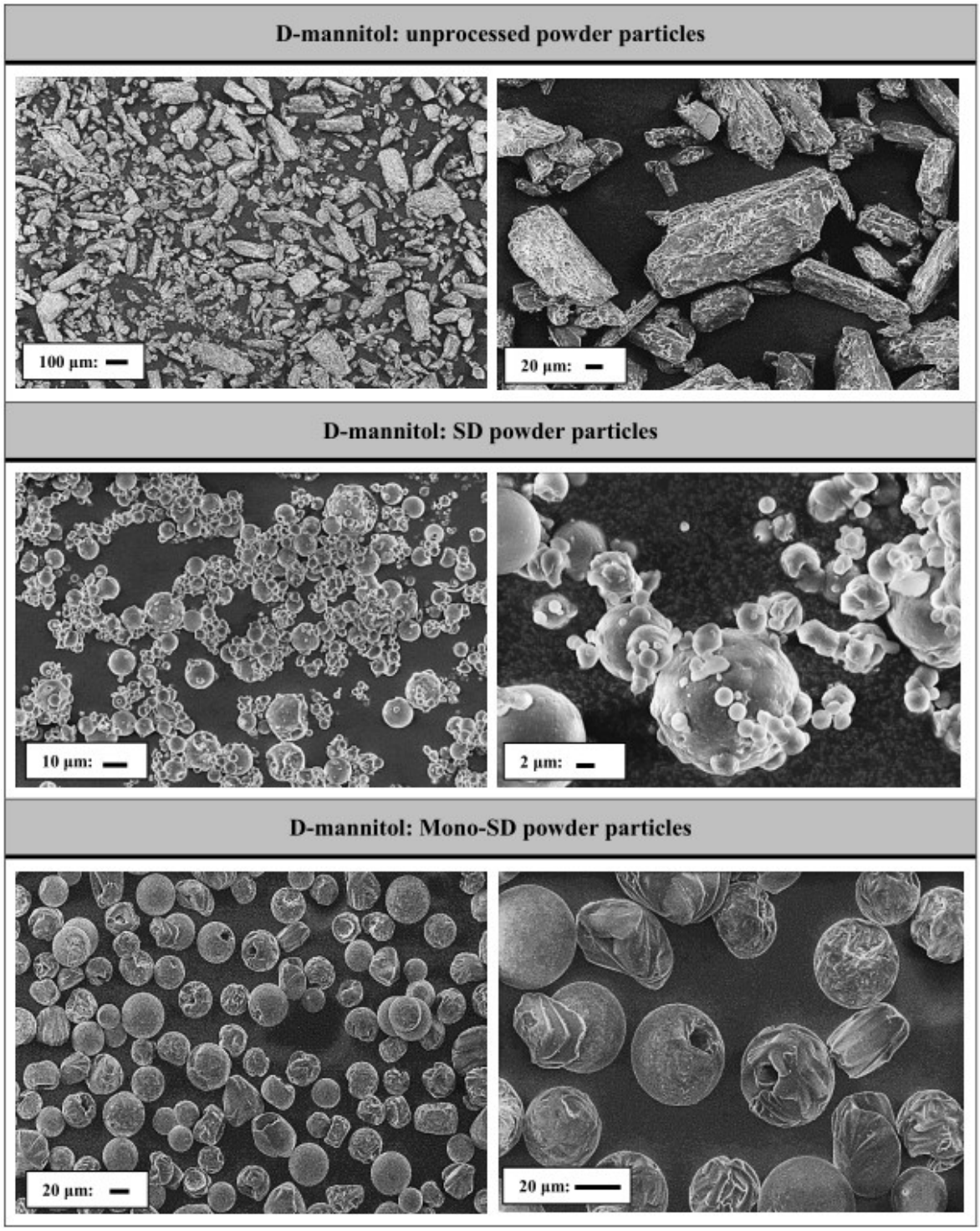

Figure 5.4: SEM images at different magnifications of some D-mannitol particles prepared using two different spray-drying systems in comparison to unprocessed powder particles. The figure shown here is a repeat of Figure 4.4 on page 114.

The results of the laser diffraction analysis are presented in Table 5.1 below. According to the geometrical particle diameters (D_{10}, D_{50} and D_{90}), different powders (i.e. unprocessed, SD and Mono-SD) for the same ingredient exhibited considerably (ANOVA, $P < 0.05$) different particle size distribution. However, the fabricated powder samples using both conventional and the new spray drying technique had an overall size range smaller than the unprocessed powders (ANOVA, $P < 0.05$). By comparing the Mono-SD powders

together, the fabricated felodipine and D-mannitol particles exhibited roughly the same size distribution. As seen in Table 5.1, the D_{50} was 31.62 ± 0.34 and 31.70 ± 0.15 µm for Mono-SD felodipine and Mono-SD mannitol, respectively.

Table 5.1: Bulk properties of the different felodipine and mannitol powders showing the geometrical parameters of the particle size distribution, the angle of repose and the corresponding flow behaviour.

Particles size parameters	Felodipine powders			D-mannitol powders		
	Unprocessed *	***SD***	***Mono-SD***	***Unprocessed***	***SD***	***Mono-SD***
D_{10} (µm)	7.21 ± 0.04	5.76 ± 0.17	13.23 ± 0.57	15.67 ± 0.05	2.65 ± 0.13	15.41 ± 0.36
D_{50} (µm)	25.21 ± 0.05	14.30 ± 0.11	31.62 ± 0.34	60.31 ± 0.17	9.50 ± 0.14	31.70 ± 0.15
D_{90} (µm)	49.29 ± 0.19	28.33 ± 0.18	43.30 ± 0.19	147.20 ± 1.39	20.05 ± 0.04	42.73 ± 0.05
Span	1.66 ± 0.00	1.57 ± 0.01	0.95 ± 0.01	2.18 ± 0.01	1.83 ± 0.03	0.86 ± 0.01
Particles (%) < 10 µm	20.18 ± 0.02	40.56 ± 0.53	7.61 ± 0.34	6.34 ± 0.03	58.7 ± 0.50	6.52 ± 0.19
Particles (%) < 25 µm	49.54 ± 0.08	85.73 ± 0.24	29.30 ± 1.04	18.05 ± 0.05	95.86 ± 0.06	27.01 ± 0.56
Angle of repose (º)	**48.01 ± 1.11****	**42.44 ± 1.20****	**14.45 ± 0.44**	**43.18 ± 1.05****	**49.47 ± 1.18****	**13.87 ± 1.50**
Flow property	**Very poor*****	**Very poor*****	**Excellent**	**Very poor*****	**Very poor*****	**Excellent**

* The results expressed the particle size distribution for the unprocessed (sieved) powder with particle size less than 53µm.

** Powder flow through the funnel with assisted tapping. Results reported as mean ± standard deviation (n = 3).

*** The classification of powder flow presented here is different from the original US Pharmacopoeia classification of powder flow. This is because the powder samples were very cohesive and they cannot flow through the funnel orifice without assisted tapping.

In contrast, there is a significant difference (ANOVA, $P < 0.05$) in particle size distribution when comparing between unprocessed powders or SD powders for felodipine and D-mannitol. For example, D_{50} was 25.21 ± 0.05 µm for unprocessed felodipine while it was 60.31 ± 0.17 µm for unprocessed D-mannitol powder. This further proves that the nature of the atomisation process in the single stream spray dryer system forces the formation of particles of fixed/desired size. Otherwise, these powders in their native state are significantly different in their particle size distributions due to different crystallisation behaviours.

Figures 5.5 and 5.6 showed that the particle size distribution curves for all felodipine and D-mannitol powders were unimodal with some skewness towards fine particles. However, the particle size distribution for Mono-SD felodipine (span of 0.95) was much narrower (ANOVA, $P < 0.05$) than the unprocessed felodipine with a span of 1.66 and SD felodipine with a span of 1.57 (Figure 5.5 and Table 5.1). Similar results were found when comparing the different D-mannitol powders. The Mono-SD powder generated via the new single-stream spray drying system has a very narrow size distribution (span of 0.86) compared with unprocessed and conventionally spray-dried samples where the size distribution was much broader (span of 2.18 and 1.83, respectively).

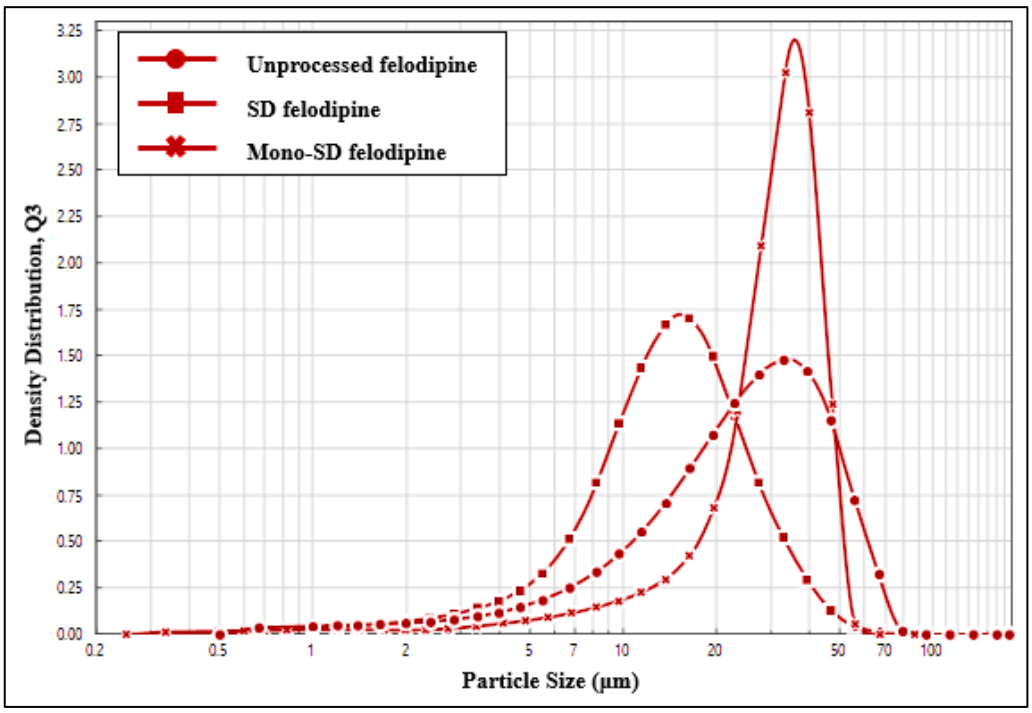

Figure 5.5: Probability density distribution obtained for particle size distribution for felodipine powders.

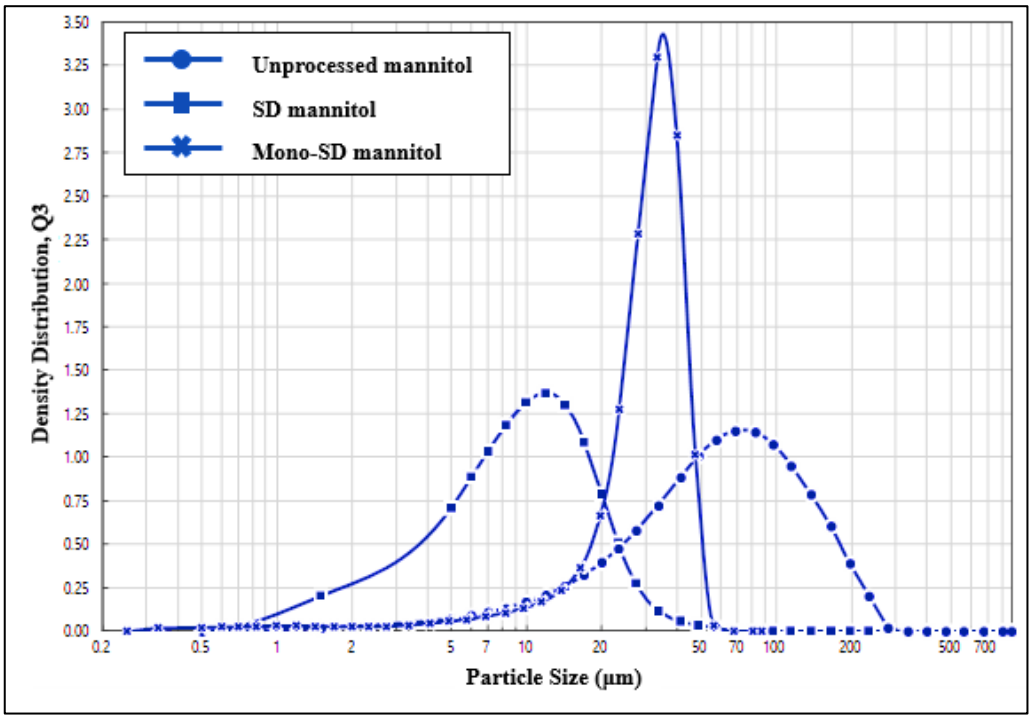

Figure 5.6: Probability density distribution obtained for particle size distribution for D-mannitol powders.

The impact of different particle size and shape distributions on the powder flowability was investigated by evaluating the repose angle (θ) for the tested powders. Typically, the smaller the angle of repose, the more flowable is the powdered material and vice versa (233). As seen in Table 5.1, the smallest repose angles were measured for the Mono-SD felodipine (θ = 14.45º) and D-mannitol powders (θ = 13.87º), and they were even smaller than the values stated in the flowability classification system outlined in the US Pharmacopoeia (236). By contrast, the unprocessed and SD powders for the same material exhibited the highest repose angles as follows: SD felodipine (θ = 42.44º), unprocessed felodipine (θ = 48.01º), SD mannitol (θ =49.47º) and unprocessed mannitol (θ = 43.18º). These results indicated that Mono-SD powders had much superior flow, whereas the unprocessed and SD powders had the poorest flow properties (practically unflowable).

These results indicate that monodisperse particles even with small particle size (D_{90} < 44 μm) exhibit less internal friction (contact points) and flow freely due to their identical spherical shape. In contrast, irregular particles with broader size distributions (unprocessed and SD powders) present pronounced internal friction (large geometrical interlocking) within the powder. Such data indicate that creating uniform binary mixtures could be problematic when using cohesive felodipine and mannitol powders (i.e. unprocessed and SD powders) due to their higher propensity to aggregate during the blending process.

5.3.2. Effect of particle properties, drug load, and mixing time on the powder blend homogeneity and content uniformity:

In this study, the blend uniformity was assessed by determining the deviation in the content uniformity of the samples which were removed from different regions in the powder blend after 10 and 30 minutes of the mixing process (316). Achieving a homogeneous binary mixture depends on the flowability of its two constituents: the drug and the excipient. When the mixing container is agitated, the ability of both the drug and the excipient to move locally (i.e. flow) between and past neighbouring particles significantly enhances the homogeneity of the mixture. Achieving a homogeneous blend is especially important when dealing with low-dose highly potent drug products. Selecting an optimal particle size distribution for the starting ingredients becomes extremely important in this case (39,87,88,318). For low-dose drugs, a larger particle size helps to improve their flowability but also could lead to the formation of pockets of drug that are difficult to distribute uniformly (86). On the other hand, micronised drug powders can enhance the statistical likelihood of an even distribution of drug particles among the prepared formulation blends (85). Yet, their biggest challenge is poor flowability causing aggregation and poor content uniformity within the blend. Zhang and Johnson studied the impact of drug particle size on the content uniformity of low-dose solid dosage forms. Their results indicated that low-dose blends (approximately 10 μg drug per 100 mg dose unit) containing a larger drug particle size (18.5 μm) failed to meet the US Pharmacopoeia requirement, whereas a blend containing smaller particle sizes (6.5 μm) passed (86).

The above represents a formidable challenge to the formulation scientist, where both large and small particle sizes cause problems with content uniformity of the low-dose drugs. Thus, the current work aimed at exploring the effect of monodispersity of both the drug and excipient in overcoming this challenge. The hypothesis is that even if particles are small in size, their monodispersity would decrease interparticle contacts and interactions, allowing better distribution of low-dose drugs within a powder blend, ultimately leading to better content uniformity.

To investigate this hypothesis, carrier and drug powders of different particles size distributions (unprocessed with the widest distribution followed by SD which has a narrower distribution and Mono-SD with the narrowest/monodisperse distribution) were combined in binary mixtures at different dilutions (1-10% w/w) followed by assessing the drug content uniformity at different mixing times. A summary of the validation process parameters for felodipine quantification method was presented in Appendix A4.

As can be seen in Figures (5.7–5.9) below, there is a significant difference in the content uniformity (ANOVA, $P < 0.05$), depending on the composition of the binary mixtures. The blends containing SD mannitol powder did not exhibit a uniform drug content across the board (Figure 5.7 and Table 5.2). Furthermore, increasing the mixing time from 10 to 30 minutes, and/or drug amount from 1 to 10% (w/w) respectively, had no significant effect (ANOVA, $P > 0.05$) on the content uniformity of any of the formulations. These results indicate that felodipine powders could not be easily mixed with SD mannitol which led to poor uniformity. This is probably due to the nature of SD mannitol powder which consists of fine spherical particles (D_{50} = 9.5μm; ~96% of total particles < 25μm) and agglomerates. Therefore, SD mannitol powder exhibits a cohesive behaviour with poor flowability due to a high number of contact points and interparticulate bonding present in its powder bed. Felodipine particles cannot diffuse easily among the SD mannitol powder particles to form a homogenous blend unless the interparticulate bonding in the powder bed is broken down, and this requires intense mixing (i.e. using a high shear mixer) and/or longer mixing time (319,320).

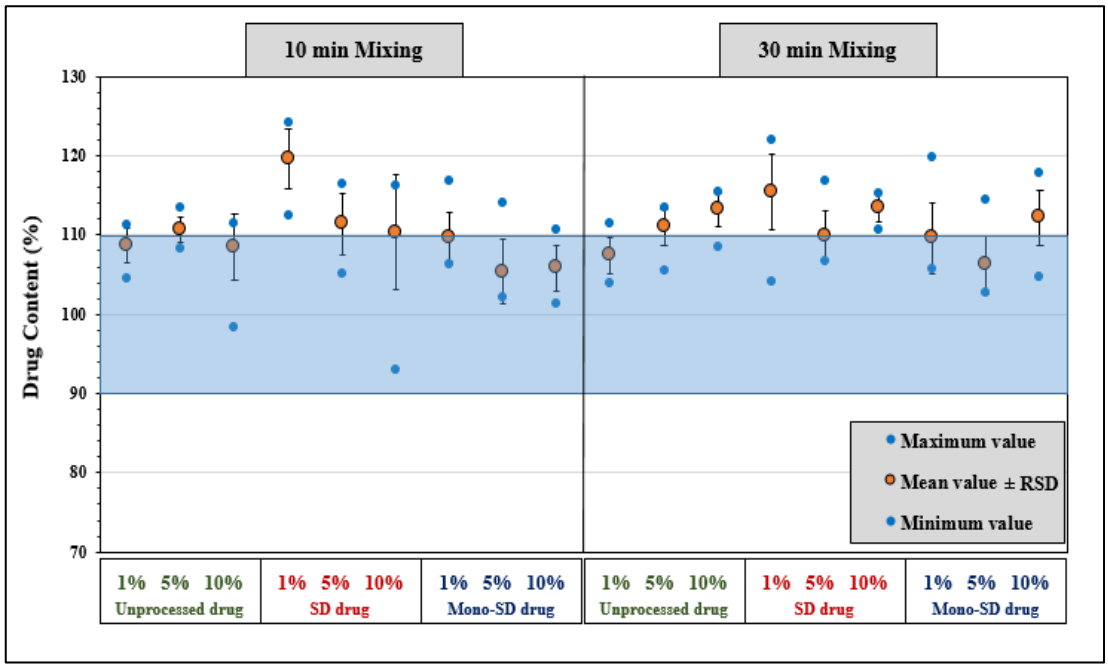

Figure 5.7: The effect of drug amount and mixing time on the content uniformity of powder blends for felodipine and SD mannitol. The presented results are for the set of six samples collected from different locations in the powder blend. The blue box refers to the samples which exhibit drug content within ±10% range of the content claim on the label.

Table 5.2: Blend uniformity data of the formulations contained SD mannitol as a drug carrier.

Mixing (min)	Drug strength (w/w)	Unprocessed Felodipine		SD Felodipine		Mono-SD Felodipine	
		Drug Assay (%)	RSD (%)	Drug Assay (%)	RSD (%)	Drug Assay (%)	RSD (%)
10	1%	108.65	2.24	119.60	3.83	109.75	3.09
	5%	110.65	1.54	111.39	3.91	105.33	4.09
	10%	108.51	4.19	110.32	7.24	105.86	2.91
30	1%	107.43	2.29	115.44	4.84	109.59	4.85
	5%	110.98	2.35	109.96	3.04	106.24	3.64
	10%	113.16	2.01	113.49	1.76	112.17	3.44

- The results exhibited the drug content (drug distribution uniformity) for the set of six samples collected from different locations in the powder blend and expressed as a mean ± RSD.
- According to FDA draft guidance, the green cells indicate that the blend is non-uniform, while the blue cell indicates that the blend is uniform. The powder blend is considered uniform when all of the tested samples are within ±10% range of the content claim on the label and the relative standard deviation (RSD) of these is ≤ 5% (316).

In general, the impact of drug proportion and mixing time on the content uniformity was very clear in the mixtures containing unprocessed mannitol as a carrier in comparison with the mixtures containing SD mannitol. As depicted in Figure 5.8 and Table 5.3, it is clear that increasing the mixing time and/ or drug strength led to improve the blend homogeneity and drug content uniformity for all mixtures except the ones prepared with unprocessed felodipine. Specifically, when mixing unprocessed mannitol with unprocessed felodipine, the mixtures did not exhibit uniformity in drug content. By contrast, when mixing unprocessed mannitol with SD or Mono-SD felodipine, the mixtures of some concentrations showed a high degree of

content uniformity (Figure 5.8 and Table 5.3). These results can be explained by the fact that the interaction (friction) between unprocessed mannitol particles and felodipine particles during the mixing process was less when using spherical spray-dried felodipine particles in comparison with unprocessed elongated irregular felodipine particles (Figures 5.2 and 5.3). As a result, SD/Mono-SD felodipine particles exhibited better diffusion properties in the powder blends than unprocessed felodipine particles.

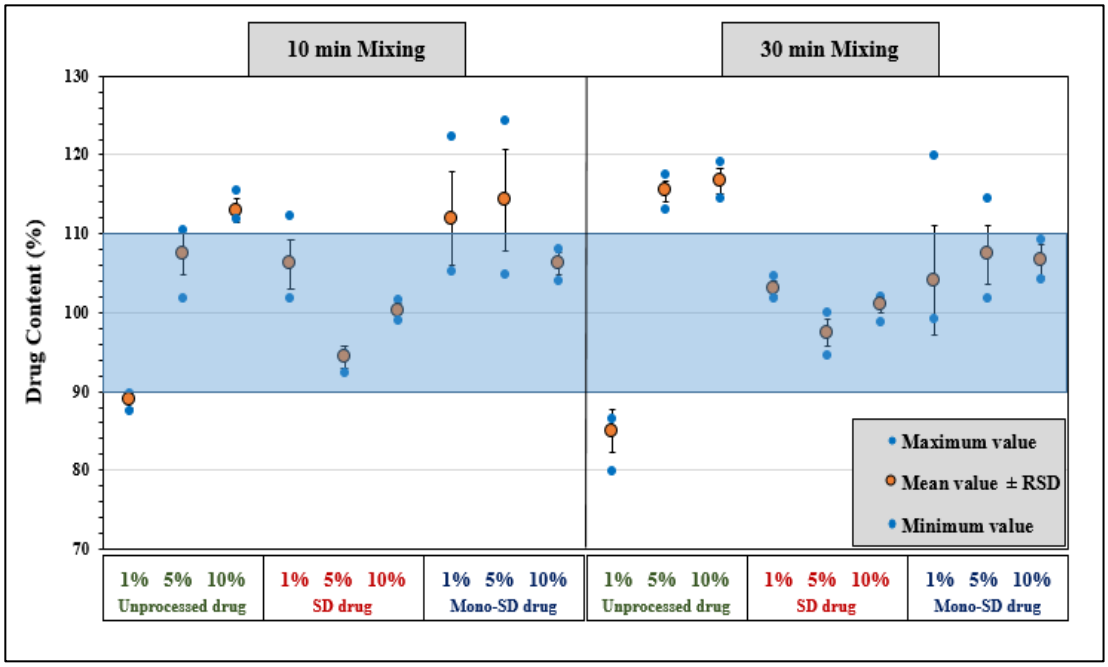

Figure 5.8: The effect of drug amount and mixing time on the content uniformity of powder blends for felodipine and unprocessed mannitol. The presented results are for the set of six samples collected from different locations in the powder blend. The blue box refers to the samples which exhibit drug content within ±10% range of the content claim on the label.

Table 5.3: Blend uniformity data of the formulations contained unprocessed mannitol as a drug carrier.

Mixing (min)	Drug strength (w/w)	Unprocessed Felodipine		SD Felodipine		Mono-SD Felodipine	
		Drug Assay (%)	RSD (%)	Drug Assay (%)	RSD (%)	Drug Assay (%)	RSD (%)
10	1%	88.89	0.90	106.18	3.14	111.94	5.92
	5%	107.41	2.66	94.30	1.41	114.32	6.44
	10%	112.90	1.48	100.27	1.00	106.22	1.48
30	1%	84.96	2.71	103.09	0.94	104.05	6.97
	5%	115.39	1.31	97.42	1.72	107.41	3.73
	10%	116.68	1.60	101.05	1.10	106.62	2.03

- The results exhibited the drug content (drug distribution uniformity) for the set of six samples collected from different locations in the powder blend and expressed as a mean ± RSD.
- According to FDA draft guidance, the green cells indicate that the blend is non-uniform, while the blue cell indicates that the blend is uniform. The powder blend is considered uniform when all of the tested samples are within ±10% range of the content claim on the label and the relative standard deviation (RSD) of these is ≤ 5% (316).

Interestingly, the mixtures containing unprocessed mannitol with SD/Mono-SD felodipine exhibit higher content uniformity than the mixtures containing SD mannitol with spray-dried felodipine (SD or Mono-SD). These results can be explained by the differences in fundamental particle properties between SD and unprocessed mannitol powders. The particle size of SD mannitol was much smaller than the unprocessed mannitol (Table 5.1). As a result, the powder bed's void (interfacial) spaces were less in the SD mannitol than the unprocessed mannitol, as seen in Figure 5.2. This can also be seen in the SEM images where SD mannitol particles showed fine spherical shape with extensive and unpredicted agglomerates, while unprocessed mannitol particles displayed elongated-irregular morphologies (i.e. subangular and prismatic crystals with sharp edges) with less uniformity in size and shape (Figure 5.4). Therefore, as compared to SD mannitol, the unprocessed mannitol has better properties for the diffusion of SD/Mono-SD felodipine particles in the powder blend (Figure 5.8 and Table 5.3).

On the other hand, unprocessed felodipine particles are not able to freely diffuse within either the unprocessed or SD system of mannitol, despite seeming less cohesive than SD-felodipine upon optical microscopy and SEM analysis. The reason for this apparent contradiction could be that the particle shape of the unprocessed felodipine is similar to the shape of unprocessed mannitol. This similarity in shape along with the fact that the shape is irregular and consists of flat surfaces potentially increases the interparticle interactions, resulting in decreased flowability and ultimately low content uniformity.

Another interesting finding was that the mixtures for unprocessed mannitol and SD felodipine exhibited significantly better homogeneity and drug content uniformity than the mixture for unprocessed mannitol with Mono-SD felodipine at both mixing times (Figure 5.8 and Table 5.3). This could be explained by the fact that SD Felodipine had a higher percentage of fines than Mono-SD Felodipine (86% vs. 30% < 25 μm) where these fines can diffuse (percolate) much easier/faster during the mixing process through the void spaces in the unprocessed mannitol powder bed (80).

Compared with the previous powder blends, the mixtures containing Mono-SD mannitol as the carrier had the highest content uniformity. As depicted below in Figure 5.9 and Table 5.4, all mixtures (except of one with unprocessed Felodipine at 1%) were uniform and the drug content uniformity was in the range from 94.93 to 106.35% and from 99.69 to 107.25% 99 after 10 and 30 minutes of mixing. In addition, the mixtures exhibited a high content uniformity even when the mixing time was too short (i.e. 10 minutes). The superior content uniformity achieved when using Mono-SD mannitol as the carrier could be explained by the monodispersity of the carrier particles allowing rapid uniform distribution of the SD Felodipine particles in between. For Mono-SD mannitol and Mono-SD felodipine mixtures, there could be another important factor at play here which is the fact that both powders had similar particle sizes (D_{50} ~ 32μm). As a result, the highest degree of content uniformity can be reached if mixed particles are as similar in their properties (i.e. shape, size, and density) as possible (77,80,321).

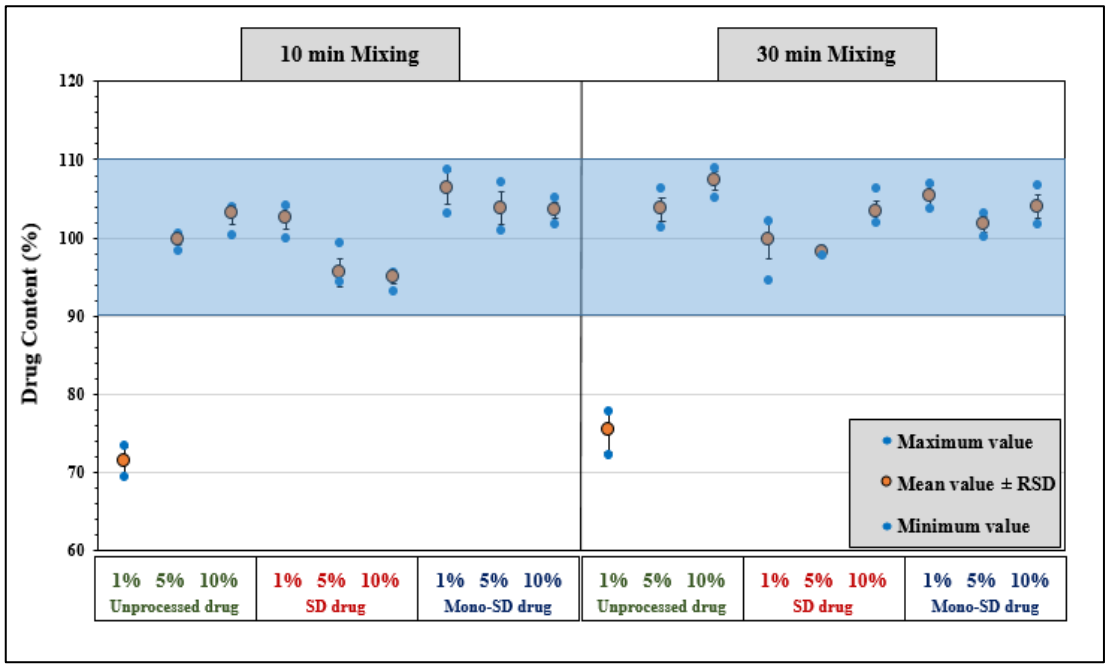

Figure 5.9: The effect of drug amount and mixing time on the content uniformity of powder blends for felodipine and Mono-SD mannitol. The presented results are for the set of six samples collected from different locations in the powder blend. The blue box refers to the samples which exhibit drug content within ±10% range of the content claim on the label (316).

Table 5.4: Blend uniformity data of the formulations contained Mono-SD mannitol as a drug carrier.

Mixing (min)	Drug strength (w/w)	Unprocessed Felodipine		SD Felodipine		Mono-SD Felodipine	
		Drug Assay (%)	RSD (%)	Drug Assay (%)	RSD (%)	Drug Assay (%)	RSD (%)
10	1%	71.43	1.80	102.57	1.43	106.35	2.10
	5%	99.81	0.76	95.62	1.79	103.80	2.11
	10%	103.04	1.22	94.93	0.88	103.49	1.01
30	1%	75.38	2.69	99.69	2.45	105.35	1.37
	5%	103.62	1.46	98.20	0.30	101.72	1.00
	10%	107.25	1.17	103.35	1.39	103.96	1.51

- The results exhibited the drug content (drug distribution uniformity) for the set of six samples collected from different locations in the powder blend and expressed as a mean ± RSD.
- According to FDA draft guidance, the green cells indicate that the blend is non-uniform, while the blue cell indicates that the blend is uniform. The powder blend is considered uniform when all of the tested samples are within ±10% range of the content claim on the label and the relative standard deviation (RSD) of these is ≤ 5% (316).

The only powder that performed poorly in terms of content uniformity was the one of Mono-SD mannitol with unprocessed felodipine at 1%. It seems that despite the monodisperse nature of the carrier, the dominating factor in the binary mixture was the poor flowability of the unprocessed felodipine (angle of repose one of the highest between studied powders at 48°). It can be observed that the % drug content was lower than 80% for this powder at both mixing times. This could mean drug loss has occurred during the mixing process, probably due to particle adhesion to the mixing container. This drug loss could also be observed when unprocessed felodipine was mixed with unprocessed mannitol at the same concentration of

1% w/w. This is not unexpected given the flaky/flat particles observed in the SEM images for unprocessed felodipine, which could create friction with the container walls due to their higher surface/contact area and prevent uniform distribution within the blend (322).

5.4. Conclusion:

Differences in particle size and shape properties for the blend components significantly impact the formulation homogeneity and drug content uniformity. The highest degree of content uniformity can be reached if the shape, size and density of the mixed particles are as similar as possible; spherical shape is preferred. However, for the low-dose drug content, the choice of the filler may assist dispersibility and uniformity of the drug throughout the blend. Although micron-sized drugs generally tend to agglomerate/aggregates, this study shows that monodisperse spherical particles have a high flowability and using filler as a monodisperse powder can enhance blend homogeneity regardless of the bulk powder properties for the low-dose micronised drug. The mixtures that contained mono-sized mannitol particles with spherical shapes, and smooth surfaces achieved high uniformity.

In contrast, the mixtures containing polydisperse mannitol powders with irregular particle shapes and uncontrolled agglomerates had a low degree of mixing uniformity. All results could be explained by the relationship between the interparticulate interactions and the properties of the particles (i.e. size, size distribution, and shape). In general, using a mono-sized filler with spherical particle shape, excellent powder flowability and particle size close to that of the drug powder can facilitate the preparation of homogeneous blends suitable for early clinical studies of low-dose drugs.

Chapter 6

CHAPTER 6

Conclusions and Recommendations

For many pharmaceutical ingredients used in the development of solid dosage forms, particle size and shape as well as their distributions are key parameters affecting materials handling and processing (9,28,29,66,68) In many cases, changes in these properties could affect material's blend homogeneity or tableting performance. This could also result in a drug product's bio-performance variation after oral administration (1,5,7,46,195). Unfortunately, most pharmaceutical ingredients are polydisperse powders containing fine particles with different morphologies and agglomerates, leading to processing and quality issues (2–4,34).

The current research has set out to develop a novel spray drying-based technology to produce monodisperse powders with adjustable particle size in order to overcome processing issues and formulate solid dosage forms with optimal critical quality attributes (CQAs). The proposed technology involves a combination of a monodisperse droplet generator (MDG) with a new drying chamber and other ancillary equipment.

The work started by investigating the effect of vibration frequency and outlet feed pressure of MDG on the droplet formation process, droplet size and the precision of producing monodisperse droplets. This investigation was conducted using a PAT stroboscopic imaging technique, which enabled direct visualisation of the produced droplets and subsequent quantification of droplet parameters (droplet size and droplet-to-droplet distance). The results in Chapter 2 indicated that MDG atomiser could be used effectively to generate a stream of monodisperse droplets with adjustable size when it is operated with optimal processing parameters (vibration frequency, feed flow rate/ feed pressure). A linear correlation was found between the predicted monodisperse droplet size and imaging measurements confirming the suitability of the technique for droplet size estimation. The diameter of droplets produced from a given pinhole size could be modulated through controlling the vibration frequency and feed flow rate/ feed pressure of the MDG atomiser. Increasing the vibration frequency leads to an increase in the number of droplets generated whilst decreasing their size. In addition, the generation process for monodisperse droplets is precise when operating within the optimal vibration frequency. However, the behaviour of droplets starts to change at longer distances (2 - 4 cm) from the MDG tip, probably due to aerodynamic resistance in the surrounding environment. This leads to loss of monodispersity through collisions and subsequently coalescence of the droplets.

To generate uniform particles from these droplets, a new spray drying system referred to as a 'single-stream spray dryer' has been designed and constructed. The new spray dryer operated in a laminar flow mode and successfully produced quasi-monodisperse particles with high repeatability when the MDG atomiser was

provided with few accessories. These included a cooling jacket to improve the stability of MDG performance when operating under high inlet temperature conditions. Furthermore, a pulsating air unit for dispersing the uniform droplets after ejection from the MDG pinhole was also implemented to overcome the early loss of monodispersity issue. The size of the generated particles could be predetermined and controlled by adjusting the MDG operation parameters and feed solution properties. The final prototype (approx. 2 metres in length) produced highly uniform quasi-monodisperse spherical particles when aqueous feed solution of metformin HCl (15% w/v) was atomised using a 35 μm MDG pinhole, and the powder yield was around 50% when the inlet temperature was 220ºC. Increasing the length of the drying chamber when constructed on a pilot-scale in the future should further improve the yield of the powders due to potentially longer droplet residence time.

In chapter 4, further testing was carried out to investigate the impact of monodisperse particles on bulk powder properties such as flowability and packing. Specifically, two pharmaceutical ingredients (D-mannitol and Metformin HCl) with different particles characteristics were chosen as model ingredients and microparticles from both were created using different spray drying systems (conventional spray dryer BUCHI B-290 and the single-stream spray dryer). Both model compounds are naturally cohesive crystalline powders, and present unfavourable processing properties (i.e. flowability and compressibility) during tableting. All the generated spray-dried ingredients (SD and Mono-SD) were fine powders with particle sizes less than 50 μm. However, significant differences in size distribution, shape, and surface morphology/habit were observed when comparing between the different D-mannitol or metformin HCl powders. The results indicated that mono-SD powders which are fine (< 50 μm) have significantly better flow and packing than the other powders (unprocessed and conventionally spray dried). The spherical uniform shape and narrow size distribution could have led to a decrease in adhesion between the particles, which eventually translated into better flowability (322,323). In the future, we expect this approach could be used for fabricating fine particles (< 50 μm) which impart a dissolution advantage, however, with exceptional flowability which are normally very contrasting properties in formulation development. The use of spray-dried uniform or monodisperse particles could also reduce the need for functional excipients and/or further production steps to improve pharmaceutical ingredients' flowability and content uniformity.

In fact, chapter 5 focused on investigating the content uniformity of binary mixtures containing monodisperse powders to understand the impact of powder particles properties on the mixing behaviour and blend homogeneity. In this investigation, different binary mixtures of felodipine and mannitol were prepared using powders with varying bulk properties: unprocessed powders, spray-dried (SD) powders and monodisperse (Mono-SD) powders. The findings indicated that the particle size and shape of the formulation ingredients as well as powder monodispersity/polydispersity have a great impact on the blend homogeneity and content uniformity. For low-dose drug formulations, it was observed that using a drug carrier (i.e. filler) with high powder flowability is very important to enhance the drug dispersibility throughout the blend. Although micron-sized drugs generally tend to agglomerate/aggregate, this study showed that using D-mannitol as a monodisperse powder/carrier could enhance blend homogeneity

regardless of the bulk powder properties of the low-dose drug. In contrast, mixtures containing polydisperse mannitol with irregular particle shapes and uncontrolled agglomerates (i.e. untreated powder or SD powder) had a low degree of mixing uniformity.

Overall, one might say that the properties of the spray-dried particles depend mainly on the atomisation conditions. Using a single-stream spray dryer equipped with an MDG atomiser is a promising approach for generating mono-sized spherical particles with adjustable size suitable for use in solid dosage form manufacturing. Better control of particle size and morphology means better control of bulk powder properties and flowability, and that ultimately translates into better performance of the solid dosage form during production and after administration.

In the future, simulations and experimental studies could be conducted to evaluate the novel single-stream drying process when utilising other operating parameters (e.g. upon scale-up) such as higher feed flow rates, higher gas rates and different drying temperatures. Such investigations might provide more information about heat/mass transfer between the atomised droplets and air streams during droplet movement inside the drying chamber. It could also improve the drying efficiency and further increase the yield by determining sources of heat loss throughout the process.

Appendix A1: A typical Heckel plot representing powder compaction.

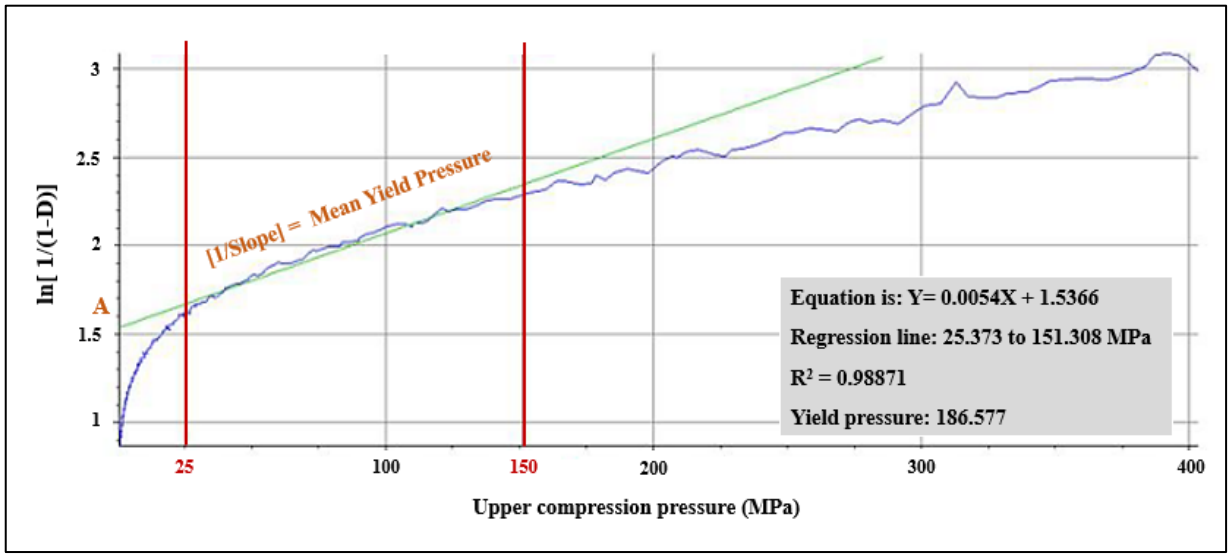

Figure A1: Typical Heckel plot for uncompressed metformin HCl compact, as an example, produced at a compression speed of 0.1 mm/s. The A value is related to powder densification and initial packing density. The slope (K) is proportional to the reciprocal of the mean yield pressure (P_y).

Figure A1 shows that the Heckel plot was typically curved at lower pressures (particle rearrangement region), followed by a liner region at higher pressures (particle deformation region). The linear part of the Heckel plot (with the best R^2 fit) is called a Heckel equation. According to the literature, the Heckel plot is never genuinely linear, although the slope changes little within certain pressure intervals (324–326). In this study, as seen in Figure A1 above, the Heckel data had the best linear regression ($R^2 \geq 0.984$) during the compression pressure between 25 and 150 MPa. Therefore, the mean yield pressure was calculated for each tested powder over the previously selected range in order to compare and evaluate the plasticity of the powders.

Appendix A2: Production of monodisperse droplets.

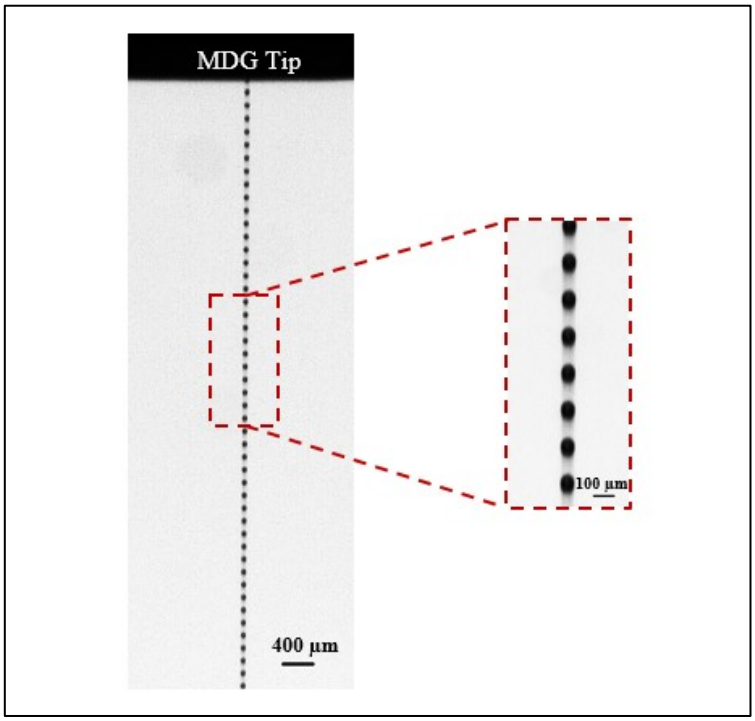

Figure A2: Monodisperse droplets chain generated using 35µm MDG atomiser orifice with vibrations frequency of 46 KHz and feed flow rate of 0.4 ml/min. The monodisperse droplets presented in this image are for an aqueous metformin 15% (w/w) solution.

According to image analysis data, the measured diameters of monodisperse droplets were 67.91 ± 6.18 and 69.72 ± 1.64 µm for D-mannitol and metformin HCl solutions when using 35µm MDG pinhole with feed flow rate at 7.24×10^{-9} and 7.10×10^{-9} m^3/s, respectively. Compared to the theoretical calculation, using equation 2.2 (chapter 2; p: 54), it has been shown that the mean measured diameter of the D-mannitol and metformin HCl droplets was corresponding with the calculated diameter, which was 67.00 and 66.55 µm, respectively. These observations were in good agreement with the predictions of Rayleigh's instability theory (169,176,327).

Appendix A3: Schematic drawing for mannitol powders packing.

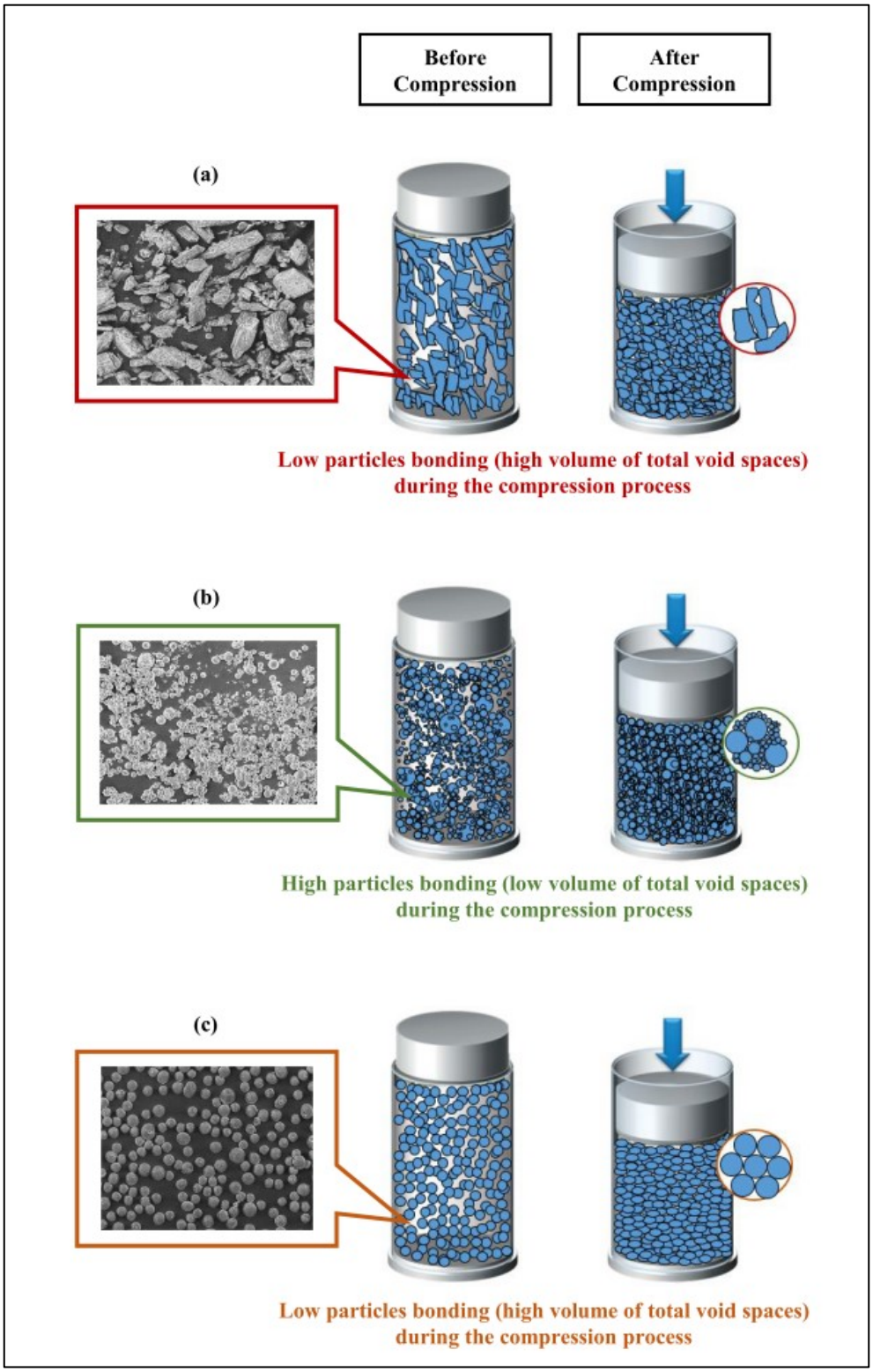

Figure A3: Schematic drawing for packing structure of three different mannitol powders before and after compression process: (a) unprocessed mannitol (cohesive powder), (b) SD mannitol (cohesive powder), and (c) Mono-SD mannitol (non-cohesive powder, free-flowing). Unprocessed mannitol powder contains a higher % of coarse particles, while the SD mannitol contains a higher % of fine particles.

Appendix A4: Analytical method assessment for felodipine quantification.

The calibration curve was prepared from dilutions of standard stock solution of felodipine substance (0.5 mg/ml), using ethanol as solvent. According to the felodipine assay described in the U. S. Pharmacopoeia 36, the absorbance of all dilution samples was determined by using the HPLC method at a UV wavelength of 362 nm. For content uniformity and analytical method investigation, six points calibration curve was obtained in a concentration range from 10 – 80 µg/ml for felodipine, which typically covers 25, 50, 75, 100, 150, and 200% of the targeted drug concentration. Three individually prepared replicates at each concentration were analysed. As seen in Table A1 below, the linear correlation between absorbance peak area and drug concentration was assessed. The calibration curve was linear in the selected concentration range, where the linear regression equation was Y = 38449X - 33251 with a correlation coefficient R^2 over 0.999. The accuracy and precision of the analytical method were also investigated using samples with the known concentrations (Table A1). Based on the mean and relative standard deviation (RSD), all the validation parameters were in the ranges acceptable according to the ICH guidelines for analytical method validation (315,328).

Table A1: Summary of the validation process parameters for felodipine quantification method.

Linear regression analysis of the calibration curve						
Standard regression equation			**Linearity range**		10 – 80 (µg/ml)	
Y=38449X - 33251			**Correlation coefficient**		R^2 = 0.9993	
Validation Parameters	**Intraday measured concentrations % Recovery [mean ± SD, (RSD %)]**			**Interday measured concentrations % Recovery [mean ± SD, (RSD %)]**		
	20 µg/ml	**40 µg/ml**	**60 µg/ml**	**20 µg/ml**	**40 µg/ml**	**60 µg/ml**
Precision (n = 6)	99.09 ± 0.05 (0.06)	101.21 ± 0.05 (0.05)	98.84 ± 0.03 (0.04)	99.19 ± 0.19 (0.20)	101.61 ± 0.17 (0.17)	101.39 ± 0.13 (0.13)
Accuracy (n = 3)	99.21 ± 0.96 (0.97)	101.45 ± 1.03 (1.02)	99.91 ± 0.77 (0.77)	-	-	-

- Precision was represented as a mean value for six injections at each concentration.
- Accuracy was represented as a mean value for three individually prepared replicates at each concentration.
- Interday variation was assessed after one week. The concentration of each run was determined from the single calibration curve run on the first day of the study.

References

1. Dave VS, Saoji SD, Raut NA, Haware R V. Excipient variability and its impact on dosage form functionality. J Pharm Sci. 2015; 104(3): 906–15.

2. Jallo LJ, Ghoroi C, Gurumurthy L, Patel U, Davé RN. Improvement of flow and bulk density of pharmaceutical powders using surface modification. Int J Pharm. 2012; 423(2): 213–25.

3. Megarry AJ, Swainson SME, Roberts RJ, Reynolds GK. A big data approach to pharmaceutical flow properties. Int J Pharm. 2019; 555: 337–45.

4. Yu W, Liao L, Bharadwaj R, Hancock BC. What is the "typical" particle shape of active pharmaceutical ingredients? Powder Technol. 2017; 313: 1–8.

5. Charoo NA. Critical excipient attributes relevant to solid dosage formulation manufacturing. J Pharm Innov. 2020; 15: 163–81.

6. Hlinak AJ, Kuriyan K, Morris KR, Reklaitis G V., Basu PK. Understanding critical material properties for solid dosage form design. J Pharm Innov. 2006; 12–6.

7. Ticehurst MD, Marziano I. Integration of active pharmaceutical ingredient solid form selection and particle engineering into drug product design. J Pharm Pharmacol. 2015; 67(6): 782–802.

8. Fonteyne M, Wickström H, Peeters E, Vercruysse J, Ehlers H, Peters BH, et al. Influence of raw material properties upon critical quality attributes of continuously produced granules and tablets. Eur J Pharm Biopharm. 2014; 87(2): 252–263.

9. Stauffer F, Vanhoorne V, Pilcer G, Chavez PF, Rome S, Schubert MA, et al. Raw material variability of an active pharmaceutical ingredient and its relevance for processability in secondary continuous pharmaceutical manufacturing. Eur J Pharm Biopharm. 2018; 127: 92–103.

10. Stauffer F, Vanhoorne V, Pilcer G, Chavez PF, Schubert MA, Vervaet C, et al. Managing active pharmaceutical ingredient raw material variability during twin-screw blend feeding. Eur J Pharm Biopharm. 2019; 135: 49–60.

11. Stauffer F, Vanhoorne V, Pilcer G, Chavez PF, Vervaet C, De Beer T. Managing API raw material variability during continuous twin-screw wet granulation. Int J Pharm. 2019; 561: 265–73.

12. Stauffer F, Vanhoorne V, Pilcer G, Chavez PF, Vervaet C, De Beer T. Managing API raw material variability in a continuous manufacturing line – Prediction of process robustness. Int J Pharm. 2019; 569: 118525.

13. Zhang D, Xu S, Du S, Wang J, Gong J. Progress of pharmaceutical continuous crystallization. Engineering. 2017; 3(3): 354–64.

14. Variankaval N, Cote AS. From form to function: crystallization of active pharmaceutical ingredients. AIChE. 2008; 54(7): 1682–8.

15. El-Zhry El-Yafi AK, El-Zein H. Technical crystallization for application in pharmaceutical material engineering: Review article. Asian J Pharm Sci. 2015; 10(4): 283–391.

16. Acharya G, Shin CS, McDermott M, Mishra H, Park H, Kwon IC, et al. The hydrogel template method for fabrication of homogeneous nano/microparticles. J Control Release. 2010; 141(3): 314-319.

17. Gratton SEA, Pohlhaus PD, Lee J, Guo J, Cho MJ, DeSimone JM. Nanofabricated particles for engineered drug therapies: A preliminary biodistribution study of PRINT^{TM} nanoparticles. J Control

Release. 2007; 121(1–2): 10–8.

18. Lee BK, Yun YH, Choi JS, Choi YC, Kim JD, Cho YW. Fabrication of drug-loaded polymer microparticles with arbitrary geometries using a piezoelectric inkjet printing system. Int J Pharm. 2012; 427(2): 305–10.

19. Liu D, Zhang H, Fontana F, Hirvonen JT, Santos HA. Microfluidic-assisted fabrication of carriers for controlled drug delivery. Lab Chip. 2017; 17(11): 1856–83.

20. Xu Q, Hashimoto M, Dang TT, Hoare T, Kohane DS, Whitesides GM, et al. Preparation of monodisperse biodegradable polymer microparticles using a microfluidic flow-focusing device for controlled drug delivery. Small. 2009; 5(13): 1575–1581.

21. Xu S, Nie Z, Seo M, Lewis P, Kumacheva E, Stone HA, et al. Generation of monodisperse particles by using microfluidics: Control over size, shape, and composition. Angew Chem Int Ed. 2005; 44(5): 724–8.

22. Patel KC, Chen XD. Production of spherical and uniform-sized particles using a laboratory ink-jet spray dryer. Asia-Pacific J Chem Eng. 2007; 2(5): 415–430.

23. Vehring R. Pharmaceutical particle engineering via spray drying. Pharm Res. 2008; 25(5): 999–1022.

24. Sugimoto T. Monodispersed Particles, 2nd Edition. Elsevier. 2019; 1–826.

25. Jillavenkatesa A, Dapkunas SJ, Lum LS. Particle Size Characterization. National Institute of Standards and Technology (NIST). Special Publication, US Government Printing Office, Washington. 2001; 960–961.

26. International Conference on Harmonisation (ICH): Q8 (R2) Pharmaceutical development. step 4 version; as revised in August 2009. Available from: https://www.ich.org/page/quality-guidelines.

27. CDER's. New Drugs at FDA: CDER's New Molecular Entities and New Therapeutic Biological Products [Internet; cited in August 2021]. Available from: https://www.fda.gov/drugs/development-approval-process-drugs/new-drugs-fda-cders-new-molecular-entities-and-new-therapeutic-biological-products.

28. Zhang J, Wu CY, Pan X, Wu C. On identification of critical material attributes for compression behaviour of pharmaceutical diluent powders. Materials. 2017; 10(7): 845.

29. Van Snick B, Grymonpré W, Dhondt J, Pandelaere K, Di Pretoro G, Remon JP, et al. Impact of blend properties on die filling during tableting. Int J Pharm. 2018; 549(1–2): 476–88.

30. Namjoshi S, Dabbaghi M, Roberts MS, Grice JE, Mohammed Y. Quality by design: Development of the quality target product profile (QTPP) for semisolid topical products. Pharmaceutics. 2020; 12(3): 287.

31. Sivaraman A, Banga A. Quality by design approaches for topical dermatological dosage forms. Res Reports Transdermal Drug Deliv. 2015; 4: 9–21.

32. Qiu Y, Chen Y, Zhang G, Yu L, Mantri R. Developing solid oral dosage forms: pharmaceutical theory and practice. second edi. Academic Press; 2016: 1–1176.

33. Leane M, Pitt K, Reynolds G, Anwar J, Charlton S, Crean A, et al. A proposal for a drug product Manufacturing Classification System (MCS) for oral solid dosage forms. Pharm Dev Technol. 2015; 20(1): 12–21.

34. Leane M, Pitt K, Reynolds GK, Dawson N, Ziegler I, Szepes A, et al. Manufacturing classification system in the real world: factors influencing manufacturing process choices for filed commercial oral solid dosage formulations, case studies from industry and considerations for continuous processing. Pharm Dev Technol. 2018; 23(10): 964–77.

35. Escotet-Espinoza MS, Moghtadernejad S, Scicolone J, Wang Y, Pereira G, Schäfer E, et al. Using a material property library to find surrogate materials for pharmaceutical process development. Powder Technol. 2018; 339: 659–76.

36. Ferreira AP, Gamble JF, Leane MM, Park H, Olusanmi D, Tobyn M. Enhanced understanding of pharmaceutical materials through advanced characterisation and analysis. AAPS PharmSciTech. 2018; 19(8): 3462–80.

37. Kuentz M, Holm R, Elder DP. Methodology of oral formulation selection in the pharmaceutical industry. Vol. 87, European Journal of Pharmaceutical Sciences. 2016; 97: 136–63.

38. Zheng J. Formulation and analytical development for low-dose oral drug products. John Wiley & Sons, Inc., New Jersey; 2009: 1–461.

39. Cartilier LH, Moës AJ. Effect of drug agglomerates upon the kinetics of mixing of low dosage cohesive powder mixtures. Drug Dev Ind Pharm. 1989; 15(12): 1911–31.

40. Huang CY, Ku MS. Asymmetry effect of particle size distribution on content uniformity and over-potency risk in low-dose solid drugs. J Pharm Sci. 2010; 99(10): 4351–62.

41. Orr NA, Sallam EA. Content uniformity of potent drugs in tablets. J Pharm Pharmacol. 1978; 30(1): 741–7.

42. Censi R, Di Martino P. Polymorph impact on the bioavailability and stability of poorly soluble drugs. Molecules. 2015; 20(10): 18759–76.

43. Uzunović A, Vranić E, Hadžidedić Š. Impairment of the in vitro release of carbamazepine from tablets. Bosn J Basic Med Sci. 2010; 10(3): 234–8.

44. FDA. Recalls, market withdrawals, & safety alerts [Internet; cited in August 2021]. Available from: https://www.fda.gov/Safety/Recalls/default.htm.

45. Van Snick B, Dhondt J, Pandelaere K, Bertels J, Mertens R, Klingeleers D, et al. A multivariate raw material property database to facilitate drug product development and enable in-silico design of pharmaceutical dry powder processes. Int J Pharm. 2018; 549(1–2): 415–35.

46. Markl D, Strobel A, Schlossnikl R, Bøtker J, Bawuah P, Ridgway C, et al. Characterisation of pore structures of pharmaceutical tablets: A review. Int J Pharm. 2018; 538(1–2): 188–214.

47. Rojas J, Buckner I, Kumar V. Co-proccessed excipients with enhanced direct compression functionality for improved tableting performance. Drug Dev Ind Pharm. 2012; 38(10): 1159–70.

48. Fujiwara M, Nagy ZK, Chew JW, Braatz RD. First-principles and direct design approaches for the control of pharmaceutical crystallization. J Process Control. 2005; 15(5): 493–504.

49. Ohta M, Buckton G. A study of the differences between two amorphous spray-dried samples of cefditoren pivoxil which exhibited different physical stabilities. Int J Pharm. 2005; 289(1–2): 31–8.

50. Ohta M, Buckton G. Determination of the changes in surface energetics of cefditoren pivoxil as a consequence of processing induced disorder and equilibration to different relative humidities. Int J Pharm. 2004; 269(1): 81–8.

51. Nofrerias I, Nardi A, Suñé-Pou M, Suñé-Negre JM, García-Montoya E, Pérez-Lozano P, et al. Comparison between Microcrystalline Celluloses of different grades made by four manufacturers using the SeDeM diagram expert system as a pharmaceutical characterization tool. Powder Technol. 2019; 342: 780–8.

52. Landín M, Martínez-Pacheco R, Gómez-Amoza JL, Souto C, Concheiro A, Rowe RC. Effect of country of origin on the properties of microcrystalline cellulose. Int J Pharm. 1993; 91(2–3): 123–31.

53. Landín M, Vázquez MJ, Souto C, Concheiro A, Gómez-amoza JL, Martínez-pacheco R. Comparison of two varieties of microcrystalline cellulose as filler-binders I. Perdnisone tablets. Drug Dev Ind Pharm. 1992; 18(3): 355–68.

54. Landín M, González MP, Souto C, Concheiro A, Gómez-Amoza JL, Martínez-Pacheco R. Comparison of two varieties of microcrystalline cellulose as filler-binders II. Hydrochlorothiazide tablets. Drug Dev Ind Pharm. 1993; 19(10): 1211–20.

55. Rojas J, López A, Gamboa Y, González C, Montoya F. Assessment of processing and polymorphic form effect on the powder and tableting properties of microcrystalline celluloses I and II. Chem Pharm Bull. 2011; 59(5): 603–7.

56. Rojas J, Buckner I, Kumar V. Co-proccessed excipients with enhanced direct compression functionality for improved tableting performance. Drug Dev Ind Pharm. 2012; 38(10): 1159–1170.

57. Bolhuis GK, Van Kamp H V., Lerk CF. On the similarity of sodium starch glycolate from different sources. Drug Dev Ind Pharm. 1986; 12(4): 621–30.

58. Rudnic EM, Kanig JL, Rhodes CT. Effect of molecular structure variation on the disintegrant action of sodium starch glycolate. J Pharm Sci. 1985; 74(6): 647–50.

59. Shah U, Augsburger L. Multiple sources of sodium starch glycolate, NF: Evaluation of functional equivalence and development of standard performance tests. Pharm Dev Technol. 2002; 7(3): 345–59.

60. Leinonen UI, Jalonen HU, Vihervaara PA, Laine ESU. Physical and lubrication properties of magnesium stearate. J Pharm Sci. 1992; 81(12): 1194–8.

61. Zarmpi P, Flanagan T, Meehan E, Mann J, Fotaki N. Impact of Magnesium Stearate Presence and Variability on Drug Apparent Solubility Based on Drug Physicochemical Properties. AAPS J. 2020; 22(75): 1–18.

62. Hagsten A, Casper Larsen C, Møller Sonnergaard J, Rantanen J, Hovgaard L. Identifying sources of batch to batch variation in processability. Powder Technol. 2008; 183(2): 213–9.

63. Zhao C, Jin C, Gao H, Wang L, Liu H, He Z. Effect of raw material variability of glipizide on the in vitro dissolution rate and in vivo bioavailability performance: The importance of particle size. Asian J Pharm Sci. 2019; 14(2): 165–73.

64. Šehić S, Betz G, Hadžidedić Š, El-Arini SK, Leuenberger H. Investigation of intrinsic dissolution behavior of different carbamazepine samples. Int J Pharm. 2010; 386(1–2): 77–90.

65. Elder D. ICH Q6A Specifications: test procedures and acceptance criteria for new drug substances and new drug products: chemical substances. In: Teasdale A, Elder D, Nims RW (Eds.), ICH Quality Guidelines: An Implementation Guide. John Wiley & Sons. 2017: 433–466.

66. Tekadle RK. Dosage form design parameters: Volume II. Academic Press; 2018: 1–794.

67. Fu X, Huck D, Makein L, Armstrong B, Willen U, Freeman T. Effect of particle shape and size on flow properties of lactose powders. Particuology. 2012; 10(2): 203–8.

68. Tekade RK. Dosage form design considerations: Volume I. Academic Press; 2018: 287–336.

69. Ganesan V, Rosentrater KA, Muthukumarappan K. Flowability and handling characteristics of bulk solids and powders - a review with implications for DDGS. Biosyst Eng. 2008; 101(4): 425–35.

70. Hart A. Effect of particle size on detergent powders flowability and tabletability. J Chem Eng Process Technol. 2015; 6(1): 1–4.

71. Aulton M, Taylor K. Aulton's pharmaceutics: the design and manufacture of medicines. fifth edit. Elsevier Ltd; 2018: 1–918.

72. Liu LX, Marziano I, Bentham AC, Litster JD, E.T.White, Howes T. Effect of particle properties on the flowability of ibuprofen powders. Int J Pharm. 2008; 362(1–2): 109–17.

73. Lumay G, Boschini F, Traina K, Bontempi S, Remy JC, Cloots R, et al. Measuring the flowing properties of powders and grains. Powder Technol. 2012; 224: 19–27.

74. Šimek M, Grünwaldová V, Kratochvíl B. Comparison of compression and material properties of differently shaped and sized paracetamols. KONA Powder Part J. 2017; 34: 197–206.

75. Fathollahi S, Faulhammer E, Glasser BJ, Khinast JG. Impact of powder composition on processing-relevant properties of pharmaceutical materials: An experimental study. Adv Powder Technol. 2020; 31(7): 2991–3003.

76. Kojima T, Elliott JA. Incipient flow properties of two-component fine powder systems and their relationships with bulk density and particle contacts. Powder Technol. 2012; 228: 359–70.

77. Venables HJ, Wells JI. Powder mixing. Drug Dev Ind Pharm. 2001; 27(7): 599–612.

78. Carson JW, Royal TA, Goodwill DJ. Understanding and eliminating particle segregation problems. Bulk Solids Handl. 1986; 6(1): 139–144.

79. Purutyan H, Carson JW. Predicting, diagnosing, and solving mixture segregation problems. Powder Bulk Eng. 2006: 1-7.

80. Tang P, Puri VM. Methods for minimizing segregation: A review. Part Sci Technol. 2004; 22(4): 321–37.

81. Mcginity JW, Ku CT, Bodmeier R, Harris MR. Dissolution and uniformity properties of ordered mixes of micronized griseofulvin and a directly compressible excipient. Drug Dev Ind Pharm. 1985; 11(4): 891–900.

82. Swaminathan V, Kildsig DO. Polydisperse powder mixtures: Effect of particle size and shape on mixture stability. Drug Dev Ind Pharm. 2002; 28(1): 41–48.

83. Alonso M, Satoh M, Miyanami K. Optimum combination of size ratio, density ratio and concentration to minimize free surface segregation. Powder Technol. 1991; 68(2): 145–52.

84. Williams JC, Khan. MI. Mixing and segregation of particulate solids of different particle-size. Chem Eng. 1973; 269: 19–25.

85. Huang CY, Sherry Ku M. Prediction of drug particle size and content uniformity in low-dose solid dosage forms. Int J Pharm. 2010; 383(1–2): 70–80.

86. Zhang Y, Johnson KC. Effect of drug particle size on content uniformity of low-dose solid dosage forms. Int J Pharm. 1997; 154(2): 179–83.

87. Yalkowsky SH, Bolton S. Particle size and content uniformity. Pharm Res. 1990; 7(9): 962–6.

88. Rohrs BR, Amidon GE, Meury RH, Secreast PJ, King HM, Skoug CJ. Particle size limits to meet USP content uniformity criteria for tablets and capsules. Journal of Pharmaceutical Sciences. 2006; 95(5): 1049–59.

89. Hassanpour A, Hare C, Pasha M. Powder flow: theory, characterisation and application. Royal Society of Chemistry; 2019: 1–222.

90. Hoag SW, Lim H-P. Particle and powder bed properties. In: Augsburger LL, Hoag SW (EDs.). Pharmaceutical Dosage Forms: Tablets. Unit Operations and Mechanical Properties: Volume I, Third edition, Informa Healthcare. 2008: 17–73.

91. Chattoraj S, Daugherity P, McDermott T, Olsofsky A, Roth WJ, Tobyn M. Sticking and Picking in Pharmaceutical Tablet Compression: An IQ Consortium Review. J Pharm Sci. 2018; 107(9): 2267–82.

92. Shargel L, Yu ABC, Wu-Pong S. Bioavailability and Bioequivalence: Introduction. In: Applied Biopharmaceutics & Pharmacokinetics. Seventh edition, McGraw-Hill Education, 2016: 1-928.

93. Dokoumetzidis A, Macheras P. A century of dissolution research: From Noyes and Whitney to the Biopharmaceutics Classification System. Int J Pharm. 2006; 321(1–2): 1–11.

94. Mosharraf M, Nyström C. The effect of particle size and shape on the surface specific dissolution rate of microsized practically insoluble drugs. Int J Pharm. 1995; 122(1–2): 35–47.

95. Chu KR, Lee E, Jeong SH, Park ES. Effect of particle size on the dissolution behaviors of poorly water-soluble drugs. Arch Pharm Res. 2012; 35(7): 1187–95.

96. Liversidge GG, Cundy KC. Particle size reduction for improvement of oral bioavailability of hydrophobic drugs: I. Absolute oral bioavailability of nanocrystalline danazol in beagle dogs. Int J Pharm. 1995; 125(1): 91–7.

97. Khadka P, Ro J, Kim H, Kim I, Kim JT, Kim H, et al. Pharmaceutical particle technologies: An approach to improve drug solubility, dissolution and bioavailability. Asian J Pharm Sci. 2014; 9(6): 304–16.

98. Junghanns J-UA, Müller RH. Nanocrystal technology , drug delivery and clinical applications. Int J Nanomedicine. 2008; 3(3): 295–309.

99. Rohrs BR, Amidon GE. Particle engineering: a formulator's perspective. I. AAPS Arden House Conf New York Harriman, 2005.

100. Blagden N, de Matas M, Gavan PT, York P. Crystal engineering of active pharmaceutical ingredients to improve solubility and dissolution rates. Adv Drug Deliv Rev. 2007; 59(7): 617–30.

101. Javadzadeh Y, Dizaj SM, Vazifehasl Z, Mokhtarpour M. Recrystallization of Drugs: Effect on Dissolution Rate. In: Glebovsky V (Ed.). Recrystallization in Materials Processing. 2015: 191–211.

102. Etzler FM, Uddin MN. Powder technology and pharmaceutical development: Particle size and particle adhesion. KONA Powder Part J. 2012; 30(30): 125–43.

103. Mihranyan A, Strømme M. Fractal aspects of powder flow and densification. Part Part Syst Charact. 2007; 24(3): 223–8.

104. Cleary PW, Sawley ML. DEM modelling of industrial granular flows: 3D case studies and the effect of particle shape on hopper discharge. Appl Math Model. 2002; 26(2): 89–111.

105. Hassan MS, Lau RWM. Effect of particle shape on dry particle inhalation: Study of flowability, aerosolization, and deposition properties. AAPS PharmSciTech. 2009; 10(4): 1252-1262.

106. Zou RP, Yu AB. Evaluation of the packing characteristics of mono-sized non-spherical particles. Powder Technol. 1996; 88(1): 71–9.

107. Burtseva L, Salas BV, Werner F, Petranovskii V. Packing of monosized spheres in a cylindrical container: models and approaches. Rev Mex Fis E. 2015; 61(1): 20–7.

108. Weitz DA. Packing in the Spheres. Science. 2004; 303(5660): 968–9.

109. He S, Gan J, Pinson D, Yu A, Zhou Z. A discrete element method study of monodisperse mixing of ellipsoidal particles in a rotating drum. Ind Eng Chem Res. 2020; 59(27): 12458–70.

110. Woodle GR, Munro JM. Particle motion and mixing in a rotary kiln. Powder Technol. 1993; 76(3): 241–5.

111. Yi H, Mittal B, Puri VM, Li F, Mancino CF. Measurement of bulk mechanical properties and modeling the load-response of rootzone sands. Part 1: Round and angular monosize and binary mixtures. Part Sci Technol. 2001; 19(2): 145–73.

112. Pereira GG, Cleary PW. Segregation due to particle shape of a granular mixture in a slowly rotating tumbler. Granul Matter. 2017; 19(2): 23.

113. He SY, Gan JQ, Pinson D, Zhou ZY. Particle shape-induced radial segregation of binary mixtures in a rotating drum. Powder Technol. 2019; 341(1): 157–66.

114. Wong LW, Pilpel N. The effect of particle shape on the mechanical properties of powders. Int J Pharm. 1990; 59(2): 145–54.

115. Rasenack N, Müller BW. Crystal habit and tableting behavior. Int J Pharm. 2002; 244(1-2): 45-57.

116. Joiris E, Di Martino P, Berneron C, Guyot-Hermann AM, Guyot JC. Compression behavior of orthorhombic paracetamol. Pharm Res. 1998; 15(7): 1122–30.

117. Lu ATK, Frisella ME, Johnson KC. Dissolution Modeling: Factors Affecting the Dissolution Rates of Polydisperse Powders. Pharm Res. 1993; 10(9): 1308–14.

118. Guo M, Fu Q, Wu C, Guo Z, Li M, Sun J, et al. Rod shaped nanocrystals exhibit superior in vitro dissolution and in vivo bioavailability over spherical like nanocrystals: A case study of lovastatin. Colloids Surfaces B Biointerfaces. 2015; 128: 410-418.

119. Guo M, Wei M, Li W, Guo M, Guo C, Ma M, et al. Impacts of particle shapes on the oral delivery of drug nanocrystals: Mucus permeation, transepithelial transport and bioavailability. J Control Release. 2019; 307: 64-75.

120. Sugimoto T. Formation of Monodispersed Nano- and Micro- Particles Controlled in Size , Shape and Internal Structure. Chem Eng Technol. 2003; 26(3): 313–21.

121. Seiffert S, Thiele J. Microfluidics: Theory and Practice for Beginners. Walter de Gruyter GmbH & Co KG; 2020: 277.

122. Dolomite. Single emulsions [Internet; cited in August 2021]. Available from: https://www.dolomite-microfluidics.com/applications/single-emulsions/.

123. Yuet KP, Hwang DK, Haghgooie R, Doyle PS. Multifunctional superparamagnetic janus particles. Langmuir. 2010; 26(6): 4281–7.

124. Wang J, Li Y, Wang X, Wang J, Tian H, Zhao P, et al. Droplet microfluidics for the production of microparticles and nanoparticles. Micromachines. 2017; 8(22): 1–23.

125. Liu Z, Fontana F, Python A, Hirvonen JT, Santos HA. Microfluidics for Production of Particles: Mechanism, Methodology, and Applications. Small. 2020; 16(9): 1904673.

126. Whelehan M, Marison IW. Microencapsulation using vibrating technology. J Microencapsul. 2011; 28(8): 669–88.

127. Xia Y, Pack DW. Uniform biodegradable microparticle systems for controlled release. J Control Release. 2002; 82(1): 137–147.

128. Berkland C, Kim K, Pack DW. Fabrication of PLG microspheres with precisely controlled and monodisperse size distributions. J Control Release. 2001; 73(1): 59–74.

129. Berkland C, Pollauf E, Varde N, Pack DW, Kim K. Monodisperse liquid-filled biodegradable microcapsules. Pharm Res. 2007; 24(5): 1007–13.

130. Mao S, Guo C, Shi Y, Li LC. Recent advances in polymeric microspheres for parenteral drug delivery part 1. Expert Opin Drug Deliv. 2012; 9(10): 1209-1223.

131. Berkland C, Pollauf E, Pack DW, Kim K. Uniform double-walled polymer microspheres of controllable shell thickness. J Control Release. 2004; 96(1): 101–11.

132. Lamichhane S, Bashyal S, Keum T, Noh G, Seo JE, Bastola R, et al. Complex formulations, simple techniques: Can 3D printing technology be the Midas touch in pharmaceutical industry? Asian J Pharm Sci. 2019; 14(5): 465–79.

133. Garcia A, Mack P, Williams S, Fromen C, Shen T, Tully J, et al. Microfabricated Engineered Particle Systems for Respiratory Drug Delivery and Other Pharmaceutical Applications. J Drug Deliv. 2012; 2012: 1–10.

134. Zhang Y, Chan HF, Leong KW. Advanced materials and processing for drug delivery: The past and the future. Adv Drug Deliv Rev. 2013; 65(1): 104–20.

135. Canelas DA, Herlihy KP, DeSimone JM. Top-down particle fabrication: Control of size and shape for diagnostic imaging and drug delivery. Wiley Interdiscip Rev Nanomedicine Nanobiotechnology. 2009; 1(4): 391–404.

136. Nunes J, Herlihy KP, Mair L, Superfine R, Desimone JM. Multifunctional shape and size specific magneto-polymer composite particles. Nano Lett. 2010; 10(4): 1113–1119.

137. Gratton SEA, Williams SS, Napier ME, Pohlhaus PD, Zhou Z, Wiles KB, et al. The pursuit of a scalable nanofabrication platform for use in material and life science applications. Acc Chem Res. 2008; 41(12): 1685–95.

138. Rolland JP, Maynor BW, Euliss LE, Exner AE, Denison GM, DeSimone JM. Direct fabrication and harvesting of monodisperse, shape-specific nanobiomaterials. J Am Chem Soc. 2005; 127(28): 10096–100.

139. Patel RP, Patel MP, Suthar AM. Spray drying technology: an overview. Indian J Sci Technol. 2009; 2(10): 44–7.

140. Al-Khattawi A, Bayly A, Phillips A, Wilson D. The design and scale-up of spray dried particle

delivery systems. Expert Opin Drug Deliv. 2018; 15(1): 47–63.

141. Nandiyanto ABD, Okuyama K. Progress in developing spray-drying methods for the production of controlled morphology particles: from the nanometer to submicrometer size ranges. Adv Powder Technol. 2011; 22(1): 1–19.

142. Shishir MRI, Chen W. Trends of spray drying: A critical review on drying of fruit and vegetable juices. Trends Food Sci Technol. 2017; 65: 49–67.

143. Ziaee A, Albadarin AB, Padrela L, Femmer T, O'Reilly E, Walker G. Spray drying of pharmaceuticals and biopharmaceuticals: Critical parameters and experimental process optimization approaches. Eur J Pharm Sci. 2019; 127: 300–18.

144. Fu N, Xiao J, Woo MW, Chen XD. Frontiers in Spray Drying. First edit. CRC Press. CRC Press; 2020: 1-116.

145. Wu WD, Patel KC, Rogers S, Chen XD. Monodisperse droplet generators as potential atomizers for spray drying technology. Dry Technol. 2007; 25(12): 1907–16.

146. Miller DA, Ellenberger D, Gil M. Spray-drying technology. In: Williams III RO, Watts AB, Miller DA (Eds.). Formulating poorly water soluble drugs. Springer; 2016: 437–525.

147. Santos D, Maurício AC, Sencadas V, Santos JD, Fernandes MH, Gomes PS. Spray Drying: An Overview. InTechOpen; 2018: 9–35.

148. Anandharamakrishnan C, Padma Ishwarya S. Spray drying techniques for food ingredient encapsulation. John Wiley & Sons Ltd.; 2015: 1–296.

149. Jain M, Lohare G, Bari M, Chavan R, Barhate S, Shah C. Spray Drying in Pharmaceutical Industry: A Review. Res J Pharm Dos Forms Technol. 2011; 4(2): 74–9.

150. Al-Achi A, Gupta MR, Stagner WC. Integrated pharmaceutics: applied preformulation, product design, and regulatory science. First Edit. John Wiley & Sons.; 2013: 467–560.

151. Vehring R, Foss WR, Lechuga-Ballesteros D. Particle formation in spray drying. J Aerosol Sci. 2007; 38(7): 728–46.

152. Van Deventer H, Houben R, Koldeweij R. New Atomization Nozzle for Spray Drying. Dry Technol. 2013; 31(8): 891–7.

153. Atuonwu JC, Stapley AGF. Reducing energy consumption in spray drying by monodisperse droplet generation: Modelling and simulation. Energy Procedia. 2017; 123: 235–42.

154. Wanning S, Süverkrüp R, Lamprecht A. Jet-vortex spray freeze drying for the production of inhalable lyophilisate powders. Eur J Pharm Sci. 2017; 96: 1–7.

155. Wanning S, Süverkrüp R, Lamprecht A. Aerodynamic Droplet Stream Expansion for the Production of Spray Freeze-Dried Powders. AAPS PharmSciTech. 2017; 18(5): 1760–9.

156. Süverkrüp R, Eggerstedt SN, Gruner K, Kuschel M, Sommerfeld M, Lamprecht A. Collisions in fast droplet streams for the production of spherolyophilisates. Eur J Pharm Sci. 2013; 49(4): 535–41.

157. Süverkrüp R, Eggerstedt S, Wanning S, Kuschel M, Sommerfeld M, Lamprecht A. Collisions and coalescence in droplet streams for the production of freeze-dried powders. Colloids Surfaces B Biointerfaces. 2016; 141: 443–9.

158. Baldelli A, Boraey MA, Nobes DS, Vehring R. Analysis of the Particle Formation Process of Structured Microparticles. Mol Pharm. 2015; 12(8): 2562–2573.

159. Baldelli A, Power RM, Miles REH, Reid JP, Vehring R. Effect of crystallization kinetics on the properties of spray dried microparticles. Aerosol Sci Technol. 2016; 50(7): 693–704.

160. Baldelli A, Vehring R. Control of the radial distribution of chemical components in spray-dried crystalline microparticles. Aerosol Sci Technol. 2016; 50(10): 1130–1142.

161. Ordoubadi M, Gregson FKA, Melhem O, Barona D, Miles REH, D'Sa D, et al. Multi-Solvent Microdroplet Evaporation: Modeling and Measurement of Spray-Drying Kinetics with Inhalable Pharmaceutics. Pharm Res. 2019; 36(7): 1-17.

162. Ordoubadi M, Gregson FKA, Wang H, Nicholas M, Gracin S, Lechuga-Ballesteros D, et al. On the particle formation of leucine in spray drying of inhalable microparticles. Int J Pharm. 2020; 592: 120102.

163. Wu WD, Amelia R, Hao N, Selomulya C, Zhao D, Chiu YL, et al. Assembly of uniform photoluminescent microcomposites using a novel micro-fluidic-jet-spray-dryer. AIChE J. 2011; 57(10): 2726–37.

164. Liu W, Chen XD, Selomulya C. On the spray drying of uniform functional microparticles. Particuology. 2015; 22: 1–12.

165. Lefebvre AH, McDonell VG. Atomization and sprays. Second Edi. Atomization and Sprays. CRC Press; 2017: 1–284.

166. Nasr GG, Yule AJ, Bendig L. Industrial sprays and atomization: design, analysis and applications. Springer Science & Business Media; 2002: 1-499.

167. Liu H. Science and engineering of droplets: fundamentals and applications. Fundamentals and Applications. William Andrew; 1999: 121–136.

168. Bachalo WD. Spray diagnostics for the twenty-first century. At Sprays. 2000; 10(3–5): 439–74.

169. Heinzen C, Berger A, Marison I. Use of vibration technology for jet break-up for encapsulation of cells and liquids in monodisperse microcapsules. In: Nedović V., Willaert R. (Eds.). Fundamentals of cell immobilisation biotechnology. Focus on Biotechnology, vol 8A. Springer, Dordrecht. 2004: 257–75.

170. Duan H, Romay F, Syedain Z, Liu BYH, Naqwi AA. A New Monodisperse Droplet Generator and its Applications. ILASS Americas 28th Annual Conf erence on Liquid Atomisation and Spray Systems, Dearborn, MI, 2016.

171. Ashgriz N. Handbook of atomization and sprays: theory and applications. Springer Science & Business Media; 2011: 1–935.

172. Kamlesh C. P, Xiao Dong C. Production of spherical and uniform-sized particles using a laboratory ink-jet spray dryer. Asia-Pacific J Chem Eng. 2007; 2(5): 415–30.

173. Brenn G, Helpiö T, Durst F. A new apparatus for the production of monodisperse sprays at high flow rates. Chem Eng Sci. 1997; 52(2): 237–44.

174. Brenn G, Lackermeier U. Drop formation from a vibrating orifice generator driven by modulated electrical signals. Phys Fluids. 1997; 9(12): 3658–69.

175. Brenn G. On the controlled production of sprays with discrete polydisperse drop size spectra. Chem

Eng Sci. 2000; 55(22): 5437–44.

176. Brenn G, Durst F, Tropea C. Monodisperse sprays for various purposes - Their production and characteristics. Part Part Syst Charact. 1996; 13(3): 179–85.

177. Schneider JM, Hendricks CD. Source of uniform-sized liquid droplets. Rev Sci Instrum. 1964; 35(10): 1349–50.

178. Duan H, Romay FJ, Li C, Naqwi A, Deng W, Liu BYH. Generation of monodisperse aerosols by combining aerodynamic flow-focusing and mechanical perturbation. Aerosol Sci Technol. 2016; 50(1): 17–25.

179. Anders K, Roth N, Frohn A. Operation Characteristics of Vibrating-Orifice Generators: The coherence length. Part Part Syst Charact. 1992; 9(1–4): 40–3.

180. König G, Anders K, Frohn A. A new light-scattering technique to measure the diameter of periodically generated moving droplets. J Aerosol Sci. 1986; 17(2): 157–67.

181. Thybo P, Hovgaard L, Andersen SK, Lindeløv JS. Droplet size measurements for spray dryer scale-up. Pharm Dev Technol. 2008; 13(2): 93–104.

182. Alamilla-Beltrán L, Chanona-Pérez JJ, Jiménez-Aparicio AR, Gutiérrez-Lopez GF. Description of morphological changes of particles along spray drying. J Food Eng. 2005; 67(1–2): 179–184.

183. Huang LX, Kumar K, Mujumdar AS. A comparative study of a spray dryer with rotary disc atomizer and pressure nozzle using computational fluid dynamic simulations. Chem Eng Process Process Intensif. 2006; 45(6): 461–70.

184. Huntington DH. The influence of the spray drying process on product properties. Dry Technol. 2004; 22(6): 1261–87.

185. Finney J, Buffo R, Reineccius GA. Effects of type of atomization and processing temperatures on the physical properties and stability of spray-dried flavors. J Food Sci. 2002; 67(3): 1108–14.

186. Tropmann A, Lass N, Paust N, Ziegler C, Zengerle R, Koltay P. Monodisperse microparticle generation from aqueous solutions. Solid-State Sensors, Actuators Microsystems Conf Int IEEE. 2011: 1460–3.

187. FDA guidance for industry: PAT — a framework for innovative pharmaceutical development, manufacturing, and quality assurance. US Dep Heal Hum Serv; 2004.

188. Yao S, Song H, Cheng Q, Liang B. The Development of PAT (Process Analytical Technology) for Drug Production and the Requirements for Domestic Pharmaceutical Engineering Education. Creat Educ. 2012; 03(07): 76–9.

189. The European Medicines Agency Road Map to 2010: Preparing the Ground for the Future. Eur Med Agency, London; 2005.

190. Schaefer C, Clicq D, Lecomte C, Merschaert A, Norrant E, Fotiadu F. A Process Analytical Technology (PAT) approach to control a new API manufacturing process: Development, validation and implementation. Talanta. 2014; 120: 114–25.

191. Rathore AS, Bhambure R, Ghare V. Process analytical technology (PAT) for biopharmaceutical products. Anal Bioanal Chem. 2010; 398(1): 137–54.

192. Lee E. Microdrop generation. Vol. 5, CRC Press: Boca Raton, Florida. CRC Press LLC; 2003.

193. Nasr GG, Yule AJ, Bendig L. Industrial Sprays and Atomization. Springer Science & Business Media; 2013: 7–33.

194. Sindayihebura D, Dobre M, Bolle L. Experimental study of thin liquid film ultrasonic atomization. In: 4th World Conference on Experimental Heat Transfer, Fluid Mechanics and Thermodynamics. Brussels, Belgium; 1997: 1249–56.

195. Mangal S, Meiser F, Morton D, Larson I. Particle engineering of excipients for direct compression: understanding the role of material properties. Curr Pharm Des. 2015; 21(40): 5877–89.

196. Okuyama K, Abdullah M, Lenggoro IW, Iskandar F. Preparation of functional nanostructured particles by spray drying. Adv Powder Technol. 2006; 17(6): 587–611.

197. Shoyele SA, Cawthorne S. Particle engineering techniques for inhaled biopharmaceuticals. Vol. 58, Advanced Drug Delivery Reviews. Elsevier; 2006: 1009–29.

198. Cun D, Wan F, Yang M. Formulation strategies and particle engineering technologies for pulmonary delivery of biopharmaceuticals. Curr Pharm Des. 2015; 21(19): 2599–610.

199. Sun B, Yeo Y. Nanocrystals for the parenteral delivery of poorly water-soluble drugs. Vol. 16, Current Opinion in Solid State and Materials Science. Elsevier Ltd; 2012: 295–301.

200. International Conference on Harmonisation (ICH): Q6A Specifications: Test procedures and acceptance criteria for new drug substances and new drug products: chemical substances; 1999. Available from: http://www.ich.org/home.html.

201. Ziaee A, Albadarin AB, Padrela L, Femmer T, O'Reilly E, Walker G. Spray drying of pharmaceuticals and biopharmaceuticals: Critical parameters and experimental process optimization approaches. Eur J Pharm Sci. 2019; 127: 300–18.

202. Ormes JD, Zhang D, Chen AM, Hou S, Krueger D, Nelson T, et al. Design of experiments utilization to map the processing capabilities of a micro-spray dryer: Particle design and throughput optimization in support of drug discovery. Pharm Dev Technol. 2013; 18(1): 121–9.

203. Huang Z, Scicolone J V., Han X, Davé RN. Improved blend and tablet properties of fine pharmaceutical powders via dry particle coating. Int J Pharm. 2015; 478(2): 447–55.

204. Trementozzi AN, Leung CY, Osei-Yeboah F, Irdam E, Lin Y, MacPhee JM, et al. Engineered particles demonstrate improved flow properties at elevated drug loadings for direct compression manufacturing. Int J Pharm. 2017; 523: 133–41.

205. Shah U V., Karde V, Ghoroi C, Heng JYY. Influence of particle properties on powder bulk behaviour and processability. Int J Pharm. 2017; 518(1–2): 138–54.

206. Yu LX, Amidon G, Khan MA, Hoag SW, Polli J, Raju GK, et al. Understanding pharmaceutical quality by design. Vol. 16, AAPS Journal. Springer New York LLC; 2014; 16(4): 771–83.

207. Yu LX. Pharmaceutical quality by design: product and process development, understanding, and control. Pharm Res. 2008; 25(4): 781–91.

208. Maury M, Murphy K, Kumar S, Shi L, Lee G. Effects of process variables on the powder yield of spray-dried trehalose on a laboratory spray-dryer. Eur J Pharm Biopharm. 2005; 59(3): 565–73.

209. Boel E, Koekoekx R, Dedroog S, Babkin I, Vetrano MR, Clasen C, et al. Unraveling particle formation: From single droplet drying to spray drying and electrospraying. Pharmaceutics. 2020; 12(7): 1–58.

210. Sano Y. Gas flow behaviour in spray dryer. Dry Technol. 1993; 11(4): 697–718.

211. Feng S, Xiao L, Ge Z, Yang L, Du X, Wu H. Parameter analysis of atomized droplets sprayed evaporation in flue gas flow. Int J Heat Mass Transf. 2019; 129: 936–52.

212. Kemp IC, Wadley R, Hartwig T, Cocchini U, See-Toh Y, Gorringe L, et al. Experimental study of spray drying and atomization with a two-fluid nozzle to produce inhalable particles. Dry Technol. 2013; 31(8): 930–41.

213. Fallahi H, Zhang J, Phan HP, Nguyen NT. Flexible microfluidics: Fundamentals, recent developments, and applications. Micromachines. 2019; 10(12): 830.

214. Jiang B, Chang S, Zheng H, Zhang W, Leng M, Zhao Y. Coalescence and separation of monodisperse droplets. In: International Conference on Applied Mechanics and Mechanical Automation (AMMA 2017); 2017: 17–23.

215. Brandenberger H, Nüssli D, Piëch V, Widmer F. Monodisperse particle production: A method to prevent drop coalescence using electrostatic forces. J Electrostat. 1999; 45(3): 227-238.

216. Desai D, Wong B, Huang Y, Ye Q, Tang D, Guo H, et al. Surfactant-mediated dissolution of metformin hydrochloride tablets: Wetting effects versus ion pairs diffusivity. J Pharm Sci. 2014; 103(3): 920–6.

217. Butt Z, Pasha RA. Effect of temperature and loading on output voltage of lead zirconate titanate (PZT-5A) piezoelectric energy harvester. In: IOP Conference Series: Materials Science and Engineering; 2016: 012016.

218. Lyras KG, Dembele S, Wen JX. Numerical simulation of flashing jets atomisation using a unified approach. Int J Multiph Flow. 2019; 113: 45–58.

219. Kamoun H, Lamanna G, Weigand B, Steelant J. High-Speed Shadowgraphy Investigations of Superheated Liquid Jet Atomisation. In: ILASS-Americas 22nd Annual Conference on Liquid Atomization and Spray Systems, Cincinnati; 2010.

220. Sher E, Bar-Kohany T, Rashkovan A. Flash-boiling atomization. Progress in Energy and Combustion Science. 2008; 34(4): 417–439.

221. Khomane KS, Bansal AK. Effect of particle size on in-die and out-of-die compaction behavior of ranitidine hydrochloride polymorphs. AAPS PharmSciTech. 2013; 14(3): 1169–77.

222. Nokhodchi A, Rubinstein MH, Ford JL. The effect of particle size and viscosity grade on the compaction properties of hydroxypropylmethylcellulose 2208. Int J Pharm. 1995; 126(1–2): 189–97.

223. Sun CC. Decoding powder tabletability: Roles of particle adhesion and plasticity. J Adhes Sci Technol. 2011; 25(4–5): 483–99.

224. Sun WJ, Chen H, Aburub A, Sun CC. A platform direct compression formulation for low dose sustained-release tablets enabled by a dual particle engineering approach. Powder Technol. 2019; 342: 856–63.

225. Rowe RC, Sheskey PJ, Quinn ME. Handbook of pharmaceutical excipients. Libros Digitales-Pharmaceutical Press; 2009: 424–428.

226. Takasaki H, Yonemochi E, Ito M, Wada K, Terada K. The importance of binder moisture content in Metformin HCL high-dose formulations prepared by moist aqueous granulation (MAG). Results Pharma Sci. 2015; 5: 1–7.

227. Al-Khattawi A, Koner J, Rue P, Kirby D, Perrie Y, Rajabi-Siahboomi A, et al. A pragmatic approach for engineering porous mannitol and mechanistic evaluation of particle performance. Eur J Pharm Biopharm. 2015; 94: 1–10.

228. Cantor SL, Kothari S, Koo OMY. Evaluation of the physical and mechanical properties of high drug load formulations: Wet granulation vs. novel foam granulation. Powder Technol. 2009; 195(1): 15–24.

229. Malvern Panalytical Morphologi®. Component Characterization of Cements using Morphologi G3-ID. Malvern Instruments Limited; 2015: 1–7.

230. Degen T, Sadki M, Bron E, König U, Nénert G. The high score suite. Powder Diffr. 2014; 29(S2): S13–8.

231. Field C. Developing a method for suitable loss on drying by TGA. PerkinElmer; 2003. Available from:https://www.perkinelmer.com/CMSResources/Images/4474504CST_AccuPikMethodSuitableLossDrying.pdf.

232. Bulk density and tapped density of powders ⟨616⟩, The United States Pharmacopeia (USP 36, Volume 1). United States Pharmacopeial Conv Inc, Rockville, MD, USA; 2013: 265–8.

233. Carr RL. Evaluating flow properties of solids. Chem Eng. 1965; 72: 163–8.

234. Hausner HH. Friction Conditions in a Mass of Metal Powder. Int J Powder Metall. 1967; 13: 7–13.

235. Sune Negre JM, Roig Carreras M, Fuster García R, Hernández Pérez C, Ruhí Roura R, García Montoya E, et al. Nueva metodología de preformulación galénica para la caracterización de sustancias en relación a su viabilidad para la compresión: Método SeDeM. Vol. 15, Ciencia y Tecnologia Pharmaceutica. 2005; 15: 125–36.

236. Powder flow ⟨1174⟩, The United States Pharmacopeia (USP 36, Volume 1). United States Pharmacopeial Conv Inc, Rockville, MD, USA; 2013: 891–4.

237. Jenike AW. Storage and flow of solids, Bulletin No. 123 of the Utah State Engineering Experiment Station. 1964; 53(26).

238. Stasiak M, Molenda M. Direct shear testing of flowability of food powders. Res Agric Eng. 2004; 50(1): 6–10.

239. Heckel RW. An analysis of powder compaction phenomena. Trans Met Soc AIME. 1961; 221(4): 1001–1008.

240. Heckel RW. Density-Pressure Relationships in Powder Compaction. Trans Met Soc AIME. 1961; 221(4): 671–5.

241. Patel S, Kaushal AM, Bansal AK. Mechanistic investigation on pressure dependency of Heckel parameter. Int J Pharm. 2010; 389(1–2): 66–73.

242. Nordström J, Klevan I, Alderborn G. A protocol for the classification of powder compression characteristics. Eur J Pharm Biopharm. 2012; 80(1): 209–16.

243. Tarlier N, Soulairol I, Bataille B, Baylac G, Ravel P, Nofrerias I, et al. Compaction behavior and deformation mechanism of directly compressible textured mannitol in a rotary tablet press simulator. Int J Pharm. 2015; 495(1): 410–9.

244. Roberts RJ, Rowe RC. The effect of punch velocity on the compaction of a variety of materials. J Pharm Pharmacol. 1985; 37(6): 377–84.

245. Fell JT, Newton JM. Determination of tablet strength by the diametral-compression test. J Pharm Sci. 1970; 59(5): 688–91.

246. Tye CK, Sun C, Amidon GE. Evaluation of the effects of tableting speed on the relationships between compaction pressure, tablet tensile strength, and tablet solid fraction. J Pharm Sci. 2005; 94(3): 465–72.

247. Chang SY, Wang C, Sun CC. Relationship between hydrate stability and accuracy of true density measured by helium pycnometry. Int J Pharm. 2019; 567: 118444.

248. Armstrong NA, Haines-Nutt RF. Elastic recovery and surface area changes in compacted powder systems. Powder Technol. 1974; 9(5–6): 287–90.

249. Sune Negre JM, Garcia E, Perez P, Aguilar Diaz JE, Roig M, Fuster R, et al. SeDeM Diagram: A New Expert System for the Formulation of Drugs in Solid Form. In: InTechOpen; 2011: 17–34.

250. Dai S, Xu B, Shi G, Liu J, Zhang Z, Shi X, et al. SeDeM expert system for directly compressed tablet formulation: A review and new perspectives. Powder Technol. 2019; 342(11): 517–27.

251. Saurí J, Millán D, Suñé-Negre JM, Pérez-Lozano P, Sarrate R, Fàbregas A, et al. The use of the SeDeM diagram expert system for the formulation of Captopril SR matrix tablets by direct compression. Int J Pharm. 2014; 461(1–2): 38–45.

252. Aguilar-Díaz JE, García-Montoya E, Suñe-Negre JM, Pérez-Lozano P, Miñarro M, Ticó JR. Predicting orally disintegrating tablets formulations of ibuprophen tablets: An application of the new SeDeM-ODT expert system. Eur J Pharm Biopharm. 2012; 80(3): 638–48.

253. Sun CC, Hou H, Gao P, Ma C, Medina C, Alvarez FJ. Development of a high drug load tablet formulation based on assessment of powder manufacturability: Moving towards quality by design. J Pharm Sci. 2009; 98(1): 239–47.

254. Broadhead J, Edmond Rouan SK, Rhodes CT. The spray drying of pharmaceuticals. Drug Dev Ind Pharm. 1992; 18(11–12): 1169–206.

255. Davis M, Walker G. Recent strategies in spray drying for the enhanced bioavailability of poorly water-soluble drugs. J Control Release. 2018; 269: 110–27.

256. Wei Y, Huang YH, Cheng KC, Song YL. Investigations of the Influences of Processing Conditions on the Properties of Spray Dried Chitosan-Tripolyphosphate Particles loaded with Theophylline. Sci Rep. 2020; 10(1): 1–12.

257. Campaña I, Benito-Calvo A, Pérez-González A, Bermúdez de Castro JM, Carbonell E. Assessing automated image analysis of sand grain shape to identify sedimentary facies, Gran Dolina archaeological site (Burgos, Spain). Sediment Geol. 2016; 346: 72–83.

258. Benmessaoud I, Koutchoukali O, Bouhelassa M, Nouar A, Veesler S. Solvent screening and crystal habit of metformin hydrochloride. J Cryst Growth. 2016; 451: 42–51.

259. Cares-Pacheco MG, Vaca-Medina G, Calvet R, Espitalier F, Letourneau JJ, Rouilly A, et al. Physicochemical characterization of d-mannitol polymorphs: The challenging surface energy determination by inverse gas chromatography in the infinite dilution region. Int J Pharm. 2014; 475(1-2): 69-81.

260. Kaialy W, Momin MN, Ticehurst MD, Murphy J, Nokhodchi A. Engineered mannitol as an alternative carrier to enhance deep lung penetration of salbutamol sulphate from dry powder inhaler. Colloids Surfaces B Biointerfaces. 2010; 79(2): 345–56.

261. Walton DE, Mumford CJ. The morphology of spray-dried particles. The effect of process variables upon the morphology of spray-dried particles. Chem Eng Res Des. 1999; 77(5): 442–60.

262. Nguyen D, Rasmuson A, Björn IN, Thalberg K. Mechanistic time scales in adhesive mixing investigated by dry particle sizing. Eur J Pharm Sci. 2015; 69: 19–25.

263. Burger A, Henck JO, Hetz S, Rollinger JM, Weissnicht AA, Stöttner H. Energy/temperature diagram and compression behavior of the polymorphs of D-mannitol. J Pharm Sci. 2000; 89(4): 457–68.

264. Debord B, Lefebvre C, Guyot-Hermann AM, Hubert J, Bouché R, Cuyot JC. Study of Different Crystalline forms of Mannitol: Comparative Behaviour under Compression. Drug Dev Ind Pharm. 1987; 13(9–11): 1533–46.

265. Childs SL, Chyall LJ, Dunlap JT, Coates DA, Stahly BC, Stahly GP. A metastable polymorph of metformin hydrochloride: Isolation and characterization using capillary crystallization and thermal microscopy techniques. Cryst Growth Des. 2004; 4(3): 441–9.

266. Hulse WL, Forbes RT, Bonner MC, Getrost M. The characterization and comparison of spray-dried mannitol samples characterization of spray-dried mannitol. Drug Dev Ind Pharm. 2009; 35(6): 712–8.

267. Barot B, Parejiya P, Patel T, Parikh R, Gohel M. Development of directly compressible metformin hydrochloride by the spray-drying technique. Acta Pharm. 2010; 60(2): 165–75.

268. Block LC, Schmeling LO, Couto AG, Silva MAS, Tagliari MP, Bresolin TMB, et al. Effect of binders on 500mg metformin hydrochloride tablets produced by wet granulation. Rev Ciencias Farm Basica e Apl. 2009; 30(2): 145-152.

269. Tao J, Jones KJ, Yu L. Cross-nucleation between D-mannitol polymorphs in seeded crystallization. Cryst Growth Des. 2007; 7(12): 2410–2414.

270. Kaialy W, Nokhodchi A. Freeze-dried mannitol for superior pulmonary drug delivery via dry powder inhaler. Pharm Res. 2013; 30(2): 458–477.

271. Holder CF, Schaak RE. Tutorial on Powder X-ray Diffraction for Characterizing Nanoscale Materials. ACS Nano. 2019; 13(7): 7359–65.

272. Pecharsky VK, Zavalij PY. Fundamentals of powder diffraction and structural characterization of materials. Second edition. Springer Science & Business Media; 2008: 1–729.

273. Bhaskar R, Li J, Xu L. A comparative study of particle size dependency of IR and XRD methods for quartz analysis. Am Ind Hyg Assoc J. 1994; 55(7): 605–9.

274. Langford JI, Louër D, Scardi P. Effect of a crystallite size distribution on X-ray diffraction line profiles and whole-powder-pattern fitting. J Appl Crystallogr. 2000; 33(3): 964–74.

275. Wilchinsky ZW. Effect of crystal, grain, and particle size on X-ray power diffracted from powders. Acta Crystallogr. 1951; 4(1): 1–9.

276. Patterson AL. The scherrer formula for X-ray particle size determination. Phys Rev. 1939; 56(10): 978–82.

277. Sain S, Kar A, Patra A, Pradhan SK. Structural interpretation of SnO2 nanocrystals of different morphologies synthesized by microwave irradiation and hydrothermal methods. CrystEngComm. 2014; 16(6): 1079–1090.

278. The cambridge crystallographic data centre (CCDC) [Internet; cited in August 2021]. Available from: https://www.ccdc.cam.ac.uk/

279. Maas SG, Schaldach G, Littringer EM, Mescher A, Griesser UJ, Braun DE, et al. The impact of spray drying outlet temperature on the particle morphology of mannitol. Powder Technol. 2011; 213(1–3): 27–35.

280. Wang A, Lu Y, Zhu R, Li S, Ma X. Effect of process parameters on the performance of spray dried hydroxyapatite microspheres. Powder Technol. 2009; 191(1–2): 1–6.

281. York P. Solid-state properties of powders in the formulation and processing of solid dosage forms. Int J Pharm. 1983; 14(1): 1–28.

282. Ekdahl A, Mudie D, Malewski D, Amidon G, Goodwin A. Effect of Spray-Dried Particle Morphology on Mechanical and Flow Properties of Felodipine in PVP VA Amorphous Solid Dispersions. J Pharm Sci. 2019; 108(11): 3657–66.

283. Ridgway K, Rupp R. The effect of particle shape on powder properties. J Pharm Pharmacol. 1969; 21(S1): 30S-39S.

284. Hou H, Sun CC. Quantifying effects of particulate properties on powder flow properties using a ring shear tester. J Pharm Sci. 2008; 97(9): 4030–9.

285. Kulkarni PA, Berry RJ, Bradley MSA. Review of the flowability measuring techniques for powder metallurgy industry. Proc Inst Mech Eng Part E J Process Mech Eng. 2010; 224(3): 159–68.

286. Ashish J, Swaroop G, Balasubramanian K. Effect of Ammonium Perchlorate Particle Size on Flow, Ballistic, and Mechanical Properties of Composite Propellant. In: NNanomaterials in Rocket Propulsion Systems Elsevier; 2019: 299–362.

287. Shah RB, Tawakkul MA, Khan MA. Comparative evaluation of flow for pharmaceutical powders and granules. AAPS PharmSciTech. 2008; 9(1): 250–8.

288. Raval MK, Patel JM, Parikh RK, Sheth NR. Studies on influence of polymers and excipients on crystallization behavior of metformin HCl to improve the manufacturability. Part Sci Technol. 2014; 32(5): 431–44.

289. Nan W, Ghadiri M, Wang Y. Analysis of powder rheometry of FT4: Effect of particle shape. Chem Eng Sci. 2017; 173: 374–83.

290. Koner JS, Rajabi-Siahboomi A, Bowen J, Perrie Y, Kirby D, Mohammed AR. A Holistic Multi Evidence Approach to Study the Fragmentation Behaviour of Crystalline Mannitol. Sci Rep. 2015; 5(1): 1–12.

291. Katikaneni PR, Upadrashta SM, Rowlings CE, Neau SH, Hileman GA. Consolidation of ethylcellulose: Effect of particle size, press speed, and lubricants. Int J Pharm. 1995; 117(1): 13–21.

292. Nokhodchi A, Ford JL, Rowe PH, Rubistein MH. The effect of moisture on the heckel and energy analysis of hydroxypropylmethylcellulose 2208 (HPMC K4M). J Pharm Pharmacol. 1996; 48(11): 1122–7.

293. Yoshinari T, Forbes RT, York P, Kawashima Y. The improved compaction properties of mannitol after a moisture-induced polymorphic transition. Int J Pharm. 2003; 258(1–2): 121–31.

294. Kosugi A, Leong KH, Urata E, Hayashi Y, Kumada S, Okada K, et al. Effect of different direct compaction grades of mannitol on the storage stability of tablet properties investigated using a kohonen self-organizing map and elastic net regression model. Pharmaceutics. 2020; 12(9): 886.

295. Tarlier N, Soulairol I, Sanchez-Ballester N, Baylac G, Aubert A, Lefevre P, et al. Deformation behavior of crystallized mannitol during compression using a rotary tablet press simulator. Int J Pharm. 2018; 547(1–2): 142–9.

296. Barot BS, Parejiya PB, Patel TM, Parikh RK, Gohel MC. Compactibility improvement of metformin hydrochloride by crystallization technique. Adv Powder Technol. 2012; 23(6): 814–23.

297. Garekani HA, Ford JL, Rubinstein MH, Rajabi-Siahboomi AR. Effect of compression force, compression speed, and particle size on the compression properties of paracetamol. Drug Dev Ind Pharm. 2001; 27(9): 935–42.

298. Šantl M, Ilić I, Vrečer F, Baumgartner S. A compressibility and compactibility study of real tableting mixtures: The impact of wet and dry granulation versus a direct tableting mixture. Acta Pharm. 2012; 62(3): 325–40.

299. Jivraj M, Martini LG, Thomson CM. An overview of the different excipients useful for the direct compression of tablets. Pharm Sci Technolo Today. 2000; 3(2): 58–63.

300. United States Pharmacopoeia. Tablet breaking force ⟨1217⟩, The United States Pharmacopeia (USP 36, Volume 1). United States Pharmacopeial Conv Inc, Rockville, MD, USA. 2013; 274–6.

301. Zatloukal Z, Šklubalová Z. The influence of orifice height on flow rate of powder excipients. Die Pharm Int J Pharm Sci. 2011; 66(12): 953–5.

302. Hancock BC, Garcia-Mundoz S. How do formulation and process parameters impact blend and unit dose uniformity? Further analysis of the product quality research institute blend uniformity working group industry survey. J Pharm Sci. 2013; 102(3): 982–6.

303. Kukkar V, Anand V, Kataria M, Gera M, Choudhury PK. Mixing and formulation of low dose drugs: underlying problems and solutions. Thai J Pharm Sci. 2008; 32: 43–58.

304. Genina N, Räikkönen H, Antikainen O, Heinämäki J, Yliruusi J. Ultrasound-assisted powder-coating technique to improve content uniformity of low-dose solid dosage forms. AAPS PharmSciTech. 2010; 11(3): 1320–7.

305. Yip CW, Hersey JA. Ordered or random mixing: Choice of system and mixer. Drug Dev Ind Pharm. 1977; 3(5): 429–38.

306. Hersey JA. Ordered mixing: a new concept in powder mixing practice. Powder Technol. 1975; 11(1): 41–4.

307. Bi M, Sun CC, Alvarez F, Alvarez-Nunez F. The manufacture of low-dose oral solid dosage form to support early clinical studies using an automated micro-filing system. AAPS PharmSciTech. 2011; 12(1): 88–95.

308. Clarke A, Doughty D. Development of liquid dispensing technology for the manufacture of low dose drug products. In: Kleinebudde P, Khinast J, Rantanen J, editors. Continuous Manufacturing of Pharmaceuticals. John Wiley & Sons Ltd; 2017: 551–75.

309. Besenhard MO, Karkala SK, Faulhammer E, Fathollahi S, Ramachandran R, Khinast JG. Continuous feeding of low-dose APIs via periodic micro dosing. Int J Pharm. 2016; 509(1–2): 123–34.

310. Wang H, Wu L, Zhang T, Chen R, Zhang L. Continuous micro-feeding of fine cohesive powders actuated by pulse inertia force and acoustic radiation force in ultrasonic standing wave field. Int J Pharm. 2018; 545(1–2): 153–62.

311. Sacher S, Heindl N, Afonso Urich JA, Kruisz J, Khinast JG. A solution for low-dose feeding in continuous pharmaceutical processes. Int J Pharm. 2020; 591: 119969.

312. Chen X, Seyfang K, Steckel H. Development of a micro dosing system for fine powder using a vibrating capillary. Part 1: The investigation of factors influencing on the dosing performance. Int J Pharm. 2012; 433(1–2): 34–41.

313. Official felodipine monograph, The United States Pharmacopeia (USP 36, Volume 2). United States Pharmacopeial Conv Inc, Rockville, MD, USA; 2013: 3538–43.

314. Torrado JJ, Illum L, Davis SS. Particle size and size distribution of albumin microspheres produced by heat and chemical stabilization. Int J Pharm. 1989; 51(1): 85–93.

315. International Conference on Harmonisation (ICH): Q2(R1) Validation of analytical procedures: Text and methodology; 2005.

316. Guidance for industry: powder blends and finished dosage units— stratified in-process dosage unit sampling and assessment, U.S. department of health and human services, Food and drug administration, Center for drug evaluation and research (CDER). Pharm CGMPs; 2003.

317. Legoix L, Gatumel C, Milhé M, Berthiaux H. Characterizing powders in order to determine their flow behavior in a mixer: From small scale observations to macroscopic in-mixer rheology for powders of various flowabilities. Powder Technol. 2017; 322: 314–31.

318. Alyami H, Dahmash E, Bowen J, Mohammed AR. An investigation into the effects of excipient particle size , blending techniques and processing parameters on the homogeneity and content uniformity of a blend containing low-dose model drug. PLoS One. 2017; 12(6): e0178772.

319. Alsulays BB, Fayed MH, Alalaiwe A, Alshahrani SM, Alshetaili AS, Alshehri SM, et al. Mixing of low-dose cohesive drug and overcoming of pre-blending step using a new gentle-wing high-shear mixer granulator. Drug Dev Ind Pharm. 2018; 44(9): 1520–7.

320. Fayed MH, Abdel-Rahman SI, Alanazi FK, Ahmed MO, Tawfeek HM. An investigation into the impact of key process variables on the uniformity of powder blends containing a low-dose drug in a gentle-wing high shear mixer. J Drug Deliv Sci Technol. 2020; 60: 102036.

321. Alchikh-Sulaiman B, Alian M, Ein-Mozaffari F, Lohi A, Upreti SR. Using the discrete element method to assess the mixing of polydisperse solid particles in a rotary drum. Particuology. 2016; 25: 133–42.

322. Corn M. The adhesion of solid particles to solid surfaces, I. A review. J Air Pollut Control Assoc. 1961; 11(11): 523–8.

323. Mullins ME, Michaels LP, Menon V, Locke B, Ranade MB. Effect of geometry on particle adhesion. Aerosol Sci Technol. 1992; 17(2): 105–18.

324. York P. A consideration of experimental variables in the analysis of powder compaction behaviour. J Pharm Pharmacol. 1979; 31(1): 244–6.

325. Çelik M, Marshall K. Use of a compaction simulator system in tabletting Research. Drug Dev Ind Pharm. 1989; 15(5): 759–800.

326. Katz JM, Buckner IS. Characterization of strain rate sensitivity in pharmaceutical materials using indentation creep analysis. Int J Pharm. 2013; 442(1–2): 13–9.

327. Rayleigh, Lord. On the instability of jets. Proc London Math Soc. 1878; S1-10(1): 4–13.

328. Shabir GA. Step-by-step analytical methods validation and protocol in the quality system compliance industry. J Valid Technol. 2005; 10: 314–25.